Acrylic-Polyurethane Based Graft-Interpenetrating Polymer Networks for High-Performance Applications

by

Nima Alizadeh

A dissertation submitted to the Graduate Faculty of
Auburn University
in partial fulfillment of the
requirements for the Degree of
Doctor of Philosophy

Auburn, Alabama
May 1, 2021

Keywords: interpenetrating polymer networks, polyurethane, acrylic-based copolymers, polymer matrix composites, finite element modeling, thermal energy storage

Approved by

Maria L. Auad, Chair, Professor of Chemical Engineering
Sabit Adanur, Professor of Mechanical Engineering
Asha-Dee Celestine, Assistant Professor of Aerospace Engineering
Vinamra Agrawal, Assistant Professor of Aerospace Engineering

Abstract

In this research, interpenetrating polymer networks (IPNs), based on of polyurethane (PU) and acrylic copolymer were synthesized for high-performance applications. Two different polymers with different mechanical and thermal properties were utilized to take advantage of the synergy of the networks. Chemical bonds between the two phases were utilized to minimize the phase separation between two polymers and enhance the final properties. The use of synthesized IPNs in transparent high fracture toughness and impact structural applications, fiber-reinforced composite, and thermal energy storage devices were studied. The stress relaxation behavior of the synthesized IPNs was also modeled.

In chapter 2, graft-interpenetrating polymer networks were synthesized for transparent protection applications. Excellent transparency was observed in IPN samples with a high percentage of styrene. Fracture toughness results indicated more than 100% improvement compared to poly(methyl methacrylate) (PMMA) and polystyrene as traditional transparent impact resistant polymers. Novel graft-IPN synthesized in this chapter has huge potential in transparent high fracture toughness applications.

In chapter 3, graft-interpenetrating polymer networks containing commercial vinyl ester were employed in carbon fiber reinforced polymer matrix composites. Enhancement in damping properties was observed in IPN structure compared to pure acrylic copolymer due to the presence of PU. No phase separation was observed in the IPN matrix, and composite samples showed good adhesion between fibers and matrix without any debonding or fiber pull-out. The composites' flexural and tensile properties were also obtained and showed enhancement compared to composite samples prepared in the literature. The results obtained in this chapter, combined with

simple manufacturing method of composites, indicate the potential of graft-IPN carbon fiber composite in different high-performance applications.

In chapter 4, the application of graft-IPNs was broadened by increasing the percentage of PU in the system. The effect of changing the monomer of the acrylic copolymer from styrene to MMA was also studied. Temperature ramp test and tensile results showed broad properties for elastomeric to more ductile applications. Excellent transparency and impact resistance for sandwich structure of pure polycarbonate (PC) sheets with novel graft-IPNs between them were also obtained. The strength of materials as an adhesive was also determined using a lap shear test. The flexible graft-IPN has vast potential to be used in transparent high impact resistance applications.

In chapter 5, the stress relaxation behavior of the IPN samples with different percentages of PU and different styrene ratios were studied using dynamic mechanical analysis under tensile and flexural tests. Synthesized glassy IPNs showed excellent compatibility between two phases with comparable resistance against relaxation to COP samples in the stress relaxation test. Rubbery samples also exhibited excellent resistance against relaxation, which shows their potential in damping applications. These experimental results were used to simulate the numerical model for the stress relaxation behavior of the samples. For this purpose, a three-dimensional FEM model was utilized with the Generalized Maxwell model and four-term Prony series constants. Good overlap between experimental and simulated stress relaxation data was observed for all samples, which shows the potential of the generated model in predicting the stress relaxation behavior of IPNs.

In the final chapter, semi-interpenetrating polymer networks were synthesized out of polyethylene glycol (PEG)-based PU and MMA-based acrylic copolymer. PU was utilized to act as a thermal

energy storage material. At the same time, acrylic copolymer was used to act as a skeleton to keep the whole system together at a higher temperature. The synthesized sample showed excellent thermal properties with cycling and shape stability. Such material has tremendous potential to be used in thermal energy storage applications such as electronics and solar cells.

Keywords: interpenetrating polymer networks, acrylic-based copolymers, polyurethane, fracture toughness, woven fiber composites, elastomeric materials, adhesives, impact resistance, finite element modeling, stress relaxation, phase change materials, thermal energy storage, viscoelastic properties, thermomechanical properties, NMR polymerization

Acknowledgments

This research would not have been possible without the help of many different individuals and parties, and I want to show my appreciation for their unlimited assistance. Present work is funded by National Science Foundation - Centers of Research Excellence in Science and Technology (NSF-CREST) Center for Sustainable Lightweight Materials (C-SLAM) award #1735971. I want to send my gratitude to my parents, Daryoush and Zahra, who have guided me throughout my life to become successful in my personal and professional life. They are my role models, and I follow them in each step of my life. I also want to thank my sister, Shima, whom I wouldn't be here without, and I will never be able to thank her enough for the amount of aid and support that she provides for me. I also thank my American family (Eric and Jennifer Halverson) and their lovely kids (Ann Maria and Hadley). I always look at them as my real family, and I never felt alone during my Ph.D. They were always there for me, and they made my Ph.D. journey much more comfortable with their presence. I am very thankful to my advisor, Dr. Maria L. Auad, for the continuous and unlimited support she has provided for me during my Ph.D. program, making my Ph.D. life productive and exciting. I am very appreciative to my advisory committee members, Dr. Sabit Adanur, Dr. Asha-Dee Celestine, and Dr. Vinamra Agrawal. They modified my thesis quality by providing great and practical suggestions for my research. It was my honor to have Dr. George Flowers serve as the university reader for my dissertation. It was one of my best experiences during my Ph.D. to work with him and learn from him. I want to thank the Center for Polymers and Advanced Composites, the Department of Chemical Engineering, and the Department of Aerospace Engineering at Samuel Ginn College of Engineering for providing all the research facilities required in my projects. I would love to thank Geoffrey Thompson, Dr. Ramsis Farag, Dr. Eldon Triggs, Dr. Royall Broughton, Emmanuel Winful, Christian Brodbeck,

Dr. Bryan Beckingham, Dr. Mehul Barde, Ehsan Hassani, Diego Gómez Maldonado, David Thorne, Haishun Du, Dr. Michael Minkler, Dr. Haibin Ning, Dr. Michael Miller, Naomi Gehling, Emma Goodlett, Elaine Manning, and Dr. Mario Eden, chair of the department of chemical engineering for their help in different aspects of my research. I could not complete my Ph.D. research without these people's continuous support in different parts of my research, such as safety, manufacturing, and characterization. I also want to thank all of the instructors that helped me during my Ph.D. study, including but not limited to Dr. Xinyu Zhang, Dr. Rashad Karimov, and Dr. Mark Carpenter. I am very grateful to have such wonderful friends and colleagues supporting me during my research. My friends and colleagues are included but not limited to Archana Bansode, Mehul barde, Yuyang Wang, Tripp Hinkle, and Xiaoliang Fu with whom I have spent an enjoyable time.

Table of Contents

List of Tables

List of Figures

List of Abbreviations

AIBN	2,2'-Azobis(2-Methyl-Propionitrile)
ALON	Aluminum-oxy-Nitride
ASTM	American Society for Testing and Materials
ATR	Attenuated Total Reflection
BisGMA	Bisphenol A bis(2-Hydroxy-3-Methacryloxypropyl) Ether
COP	Acrylate-Based Copolymer
DBTDL	Dibutyltin Dilaurate
DCH	Hexamethylene Diisocyanate
DGEBA	Diglycidyl Ether of Bisphenol A
DMA	Dynamic Mechanical Analysis
DSC	Differential Scanning Calorimetry
DTRT	Dynamic Temperature Ramp Test
FEM	Finite Element Method
FTIR	Fourier Transform Infrared Spectroscopy
HS	Hard Segment
IPN	Interpenetrating Polymer Network
IPN_G	Glassy IPN
IPN_R	Rubbery IPN
MMA	Methyl Methacrylate
NCO	Isocyanate
NMR	Nuclear Magnetic Resonance
OOP	Out-of-Plane

PANI	Polyaniline
PC	Polycarbonate
PCM	Phase Change Material
PEG	Polyethylene Glycol
PMC	Polymer Matrix Composite
PMMA	Poly-Methyl Methacrylate
POM	Polarized Optical Microscopy
PS	Polystyrene
PTMG	Poly(Tetramethylene Ether) Glycol
PU	Polyurethane
SEM	Scanning Electron Microscopy
SENB	Single Edge Notched Bend
SS	Soft Segment
TDI	Toluene Diisocyanate
TEM	Transmission Electron Microscope
TES	Thermal Energy Storage
TGA	Thermogravimetric Analysis
TPB	Triphenyl Bismuth
TRIOL	2-Ethyl-2-(Hydroxymethyl)-1,3-Propanediol
UPW	Ultrapure Water
UV	Ultra-Violet
VER	Vinyl Ester Resin
XRD	X-ray Diffraction

Chapter 1
Introduction

1.1. Polymers

Polymers have high chemical resistance [1], high mechanical properties [2], low density, easy and cheap manufacturing process, and good flexibility and impact resistance [3]. Moreover, gas permeability, tailorable properties [4], flame, and smoke resistance [5], excellent bearing, abrasion and wear resistance properties [6, 7], easier sterilization [8], superior insulation [7, 9] are other advantages of different polymers in comparison of traditional materials. These unique properties make polymers great candidate in various applications such as food packaging, electrical devices, office appliances, automobile industry, films such as photographic and magnetic films, protective shields such as helmets and canopies, medical applications such as heart valves, prosthetics, and tissue engineering, fabrics such as wearing apparel, flame resistance applications such as firefighters clothing, coating applications, adhesive bandings, friction materials, foams, decorative applications, crack repairments, insulator applications such as wire and cable insulators, defense and aerospace applications [7, 10], optics applications such as fiber optics, additive manufacturing, dental applications, housing and construction, petroleum and chemical industry such as engine oils [7] matrix in composites [11], damping applications such as shock absorber [12, 13], and so many other general, engineering, and specialty applications [7].

1.2. Multicomponent polymeric materials

Polymer blends are macroscopic homogeneous polymer mixture with the properties of their precursors. Polymer blends are noticed for producing polymers with lower prices, extending the engineering applications of polymers, enhancing specific properties, synthesizing high-performance polymer out of polymer waste, improving processability, and quick formulation change. Polymer blends are divided into miscible, partially miscible, and immiscible blends [14]. Miscible polymer blends show one phase in a specific situation, such as temperature and pressure [15]. Figure 1.1 shows the different kinds of polymer blends. Figure 1.1.a exhibits the mixtures of two polymers with no chemical bonds between them, which is called a polymer blend [16-18]. Figure 1.1.b shows the graft copolymer where chains of one polymer are attached as a side chain to the chains of another polymer [17-19]. Figure 1.1.c shows the structure of a block copolymer where chains of two polymers are bonded to each other end to end [16, 18, 19]. Figure 1.1.d represents the structure of A-B graft copolymer, where at least two polymers are chemically bonded together via several points [16, 18, 19]. Figure 1.1.e, f, and g belong to different kinds of interpenetrating polymer networks (IPNs). Figure 1.1.e shows the structure of semi-IPN where one polymer in the system is crosslinked while another polymer is linear. Figure 1.1.f represents a full-IPN where both of the polymers in the IPN system are crosslinked [16, 18]. Figure 1.1.g shows the structure of graft-IPNs where both of the polymers are crosslinked into the system, and two networks are bonded together via chemical bonds [15, 16, 18, 19]. The graft-IPN was utilized in this research to minimize the phase separation between two systems and maximize the properties of the IPN.

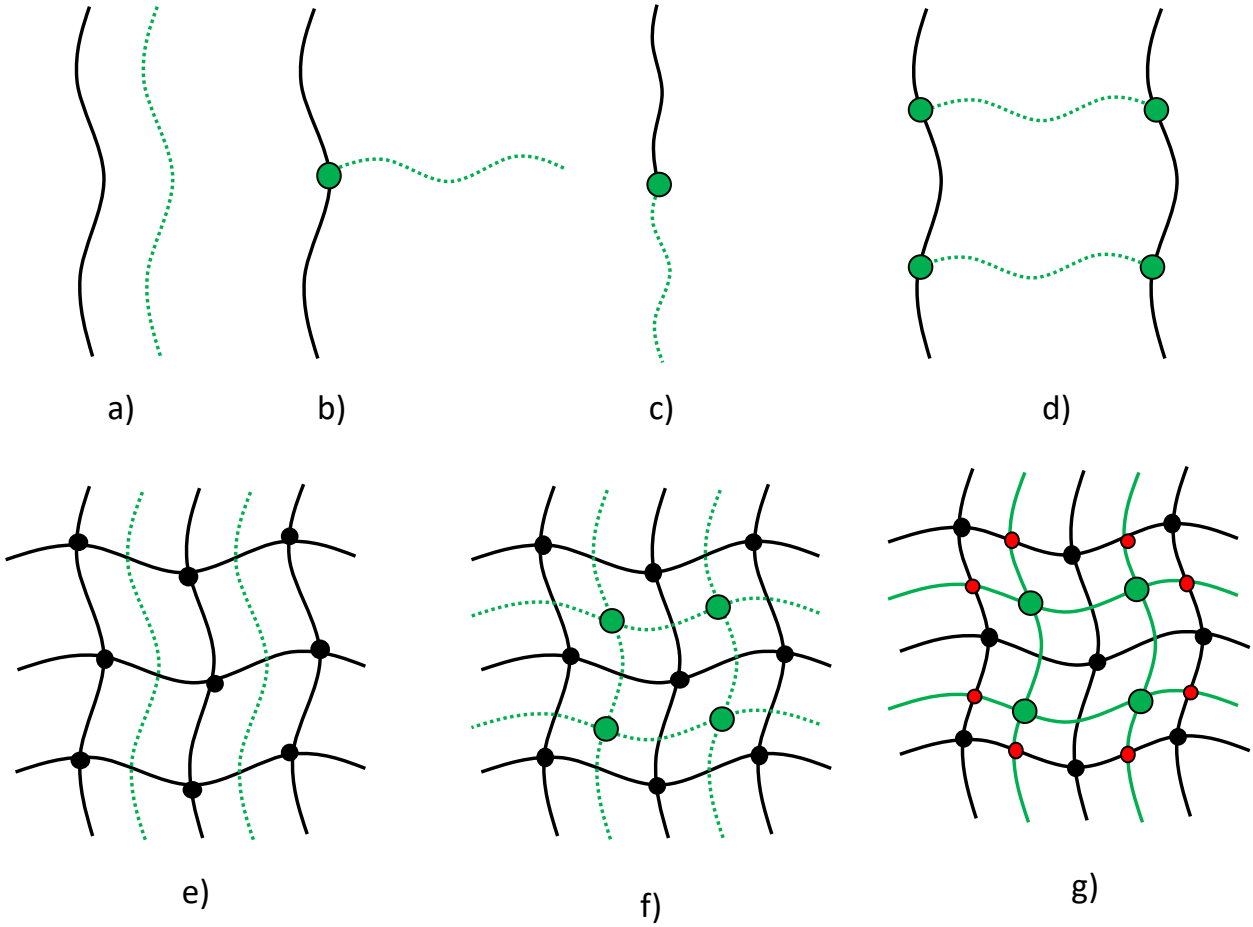

Figure 1.1. Different kinds of multicomponent polymeric materials a) polymer blend b) graft copolymer c) block copolymer d) AB-crosslinked polymer e) semi-IPN f) full-IPN g) graft-IPN.

Almost all of the polymers are immiscible due to the very low entropy of mixing and high enthalpy of mixing on blending of two polymers. Therefore, IPNs are used to enhance the compatibility between two polymers [18].

1.2.1. Interpenetrating polymer networks (IPNs)

An interpenetrating polymer network is a polymer consisting of two polymers. These two polymers are entangled with each other, and it is impossible to separate them without breaking the

chemical bonds [15]. A solvent swells an IPN; however, it does not dissolve the IPN. Li et al. mentioned that while there is phase separation in IPNs, these materials show highly uniform structures due to forced compatibility [20]. Physical entanglement, forced compatibility, the synergism of the networks and cellular, multi-phase, and continuous microstructure causes excellent thermal stability and mechanical properties within the IPNs [21]. To synthesize the IPN successfully, several factors, such as Kinetic (reaction rate), thermodynamic (Gibbs free energy), and crosslinking density, are playing a significant role in enhancing the compatibility between two phases [22, 23]. The morphology of the IPNs highly influences the final properties of the IPNs [23].

1.2.1.1. Different kinds of IPNs

Latex IPN is a kind of IPN when two linear polymers are mixed in latex mode and crosslinked simultaneously; the product is sometimes called an interpenetrating elastomeric network [18]. In latex IPNs, if monomers are synthesized simultaneously, the final product will be more uniformed. However, if one polymer is synthesized first, depending on the speed of diffusion of the second monomer into the first polymer network, the structure could be varied from a homogenous system to a core-shell structure [24]. Sheu et al. synthesized polystyrene (PS)/PS latex IPN. Seeded emulsion polymerization of styrene into the monodisperse crosslinked polystyrene latex was utilized, and the mechanism of phase separation for full-IPN was suggested. It was observed that increasing the crosslinking point of the second polymer increases the phase separation between two polymers. It was indicated that full PS/PS IPN shows less phase separation than semi PS/PS IPN due to the slower phase separation rate [25].

Gradient IPNs are other kinds of IPNs where one polymer network grows on one surface of IPN film, and another polymer grows on the other side of it [26]. In other words, the gradient IPN is one kind of IPN where one polymer is more prevalent on one side of the IPN while the other polymer is more prevalent on the other side. Moreover, in the middle of the gradient IPN, there is a similar composition of materials [16, 19]. Expressly, the gradient IPN is a combination of an infinite number of thin layers where the properties are changing layer by layer [21, 27]. Researchers have synthesized the gradient IPN with hard external part and soft internal part, and intermediate gradient part, which is useful for damping applications [28]. The materials' damping ability is defined as their ability to convert the mechanical properties to thermal energy via mechanical vibration [29]. LV et al. worked on the damping properties of the continuous gradient polyurethane/epoxy IPNs. The gradient IPN showed the broadest peak for *tan δ*, indicating the highest damping properties for gradient IPN. While the graded IPNs, which consisted of homogenous layers in its structure, showed the lowest damping properties. These high damping properties of gradient IPNs are due to their infinite number of layers, which broaden the glass transition temperature. The synthesized gradient IPNs had two surfaces, one rigid phase with epoxy as a continuous phase and another flexible surface with PU as continuous phase [21]. Thermoplastic IPNs are other kinds of IPNs where the IPN can flow if they are exposed to a higher temperature [23].

IPNs can be classified as sequential or simultaneous IPN based on the synthesis method. The IPN is called sequential when synthesis of polymer 1 happening first while swelling the monomers of polymer 2 inside the network. After completion of polymerization of polymer 1, polymer 2 is synthesized in-situ into the network of polymer 1. In sequential IPN, the first polymer that is synthesized is considered the continuous phase. In simultaneous IPN, the polymerization of the two polymers starts at the same time, while no interfering reaction is occurring. For example, a

polymer is synthesized via free radical polymerization, while the other one is synthesized via step-growth polymerization. Therefore, the coincidence between the polymerization of the two polymers might not happen; however, the onset of the polymerization in simultaneous polymerization remains the same [16, 19, 30]. Figures 1.2 and 1.3 show a simple schematic of simultaneous and sequential IPNs, respectively [19].

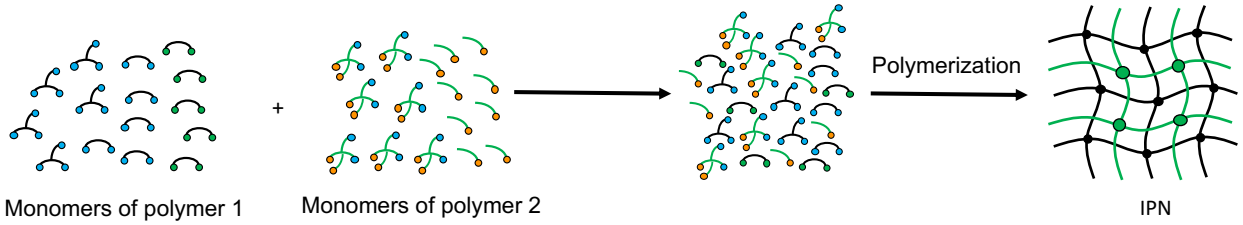

Figure 1.2. Simple schematic for simultaneous interpenetrating polymer networks.

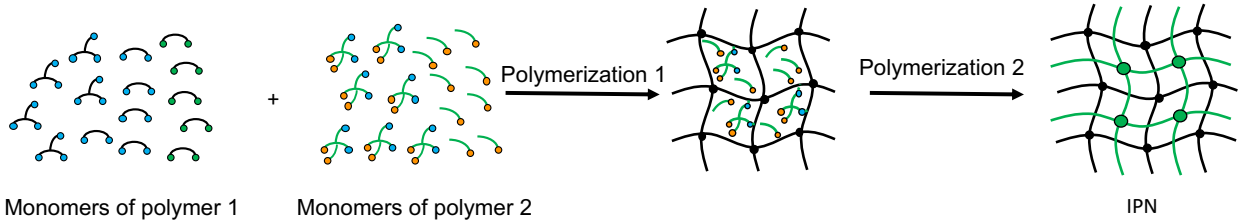

Figure 1.3. Simple schematic for sequential interpenetrating polymer networks.

The IPNs can be classified based on their domain size. An IPN with a larger domain size in micron-scale, IPN in 1000 Å, which is considered as intermediate structure, IPN with fine structures with 100 Å domain size, and IPN, which are not resolvable at all, are different kinds of IPNs based on their domain size [31].

1.2.1.2. Historical development of IPNs

Table 1.1 shows the historical development of the IPNs and the materials related to it. The development of IPNs started with mixing sulfur and white lead with India-rubber by Goodyear. The product was resistant to high and low temperature [18, 32]. Then Aylsworth, who was the chemist of Thomas Edison, invented the new composition out of rubber with different crosslinking agents [33]. Staudinger was the first person who understood the chainlike properties of the polymeric materials [34]. Ostromislensky understood the structure of the graft-copolymer, which is published in his patent. Ostromislensky dissolved the rubber in styrol and cured the polymer in solution form [18, 35]. During these years, numerous advances happened with different kinds of polymer blends, as shown in Table 1.1 [18, 36-38]. Amos et al. studied the rubber toughened plastics and successfully synthesized high-impact polystyrene and acrylonitrile-butadiene-styrene plastics [39]. Lunsted et al. synthesized block copolymer out of polyoxyalkylene compounds as surfactants. Polyoxypropylene polymer was used in the system as the hydrophobic element [18, 40]. Staudinger and Hutchinson were the first research group that synthesized interpenetrating polymer networks out of polystyrene and an organic compound. The product was a transparent plastic [41]. Millar et al. was the group that used the term "interpenetrating polymer networks." They synthesized IPNs from styrene and divinylbenzene. However, as mentioned above, the first IPN was manufactured by Aylsworth out of natural rubber, sulfate, and phenol-formaldehyde resins [18, 33, 42]. H. Frisch was interested in polymeric catenanes, which are IPNs consisting of rings physically bonded together [18]. Frisch et al. synthesized an IPN out of two elastomers. The final product was called interpenetrating elastomeric network [43]. It should be added that K. Frisch, who was the brother of H. Frisch, was one of the top polyurethane (PU) scientists. His group always used PU as one of the components of the IPNs that they developed [18]. Sperling et al. synthesized a sequential IPN out of poly(ethyl

acrylate) and polystyrene. Ultraviolet photopolymerization was used to polymerize both of the polymers with desirable initiators [44].

Table 1.1. History of IPNs and related materials [18].

Event	First investigators	Year
Vulcanization of rubber	Goodyear	1844
IPN type structure	Aylsworth	1914
Polymer structure elucidated	Staudinger	1920
Graft copolymers	Ostromislensky	1927
Interpenetrating polymer networks	Staudinger and Hutchinson	1951
Block copolymers	Dunn and Melville	1952
HiPS and ABS	Amos, McCurdy, and McIntire	1954
Block copolymer surfactants	Lunsted	1954
Homo-IPNs	Millar	1960
Thermoplastic elastomers	Holden and Milkovich	1966
AB crosslinked copolymers	Bamford, Dyson, and Eastmond	1967
Sequential lPNs	Sperling and Friedman	1969
Latex lENs	Frisch, Klempner, and Frisch	1969
Simultaneous interpenetrating networks	Sperling and Arnts	1971
IPN nomenclature	Sperling and Arnts	1974
Thermoplastic IPNs	Davison and Gergen	1977

1.2.1.3. IPN's applications

Several research groups synthesized the full and semi-IPN with different methods. The phase separation of the IPNs and the potentials of synthesized IPN in various applications such as self-healing applications [45], conductive polymers [46], artificial muscle [47], dental applications [48], phase change applications [49], biomedical applications [50], noise and vibration damping [51], coatings [18],

adhesives [18], impact-resistant plastics [52, 53], tough plastics [18], and electrical insulation [18] were studied.

Peterson et al. utilized an IPN for self-healing applications. The lack of liquid-filled capsules in this system simplified the process. The IPN can be used in applications where liquid-based healing is not effective as well. The semi-IPN was synthesized out of methacrylated phenyl glycidyl ether as the linear phase and diglycidyl ether of bisphenol A (DGEBA) and 4,40 -methylene biscyclohexanamine as the crosslinked polymer in the system. The synthesized IPNs show great potential to be used in fiber-reinforced composite susceptible to fatigue-induced damage [45].

Interpenetrating polymer networks were used in conductive applications. Jeevananda et al. synthesized conducting IPNs out of a castor oil-based polyurethane (PU) with poly(methyl methacrylate) (PMMA) and polyaniline (PANI) doped with camphor sulphonic acid. PANI is not soluble in a regular organic solvent; therefore, extensive research was done on the PANI blends and its composite. Thus, combining the high conductivity of PANI with other polymers with high mechanical properties produces IPN with desirable properties for a wide range of applications. It was observed that the initial thermal stability of PANI was enhanced by utilizing it into the IPN system due to the reduction in moisture absorbance of PANI [46].

Ha et al. utilized electroactive polymer in artificial muscle applications. Electroelastomers based on acrylic copolymer elastomers were used in IPN structure due to their large-strain and high mechanical properties. The acrylic elastomer films were used as the first polymer of IPN, and 1,6-hexanediol diacrylate liquid as the cross-linkable polymer to form the second polymer with a higher young modulus. It was mentioned that although an optimum amount of poly(1,6-hexanediol diacrylate) is required to support the highly prestrain acrylic elastomer networks, increasing the

amount of poly(1,6-hexanediol diacrylate) decreases the electrically induced strain due to the higher young modulus provided by poly(1,6-hexanediol diacrylate) [47].

The application of polymers in dental work was started with using PMMA in 1930's [54]. Bowen et al. was the first group who used thermoset polymers for dental applications [55]. The denture- based IPNs are semi-IPNs with just one of the polymer crosslinked while the other one is linear[48]. Multifunctional monomers like bisphenol A bis(2-hydroxy-3-methacryloxypropyl) ether (BisGMA) are used to form the crosslinked part of the IPN. In contrast, the mono-functional part is used to create the linear portion of the semi-IPN. There are a couple of requirements that should be fulfilled to form the semi-IPN. In an IPN that is made of the photopolymerization process, the monofunctional methyl methacrylate (MMA) should be polymerized first due to the low reactivity of the monofunctional MMA via photopolymerization. Then the crosslinked MMA precursors swell the monofunctional polymer to form the final semi-IPN. The fiber-reinforced composite could be used in dental applications where fibers reinforce the IPN matrix by increasing the strength and flexural modulus of the system. The durable adhesion and bonding between the fibers and matrix could be reached by applying a semi-IPN as a polymer matrix into the system [48].

Zhang et al. synthesized semi-IPNs out of polyethylene glycol (PEG) and a network gel for phase change applications. Results indicated that the latent heat of the semi-IPN is close to the PEG Mn=10000 g/mol. Higher shape stability of the semi-IPN in comparison to the pure PEG with different molecular weights was observed. This fact proves the positive effect of a 3D structure for keeping PEG from moving freely and lose its original shape in semi-IPN. Synthesized semi-IPNs also showed excellent heat-shielding properties and cycling stability due to the high latent heat. It offers a wide range of applications of this material in the heat management field [49].

Szilagyi et al. synthesized an interpenetrating polymer network composed of poly(vinyl alcohol) and poly(N-isopropylacrylamide) as a hydrogel. Poly(N-isopropylacrylamide) has thermally induced volume change, which makes it a good material for drug delivery systems. However, in some applications, dramatic volume change could be a significant disadvantage. The formation of the IPNs could ensure the stability of the morphology [56]. The volume phase transition temperature of the synthesized IPN was due to the presence of a hydrophilic neutral or anionic co-monomer of poly(N-isopropylacrylamide). The synthesized sheet of IPN became opaque when it exceeded the critical temperature. This shows the potential of these materials in controlling UV light radiation [57].

1.2.1.4. IPNs: Improvement in polymers' thermal properties

Several research groups tried to enhance the properties of polymers by utilizing IPNs. IPNs, regardless of the composition and other factors in synthesis, show better thermal stability than their constituent materials [58]. Vlad et al. synthesized the IPN out of PU and polysiloxane. It was observed that the IPNs are superior regarding their thermal stability. Two separate glass transition temperatures for all of the samples were observed, indicating a considerable phase separation between two polymers [59].

Mathew et al. studied the thermal stability of natural rubber / PS semi- and full-IPNs developed with the sequential technique. Higher thermal stability was achieved by increasing the percentage of PS into the IPN. Full-IPN with crosslinked PS showed better interpenetration between two polymers and, therefore, higher thermal stability in comparison to the semi-IPN with linear PS in it [60].

1.2.1.5. IPNs: Improvement in polymers' toughness and mechanical properties

Many different research groups tried to enhance the impact resistance and toughness properties of plastics by adding rubbery materials with higher toughness such as PU to brittle plastics such as PMMA and vinyl ester resin (VER). The objective of their work was to produce novel materials for windshield-like applications. The product generally consisted of a highly rigid continuous matrix with a large number of elastomeric domains. Incorporating these properties synthesized the novel materials with immense potential in transparent protective applications [26, 31, 61-69].

Kim et al. synthesized full-IPNs, semi-IPNs, and polymer blends out of PU and PMMA with the simultaneous method. It was observed that the interpenetration happening in the IPNs is playing a key role in decreasing the phase separation and domain size in contrast to the linear polymer blends and the semi-IPNs, which was called pseudo-IPN in this paper [31].

Klempner et al. synthesized the IPN out of PU and PMMA. It was indicated that increasing the percentage of PU in the IPN to make it a continuous phase decreases the modulus of the system, whereas increasing the amount of PMMA as a glassy phase inverses the continuous phase to glassy and therefore increases the modulus of the system. Also, it was mentioned that the linear PU has a higher modulus compared to the crosslinked PU due to the higher crystallization in the linear PU [63].

Jajam et al. synthesized an IPN using PU as the flexible phase and PMMA as the rigid phase. The sample with 25 wt% of PU showed the lowest damage with the smallest crack in it due to the flexible nature of the PU and a higher degree of roughness provided by PU. Approximately 60% improvement was observed in quasi-static crack initiation toughness (K_{IC}) by utilizing PU in comparison to neat PMMA [70].

Auad et al. synthesized the IPN out of PU and PMMA. The IPN was synthesized with the sequential method. It was observed from TEM images that increasing the molecular weight of poly(tetramethylene ether) glycol (PTMG) as a diol increases the domain size of the PMMA into the system. An increase in PU domain in samples with a higher percentage of PU was also observed. PU, which cured first, produces the continuous matrix, while the PMMA phase produces round domains into PU. All of the IPN samples possessed good transparency; however, the samples with a lower percentage of PU owned higher transparency. The apparent increase in storage modulus was observed in samples with a higher percentage of PMMA due to the higher stiffness provided by PMMA. The results also suggested that the increase in the molecular weight of diol increases the fracture toughness of the samples due to the rise of the soft segment in PU [10]. Bird et al. synthesized an IPN out of PU and PMMA. Different samples were synthesized with varying percentages of PU and PMMA. The effect of changing the isocyanate from 1,6-diisocyanatohexane (DCH) to toluene diisocyanate (TDI) and adding an inhibitor to the PMMA system was also studied. It was observed that samples with an inhibitor which pushes the IPN to follow the sequential method have better compatibility [23, 71].

The samples with TDI as isocyanate showed a dark yellow-orange color in the final product. However, the samples with DCH produced clear IPNs. The benzene ring in the TDI structure is responsible for the change in color. Rosu et al. indicated that the urethane group's scission and oxidation of the methylene group between the benzene rings caused by UV light in aromatic PU is responsible for the degradation of PU and, therefore, change in surface color [72]. Samples with DCH showed higher stiffness due to the more open structure provided by DCH and, therefore, higher compatibility. The fracture toughness of the samples showed an increase in toughness as the percentage of PU increases, and the brittle failure of the PMMA changed to ductile failure by

adding PU into the system. It was also observed that increasing the molecular weight of the diol increases the molecular weight between crosslinking points and therefore increases the flexibility of the IPNs [23].

The effect of changing the ratio of triol/PTMG was checked in the final properties of the IPNs. More phase separation was observed by increasing the amount of diol into the system. This was expected due to the higher domain size provided by higher flexible chains of PU. Moreover, the samples with a higher amount of diols showed a higher swelling ratio due to the reasons mentioned above. The excellent transparency was observed in all samples with a small decrease in samples with a higher diol amount due to the reason mentioned above [23, 73].

Dadbin et al. checked the effect of changing the molecular weight of the soft segment of PU on the morphology of the simultaneous IPN out of PU and poly(allyl diglycol carbonate) [74].

Babkina et al. suggested that sequential polymerization forms a considerable number of topological engagements, which improve the compatibility of the IPNs based on PU [75]. The results also indicated that following the simultaneous polymerization does not allow PU to be the continuous phase into the system. However, the polymerization of the two systems occurs completely separated from each other [75].

Xiao et al. studied the effect of changing the molecular weight of polyols in different IPNs, one with PU/PMMA and another with PU/ poly(methyl methacrylate-methacrylic acid). The results showed higher mechanical properties and better compatibility for the samples with a lower molecular weight of polyols [76]. The lower interpenetration provided by loose PU chains with higher molecular weight polyols results in higher phase separation [74].

Frisch et al. synthesized the IPN with PU and acrylate copolymer. The glass transition results indicated better interpenetration for full-IPN samples rather than the semi-IPN samples. However,

all of the samples showed some heterogeneous behavior. The full-IPNs exhibited higher enhancement in modulus number and other mechanical properties due to better adhesion between two phases. The sharp drop in elongation of the samples, with 60 wt% of PU, revealed that phase inversion occurred in the system. It was also mentioned that increasing the catalyst increases the rate of polymerization and increases the phase separation. This fact might be due to the lower time provided for monomers to disperse into the polymer network [58].

Akay et al. synthesized various linear and network forms of IPN out of PU/PMMA with simultaneous and sequential polymerization methods. Glass transition temperature of all the samples started to increase by adding more PMMA into the system. However, the samples between 20 to 80 wt% PU showed a flat peak indicating that several transition mechanisms are happening in a wide range of temperatures. The simultaneous IPN offered a uniform surface with no aggregation of PMMA. However, the sequential IPNs showed an ununiform surface, which resulted in premature failure under small elongation. The ultimate tensile strength started to increase by increasing the content of PMMA gradually, and it followed a rapid climb up due to phase inversion occurring into the system [77].

Morin et al. synthesized PU-PMMA interpenetrating polymer networks. Due to the incompatibility of PMMA and PU, the sequential method was utilized to synthesize the IPN. The samples' failure changed from brittle failure to ductile failure by adding more PU into the system. Moreover, enhancement in impact-resistant was observed in samples with a high content of PU [78].

1.2.1.6. Different approaches to enhance the polymers' compatibility in IPNs

Different research groups tried to solve the phase separation between polymers in IPNs. Lee et al. mentioned that the pressure has a positive effect on the compatibility of two polymers in IPNs.

They also compared the phase separation of the full IPN and the semi-IPN with linear PS and PU. The results showed that the highest compatibility belongs to full-IPN, while the semi-IPN with cured PS has the lowest compatibility. This shows the effect of the mobility of the monomers in phase separation of the samples [79].

Another approach to solving the immiscibility of the polymer blends is by utilizing interfacial agents. These agents decrease the disperse phase's domain size by working as a barrier at the interphase region and, therefore, increasing the compatibility between two phases [80].

1.2.1.7. Graft-interpenetrating polymer networks (graft-IPNs)

Other research groups tried to enhance the interfacial bonding, compatibility, and interpenetration of the two polymers and improve the properties of the IPN by utilizing the chemical bonds between the two polymers. As mentioned before, the product is called graft-IPNs.

Fan et al. synthesized the simultaneous IPN with a negligible number of chemical bonds between two polymers out of vinyl ester resin (VER) and PU. The VE was mixed with styrene for manufacturing the final product. However, the morphology difference between full-IPN and Graft-IPN was not studied in this paper [81].

Huang et al. synthesized the graft-IPNs out of PU and nitrolignin with different ratios of NCO/OH. The results showed enhancement in mechanical properties by increasing the proportion of NCO/OH into the system [82]. Sung et al. tried to enhance the properties of the epoxy by utilizing the graft-IPN. The results showed that the polydimethylsiloxane could be used in graft-IPN alongside with multifunctional epoxies to enhance the toughness of the brittle epoxies [83]. A similar research group found out that adding polypropylene glycol as the third component shows better

compatibility compared to epoxy/polypropylene glycol or epoxy/polydimethylsiloxane with better damping properties [84].

Kostrzewa et al. tried to improve the toughness properties of the diglycidyl ether of bisphenol A (DGEBA) with the help of PU. The produced graft-IPN showed excellent compatibility with enhanced properties [85].

Hsieh et al. also tried to improve the properties of the DGEBA by synthesizing graft-IPN out of DGEBA and urethane-modified bismaleimide. The results revealed that IPN with poly(butylene adipate)-based PU has improvement in toughening properties, while the graft-IPN with poly(oxypropylene)-based PU shows enhancement in the fracture energy [86].

Wang et al. tried to modify the properties of the graft-IPN out of PU and DGEBA with the help of short carbon fiber and micro hollow glass bead as reinforcements. The improvement in damping properties, thermal properties, and tensile strength was observed [12]. Lin et al. utilized a similar graft-IPN with Ultra-high-molecular-weight polyethylene fiber to synthesize the novel composites [87].

Pissis et al. studied the chain mobility and miscibility of the semi-IPN out of linear PU and polycyanurate and full sequential IPN out of crosslinked PU and polycyanurate. It was observed that the formation of the chemical interaction between the cyanate group and urethane group of the PU in semi-IPN enhances the miscibility of two polymers and synthesizes the homogenous IPN on 2 nm scale. It was also mentioned that the full IPN with lower content of polycyanurate results in the phase separation in full IPN. Moreover, they observed better miscibility in the semi-IPN system rather than the full IPN system [88].

Sundararajan et al. synthesized graft semi-IPNs out of poly(2-hydroxyethyl methacrylate) and crosslinked poly(ethylene glycol) (PEG) via the simultaneous method for phase change

application. Tetraethyl orthosilicate as a crosslinker is crucial in the system to avoid moisture absorption [89]. It was observed that the crystal size and degree of crystallization were reduced by increasing the amount of 2-hydroxyethyl methacrylate into the system.

1:1:4 molar ratio of tetraethyl orthosilicate: PEG: 2-hydroxyethyl methacrylate was found to have the highest latent enthalpy, 145 J/g. The transition temperature for all of the IPN samples between 50-60ºC and cycling stability make this IPN a good candidate in the military and civil applications such as biomedical and biological carrying systems, heat management of electronics, temperature-controlled greenhouse, and cooling the collector of microwave antenna of ships, and airborne helicopter [89-92].

Jiang et al. synthesized the graft semi-IPN as phase change material (PCM) out of PEG as the functional branch chain with solid-liquid phase changeability and cellulose diacetate as the skeleton to support materials into the system. The chemical bonding was utilized to attach two constituents. However, this novel material was not called IPN in this paper. The enthalpy of melting started to increase in samples with a higher percentage of PEG due to the higher crystallinity provided by PEG and less hindrance coming from the second polymer. Moreover, cellulose diacetate is considered as an impurity for PEG, which destroys the perfection of the crystals into the system and therefore decreases the heat of enthalpy. The enthalpy of transition started to increase by increasing the molecular weight of PEG. However, after reaching the maximum, it started to decrease due to the steric hindrance [93].

Sundaram et al. mixed PU as the elastomeric phase and acrylate-based copolymer (COP) as a stiff phase to synthesize the graft-IPN. High transparency was observed in IPN samples with different percentages of PU:COP demonstrating high compatibility between two polymers. The fracture properties improved by increasing the amount of PU into the system. The graft-IPN with 70 wt%

of PU showed the most significant improvement in fracture due to the higher flexibility coming from PU. Moreover, the samples with higher molecular weight diol showed 6% more improvement in fracture toughness due to the higher mobility provided by longer chains of diols. The brittle crack growth behavior of the samples with a higher percentage of PMMA changed to ductile crack growth in samples with 60 wt% PU due to the reason mentioned above. The improvement in crack initiation toughness was also observed over commercially available materials such as polycarbonate and PMMA [94].

Hsieh et al. synthesized two different kinds of graft-IPNs. The first one was with polyurethanes (PU) based on poly(butylene adipate) and diglycidylether of bisphenol A (epoxy), and the second one was PU based on poly(oxypropy1ene) polyols and epoxy. Simultaneous polymerization was utilized to synthesize the IPNs. The tensile strength improved by adding more PU into the system due to not only better interpenetration but also the grafting between two polymers. However, the IPNs with 20 wt% PU showed the highest tensile strength, and then the strength started to decrease due to the phase inversion happening into the system. IPNs with (PU) based on poly(butylene adipate) into the system exhibited higher tensile strength, perhaps due to the higher compatibility between the two phases. The dynamic mechanical analysis, however, showed two peaks for all of the samples, which indicates that massive phase separation is happening in all of the samples due to the low compatibility between two phases [95].

Similar trends, which were observed for tensile strength, were found for the impact strength and toughening properties of the IPNs. The formation of the micro-separated phase and agglomeration of the rubbery phase is responsible for the drop in toughening properties. Higher heterogeneous samples showed higher fracture energy properties because the phase-separated rubbery domains

stopped the crack from propagation. However, more homogenous IPN was needed for having better impact strength into sample [96].

Bird et al. also tried to increase the miscibility in IPNs by utilizing chemical bonds between two networks. BisGMA and triethyleneglycol dimethacrylate were used as copolymer constituents in IPN. BisGMA has hydroxyl groups in its structure, making it capable of forming chemical bonds between two polymer phases. BisGMA has also structural features similar to polycarbonate (PC), two aromatic rings, which give high stiffness to BisGMA [23]. The graft-IPN with a rougher surface and, therefore, higher ability in absorbing energy was obtained by adding PU into the system. However, the enhancement in fracture toughness was not good enough [23].

Ballestero et al. tried to synthesize graft-IPNs out of PU as a flexible phase and MMA, triethylene glycol dimethacrylate, and styrene; three different rigid polymers, which considered as hard phase. Samples with triethylene glycol dimethacrylate instead of MMA showed higher heterogeneity into the system. The IPN samples with MMA and different molecular weights of diols showed excellent compatibility and interpenetration. Slightly higher fracture toughness was observed in IPNs with a higher molecular weight of diols due to the higher flexibility. Besides, the samples with 70 wt% of copolymer exhibited the most fracture toughness [97].

1.3. Polymers and their high-performance applications for IPNs

1.3.1. Transparent polymeric materials (amorphous glassy polymers)

Amorphous, glassy polymers are one kind of transparent materials with tremendous potential in transparent protective applications. Polymers such as polycarbonate and polyvinyl butyral were already used in laminated glass structures [98]. In transparent, protective polymeric materials, there

are two main groups: acrylates such as Plexiglas® and Acrylite® and polycarbonates such as Lexan® and Tuffak® [23].

Amorphous, glassy polymers are mostly used as the intermediate, backing, and adhesive inter-layers in transparent armors. The mechanical properties of polymers and their chemical, heat, and humidity resistance are the biggest concerns of using them in transparent advanced applications. Improvement in such properties extends the transparent protective applications of amorphous, glassy polymers [99].

1.3.1.1. Poly(methyl methacrylate)

Poly(methyl methacrylate) (PMMA), also called an acrylic polymer, is the polymer that most similar to glass regards to the transparency and wearing resistance [99]. Acrylics, such as the one produced by CYRO Industries, are widely used as enclosures, aircraft, hockey rinks, and other impact resistant applications [100]. Relatively low fracture toughness, high rate of increase in ballistic protection by increasing the thickness, relatively high elastic stiffness, high ultra-violet (UV), chemical, and scratch resistance are desirable properties of PMMA, which make it a good candidate for transparent applications. Moreover, manufacturing complicated shapes are possible with PMMA due to the ease of manufacturing [99]. PMMA is a vinyl polymer, which is synthesized via free radical polymerization. The simple schematic of synthesizing PMMA out of methyl methacrylate is shown in Figure 1.4 [101]. The high flexibility of the PMMA is coming from long carbonyl ester [97]. This material was first synthesized by Röhm and then patented under Plexiglas® by Rohm and Haas Company [102]. It was first used as cockpit canopies in World War II [103]. PMMA is sensitive to scratch, and it is fragile, which restricts its transparent applications. Blending PMMA with other polymers is used to solve their disadvantages. Different research groups tried to improve

the properties of the PMMA by adding polystyrene (PS) [104], ethylene-co-vinyl acetate [105], rubber [106], high-density polyethylene [107], cellulose acetate hydrogen phthalate [108], polyvinyl methyl ether, and poly(vinylidene fluoride) [109].

Lee et al. studied the effect of curing temperature, pressure, and curing in the water on the final properties of the auto polymerized PMMA. The results showed that the curing temperature is the most critical factor in the hardness of the cured PMMA, while pressure does not have a significant effect. They also mentioned that the polymerization in the aqueous environment would help to remove the residual monomers and therefore enhance the hardness of the PMMA [110].

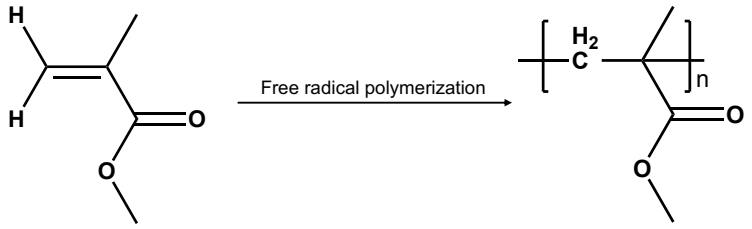

Figure 1.4. Polymerization of PMMA [101].

[Adapted by permission from Elsevier: Elsevier, Sensors and Actuators B: Chemical, 130, 2, 836-841, Copyright 2008]

1.3.1.2. Polycarbonate (PC)

Due to the higher fracture toughness of PC compared to PMMA, it is an excellent choice for the backing layer of the transparent armor systems. PC is stronger and lighter than acrylates. Moreover, PC shows higher impact resistance properties than acrylates [111]. However, the UV, chemical, and scratch-resistance of PC are relatively low, and they are expensive [111]. Therefore, UV-stabilizers and a hard coating are required to increase resistant properties [99, 112]. PC is widely

used in different applications, such as helmets, riot shields, automotive bumpers, and cases for power tools [23]. Figure 1.5 shows the structure of PC [103].

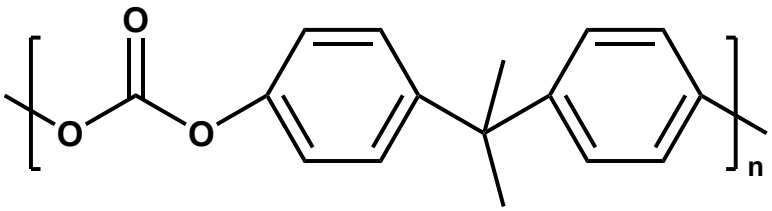

Figure 1.5. Chemical structure of PC.

1.3.1.3. Polystyrene (PS) and vinyl ester resin (VER)

Polystyrene (PS) is an aromatic polymer. The low price of PS makes it applicable in many different commercial applications, such as packing materials, drinking cups, and various plastic models [113]. Bisphenol-A based dimethacrylate resins are considered as high viscosity material. Therefore, vinyl ester resins are mostly synthesized with low viscosity materials such as MMA and styrene [97, 114]. Vinyl ester resin (VER) is a good candidate as a matrix for high-performance composites due to the high thermal and mechanical properties of epoxy resins and the rapid cure properties of unsaturated polyesters resins [115]. These materials are frequently used in military and civilian applications due to their high modulus, low cost, and low weight [97]. However, their brittle nature is their most significant disadvantage. Therefore, enhancing their fracture toughness would broaden their applications. Several techniques for toughening the VER were proposed. Methods include changing the percentage of styrene into the system, utilizing rubber modifiers in order of phase separation upon curing, and using nanostructured thermoplastic fiber mats for interlaminar

toughening [116]. Figure 1.6 shows the structure of bisphenol A bis(2-hydroxy-3-methacryloxypropyl) ether (BisGMA) as an example of VER and styrene.

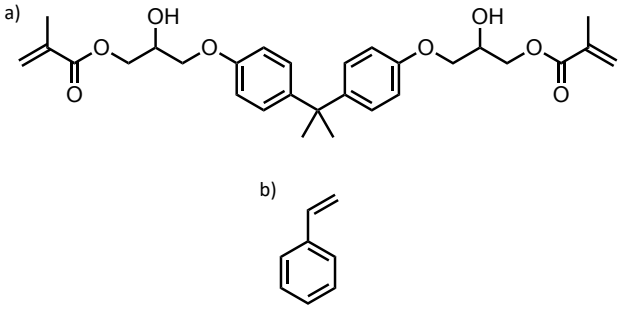

Figure 1.6. Chemical structure of a) BisGMA b) styrene.

1.3.1.4. Polyurethane (PU)

There is a wide range of PU with different structures due to the variation of diisocyanate, diols, and triols, which are used for synthesizing PU. The urethane group is, however, common in all of the different structures of PU, which is shown in Figure 1.7. The issue with PU is the slight tinting in PU structure, which could affect the optical transparency of PU, especially in high thickness [99].

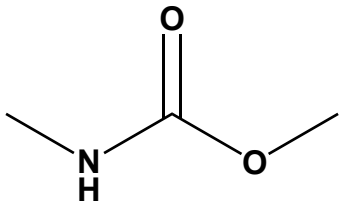

Figure 1.7. Urethane group structure.

Bayer et al. was the first group who discovered polyurethane (PU) in 1937 at I.G. Ferbenindustri, Germany. Bayer synthesized Polyurea out of aliphatic isocyanate and diamine. Then PU was

synthesized out of aliphatic isocyanate and glycol with elastomeric properties [117, 118]. PU was considered a protective material in 1970. However, the lack of transparency was a big challenge against it, in any case. Simula Technologies has since improved the transparency in PU. Research also shows that the PU is better than acrylic polymers and PC regarding impact-resistant properties when an equal weight of all materials is considered [119].

Figure 1.8 shows the general structure of the PU polymers [4]. Due to its structural properties consisting of the soft and hard segment, the properties of the PU is tailorable. PU has a wide range of applications, from rigid like glass to more flexible applications like elastomers such as coatings, adhesives, fibers, and foams [4]. Utilizing the low molecular weight reactants results in stiff and rigid PU due to the higher number of functional groups into the system, while using the high molecular weight reactants is synthesized the flexible PU with a lower number of crosslinking point into the system [117]. Li et al. [120] and Panwiriyarat et al. [121] studied the effect of changing the molecular weight of diols on the PU. Moreover, Wu et al. indicated the application of PU synthesized with polyether and curing agent as golf ball [122]. Although PU has high fracture toughness, however, its lower transparency in comparison to other materials in advanced applications restrict its application [99]. Nowadays, PU coatings demand high glassy properties with improved scratch and corrosion resistant [117, 118].

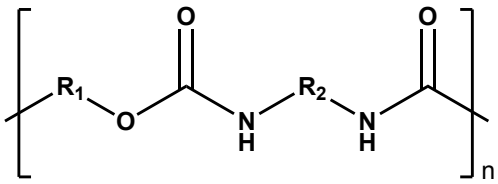

Figure 1.8. Polyurethane structure.

Hydroxyl and isocyanate, and isocyanate and water reactions are the most important reactions in manufacturing polyurethane, which forms polyurethane foams [123]. Polyurethane could be synthesized out of alcohol and isocyanate during the polyaddition polymerization [4]. Polyurethane could also be synthesized by the reaction between PU prepolymer and curing agent. The PU prepolymer is synthesized by the reaction between the polyol and diisocyanate. Diamine or glycol is a curing agent for synthesizing PU. There are also many other methods for synthesizing aliphatic PU [118, 124-129].

The catalysts usually are utilized to increase the rate of step-growth polymerization in PU. Catalysts for synthesizing PU increase the rate of polymerization, balancing the chain propagation and foaming reaction and quickening the completion of the reaction [130]. The catalyst could affect the morphology and structure of PU. For instance, catalysts consisting of organotin compounds dominate the reaction between isocyanate and hydroxyl groups, while tertiary amines speed the reaction between isocyanate and water to produce foams [123]. Triphenyl bismuth (TPB) got attention as one of the major catalysts for synthesizing PU via polyaddition condensation. Dibutyltin dilaurate (DBTDL) and TPB usually are used together as catalysts for PU. Because DBTDL is the primary driving force for step-growth polymerization, it activates TPB as a catalyst while TPB is moderating the polymerization process due to the low catalytic activity. Therefore, the ratio of PU polymerization is adjustable by adjusting the ratio of DBTDL and TPB. It also promotes the isocyanate-hydroxyl reaction against isocyanate-water reaction to avoid foam formation [123, 131]. DBTDL is more likely to participate in hydroxyl reaction than water due to the higher nucleophilic oxygen in the hydroxyl group. Luo et al. found out that the TPB, DBTDL, and DBTDL-TPB complex obtained from a mixture of two catalysts take advantage of high activity of DBTDL, completion cure of TPB, and moderate curing of DBTDL-TPB complex [123].

Segmented polyurethane with soft segments and hard segments attract attention in recent years due to their wide range of general and advanced applications [132]. Segmented PU contains two different segments: hard and soft. The soft segment (SS) are amorphous parts of the PU, while the hard segment (HS) acts as the filler to restrict the mobility of the soft segment. The segmented PU consists of a soft segment typically synthesized by flexible polyether and polyester diols, which gives elasticity to the system, and a hard segment, mostly synthesized by the reaction between a diisocyanate and short diols to bear the loads. The reaction of diol and isocyanate provided hydrogen bonding and therefore provide physical entanglement in the system as well [133, 134]. Segmented PU was first introduced by Cooper and Tobolsky in 1966 [135]. Different variables such as synthesis method, the chain length of the SS, the structure of SS and HS, and symmetry of diisocyanate affect phase mixing and, therefore, the final properties of the PU [117]. Frontini et al. studied the effect of changing the SS:HS ratio on the final properties of thermoplastic PU. 80/20 HS/SS ratio samples showed the highest fracture toughness [136]. Segmented PU also delivers excellent ballistic performance. Figure 1.9 shows the performance of the thick PU layer, which is closing and healing the projectile pathway. Figure 1.9.c shows the schematic of the soft and hard segment of PU, which helps it in ballistic resistance [137].

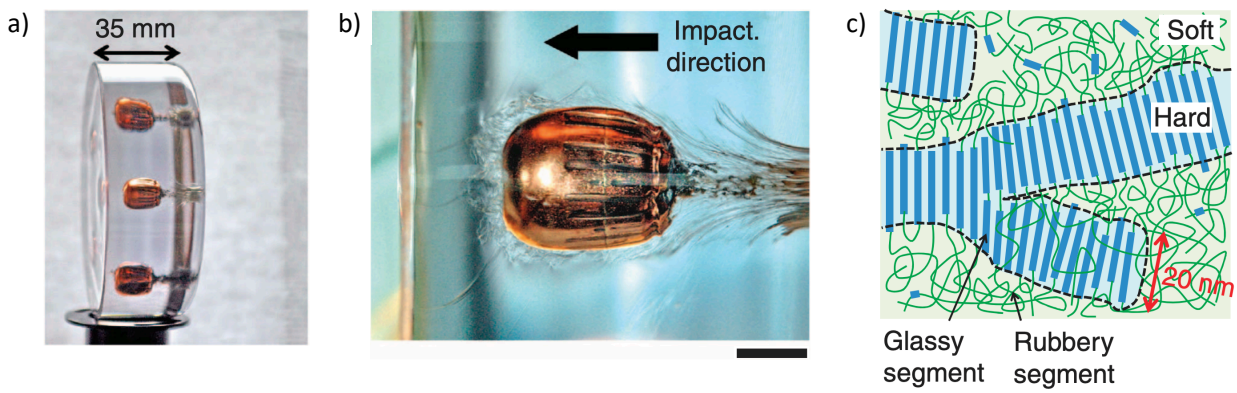

Figure 1.9. Macroscopic ballistic impact tests a) photograph of a polyurethane disc impacted by copper jacketed 9 mm lead projectiles b) magnified view of the projectile and penetration path c) schematic of the nanostructure of soft and hard segments of PU [137].

Lee et al. studied the polystyrene-polydimethylsiloxane diblock-copolymer, which shows the analogous behavior to the soft and hard segment of PU. PS is the glassy polymer, and polydimethylsiloxane is the rubbery polymer. The combination of elastic recovery and flow of the fluid and fragmented layers were mentioned as the reason behind the excellent ballistic properties of the copolymer. As shown in Figure 1.10, the initial structure is highly compressed; therefore, the ordered structure joins the granular phase with a higher disorder. The temperature in this structure is higher than the glass transition of the PS (the hard segment of PU). When the temperature is going higher, the granular structure becomes more homogenous. The combination of highly compressed chains with liquids is highly capable of absorbing the impact energy and therefore enhances the ballistic properties of the materials [137].

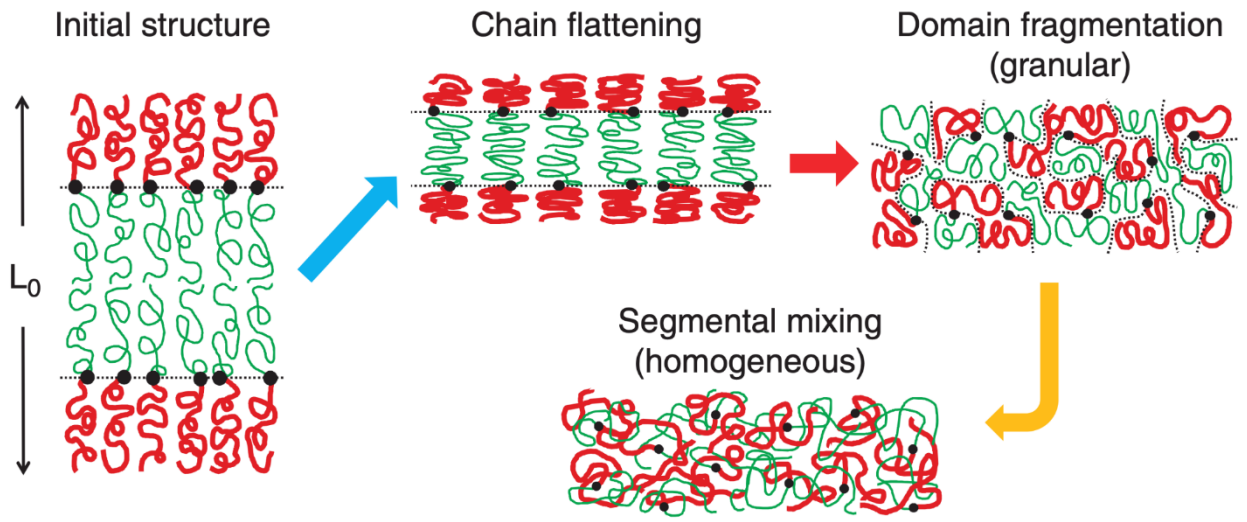

Figure 1.10. Schematic of mechanically driven transformation into a fragmented and segmentally mixed fluid phase in diblock-copolymer [137].

[Reprinted by permission from Springer Nature: Springer Nature, Nature Communications, 3, 1164, Copyright 2012]

Hazell et al. utilized thermosetting polyurethane replacement resin with glass as face and PC as the surrounding material, and they modeled the penetration behavior of bullet into the system. It was observed that the presence of PU in the system restricts the penetration of a bullet. Moreover, their results indicated that using higher thickness glass increases the ballistic performance of the system [138].

O'Sickey et al. [139] synthesized poly(urethane urea) with poly(propylene glycol) soft segments. They observed that while changing the hard segment content does not significantly affect the morphology of the final sample, increasing the soft segments increases the domains and the phase separation into the system.

Schemmer et al. [134] synthesized the thermoplastic polyurethane elastomers with aliphatic hard segments based on novel long-chain diisocyanates. The synthesized PU showed significant elastic improvement with enhanced flexibility and a higher melting point by utilizing short-chain diol in the hard segment. It was observed that an increase in hydrogen bonding due to the short-chain diol decreases the phase separation of the system.

Rinaldi et al. synthesized the transparent poly(urethane urea) with tunable mechanical properties. Increasing the hard domain of PU increases the interdomain spacing and the mechanical properties by increasing the content of the hard segment to become a continuous phase. The glass transition shifted to a higher temperature by decreasing the molecular weight of soft segments due to an increase in urethane groups. It was also observed that the presence of the urethane group enhances the intermolecular interaction and improves the protection properties of the polymer [140].

Many other research groups utilized different kinds of PU for various applications [129, 141].

1.3.2. Polyethylene glycol (PEG)

PEG was reported as one of the most promising PCMs due to the larger melting enthalpy, high resistant corrosion, and wide melting temperature rate [142]. The phase change properties of the PEG is highly dependent on its molecular weight. However, PEG should be sealed into a package to prevent leakage after the solid-liquid phase transition. Sealing PEG increases the price of the final product and restricts PEG's widespread use [113].

Su et al. synthesized the polymeric solid-solid PCM out of PU (PUPCM). PEG was mixed with 4,40-diphenylmethane diisocyanate as the soft segment for synthesizing the prepolymer. Then the prepolymer was mixed with 1,4-butanediol as the chain extender and hard segment for

synthesizing the final PU. The hard segments consist of benzene groups, limiting the mobility of the segment, while the soft segments include flexible chains. The PUPCM showed no shape change even after 100ºC, while the PEG started to lose its shape after passing its melting point. This observation suggests that in PUPCM, only the soft segments go through the solid-liquid phase change, and the hard segment acts as the supporting agent to keep the shape of material [143]. The high transition enthalpy, good thermal stability, and solid-solid phase change behavior of synthesized PUPCM show the considerable potential of PUPCM in many applications [143].

Sari et al. synthesized the polystyrene-graft-PEG6000 copolymers, where styrene is considered a hard phase, and PEG is considered as a soft phase. The synthesized graft copolymer showed a suitable solid-solid phase change range and high latent enthalpy. It was mentioned that the phase change enthalpy could be increased by increasing the amount of PEG in copolymer system. Thermal cycle results indicated the excellent stability of the copolymer after thermal cycling. Besides, the copolymer showed higher thermal conductivity and thermal stability compared to its constituents[90].

Cao et al. synthesized the novel hyperbranched PU out of PEG and hyperbranched polyester as a chain extender for phase change applications. The results indicated that the PU keeps its structure even in temperatures higher than the melting point of PEG. In the PU structure, the hard segments act as the skeleton, supporting the free PEG chains in temperatures higher than their melting point. The results also showed, increasing the percentage of PEG increases the thermal heat enthalpy and transition temperature due to the higher quantity of crystals provided by PEG. However, introducing the hard segment into the system lowers the quality of the crystals and therefore decreases the heat of enthalpy. Wide-angle X-ray diffraction showed that the crystal structure has not changed during the polymerization process, while the crystals are smaller in PU structure than

neat PEG due to the hindrance of the hard segment. The results also indicated that thermal stability, transition temperature, and latent heat are adjustable by changing the components into the system [144]. The synthesized PU shows the tremendous protentional in phase change applications.

Li et al. synthesized a solid-solid phase change material out of PEG10000, 4,40-Diphenylmethane diisocyanate, and pentaerythritol. The results showed that the novel material had a high transition enthalpy and an appropriate transition point. Moreover, the thermal stability of PEG improved by synthesizing the copolymer out of PEG, and the copolymer kept its solid shape after the transition temperature of PEG due to the presence of the hard segment into the system [92]. Another research group synthesized PEG/4,40-Diphenylmethane diisocyanate/polyvinyl alcohol copolymer as PCMs. PEG was used as the heat storage material, while polyvinyl alcohol was used as the supporting material. The copolymer showed high latent heat enthalpy and suitable transition temperature. The decay in latent heat enthalpy was observed due to the restriction of crosslinking points and supporting materials. The copolymer showed better thermal resistance in comparison to neat PEG due to the presence of supporting materials in the system [91].

1.3.3. High-performance applications

1.3.3.1. Transparent protection applications

Glass is considered one of the most conventional materials in transparent applications. Modern glass is an amorphous material, which consists of silica, calcium oxide, and sodium oxide [145]. However, glass is susceptible to shattering, which produces dangerous shards. Tempered glass is one of the alternatives for conventional glasses. Tempered glass is chemically and thermally heated. This process allows for tempered glass to be four times stronger than traditional glass [98].

Moreover, it breaks into smaller pieces compared to the conventional glass while being less sharp [98].

Transparent, impact-absorbing materials can be used as windshields for automobiles or airplanes, protective enclosures for banks, jewelry and historical documents, safety masks, etc. [23]. It also could be used for protecting individuals, such as political leaders or security enforcement [146]. They also are used in the canopies to keep pilots safe in helicopters and fighter jets [147]; moreover, in riots, transparent, high impact absorbance material is required to protect the police [148].

Some of the requirements to be considered for transparent armor include ballistic resistance, optical transparency, low density, and high impact resistance. These materials consist of a hard face for inducing the erosion of a projectile by dispersing the kinetic energy. However, the absorber transfers the kinetic energy to other forms of energy, such as heat [138]. Laminated glass is the traditional material used for armor applications. Laminated glass, known as bullet-proof glass, consists of layered glass with plastics in between them [149]. Harsh blows are required to break through the plastic layers; therefore, these glasses could withstand bullets. However, after a couple of impacts, laminated glasses lose their transparency due to the cracks' propagation into them [23]; moreover, to get desirable penetration resistance, high thickness and high mass of these materials are required. These facts restrict the application of these materials in transparent armor systems [99]. Figure 1.11 shows the two different structures of the traditional laminated glasses [150, 151].

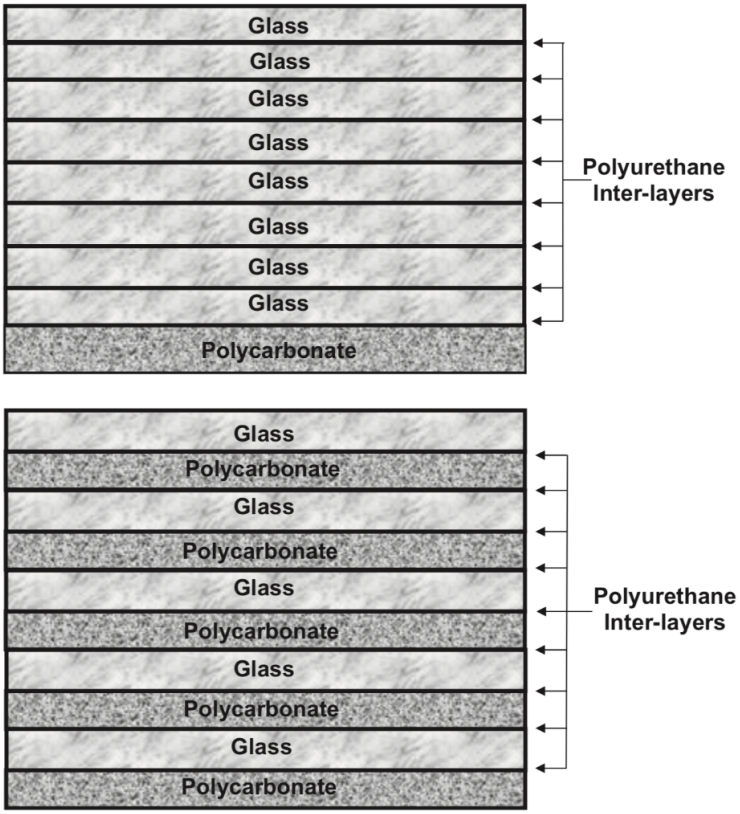

Figure 1.11. The traditional structure of transparent armor systems with laminated glasses [99].

[Reprinted by permission from Elsevier: Elsevier, Materials & Design 34, 808-819, Copyright 2012]

Besides high protection capabilities, the armor vehicles should be as low dense as possible to ensure higher mobility and gas efficiency. Moreover, as all of the transparent parts of the armor vehicles are located on top of the vehicle, it raises the center of gravity for the vehicle, therefore decreases the handling stability of the vehicles [99]. Sands et al. reported that utilizing the traditional materials contribute to 30% of the whole mass of the body armor while only covering 15% of the vehicle [152]. It was also calculated that $5.2 million was spent every month in 2005 to replace damaged windshields and door windows of the High Mobility Multi-purpose Wheeled Vehicle [153].

The more recent transparent armor systems consist of three layers: a hard strike face**,** an energy-absorbing intermediate layer, and a back layer or spall. As shown in Figure 1.12, the strike layer is glass or transparent ceramic. The intermediate layer consists of glass or poly-methyl methacrylate (PMMA), and the back layer is made of polycarbonate (PC). The strike layer usually has high optical transparency, good impact damage resistance, and suitable environmental resistance. The intermediate layer has high optical transparency, good environmental resistance, high kinetic energy absorption, high bending stiffness for supporting the strike face layer, and an excellent ability to localize the damage. The spall, or back layer, also presents high optical transparency and high chemical, environmental, and scratch-resistance. Generally, there is polymeric adhesive inter-layer between these main layers to adhere them together [99]. As shown in Figure 1.12, newer transparent armor systems have lower density and thickness in comparison to traditional systems [153, 154].

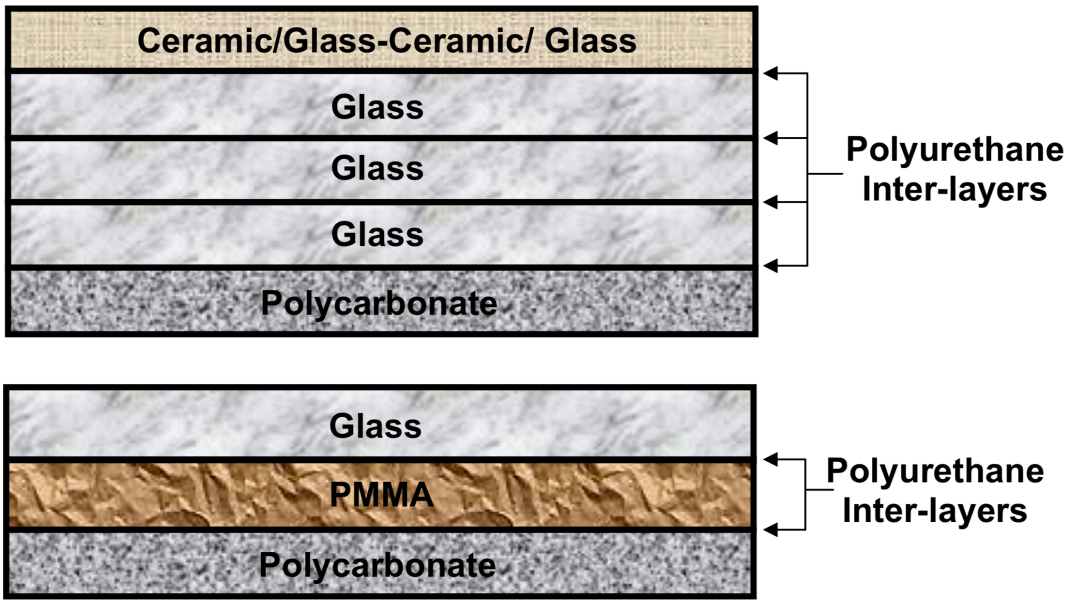

Figure 1.12. Newer structural design for transparent armor systems [99].

Glass (soda-lime glass), glass ceramics, mono-crystalline, and sub-micron grain size polycrystalline ceramics, and thermoplastic and thermosetting amorphous glassy polymers are the most common transparent materials being used in newer armor systems [99, 152, 155-157]. Table 1.2 and 1.3 show a summary of the properties of materials that are used in transparent armors [99].

Table 1.2. Properties of glass and ceramics in transparent armor applications [99].

Property	Units	ALON	Fused silica	Sapphire	Spinel
Density	kg/m^3	3.69×10^3	2.21×10^3	3.97×10^3	3.59×10^3
Areal density (at 1"thickness)	kg/m^2	93.89	55.85	100.97	90.86
Elastic modulus	Pa	334×10^9	70×10^9	344×10^9	260×10^9
Mean flexure strength	Pa	380×10^6	48×10^6	742×10^6	184×10^6
Fracture toughness	$Pa\ m^{1/2}$	2.4×10^6	0.78×10^6	3.0×10^6	1.7×10^6
Knoop hardness	Pa	17.7×10^9	4.5×10^9	19.6×10^9	14.9×10^9
Transmission in visual spectrum	%	82-85	91-92	75-82	-
Maturity of technology		Relatively new technology (becoming commercially viable)	Well established technology	Well established technology	Established, continued advancements
Cost		3–5 times that of glass	Lowest material and processing costs	Higher than ALON™	Lower than ALON™
Manufacturing costs		High due to high processing temperature, proprietary powder, and surface finish requirements	Relatively low due to lower melting temps	High due to high temperature processing and surface finish requirements	Moderate due to surface finish requirements
Bottleneck		Cost and limited dimensions	Limited ballistic protection enhancement	Cost and limited dimensions	Limited dimensions

Commercial availability		Sumert Corp., limited availability	Widely available	Widely available in smaller sizes	In the process of becoming more commercially available
Environmental resistance		Low chemical reactivity and highly scratch resistant		Low chemical reactivity and highly scratch resistant	

[Adapted by permission from Elsevier: Elsevier, Materials & Design 34, 808-819, Copyright 2012]

Table 1.3. Properties of polymeric materials in transparent armor applications [99].

Property	**Units**	**Lexan polycarbonate**	**Stimula polyurethane**	**Plexiglass G PMMA**
Density	kg/m^3	1.2×10^3	1.104×10^3	1.19×10^3
Areal density	kg/m^2	30.27	27.83	30.27
Tensile strength	Pa	66×10^6	62×10^6	72×10^6
Tensile modulus	Pa	2.208×10^9	689×10^6	3.102×10^9
Shear strength	Pa	45×10^6	-	62×10^6
Shear modulus	Pa	1.000×10^9	-	1.151×10^9
Compressive strength	Pa	83×10^6	72×10^6	124×10^6
Compressive modulus	Pa	1.660×10^9	1.241×10^9	3.030×10^9
Flexural strength	Pa	104×10^6	89×10^6	104×10^6
Flexural modulus	Pa	2.586×10^9	2.020×10^9	3.280×10^9
Max operation temperature	°C	121	149	95
Glass transition temperature	°C	145	-75	100
Manufacturing process		Extrusion and injection molding	Casting and liquid injection molding	Casting and later thermoforming
Main limitations		Degradation from chemical, UV-irradiation, scratches, abrasion	Slight tinting in thicker sections	Relatively brittle

[Adapted by permission from Elsevier: Elsevier, Materials & Design 34, 808-819, Copyright 2012]

The higher hardness and young modulus are required in strike face to defeat the projectile at this step. Crystalline ceramics provide exceptional strength, which makes ceramics an excellent choice for strike face layer. Materials like Al_2O_3-based sapphire, sub-micron grain-size polycrystalline transparent ceramics like aluminum-oxy-nitride (ALON™ [158]) and magnesium-aluminate, which is called spinel, are several examples of transparent, crystalline ceramics [159]. Excellent mechanical properties, higher durability and chemical resistance, and an increase in protection in comparison to glasses make ceramics a good option in transparent armor applications. However, their commercial availability, cost, and difficulty in manufacturing limit their applications [23, 97, 99, 160-165].

Like glasses, ceramics are brittle; therefore, ceramics used as strike face layers show extensive cracking after being exposed to the first projectile. These cracks will weaken the properties of the transparent armors and decrease the transparency [97, 166].

The intermediate layer is the section with the most significant quantity used in transparent systems; therefore, a lower density of materials will have a considerable impact on the mass efficiency of the final product. As mentioned before, the intermediate layer provides the back support for the strike layer; therefore, a higher young modulus and larger thickness of the intermediate layer is required for this purpose [99]. Amorphous polymers such as PMMA, glass ceramics, and glass are materials used for the intermediate layer due to their density and young modulus. However, amorphous polymers have the lowest density, making them the best choice for the intermediate layer in transparent systems. For instance, PMMA shows the high fracture toughness with fine-scale fragments, limiting the transparency damage due to a single impact. Improvement in the

mechanical properties of the amorphous polymers makes them excellent materials for transparent armor applications [99].

Spall or backing layer prohibits the strike face and intermediate fragments from entering the cabin. The most important property of the backing layer is ductility. PU and PC, as two amorphous glassy polymers, are the best option for the backing layer due to the highest flexibility among the materials and low density, which is crucial for military vehicles [99].

Overall, excellent transparency, low density, high environmental resistance, and toughness make amorphous glassy polymers a good candidate to be used in different layers of transparent armor systems [97, 99].

1.3.3.2. Polymer matrix composites (PMCs)

Polymer matrix composites have been widely used in different applications due to their relatively low cost, easy processing, and tailorable properties compared to ceramic and metal matrix composites [167]. PMCs can be used in aerospace and military applications, sporting goods, damping applications [12], and biomedical applications [168, 169]. For instance, Sierra Nevada's Dream Chaser space plane and SpaceX's Falcon Heavy's fairing used PMCs in their structure [170]. Polymer matrix Continuous fiber-reinforced composites are ideal for applications where high thermomechanical, mechanical, and low weight is desirable. Specifically, Carbon fiber composites exhibit high specific strength and specific stiffness, with excellent fatigue and creep resistance. Furthermore, PMCs' properties are changeable by changing the polymer and fiber materials and their composition [167].

1.3.3.3. Thermal energy storage (TES)

Phase change materials (PCMs) undergo phase change transformation in the narrow temperature range by utilizing latent heat. These materials should have large latent heat and high thermal conductivity for phase change applications. Phase change materials have attracted much attention in recent years due to their high latent heat, making them usable for thermal energy storage (TES) [171, 172]. Table 1.4 shows the different thermal energy storage applications of PCMs. All of these applications can be separated into either thermal protection or thermal storage. The difference between these two applications is the heat conductivity of the PCM. In thermal protection, it is ideal to have low conductivity, whereas, for thermal storage, high conductivity is required to provide sufficient capacity to dispose of energy quickly [92, 171, 173-180].

Table 1.4. PCM-TES applications [171].

Applications	
Thermal storage of solar energy	Thermal protection of electronic devices (integrated into the appliance)
Passive storage in bioclimatic building/architecture (HDPE + paraffin)	Medical applications: transport of blood, operating tables, hot-cold therapies
Cooling: use of off-peak rates and reduction of installed power, ice bank	Cooling of engines (electric and combustion)
Heating and sanitary hot water: using off-peak rate and adapting unloading curves	Thermal comfort in vehicles
Safety: temperature maintenance in rooms with computers or electrical appliances	Softening of exothermic temperature peaks in chemical reactions
Thermal protection of food	Spacecraft thermal systems
Food agroindustry, wine, milk products (absorbing peaks in demand), greenhouses	Solar power plants
Insulation clothes	

Traditional PCMs, such as hydrated salts, fatty acids [181], fatty alcohols [182], fatty hydrocarbons [183], paraffin waxes [184], and polyethylene glycol (PEG), have problems with leakage [89, 185]. Therefore, new methods such as utilizing microcapsules [186], and copolymerization were used to overcome the leakage problem. PCMs could be classified into three different groups based on their transition states: solid-solid PCMs, solid-liquid PCMs, and liquid–gas PCMs. In the solid-solid phase change, the crystalline structure phase changes into another crystalline structure or an amorphous phase to save the latent heat. Solid-solid PCMs consist of organic, inorganic, and polymer-based PCMs. The most important advantages of polymeric solid-solid PCMs in comparison to the traditional PCMs are no leakage, no liquid or gas formation, minimal volume change, longer service life, corrosion resistance, no need to be sealed, and the simple and cost-effective fabrication process [90, 91, 144, 187]. There are two different kinds of polymeric solid-solid PCMs. One is the mixture of a PCM with another compound with a higher melting point as supporting material. Therefore, as long as the mixture temperature does not reach the melting point of supporting material, the mixture keeps its shape, although the PCM phase changes from solid to liquid to store the energy. This kind is called shape stabilized PCMs [188]. The most critical disadvantageous of this material is the phase segregation during the heating and cooling cycles [90]. The other type of PCM is synthesized by grafting or copolymerizing two different polymers. The high transition temperature, low transition enthalpy, and thermal instability are reported as the defects of polymeric solid-solid PCMs [143]. Therefore, semi-IPN composites are utilized for TES applications due to their excellent stability. Additionally, The superposition phase change effect of two phases provides high heat enthalpy for the system [49].

1.4. Research objectives

The current research is focused on synthesizing novel graft-interpenetrating polymer networks for high-performance applications. Grafting two polymers, choice of monomers, the proportion of polymers and their precursors, curing profile, and different types of IPNs have been studied in the following objectives. The stress relaxation behavior of the synthesized graft-IPNs was also simulated. Acrylic-polyurethane based graft-IPNs could be excellent alternatives for traditional materials in high-performance applications discussed in these objectives.

Chapter 2: High-fracture-toughness acrylic-polyurethane-based graft-interpenetrating polymer networks for transparent applications

In this chapter, the phase separation between two phases of IPN was addressed by generating chemical bonds between two polymers to synthesize graft-IPNs. PU was used as the elastomeric phase to obtain high impact resistant IPN. The acrylic copolymer based on bis(2-hydroxy-3-methacryloxypropyl) ether (BisGMA) resin and styrene was used as a rigid phase to provide high stiffness into the system. BisGMA was utilized due to its secondary hydroxyl groups, which react with isocyanate groups of PU precursors and generate chemical bonds between two polymers. The effect of changing the percentage of BisGMA:Styrene on phase separation of the final IPNs was studied to minimize the phase separation between two polymers. Synthesizing graft-IPNs with excellent transparency and fracture toughness was the goal of this objective.

Chapter 3: Mechanical performance of vinyl ester-polyurethane interpenetrating polymer network composites

In the third chapter, the graft-IPN matrix with PU and acrylic copolymer was utilized in carbon fiber reinforced composite. A commercial vinyl ester with extra styrene was used to synthesize the IPN matrix. After evaluating different manufacturing methods, a simple hand layup process was utilized for manufacturing composite. The mechanical and thermomechanical behavior of the IPN matrix composite was studied. Manufacturing IPN matrix composite with excellent mechanical and thermomechanical properties was targeted in this objective.

Chapter 4: Flexible acrylic-polyurethane based graft-interpenetrating polymer networks for high impact structural applications

In chapter 4, to broaden the application of novel graft-IPN, which was synthesized in the second chapter, the PU to copolymer composition was changed to obtain the graft-IPN with higher flexibility and elastomeric properties. Moreover, methyl methacrylate (MMA) was used to substitute styrene in the system to check the effect of two different monomers in final properties and compatibility in IPN. Synthesizing flexible IPNs with broad thermo-mechanical properties, excellent transparency, and impact resistance with different PU to copolymer composition was the target of the current objective.

Chapter 5: Mechanical characterization and modeling stress relaxation behavior of acrylic-polyurethane-based graft-interpenetrating polymer networks

In chapter 5, flexure and tension stress relaxation behavior of the graft-IPNs with different PU to copolymer compositions and BisGMA to styrene compositions were studied and modeled using a Generalized Maxwell model and the Prony series in a three-dimensional setting. MATLAB was utilized to find Prony series coefficients by the curve-fitting tool. Numbers obtained from

MATLAB were plugged into to FEniCS, an open-source finite-element framework, to finish the modeling. Generating the model with good overlap with experimental stress-relaxation behavior of IPNs was the goal of this objective.

Chapter 6: Acrylic-polyurethane based graft semi-interpenetrating polymer networks for thermal energy storage

In the final chapter, the graft semi-IPN was synthesized based on linear PU with PEG8000 for thermal energy storage applications. Acrylic copolymer with BisGMA and MMA was used as the second polymer. Utilizing acrylic copolymer in IPN structure destroys the perfection of crystallization in PEG and therefore decreases PEG phase change properties. However, the presence of the acrylic copolymer is required because copolymer acts as a skeleton to support PEG-based PU and thus avoids leakage in the system. Synthesizing PEG-based PU IPN with promising thermal properties and shape and cycling stability was the goal for this objective.

References

1. Stevens, M. P., *Polymer chemistry*. Oxford university press New York: 1990; Vol. 2.

2. Ou, R.; Zhao, H.; Sui, S.; Song, Y.; Wang, Q., Reinforcing effects of Kevlar fiber on the mechanical properties of wood-flour/high-density-polyethylene composites. *Composites Part A: Applied Science and Manufacturing* **2010,** *41* (9), 1272-1278.

3. Allcock, H. R., Inorganic—Organic Polymers. *Advanced Materials* **1994,** *6* (2), 106-115.

4. Petrovic, Z. S., *Handbook of Polymer Synthesis, Characterization, Processing*. A John Wiley & Sons, Inc.: 2013.

5. Gallucci, R. R.; Kernick III, W. A.; Sanner, M. A.; Singh, R. K., Flame resistant polymer blends. Google Patents: 2010.

6. Lin, P.; Zhang, R.; Wang, X.; Cai, M.; Yang, J.; Yu, B.; Zhou, F., Articular Cartilage Inspired Bilayer Tough Hydrogel Prepared by Interfacial Modulated Polymerization Showing Excellent Combination of High Load-Bearing and Low Friction Performance. *ACS Macro Letters* **2016,** *5* (11), 1191-1195.

7. Odian, G., *Principles of polymerization*. John Wiley & Sons, Inc.: Hoboken, New Jersey, 2004.

8. Sintzel, M. B.; Merkli, A.; Tabatabay, C.; Gurny, R., Influence of Irradiation Sterilization on Polymers Used as Drug Carriers—A Review. *Drug Development and Industrial Pharmacy* **1997,** *23* (9), 857-878.

9. Matsuoka, R.; Naito, K.; Irie, T.; Kondo, K. In *Evaluation methods of polymer insulators under contaminated conditions*, IEEE/PES Transmission and Distribution Conference and Exhibition, 6-10 Oct. 2002; 2002; pp 2197-2202 vol.3.

10. Alizadeh, N.; Bird, S. A.; Mendez, R. B.; Jajam, K. C.; Alexander, A. C.; Tippur, H. V.; Auad, M. L., Chapter 11 - Synthesis and Characterization of High Performance Interpenetrating Polymer Networks With Polyurethane and Poly(methyl methacrylate). In *Unsaturated Polyester Resins*, Thomas, S.; Hosur, M.; Chirayil, C. J., Eds. Elsevier: 2019; pp 243-255.

11. Wang, X.; Jiang, M.; Zhou, Z.; Gou, J.; Hui, D., 3D printing of polymer matrix composites: A review and prospective. *Composites Part B: Engineering* **2017,** *110*, 442-458.

12. Wang, T. M.; Chen, S. B.; Wang, Q. H.; Pei, X. Q., Damping analysis of polyurethane/epoxy graft interpenetrating polymer network composites filled with short carbon fiber and micro hollow glass bead. *Materials & Design* **2010,** *31* (8), 3810-3815.

13. Askarbekov, R.; Herak, D.; Mizera, C. In *Mechanical Behavior of Rubber Samples Under Relaxation*, Proceedings of the International Scientific Conference, 2016.

14. Utracki, L. A.; Mukhopadhyay, P.; Gupta, R. K., Polymer Blends: Introduction. In *Polymer Blends Handbook*, Utracki, L. A.; Wilkie, C. A., Eds. Springer Netherlands: Dordrecht, 2014; pp 3-170.

15. BOUDENNE, A.; IBOS, L.; CANDAU, Y., *Handbook of Multiphase Polymer Systems*. A John Wiley & Sons, Ltd., Publication: 2011.

16. Sperling, L. H.; Mishra, V., The current status of interpenetrating polymer networks. *Polymers for Advanced Technologies* **1996,** *7* (4), 197-208.

17. Sperling, L. H., Interpenetrating polymer networks and related materials. **1977,** *12* (1), 141-180.

18. Sperling, L. H., *Interpenetrating Polymer Networks and Related Materials*. Plenum Press,: New York, 1981; Vol. 12 (1).

19. Sperling, L. H., Interpenetrating Polymer Networks: An Overview. In *Interpenetrating Polymer Networks*, American Chemical Society: 1994; Vol. 239, pp 3-38.

20. Li, B.; Bi, X.; Zhang, D.; Whang, F., Forced Compatibility and Mutual Entanglements in Poly (Vinyl Acetate)/Poly (Methyl Acrylate) IPNs. *Technomic Publishing Company, Advances in Interpenetrating Polymer Networks.* **1989,** *1*, 203-220.

21. Lv, X.; Huang, Z.; Huang, C.; Shi, M.; Gao, G.; Gao, Q., Damping properties and the morphology analysis of the polyurethane/epoxy continuous gradient IPN materials. *Composites Part B: Engineering* **2016,** *88*, 139-149.

22. Anslyn, E. V.; Dougherty, D. A.; Sausalito, C. U. S., *Modern physical organic chemistry*. University Science Books www.uscibooks.com: CA, 2006.

23. Bird, S. A. Interpenetrating Polymer Networks with Polyurethane and Methacrylate-based Polymers. Auburn University, Auburn, AL, 2013.

24. George, S. C.; Thomas, S., *Manufacturing of Multiphase Polymeric Systems, in Handbook of Multiphase Polymer Systems*. John Wiley & Sons Ltd.: 2011.

25. Sheu, H. R.; El-Aasser, M. S.; Vanderhoff, J. W., Phase separation in polystyrene latex interpenetrating polymer networks. *Journal of Polymer Science Part A: Polymer Chemistry* **1990,** *28* (3), 629-651.

26. Dave, V. J.; Patel, H. S., Synthesis and characterization of interpenetrating polymer networks from transesterified castor oil based polyurethane and polystyrene. *Journal of Saudi Chemical Society* **2017,** *21* (1), 18-24.

27. Qin, C.-L.; Cai, W.-M.; Cai, J.; Tang, D.-Y.; Zhang, J.-S.; Qin, M., Damping properties and morphology of polyurethane/vinyl ester resin interpenetrating polymer network. *Materials Chemistry and Physics* **2004,** *85* (2), 402-409.

28. Thomas, D. A.; Sperling, L. H., Interpenetrating Polymer Networks, in Polymer Blends. Academic Press, Inc.: 1978

29. Shin, J.; Choi, K.; Shiko, S.; Choi, H.; Bae, D., Mechanical damping behavior of Al/C60-fullerene composites with supersaturated Al–C phases. *Composites Part B: Engineering* **2015,** *77*, 194-198.

30. Mita, I.; Akiyama, S., Macromolecular Design of Polymeric Materials. In *PLASTICS ENGINEERING-NEW YORK*, Marcel Dekker, Inc.: 1997; pp 393-406.

31. Kim, S. C.; Klempner, D.; Frisch, K. S.; Radigan, W.; Frisch, H. L., Polyurethane Interpenetrating Polymer Networks. I. Synthesis and Morphology of Polyurethane-Poly(methyl methacrylate) Interpenetrating Polymer Networks. *Macromolecules* **1976,** *9* (2), 258-263.

32. Goodyear, C. Improvement in Indiarubber Fabric. 3633, 1844.

33. Aylsworth, J. W. PLASTIC COMPOSITION. 1,111,284, 1914.

34. Staudinger, H., Über Polymerisation. *Berichte der deutschen chemischen Gesellschaft (A and B Series)* **1920,** *53* (6), 1073-1085.

35. Ostromislensky, I. Process for Manufacturing Plastic Compositions and Products Obtained Thereby. 1,613,673, 1927.

36. Dunn, A. S.; Stead, B. D.; Melville, H. W., The synthesis of block copolymers of styrene and methyl methacrylate. *Transactions of the Faraday Society* **1954,** *50* (0), 279-290.

37. Bamford, C. H.; Dyson, R. W.; Eastmond, G. C., Studies in network formation. *Journal of Polymer Science Part C: Polymer Symposia* **1967,** *16* (4), 2425-2434.

38. Sperling, L. H.; Arnts, R. R., Simultaneous interpenetrating networks. *Journal of Applied Polymer Science* **1971,** *15* (9), 2317-2319.

39. Amos, L.; McCurdy, L.; McIntire, O. R. 2,694, 692, 1954.

40. Lundsted, L. G.; Ile, G.; Mich Polyoxyalkylene Compounds. 2,674,619, 1954.

41. Peter, S. J. J.; Malcolm, H. H. Process for the Production of Strain-Free Masses From CrossLinked Styrene-Type polymers. 2,539,377, 1951.

42. Millar, J. R., 263. Interpenetrating polymer networks. Styrene–divinylbenzene copolymers with two and three interpenetrating networks, and their sulphonates. *Journal of the Chemical Society (Resumed)* **1960,** (0), 1311-1317.

43. Frisch, H. L.; Klempner, D.; Frisch, K. C., A topologically interpenetrating elastomeric network. *Journal of Polymer Science Part B: Polymer Letters* **1969,** *7* (11), 775-779.

44. Sperling, L. H.; Friedman, D. W., Synthesis and mechanical behavior of interpenetrating polymer networks: Poly(ethyl acrylate) and polystyrene. *Journal of Polymer Science Part A-2: Polymer Physics* **1969,** *7* (2), 425-427.

45. Peterson, A. M.; Kotthapalli, H.; Rahmathullah, M. A. M.; Palmese, G. R., Investigation of interpenetrating polymer networks for self-healing applications. *Composites Science and Technology* **2012,** *72* (2), 330-336.

46. Jeevananda, T.; Siddaramaiah, Synthesis and characterization of polyaniline filled PU/PMMA interpenetrating polymer networks. *European Polymer Journal* **2003,** *39* (3), 569-578.

47. Ha, S. M.; Yuan, W.; Pei, Q.; Pelrine, R.; Stanford, S., Interpenetrating Polymer Networks for High-Performance Electroelastomer Artificial Muscles. *Advanced Materials* **2006,** *18* (7), 887-891.

48. Vallittu, P. K., Interpenetrating Polymer Networks (IPNs) in Dental Polymers and Composites. *Journal of Adhesion Science and Technology* **2009,** *23* (7-8), 961-972.

49. Zhang, Y.; Xiu, J.; Tang, B.; Lu, R.; Zhang, S., Novel semi-interpenetrating network structural phase change composites with high phase change enthalpy. *AIChE Journal* **2018,** *64* (2), 688-696.

50. Qadri, M. F.; Malviya, R.; Sharma, P. K., Biomedical Applications of Interpenetrating Polymer Network System. *Open Pharmaceutical Sciences Journal* **2015,** *2* (1), 21-30.

51. Sperling, L.; Thomas, D. Vibration or sound damping coating for vibratory structures. 3,833,404, Sept. 3, 1974.

52. Solak, T. A.; Duke, J. T. Polymerizates of olefinic nitriles and diene-nitrile rubbers. 3,426,102, Feb. 4, 1969.

53. Bruno, V. Impact-resistant plastic compositions comprising a styrene polymer and a cross-linked acrylic acid ester polymer, and process for preparing same. 3,055,859, Sept. 25, 1962.

54. Sweeney, W. T.; Paffenbarger, G. C.; Beall, J. R., Acrylic Resins for Dentures. *The Journal of the American Dental Association* **1942,** *29* (1), 7-33.

55. Bowen, R. L., Properties of a silica-reinforced polymer for dental restorations. *The Journal of the American Dental Association* **1963,** *66* (1), 57-64.

56. Sperling, L. H., *Polymeric multicomponent materials : an introduction*. Wiley: New York, 1998; p xviii, 397 p.

57. Szilágyi, A.; Zrínyi, M., Temperature induced phase transition of interpenetrating polymer networks composed of poly(vinyl alcohol) and copolymers of N-isopropylacrylamide with acrylamide or 2-acrylamido-2-methylpropyl-sulfonic acid. *Polymer* **2005,** *46* (23), 10011-10016.

58. Frisch, K. C.; Klempner, D.; Frisch, H. L., Recent advances in interpenetrating polymer networks. *Polymer Engineering & Science* **1982,** *22* (17), 1143-1152.

59. Vlad, S.; Vlad, A.; Oprea, S., Interpenetrating polymer networks based on polyurethane and polysiloxane. *European Polymer Journal* **2002,** *38* (4), 829-835.

60. Mathew, A. P.; Packirisamy, S.; Thomas, S., Studies on the thermal stability of natural rubber/polystyrene interpenetrating polymer networks: thermogravimetric analysis. *Polymer Degradation and Stability* **2001,** *72* (3), 423-439.

61. Kim, S. C.; Klempner, D.; Frisch, K. C.; Frisch, H. L., Polyurethane Interpenetrating Polymer Networks. II. Density and Glass Transition Behavior of Polyurethane-Poly(methyl methacrylate) and Polyurethane-Polystyrene IPN's. *Macromolecules* **1976,** *9* (2), 263-266.

62. Kim, S. C.; Klempner, D.; Frisch, K. C.; Frisch, H. L., Polyurethane Interpenetrating Polymer Networks. 4. Volume Resistivity Behavior of Polyurethane-Poly(methyl methacrylate) Interpenetrating Polymer Networks. *Macromolecules* **1977,** *10* (6), 1191-1193.

63. Kim, S. C.; Klempner, D.; Frisch, K. C.; Frisch, H. L., Polyurethane Interpenetrating Polymer Networks .3. Viscoelastic Properties of Polyurethane-Poly(Methyl Methacrylate) Interpenetrating Polymer Networks. *Macromolecules* **1977,** *10* (6), 1187-1191.

64. Allen, G.; Bowden, M. J.; Blundell, D. J.; Hutchinson, F. G.; Jeffs, G. M.; Vyvoda, J., Composites formed by interstitial polymerization of vinyl monomers in polyurethane elastomers: 1. Preparation and mechanical properties of methyl methacrylate based composites. *Polymer* **1973,** *14* (12), 597-603.

65. Kim, S. C.; Klempner, D.; Frisch, K. C.; Frisch, H. L., Polyurethane interpenetrating polymer networks. V. Engineering properties of polyurethane–poly(methyl methacrylate) IPN's. *Journal of Applied Polymer Science* **1977,** *21* (5), 1289-1295.

66. Ajithkumar, S.; Patel, N. K.; Kansara, S. S., Sorption and diffusion of organic solvents through interpenetrating polymer networks (IPNs) based on polyurethane and unsaturated polyester. *European Polymer Journal* **2000,** *36* (11), 2387-2393.

67. Chen, C. H.; Chen, W. J.; Chen, M. H.; Li, Y. M., Simultaneous full-interpenetrating polymer networks of blocked polyurethane and vinyl ester Part I. Synthesis, swelling ratio, thermal properties and morphology. *Polymer* **2000,** *41* (22), 7961-7967.

68. Kinloch, A. J.; Guild, F. J., Predictive modeling of the properties and toughness of rubber-toughened epoxies. *Advances in Chemistry Series* **1997,** (252).

69. Huang, Y.; Kinloch, A. J.; Hunston, D. L.; Riew, C. K. In *Mechanisms of toughening thermoset resins*, United States, 1993-12-31; American Chemical Society, Washington, DC (United States): United States, 1993.

70. Jajam, K. C.; Bird, S. A.; Auad, M. L.; Tippur, H. V., Tensile, fracture and impact behavior of transparent Interpenetrating Polymer Networks with polyurethane-poly(methyl methacrylate). *Polym. Test* **2013,** *32* (5), 889-900.

71. Bird, S. A.; Clary, D.; Jajam, K. C.; Tippur, H. V.; Auad, M. L., Synthesis and characterization of high performance, transparent interpenetrating polymer networks with polyurethane and poly(methyl methacrylate). *Polymer Engineering & Science* **2013,** *53* (4), 716-723.

72. Rosu, D.; Rosu, L.; Cascaval, C. N., IR-change and yellowing of polyurethane as a result of UV irradiation. *Polymer Degradation and Stability* **2009,** *94* (4), 591-596.

73. Brydson, J.A*., Plastics Materials. 7 ed. 1999: Butterworth-Heinemann.*

74. Dadbin, S.; Frounchi, M., Effects of polyurethane soft segment and crosslink density on the morphology and mechanical properties of polyurethane/poly(allyl diglycol carbonate) simultaneous interpenetrating polymer networks. *Journal of Applied Polymer Science* **2003,** *89* (6), 1583-1595.

75. Babkina, N. V.; Lipatov, Y. S.; Alekseeva, T. T.; Sorochinskaya, L. A.; Datsyuk, Y. I., Effect of spatial constraints on phase separation during polymerization in sequential semi-interpenetrating polymer networks. *Polymer Science Series A* **2008,** *50* (7), 798-807.

76. Xiao, H. X.; Frisch, K. C.; Frisch, H. L., Interpenetrating polymer networks from polyurethanes and methacrylate polymers. I. Effect of molecular weight of polyols and NCO/OH ratio of urethane prepolymers on properties and morphology of IPNs. *Journal of Polymer Science: Polymer Chemistry Edition* **1983,** *21* (8), 2547-2557.

77. Akay, M.; Rollins, S. N., Polyurethane-poly(methyl methacrylate) interpenetrating polymer networks. *Polymer* **1993,** *34* (9), 1865-1873.

78. Morin, A.; Djomo, H.; Meyer, G. C., Polyurethane-poly(methyl methacrylate) interpenetrating polymer networks: Some mechanical properties. *Polymer Engineering & Science* **1983,** *23* (7), 394-398.

79. Lee, D. S.; Kim, S. C., Polyurethane interpenetrating polymer networks (IPN's) synthesized under high pressure. 3. Morphology and Tg behavior of polyurethane-polystyrene semi-IPN's and linear blends. *Macromolecules* **1984,** *17* (11), 2222-2227.

80. Cerclé, C.; Favis, B. D., Generalizing interfacial modification in polymer blends. *Polymer* **2012,** *53* (20), 4338-4343.

81. Fan, L. H.; Hu, C. P.; Ying, S. K., Thermal analysis during the formation of polyurethane and vinyl ester resin interpenetrating polymer networks. *Polymer* **1996,** *37* (6), 975-981.

82. Huang, J.; Zhang, L., Effects of NCO/OH molar ratio on structure and properties of graft-interpenetrating polymer networks from polyurethane and nitrolignin. *Polymer* **2002,** *43* (8), 2287-2294.

83. Sung, P.-H.; Lin, C.-Y., Polysiloxane modified epoxy polymer networks—I. Graft interpenetrating polymeric networks. *European Polymer Journal* **1997,** *33* (6), 903-906.

84. Sung, P.-H.; Lin, C.-Y., Polysiloxane modified epoxy polymer network—ii. dynamic mechanical behavior of multicomponent graft-ipns (epoxy/polysiloxane/polypropylene glycol). *European Polymer Journal* **1997,** *33* (3), 231-233.

85. Kostrzewa, M.; Hausnerova, B.; Bakar, M.; Siwek, E., Effects of various polyurethanes on the mechanical and structural properties of an epoxy resin. *Journal of Applied Polymer Science* **2011,** *119* (5), 2925-2932.

86. Hsieh, K. H.; Han, J. L.; Yu, C. T.; Fu, S. C., Graft interpenetrating polymer networks of urethane-modified bismaleimide and epoxy (I): mechanical behavior and morphology. *Polymer* **2001,** *42* (6), 2491-2500.

87. Lin, S. P.; Han, J. L.; Yeh, J. T.; Chang, F. C.; Hsieh, K. H., Composites of UHMWPE fiber reinforced PU/epoxy grafted interpenetrating polymer networks. *European Polymer Journal* **2007,** *43* (3), 996-1008.

88. Pissis, P.; Georgoussis, G.; Bershtein, V. A.; Neagu, E.; Fainleib, A. M., Dielectric studies in homogeneous and heterogeneous polyurethane/polycyanurate interpenetrating polymer networks. *Journal of Non-Crystalline Solids* **2002,** *305* (1), 150-158.

89. Sundararajan, S.; Samui, A. B.; Kulkarni, P. S., Interpenetrating phase change polymer networks based on crosslinked polyethylene glycol and poly(hydroxyethyl methacrylate). *Solar Energy Materials and Solar Cells* **2016,** *149*, 266-274.

90. Sarı, A.; Alkan, C.; Biçer, A., Synthesis and thermal properties of polystyrene-graft-PEG copolymers as new kinds of solid–solid phase change materials for thermal energy storage. *Materials Chemistry and Physics* **2012,** *133* (1), 87-94.

91. Zhou, X.-M., Preparation and characterization of PEG/MDI/PVA copolymer as solid–solid phase change heat storage material. *Journal of Applied Polymer Science* **2009,** *113* (3), 2041-2045.

92. Li, W.-D.; Ding, E.-Y., Preparation and characterization of cross-linking PEG/MDI/PE copolymer as solid–solid phase change heat storage material. *Solar Energy Materials and Solar Cells* **2007,** *91* (9), 764-768.

93. Jiang, Y.; Ding, E.; Li, G., Study on transition characteristics of PEG/CDA solid–solid phase change materials. *Polymer* **2002,** *43* (1), 117-122.

94. Sundaram, B. M.; Mendez, R. B.; Auad, M. L.; Tippur, H. V., Quasi-static and dynamic mechanical behavior of transparent graft-interpenetrating polymer networks (graft-IPNs). *Polymer Testing* **2018,** *70*, 348-362.

95. Hsieh, K. H.; Han, J. L., Graft interpenetrating polymer networks of polyurethane and epoxy. I. mechanical behavior. *Journal of Polymer Science Part B: Polymer Physics* **1990,** *28* (5), 623-630.

96. Hsieh, K. H.; Han, J. L., Graft interpenetrating polymer networks of polyurethane and epoxy. II. Toughening mechanism. *Journal of Polymer Science Part B: Polymer Physics* **1990,** *28* (6), 783-794.

97. Méndez, R. B. Sequential graft-Interpenetrating polymer networks based on polyurethane and acrylic/ester copolymers. Auburn University, Auburn, AL, 2015.

98. Girard, J. E., *Criminalistics: forensic science, crime, and terrorism.* 2 ed.; Jones & Bartlett Learning. 3.: 2011.

99. Grujicic, M.; Bell, W. C.; Pandurangan, B., Design and material selection guidelines and strategies for transparent armor systems. *Materials & Design* **2012,** *34*, 808-819.

100. Plunkett, J.W., Plunkett's Chemicals, Coatings, & Plastics Industry Almanac. 2005, Houston: Plunkett Research Ltd.

101. Sun, Y.; Satyanarayan, M. V. D.; Nguyen, N. T.; Kwok, Y. C., Continuous flow polymerase chain reaction using a hybrid PMMA-PC microchip with improved heat tolerance. *Sensors and Actuators B: Chemical* **2008,** *130* (2), 836-841.

102. Cohen, S.R. and M.G. Rubin, ArteFill, in Augmentation Fillers, N.S. Sadick, Editor. 2010, Cambridge University Press. p. 54.

103. Ashby, M.; Johnson, K., *Materials and Design: The Art and Science of Material Selection in Product Design. third edition*. Elsevier: 2014.

104. Guo, S.; Ait-Kadi, A.; Bousmina, M., A modified model predictions and experimental results of weld-line strength in injection molded PS/PMMA blends. *Polymer* **2004,** *45* (9), 2911-2920.

105. Bernini, U.; Malinconico, M.; Martuscelli, E.; Mormile, P.; Novellino, A.; Russo, P.; Volpe, M. G., Ultra-tough synthetic glasses made by reactive blending of PMMA and EVA rubbers: opto-thermal characterization. *Journal of Materials Processing Technology* **1995,** *55* (3), 224-228.

106. Cangialosi, D.; Fuochi, P.; Lavalle, M.; McGrail, P. T.; Emmerson, G.; Spadaro, G., Electron beam induced polymerisation of MMA in the presence of rubber: a novel process to produce tough materials. *Radiation Physics and Chemistry* **2002,** *63* (1), 63-68.

107. Giancola, G.; Lehman, R. L.; Idol, J. D., Melt processing and domain morphology of PMMA/HDPE polymer blends prepared from powder precursors. *Powder Technology* **2012,** *218*, 18-22.

108. Vijayalakshmi Rao, R.; Ashokan, P. V.; Shridhar, M. H., Study of cellulose acetate hydrogen phthalate(CAP)-poly methyl methacrylate (PMMA) blends by thermogravimetric analysis. *Polymer Degradation and Stability* **2000,** *70* (1), 11-16.

109. Sasaki, H.; Kanti Bala, P.; Yoshida, H.; Ito, E., Miscibility of PVDF/PMMA blends examined by crystallization dynamics. *Polymer* **1995,** *36* (25), 4805-4810.

110. Lee, S.-y.; Lai, Y.-l.; Hsu, T.-s., Influence of polymerization conditions on monomer elution and microhardness of autopolymerized polymethyl methacrylate resin. *European Journal of Oral Sciences* **2002,** *110* (2), 179-183.

111. Krauthammer, T.; Marchand, K. A.; Mlakar, P. F.; Conrath, E. J., *Structural Design for Physical Security*. American Society of Civil Engineers.: 1999.

112. Hsieh, A. J.; DeSchepper, D.; Moy, P.; Dehmer, P. G.; Song, J. W., The Effects of PMMA on Ballistic Impact Performance of Hybrid Hard/Ductile All-Plastic- and Glass-Plastic-Based Composites. *U.S. Army Research Laboratory* **2004**.

113. Natta, G.; Corradini, P.; Bassi, I. W., Crystal structure of isotactic polystyrene. *Il Nuovo Cimento (1955-1965)* **1960,** *15* (1), 68-82.

114. Pham, S.; Burchill, P. J., Toughening of vinyl ester resins with modified polybutadienes. *Polymer* **1995,** *36* (17), 3279-3285.

115. Scott, T. F.; Cook, W. D.; Forsythe, J. S., Kinetics and network structure of thermally cured vinyl ester resins. *European Polymer Journal* **2002,** *38* (4), 705-716.

116. Liang, G. Z.; Zuo, R. L.; Lu, T. L.; Wang, J. L., Modification of vinyl ester resin by a new thermoset liquid crystalline diacrylate. *Journal of Materials Science* **2005,** *40* (8), 2089-2091.

117. Chattopadhyay, D. K.; Raju, K. V. S. N., Structural engineering of polyurethane coatings for high performance applications. *Progress in Polymer Science* **2007,** *32* (3), 352-418.

118. Bayer, O., Das Di-Isocyanat-Polyadditionsverfahren (Polyurethane). *Angewandte Chemie* **1947,** *59* (9), 257-272.

119. Patel, P. J.; Gilde, G. A.; Dehmer, P. G.; McCauley, J. W., Transparent armour. *The AMPTIAC Newsletter 4 (3)* 2000.

120. Li, F.; Hou, J.; Zhu, W.; Zhang, X.; Xu, M.; Luo, X.; Ma, D.; Kim, B. K., Crystallinity and morphology of segmented polyurethanes with different soft-segment length. *Journal of Applied Polymer Science* **1996,** *62* (4), 631-638.

121. Panwiriyarat, W.; Tanrattanakul, V.; Pilard, J.-F.; Pasetto, P.; Khaokong, C., Effect of the diisocyanate structure and the molecular weight of diols on bio-based polyurethanes. *Journal of Applied Polymer Science* **2013,** *130* (1), 453-462.

122. Shenshen Wu, N. D., Mass. POLYURETHANE GOLF BALL. 5,334,673, 1994.

123. Luo, S.-G.; Tan, H.-M.; Zhang, J.-G.; Wu, Y.-J.; Pei, F.-K.; Meng, X.-H., Catalytic mechanisms of triphenyl bismuth, dibutyltin dilaurate, and their combination in polyurethane-forming reaction. *Journal of Applied Polymer Science* **1997,** *65* (6), 1217-1225.

124. Kušan, J.; Keul, H.; Höcker, H., Cationic Ring-Opening Polymerization of Tetramethylene Urethane. *Macromolecules* **2001,** *34* (3), 389-395.

125. Ihata, O.; Kayaki, Y.; Ikariya, T., Synthesis of Thermoresponsive Polyurethane from 2-Methylaziridine and Supercritical Carbon Dioxide. *Angewandte Chemie International Edition* **2004,** *43* (6), 717-719.

126. Blattmann, H.; Fleischer, M.; Bähr, M.; Mülhaupt, R., Isocyanate- and Phosgene-Free Routes to Polyfunctional Cyclic Carbonates and Green Polyurethanes by Fixation of Carbon Dioxide. *Macromolecular Rapid Communications* **2014,** *35* (14), 1238-1254.

127. Unverferth, M.; Kreye, O.; Prohammer, A.; Meier, M. A. R., Renewable Non-Isocyanate Based Thermoplastic Polyurethanes via Polycondensation of Dimethyl Carbamate Monomers with Diols. *Macromolecular Rapid Communications* **2013,** *34* (19), 1569-1574.

128. Maisonneuve, L.; Lamarzelle, O.; Rix, E.; Grau, E.; Cramail, H., Isocyanate-Free Routes to Polyurethanes and Poly(hydroxy Urethane)s. *Chemical Reviews* **2015,** *115* (22), 12407-12439.

129. Chen, Z.; Hadjichristidis, N.; Feng, X.; Gnanou, Y., Poly(urethane–carbonate)s from Carbon Dioxide. *Macromolecules* **2017,** *50* (6), 2320-2328.

130. Frisch, K. C.; Rumao, L. P., Catalysis in Isocyanate Reactions. *Journal of Macromolecular Science, Part C* **1970,** *5* (1), 103-149.

131. Jr., R. R.; L.Chan, M. Propellant binders cure catalyst. 4,379,903, 1983.

132. Lucio, B.; de la Fuente, J. L., Rheological cure characterization of an advanced functional polyurethane. *Thermochimica Acta* **2014,** *596*, 6-13.

133. Eceiza, A.; Martin, M. D.; de la Caba, K.; Kortaberria, G.; Gabilondo, N.; Corcuera, M. A.; Mondragon, I., Thermoplastic polyurethane elastomers based on polycarbonate diols with different soft segment molecular weight and chemical structure: Mechanical and thermal properties. *Polymer Engineering & Science* **2008,** *48* (2), 297-306.

134. Schemmer, B.; Kronenbitter, C.; Mecking, S., Thermoplastic Polyurethane Elastomers with Aliphatic Hard Segments Based on Plant-Oil-Derived Long-Chain Diisocyanates. *Macromolecular Materials and Engineering* **2018,** *303* (4), 1700416.

135. Cooper, S. L.; Tobolsky, A. V., Properties of linear elastomeric polyurethanes. *Journal of Applied Polymer Science* **1966,** *10* (12), 1837-1844.

136. Frontini, P. M.; Rink, M.; Pavan, A., Development of polyurethane engineering thermoplastics. II. Structure and properties. *Journal of Applied Polymer Science* **1993,** *48* (11), 2023-2032.

137. Lee, J.-H.; Veysset, D.; Singer, J. P.; Retsch, M.; Saini, G.; Pezeril, T.; Nelson, K. A.; Thomas, E. L., High strain rate deformation of layered nanocomposites. *Nature Communications* **2012,** *3*, 1164.

138. Hazell, P. J.; Edwards, M. R.; Longstaff, H.; Erskine, J., Penetration of a glass-faced transparent elastomeric resin by a lead–antimony-cored bullet. *International Journal of Impact Engineering* **2009,** *36* (1), 147-153.

139. O'Sickey, M. J.; Lawrey, B. D.; Wilkes, G. L., Structure-property relationships of poly(urethane urea)s with ultra-low monol content poly(propylene glycol) soft segments. I. Influence of soft segment molecular weight and hard segment content. *Journal of Applied Polymer Science* **2002,** *84* (2), 229-243.

140. Rinaldi, R. G.; Hsieh, A. J.; Boyce, M. C., Tunable microstructures and mechanical deformation in transparent poly(urethane urea)s. *Journal of Polymer Science Part B: Polymer Physics* **2011,** *49* (2), 123-135.

141. Li, Z.; Shen, Y.; Gu, X.; Li, J.; Gao, Y., A novel underwater acoustically transparent material: Fluorosilicone polyester polyurethane. *Journal of Applied Polymer Science* **2019,** *136* (34), 47894.

142. Zalipsky, S.; Harris, J. M., Introduction to Chemistry and Biological Applications of Poly(ethylene glycol). In *Poly(ethylene glycol)*, American Chemical Society: 1997; Vol. 680, pp 1-13.

143. Su, J.-C.; Liu, P.-S., A novel solid–solid phase change heat storage material with polyurethane block copolymer structure. *Energy Conversion and Management* **2006,** *47* (18), 3185-3191.

144. Cao, Q.; Liu, P., Hyperbranched polyurethane as novel solid–solid phase change material for thermal energy storage. *European Polymer Journal* **2006,** *42* (11), 2931-2939.

145. Bertino, A.J., *Forensic Science Fundamentals & Investigations. 2009.*

146. Holden, H., To Be a U.S. Secret Service Agent. 2006: Zenith Press.

147. Jarrett, D.N., Cockpit Engineering. 2005: Ashgate Publishing Limited.

148. Clugston, M. and R. Flemming, Advanced Chemistry. 2000: Oxford University Press.

149. Varasdi, J.A., *Myth Information. 1989, New York: Ballantine Books.*

150. Bless, S.; Chen, T., Impact damage in layered glass. *International Journal of Fracture* **2010,** *162* (1), 151-158.

151. DOLAN, A. M. Ballistic Transparent Armor Testing Using a Multi-hit Rifle Pattern. KETTERING UNIVERSITY, 2007.

152. Sands, J.; Patel, P.; Dehmer, P.; Hsieh, A.; Boyce, M., Protecting the future force: transparent materials safeguard the Army's vision. *AMPTIAC Q* **2004,** *8* (4), 28-36.

153. Franks, L. P.; Barnak, D. H. a. R. *Transparent Armor Cost Benefit Study*; 2008.

154. Straßburger, E., Ballistic testing of transparent armour ceramics. *Journal of the European Ceramic Society* **2009,** *29* (2), 267-273.

155. Schwartz, M., *Innovations in materials manufacturing, fabrication, and environmental safety*. CRC press: 2010.

156. Zanotto, E. D., Bright future for glass-ceramics. *American Ceramics Society Bulletin* **2010,** *89* (8), 19-27.

157. AREVA T&D UK Ltd. *Registered Office. St. Leonards, Avenue, Stafford ST17 4 LX.*

158. Raytheon electronic systems. Lexington laboratory, 131 spring street. Lexington MA 02421. Registered trademark no. 2554362,. **2002**.

159. Sands, J. M.; Fountzoulas, C. G.; Gilde, G. A.; Patel, P. J., Modelling transparent ceramics to improve military armour. *Journal of the European Ceramic Society* **2009,** *29* (2), 261-266.

160. Haney, E. J.; Subhash, G., Analysis of interacting cracks due to sequential indentations on sapphire. *Acta Materialia* **2011,** *59* (9), 3528-3536.

161. Su, M.; Zhou, Y.; Wang, K.; Yang, Z.; Cao, Y.; Hong, M., Highly transparent AlON sintered from powder synthesized by direct nitridation. *Journal of the European Ceramic Society* **2015,** *35* (4), 1173-1178.

162. Liu, X. J.; Chen, F.; Zhang, F.; Zhang, H. L.; Zhang, Z.; Wang, J.; Wang, S. W.; Huang, Z. R., Hard transparent AlON ceramic for visible/IR windows. *International Journal of Refractory Metals and Hard Materials* **2013,** *39*, 38-43.

163. http://www.surmet.com/technology/alon-optical-ceramics/index.php.

164. Krell, A.; Strassburger, E., Hierarchy of Key Influences on the Ballistic Strength of Opaque and Transparent Armor. *Advances in Ceramic Armor III: Ceramic and Engineering Science Proceedings* **2007,** *28* (5), 45-55.

165. Basu, B.; Balani, K., *Advanced Structural Ceramics*. John Wiley & Sons, Inc.: 2011.

166. Wang, Q.; Chen, Z.; Chen, Z., Design and characteristics of hybrid composite armor subjected to projectile impact. *Materials & Design* **2013,** *46*, 634-639.

167. Chung, D. D. L., *carbon Fiber Composites*. Reed Elsevier group: 1994.

168. Xiong, W.; Cai, C. S.; Xiao, R. C., Chapter 8: The use of carbon fiber-reinforced polymer (CFRP) composites for cable-stayed bridges. In *Advanced Composites in Bridge Construction and Repair*, Kim, Y. J., Ed. Woodhead Publishing: 2014; pp 210-264.

169. Han, S.; Chung, D. D. L., Increasing the through-thickness thermal conductivity of carbon fiber polymer–matrix composite by curing pressure increase and filler incorporation. *Composites Science and Technology* **2011,** *71* (16), 1944-1952.

170. Daily, C.; Barnard, D. J.; Jones, R. W.; McClelland, J. F.; Bowler, N., Dielectric and infrared inference of thermo-oxidative aging of a bismaleimide composite material. *Composites Part B: Engineering* **2016,** *101*, 167-175.

171. Zalba, B.; Marín, J. M.; Cabeza, L. F.; Mehling, H., Review on thermal energy storage with phase change: materials, heat transfer analysis and applications. *Applied Thermal Engineering* **2003,** *23* (3), 251-283.

172. Khan, Z.; Khan, Z.; Ghafoor, A., A review of performance enhancement of PCM based latent heat storage system within the context of materials, thermal stability and compatibility. *Energy Conversion and Management* **2016,** *115*, 132-158.

173. Abhat, A.; Aboul-Enein, S.; Malatidis, N. A. In *Heat-of-Fusion Storage Systems for Solar Heating Applications*, Thermal Storage of Solar Energy, Dordrecht, 1981//; den Ouden, C., Ed. Springer Netherlands: Dordrecht, 1981; pp 157-171.

174. Ismail, K. A. R.; Henríquez, J. R., Thermally effective windows with moving phase change material curtains. *Applied Thermal Engineering* **2001,** *21* (18), 1909-1923.

175. Vakilaltojjar, S. M.; Saman, W., Analysis and modelling of a phase change storage system for air conditioning applications. *Applied Thermal Engineering* **2001,** *21* (3), 249-263.

176. Bédécarrats, J. P.; Strub, F.; Falcon, B.; Dumas, J. P., Phase-change thermal energy storage using spherical capsules: performance of a test plant. *International Journal of Refrigeration* **1996,** *19* (3), 187-196.

177. Espeau, P.; Mondieig, D.; Haget, Y.; Cuevas-Diarte, M. A., 'Active' Package for Thermal Protection of Food Products. *Packaging Technology and Science* **1997,** *10* (5), 253-260.

178. Salyer, I. O.; Sircar, A. K. In *Phase Change Katerials For Heating And Cooling Of Residential Buildings And Other Applications*, Proceedings of the 25th Intersociety Energy Conversion Engineering Conference, 12-17 Aug. 1990; 1990; pp 236-241.

179. Pal, D.; Joshi, Y., Application of Phase Change Materials for Passive Thermal Control of Plastic Quad Flat Packages: a Computational Study. *Numerical Heat Transfer, Part A: Applications* **1996,** *30* (1), 19-34.

180. Mulligan, J. C.; Colvin, D. P.; Bryant, Y. G., Microencapsulated phase-change material suspensions for heat transfer in spacecraft thermal systems. *Journal of Spacecraft and Rockets* **1996,** *33* (2), 278-284.

181. Sarı, A.; Alkan, C.; Altıntaş, A., Preparation, characterization and latent heat thermal energy storage properties of micro-nanoencapsulated fatty acids by polystyrene shell. *Applied Thermal Engineering* **2014,** *73* (1), 1160-1168.

182. Gunasekara, S. N.; Pan, R.; Chiu, J. N.; Martin, V., Polyols as phase change materials for surplus thermal energy storage. *Applied Energy* **2016,** *162* (C), 1439-1452.

183. Schiffres, S. N.; Harish, S.; Maruyama, S.; Shiomi, J.; Malen, J. A., Tunable Electrical and Thermal Transport in Ice-Templated Multilayer Graphene Nanocomposites through Freezing Rate Control. *ACS Nano* **2013,** *7* (12), 11183-11189.

184. Xiao, X.; Zhang, P.; Li, M., Preparation and thermal characterization of paraffin/metal foam composite phase change material. *Applied Energy* **2013,** *112* (C), 1357-1366.

185. Farid, M. M.; Khudhair, A. M.; Razack, S. A. K.; Al-Hallaj, S., A review on phase change energy storage: materials and applications. *Energy Conversion and Management* **2004,** *45* (9), 1597-1615.

186. Sari, A.; Alkan, C.; Doguscu, D. K.; Bicer, A., Micro/nano-encapsulated n-heptadecane with polystyrene shell for latent heat thermal energy storage. *Solar Energy Materials and Solar Cells* **2014,** *126*, 42-50.

187. Hong, Y.; Xin-shi, G., Preparation of polyethylene–paraffin compound as a form-stable solid-liquid phase change material. *Solar Energy Materials and Solar Cells* **2000,** *64* (1), 37-44.

188. Sarı, A., Form-stable paraffin/high density polyethylene composites as solid–liquid phase change material for thermal energy storage: preparation and thermal properties. *Energy Conversion and Management* **2004,** *45* (13), 2033-2042.

Chapter 2

High-fracture-toughness acrylic-polyurethane-based graft-interpenetrating polymer networks for transparent applications

2.1. Introduction

Transparent polymeric materials with high impact resistance demonstrate good potential for a wide range of applications such as safety enclosures, aerospace applications, windshields, safety goggles, and many more [1, 2]. Traditionally, glass has been used as the staple transparent material in general consumer and engineering applications [3, 4]. However, glass has high density and low impact resistance, restricting its use in high-performance applications [5]. Recently, the development of transparent and high impact resistance polymeric materials for engineering applications has attracted widespread attention [6]. Ease of processing, low density, tunable mechanical properties, excellent impact resistance, and fracture toughness of these new polymeric materials are some of the significant reasons which make them suitable candidates for advanced applications [6, 7].

While the direct blending of polymers is one method for formulating polymers with enhanced properties [8], the final mixing process presents challenges due to phase separation to occur [9, 10]. To overcome phase separation between dissimilar polymers while also improving the compatibility of the solid-state material, different polymerization processes have been developed including graft and block copolymers and interpenetrating polymer networks (IPNs) [11].

Interpenetrating polymer networks are classified as a multi-component system where one polymer is synthesized in the presence of another [12]. Most multi-component polymeric materials form immiscible phases due to the low entropy of mixing [12]. IPNs attract much attention in multi-component materials due to their physical entanglement, which brings about forced compatibility into the system, therefore increasing miscibility between the two phases [12]. Synthetic method,

degree of polymerization, and degree of crosslinking are factors influencing the final morphology of IPNs [13]. There are many different ways to classify interpenetrating polymer networks based on their physical and chemical properties. A full-IPN is one kind of interpenetrating polymer network where both polymers are crosslinked, in semi-IPN's only one of the polymer is crosslinked, while the other polymer is linear [14], and in graft-IPN both polymers are crosslinked, and a controlled amount of bonding is allowed between the two polymers [11, 15]. Latex IPN is another kind of IPN where the IPN is in the form of latex; therefore, it is a so-called interpenetrating elastomeric network [12, 16]. IPNs can also be classified as simultaneous or sequential based on the synthetic method applied. In sequential IPNs, the first polymer network is formed, swollen in the monomers of the second polymer, which is then polymerized, forming the second polymer network. In simultaneous polymerization, polymerization of the two polymer networks occurs at the same time, and no interfering reactions occur [10, 17, 18].

In the literature, numerous groups have studied IPN systems, such as Millar et al. [19], and Aylsworth and Edison [10, 12, 20-22], who have utilized different monomers to investigate various aspects of IPNs. Extensive research on this topic has also been performed by the authors [23, 24]. In previous studies, the effect of different parameters such as curing profile, the composition of two polymer systems [5, 7, 25-27], the substitution of aliphatic and aromatic isocyanate [25], the impact of the molecular weight of diol [7], simultaneous and sequential polymerization method [25], and using chemical bonds to synthesize graft-IPNs [28], have been studied. Overall, these studies suggested IPNs containing aliphatic isocyanate with 1400 g/mol diol and following a sequential synthetic method, and chemical bonds between the two phases presented better transparency and thermomechanical properties due to reduced phase separation from improved compatibility provided between the two phases. It was also observed that utilizing PU with an acrylic copolymer, such as PMMA based

copolymers, led to an improvement of ~150% in fracture toughness of the acrylic copolymer. The enhancement in phase compatibility of the IPNs was also addressed [6, 25, 28-33].

In this work, the impact of varying the acrylic copolymer precursors and the chemical bonding between the two polymer networks was investigated towards the overall goal of synthesizing novel graft-IPNs with excellent compatibility, transparency, and superior fracture toughness. For the first time, styrene, as one of the acrylic copolymer monomers, was utilized in the graft-IPN system. Two methods were utilized to monitor the polymerization of the two phases in the IPN systems. The compatibility of the two phases was evaluated using a transmission electron microscope (TEM), a dynamic mechanical analyzer (DMA), and UV-Vis spectroscopy, while scanning electron microscope (SEM) and quasi-static fracture tests were used to investigate the mechanism of the fracture toughness.

2.2. Experimental

2.2.1. Materials

In this work, the polyurethane (PU) phase was synthesized from the following compounds: 2-ethyl-2-(hydroxymethyl)-1,3-propanediol (TRIOL, MW=134.18 g/mol, crosslinker) purchased from Acros Organics, poly(tetramethylene ether) glycol (PTMG, MW=approximately 1400 g/mol) purchased from Aldrich, hexamethylene diisocyanate (DCH) purchased from TCI, and dibutyltin dilaurate (DBTDL) and triphenylbismuth (TPB) as catalysts purchased from Pfaltz & Bauer and Alfa Aesar, respectively. Ethyl acetate, purchased from Alfa Aesar, was the solvent used for the catalyst mixture. To synthesize the acrylic copolymer, styrene was purchased from Alfa Aesar, bisphenol A bis(2-hydroxy-3-methacryloxypropyl) ether (BisGMA) was purchased from Esstech, and 2,2'-azobis(2-methyl-propionitrile) (AIBN, thermal initiator) was purchased from Matrix

Scientific. 4Å molecular sieves, purchased from Alfa Aesar, were used to remove the moisture from DCH, styrene, TRIOL, and PTMG.

2.2.2. Methods

2.2.2.1. Synthesis of graft-IPNs

TRIOL (0.19 eq) and PTMG (0.12 eq) were heated to 60°C, and the molten TRIOL and PTMG were mixed with a stirrer. Next, DCH (0.31 eq + calculated amount of DCH to react with BisGMA), was added to the mixture, and the mixture was stirred. The PU phase accounted for 25 wt% of the final composition for all specimens.

For the second phase, different percentages of BisGMA were dissolved into styrene, and then AIBN (1 wt% of total co-monomer mass) was dissolved into the mixture. Then PU monomers and acrylic phase monomers were mixed. 600 μL DBTDL per 50 grams of PU (0.02 M Ethyl acetate solution) and 600 μL TPB (0.001 M Ethyl acetate solution) were added to the monomer mixture at the end of this stage for the poly-addition polymerization of the PU phase. Finally, the mixture was cured in closed aluminum molds for 24 hours at 40°C, followed by 24 hours at 60°C and finally 24 hours at 80°C.

Figure 2.1 shows the polyaddition polymerization chemistry of the polyurethane network. The simple schematic of the reaction occurring for acrylic copolymer synthesis and IPN network structure is shown in Figure 2.2 and Figure 2.3, respectively.

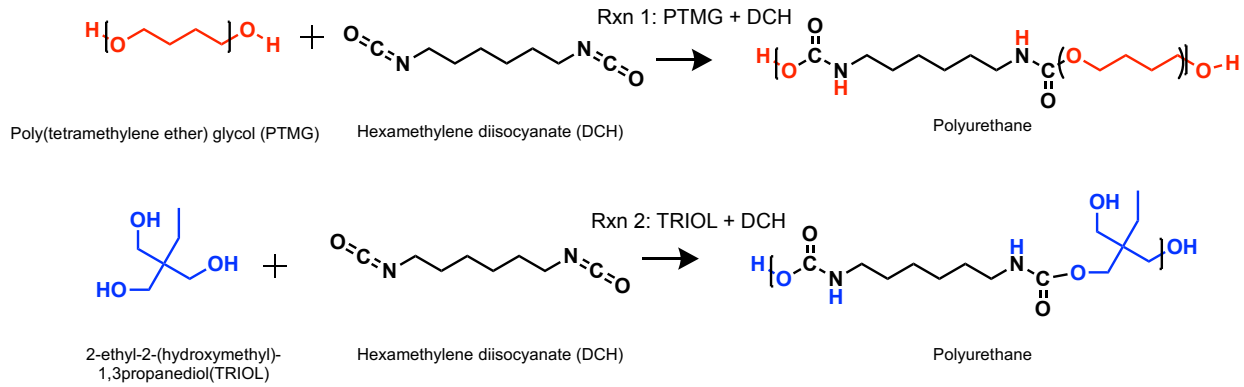

Figure 2.1. Two polyaddition polymerization reactions that form the polyurethane phase. (Top) reaction between PTMG and DCH and (Bottom) reaction between TRIOL and DCH.

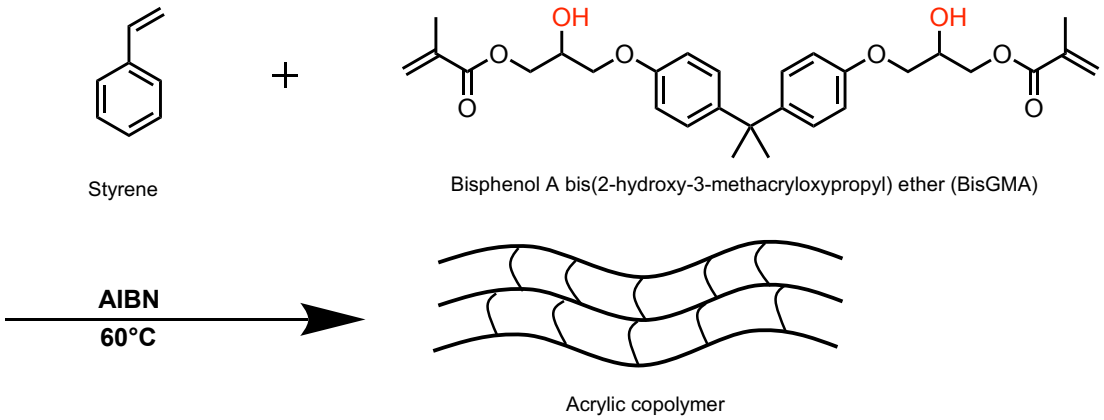

Figure 2.2. Free radical polymerization of the acrylic copolymer from styrene and BisGMA.

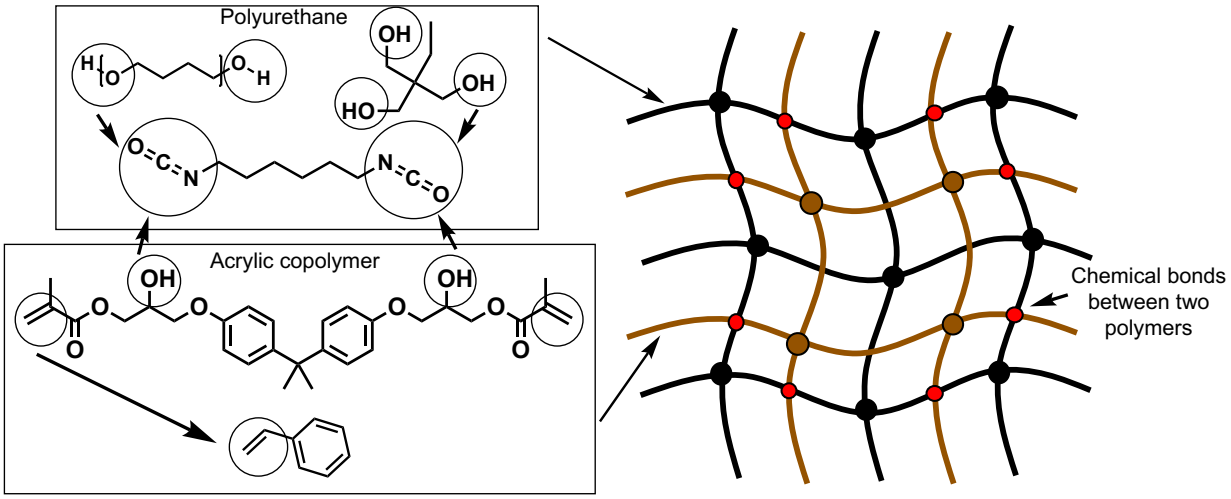

Figure 2.3. A simple schematic of IPN network structure.

2.2.2.2. Characterization

Fourier transform infrared spectroscopy (FTIR) was performed with a Nicolet 6700 FTIR spectrometer from Thermo Scientific (USA) in attenuated total reflection (ATR) infrared mode. FTIR experiments were performed from 400-4000 cm^{-1} wavenumber with 64 scans and using a 4 cm^{-1} resolution.

Low-field ^{1}H nuclear magnetic resonance spectroscopy was performed on an Oxford Pulsar 60 MHz (1.4 Tesla) NMR spectrometer using Wilmad class B eight-inch high-throughput tubes (5 mm outer diameter, 4 mm internal diameter). The 1H NMR experiment was conducted as an arrayed experiment in the Oxford Spin flow Software with 64 scans/run, a recycle delay of 2 seconds, and a spectral width of 50,000 Hz. This combination of the parameters yields an approximate sampling time of 5 minutes and 48 seconds per spectrum. The spectra were analyzed using Mnova software.

A Zeiss EVO 50 variable pressure scanning electron microscope (SEM) with digital imaging and energy dispersive spectroscopy (with the IPNs sputter-coated with an EMS 550X auto sputter

coating device with carbon coating attachment) was used to study the surface morphology of the specimens. The specimens were immersed in the liquid nitrogen, broken, and the fracture events visualized using SEM. A Zeiss EM 10C 10CR transmission electron microscope (TEM) was used to examine the interior morphology of the samples. Samples were stained using a 2.5% aqueous solution of osmium tetroxide (OsO_4) for one week, as reported by Kato prior to microtoming [34]. A Cary 60 UV/Vis spectrometer from Agilent (USA) was used to verify the transparency of the samples (250-800 nm wavelength).

TA Instruments RSA 3 dynamic mechanical analyzer (DMA) was used for studying the thermomechanical properties of the IPNs. Flexural tests were performed on the samples from 25-200°C with a sinusoidal strain amplitude of 0.1% and 0.1 Hz frequency and a 5°C/min heating rate.

The fracture toughness properties of specimens were characterized using quasi-static fracture tests performed in a 3-point bending condition following ASTM D5045 [35]. Equations 2.1, 2.2, and 2.3 were used to calculate the plane-strain fracture toughness K_{Ic}, where a is crack length, W is specimen width, B is specimen thickness, and $0 < x < 1$.

$$K_{Ic} = \left(\frac{P_Q}{BW^{1/2}}\right) f(x) \qquad [2.1]$$

$$f(x) = 6x^{1/2}\,\frac{[1.99 - x(1-x)(2.15 - 3.93x + 2.7x^2)]}{(1+2x)(1-x)^{3/2}} \qquad [2.2]$$

$$x = \frac{a}{W} \qquad [2.3]$$

Cured specimens were cut to bars of dimensions 55 mm × 12 mm × 3 mm using Boss Laser LS 3655. An edge notch 4 mm in length was cut into the samples with a saw, and the edge tip

subsequently sharpened with a razor blade. The single edge notched bend (SENB) test was performed on the specimens using an Instron 5565 with 1 kN static load cell. The load and displacement data were recorded up to crack initiation and during stable crack growth. The load at crack initiation (P) was used to calculate K_{Ic}. MATLAB was utilized to calculate K_{Ic} with Equations 2.1, 2.2, and 2.3, and at least five specimens were tested for each composition [31].

2.3. Results and discussion

2.3.1. Analysis of isocyanate conversion by FTIR measurements

The compositions (using a 10 g sample basis) of synthesized materials investigated with FTIR and NMR spectroscopy and their corresponding nomenclature are shown in Table 2.1. The isocyanate conversion (NCO) was studied using FTIR spectroscopy. The measurement is based on the decay in intensity of the peak assigned to isocyanate absorption during polymerization. The absorption peak of the isocyanate group is assigned to approximately 2270 cm^{-1}. C-H stretch absorption happening within 2850-3000 cm^{-1} was used as an internal standard due to the constant concentration of this band during the reaction [36]. The isocyanate conversion was calculated with the help of equation 2.4 [37] shown below:

$$p = 1 - \frac{\frac{A_{NCO}}{A_{CH_2}}}{\left(\frac{A_{NCO}}{A_{CH_2}}\right)_0} \quad [2.4]$$

where p is the isocyanate conversion, A_{NCO} is the integrated absorbance for the isocyanate group. A_{CH_2} is the integrated absorbance for the C-H stretch absorption and $\left(\frac{A_{NCO}}{A_{CH_2}}\right)_0$ is the relative absorbance extrapolated to time zero.

Table 2.1. Prepared sample compositions used for FTIR and NMR spectroscopy.

	Polyurethane 25 wt%			**Acrylic copolymer 75 wt%**	
Sample	**PTMG wt%**	**TRIOL wt%**	**DCH wt%**	**Styrene wt%**	**BisGMA wt%**
PU-PT	70.8	7.2	22	--	--
PU-P	89	--	11	--	--
PU-B	--	--	24.7	--	75.3
PU-PTB	14.2	1.4	24.2	--	60.2
IPN80/20	16.9	1.7	9.9	57.2	14.3
COP80/20	--	--	--	80	20

FTIR spectra for PU-PT at 0, 18, 36, 64 min, and three days are shown in Figure 2.4, where the isocyanate absorption peak (2270 cm^{-1}) decreases during polymerization while the C-H stretch absorption peak (2800-3000 cm^{-1}) remains constant. This indicates the isocyanate groups react with the hydroxyl group of the TRIOL and PTMG to form the PU network as expected.

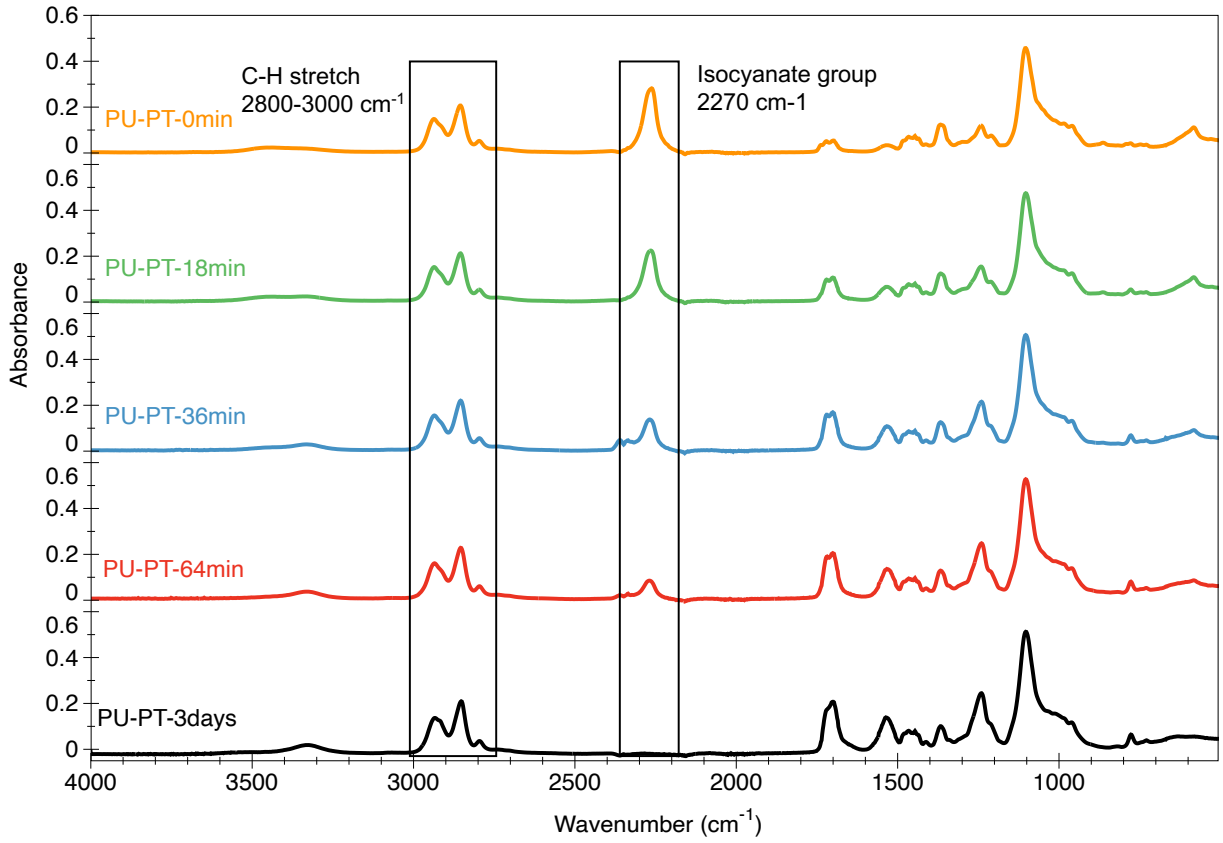

Figure 2.4. FTIR spectra of the PU-PT sample at five different times.

The isocyanate conversion versus time data extracted from the FTIR spectra is shown in Figure 2.5. While initial polymerization rates across the series are similar (except for PU-B), PU-P is the first to reach near completion. PU-B clearly shows the slowest polymerization rate, likely due to the secondary hydroxyl groups in the BisGMA and the corresponding steric hindrance compared to the PTMG primary hydroxyl group [38]. PU-PTB shows a higher polymerization rate in comparison to PU-PT due to the presence of BisGMA, which provides more hydroxyl groups into the system. PU-PT and IPN80/20 follow the same trend due to the dominant behavior of PU in isocyanate conversion and the steric effect of acrylic copolymer into the IPN system.

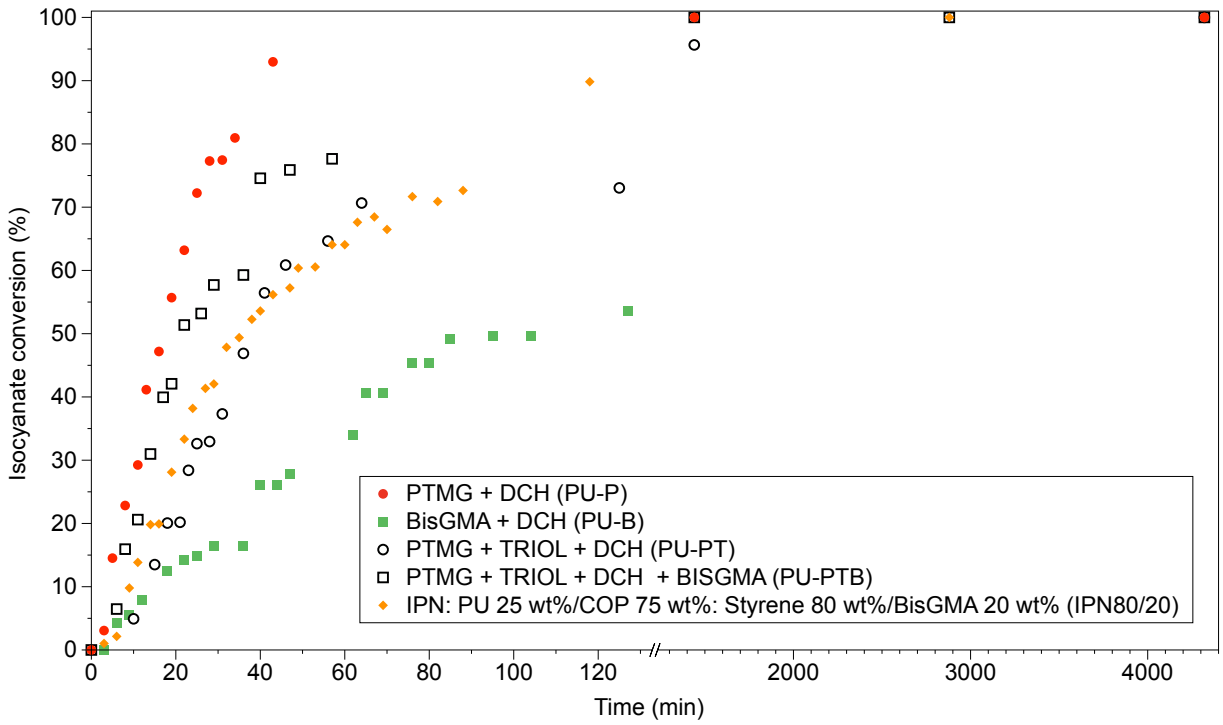

Figure 2.5. Isocyanate conversion of PTMG + TRIOL + DCH (PU-PT), IPN80/20 and its constituents.

FTIR spectroscopy was also utilized for pure acrylic copolymer with 20 wt% BisGMA and 80 wt% styrene (COP80/20) to characterize their free radical polymerization at 60ºC, which forms the second polymer network in IPN80/20. Samples were cured for 24 hours at 60ºC and then cured for 24 hours at 80ºC and their FTIR spectra were obtained at the beginning of the synthesis and after two days of curing (Figure 2.6). Peaks at 774 and 908 cm^{-1} corresponding to the out-of-plane (oop) bending of =C-H and at 1600-1660 cm^{-1} corresponding to C=C can be used to track polymerization. Both of these peaks decrease during free radical polymerization due to the consumption of double bonds. Moreover, a peak corresponding to sp^3 C-H stretching appears after

two days of curing in range of 2850-3000 cm^{-1} as additional confirmation of consumption of C=C-H to form sp^3 C-H.

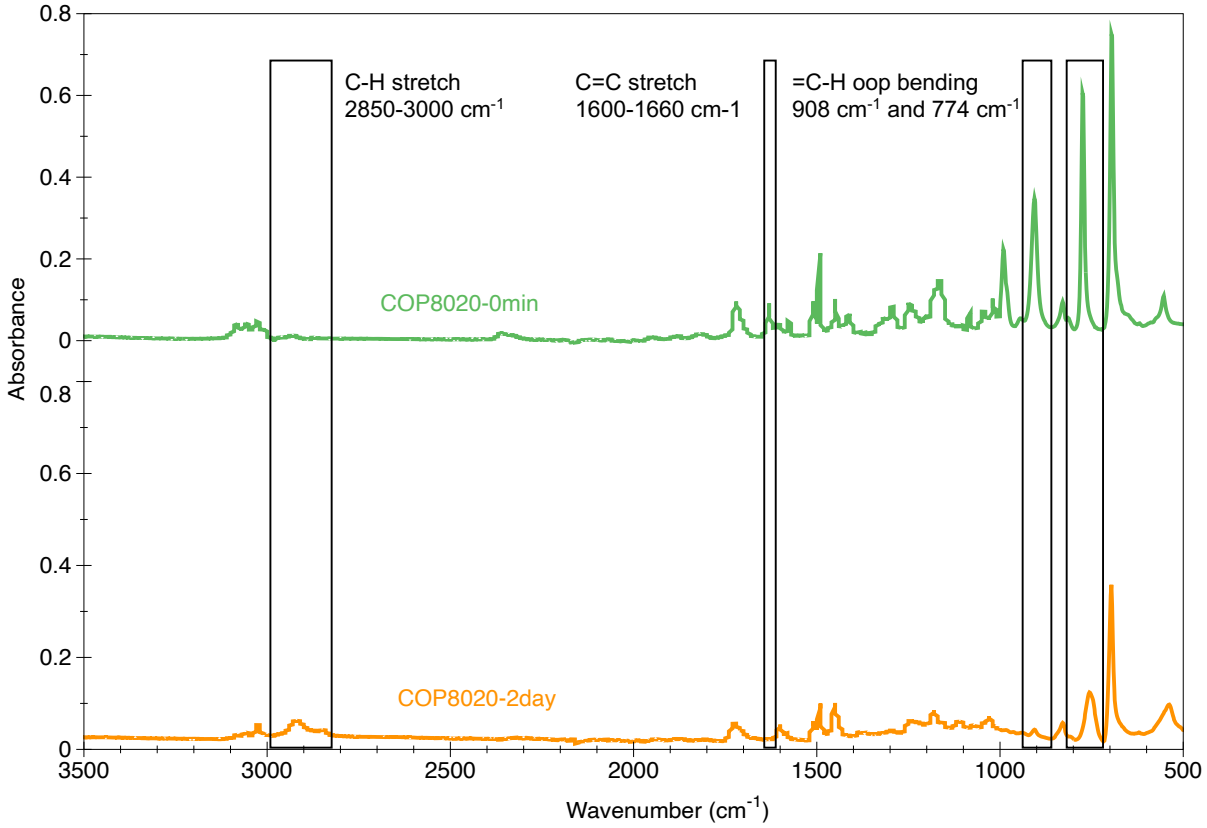

Figure 2.6. FTIR spectra of the acrylic copolymer at 0 min (top) and after two days of curing (bottom).

2.3.2. Analysis of isocyanate conversion via low-field NMR spectroscopy

Reaction progress for PU-P and PU-PT were also tracked using an Oxford Instruments Pulsar 60 MHz NMR spectrometer. Briefly, an initial spectrum of PTMG was collected prior to the addition of DCH and two drops of each catalyst, DBTDL and TPB, dissolved in ethyl acetate. The reaction mixture was agitated via stirring with copper wire and manual shaking of the tube before being

placed into the probe bore. The spectrometer was tuned and matched to the sample, and then an arrayed experiment was commenced. Note that the lag time (time from the addition of the catalyst to start of the NMR spectroscopy tracking experiment) was accounted for in both the reaction progress diagram, Figure 2.7, and the subsequent data analysis.

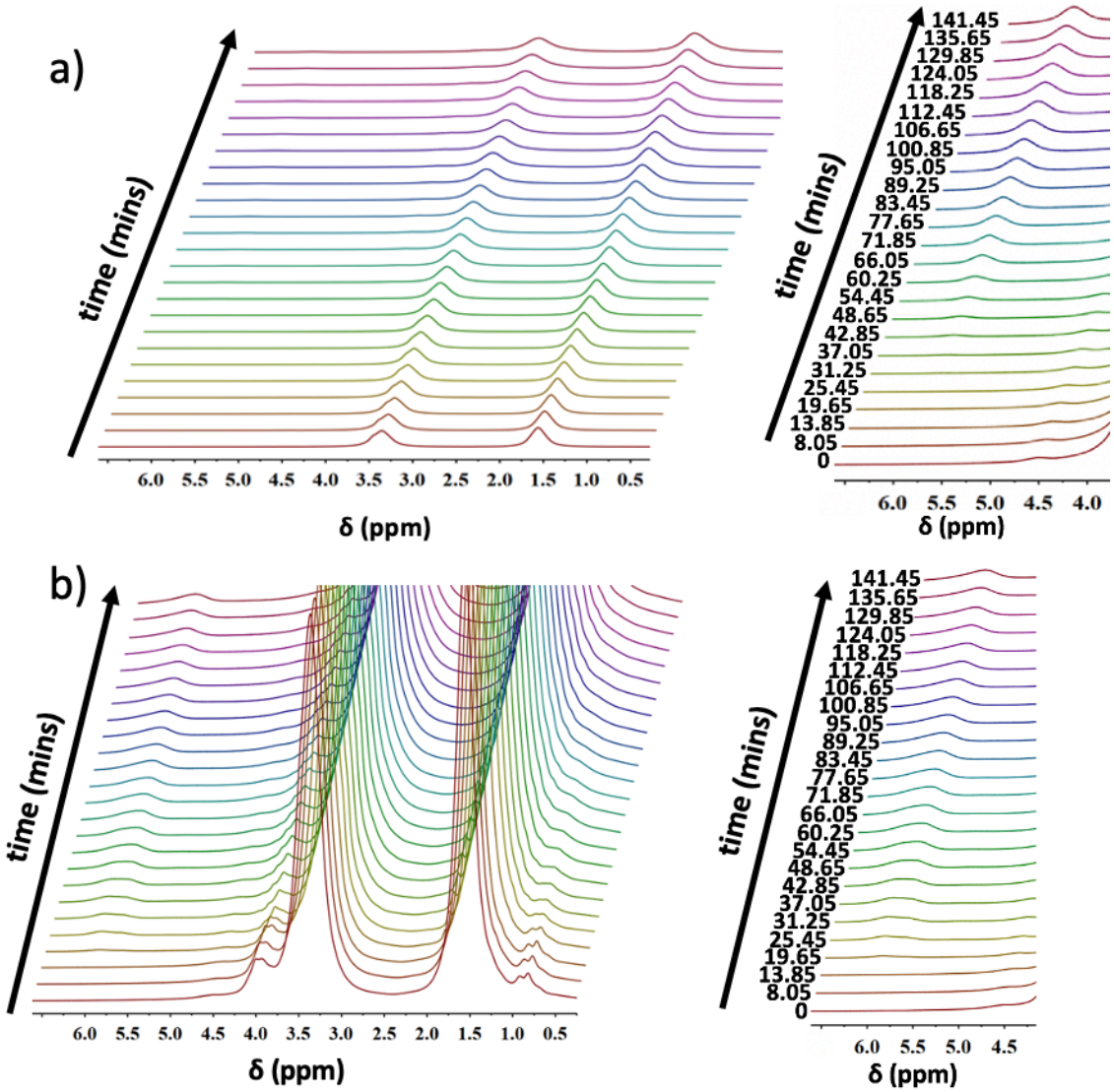

Figure 2.7. (left) NMR spectra from in-situ reaction monitoring of a) PU-P and b) PU-PT with (right) spectra enlarged to show polyurethane linkage peak.

Tetramethylsilane (a standard additive used to align most 1D ^{1}H NMR spectra) was not used here to eliminate any possible interactions with the reaction media. Instead, all spectra were shifted based on the far right peak attributed to the PTMG backbone of the PU-P (1.56 ppm) [36]. This peak also served as an internal calibration standard as the underlying protons associated with this peak (for both systems) are conserved; for the PU-PT system, the TRIOL aliphatic arm also contributes to this peak, so five additional protons are accounted for as shown in Figure 2.8.

Unfortunately, due to the spectral overlap in the aliphatic region of the NMR spectra, Figure 2.7, the consumption of hydroxyl groups could not be tracked directly. However, in both cases, the formation of urethane linkages can be traced through the formation of N-H protons. By utilizing this method, we combine the advantages of more traditional differential scanning calorimetry reaction tracking through heat evolution and that of the FTIR spectroscopy through bond identity, as discussed in this paper. Furthermore, as has been discussed elsewhere, an additional advantage of the low-field NMR spectrometer used here is the soft-lock algorithm, which eliminates the need for deuterated solvents and allows for examination of protons without any adulteration of the reaction media [39].

As shown in Figure 2.7, the peak at 5.94 ppm grows in intensity over time due to the continuous formation of secondary amine peaks as urethane linkages are formed. In the case of PU-P, each urethane linkage is strictly from the consumption of -OH groups on the PTMG chain ends. However, for PU-PT this metric of conversion is complicated by the presence of additional hydroxyl groups on the arms of the TRIOL. Nonetheless, the overall conversion to isocyanate linkages was tracked as a function of peak area and number of protons via Equation 2.5,

$$Conversion = 100 \times \frac{A_{5.94}N_{1.56}}{A_{1.56}N_{5.94}} \quad [2.5]$$

Where A_i is the peak areas at i ppm, and N_j is the number of protons associated with the peak at j ppm. Peak areas (A_i) were extracted from Gaussian fits to the peaks after spectral shifting, automatic phasing, and automatic baselining in the Mnova software. For PU-P $N_{1.56}$=76.665 and $N_{5.94}$=2.0157, while for PU-PT $N_{1.56}$=81.70375 and $N_{5.94}$=6.04704. These values are calculated for each chemistry from the reaction stoichiometry and chemical structures shown in Figure 2.8.

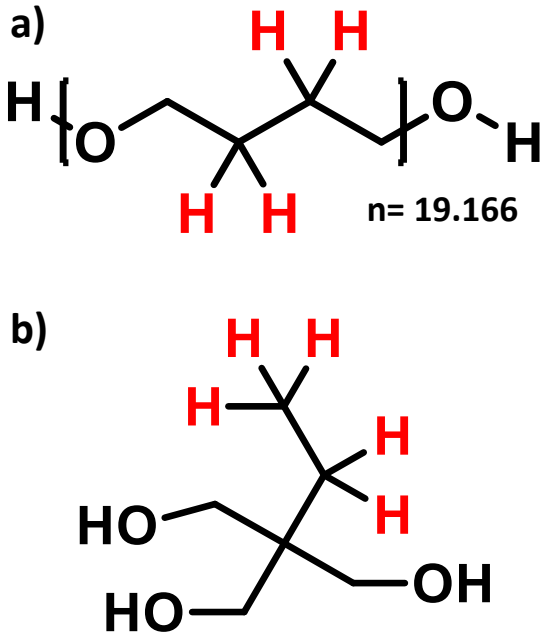

Figure 2.8. Protons used in the calculation of $N_{1.56}$ are highlighted in red for a) PTMG and b) TRIOL.

In PU-P, this analysis assumes only one DCH molecule is present in the "repeat unit" of the network, while PU-PT has the potential for up to three DCH molecules; two amine protons and

six amine protons, respectively. This is important as the network is complicated by the availability of hydroxyl groups from these two different mer units. Extracted conversion versus time data and their comparison by FTIR data is shown in Figure 2.9.

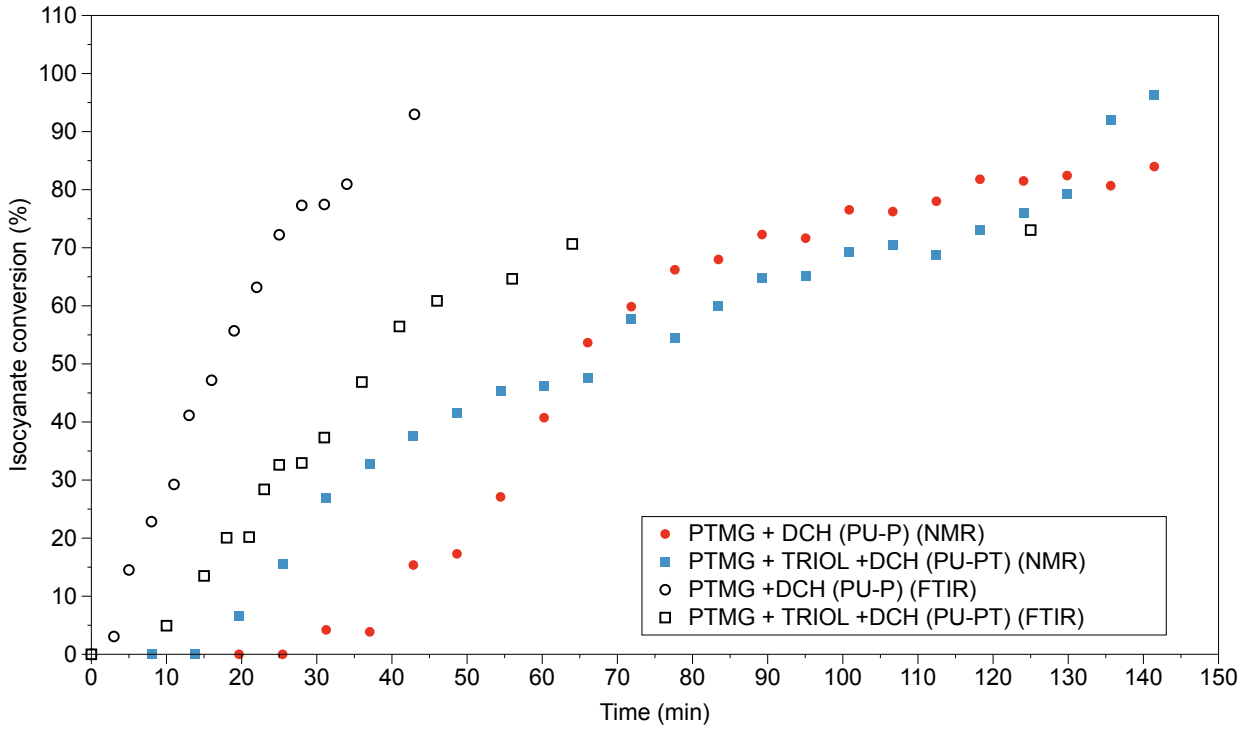

Figure 2.9. Reaction progress for both systems as a function of isocyanate conversion.

As shown in Figure 2.9, both systems exhibit a lag time at the beginning of the reaction in the NMR instrument, which we attribute to the low reaction rate at room temperature as the reaction media approaches the spectrometer operating temperature of 37°C. However, the reaction can be effectively tracked over time as the DCH is incorporated within the polymeric structure, and isocyanate groups are converted into secondary amines within the urethane linkages. While the data points appear to be non-continuous, it is essential to note that the spectrometer is averaging the signal over 64 scans acquired over a cycle time of approximately 5 minutes and 48 seconds,

i.e., the resulting isocyanate conversion is time-averaged. Additionally, the conversion in each case reaches a maximum at approximately the same time as extracted from FTIR spectroscopy after accounting for the thermal lag time. Overall, we find this method to provide adequate and facile means to track both reaction progress and bond-specific formation.

2.3.3. Network morphology

A series of IPNs with different styrene to BisGMA content in the acrylic network were synthesized, and their morphology was examined with TEM (Figure 2.10). The lines are observed in Figure 2.10.a, b, and c are tool marks produced during the microtoming procedure. The pure acrylic copolymer (Figure 2.10.a) shows a homogeneous dispersion of the polymeric component throughout the copolymer sample and is utilized as the control experiment for comparisons. No clear OsO_4 stained domains are observed in this sample. In the IPN samples, the polyurethane regions become black after sample staining, while the acrylic phase does not interact with OsO_4 and remains clear. Figures 2.10.b, c, and d display TEM images of IPN with 70, 80, and 90 wt% of styrene, respectively. In Figure 2.10.b, a distinct black domain is observed in the sample due to the incompatibility of the two polymers containing 70 wt% styrene. However, the IPN composed of 80 wt% styrene shows a fine dispersion of the two polymers with no well-defined domains in the image. As described by Bird et al., the absence of defined domain shapes indicates a good interpenetration of two phases [25]. The finest phase domains of the samples, as observed by TEM, typically indicate the highest level of interpenetration between the two polymers [30]. Figure 2.10.d corresponds to the IPN system with 90 wt% styrene and demonstrates good interpenetration between two polymers with less phase separation compared to a sample with 70 wt% of styrene.

The smaller size and thereby higher mobility of styrene in comparison to BisGMA within the polyurethane network likely improve swelling of the forming polyurethane network and decreases phase separation.

It was also observed that utilizing a linear isocyanate (such as DCH) has a positive effect on the compatibility of two phases [25]. Ballestero et al. also used TEM to study the impact of post-curing processes on domain size and interpenetration of polyurethane similar with PMMA and observed better dispersion between two polymers after post-curing due to the additional chemical bonds formed between the two polymer networks during this process [28].

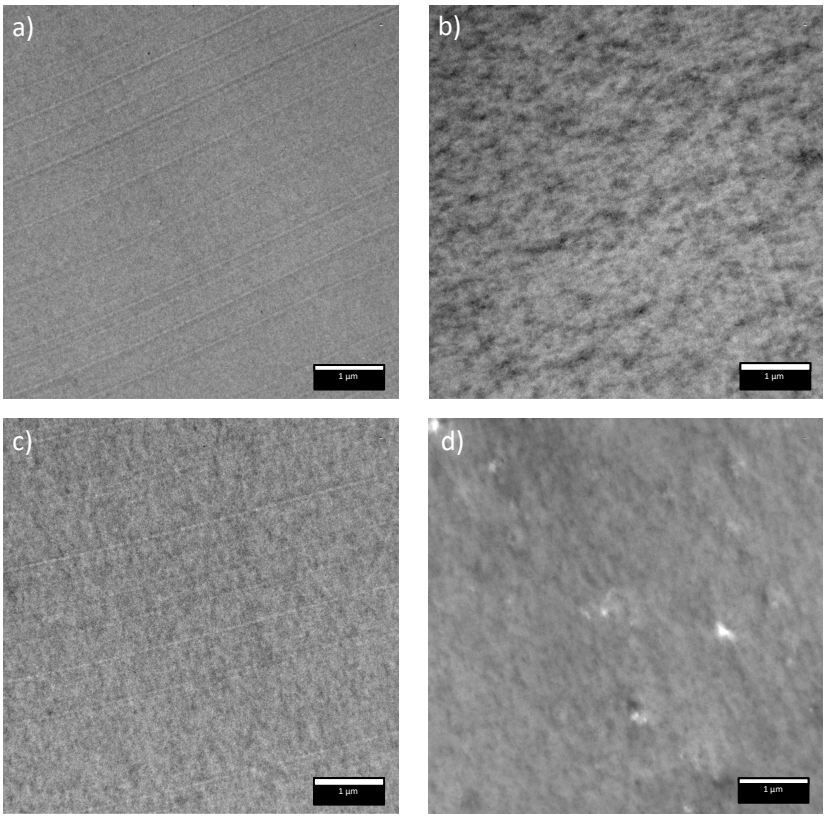

Figure 2.10. TEM images of a) copolymer: styrene 80 wt%/BisGMA 20 wt%; IPN samples with 25 wt% PU and 75 wt% acrylic copolymer with various acrylic copolymer precursors: b) IPN:

styrene 70 wt%/BisGMA 30 wt%; c) IPN: styrene 80 wt%/BisGMA 20 wt%; d) IPN: styrene 90 wt%/BisGMA 10 wt%.

2.3.4. Degree of transparency

IPN transparency was investigated using UV-Visible spectrophotometry with the results for the IPNs of varied styrene to BisGMA composition shown in Figure 2.11. Transparency is a strong function of composition as samples with 50 wt% styrene show almost no transparency while increasing styrene content leads to increasing transparency. For IPN samples with 80 wt% styrene (Figure 10.c) and 90 wt% styrene (Figure 10.d), the domain sizes are below 380 nm on average; for these samples, good transparency was observed. In the case of IPN sample with 70 wt% styrene (Figure 10.b), it shows the domain in the range of the light wavelength, and the transmittance is considerably reduced. Ultimately, samples with 80 and 90 wt% of styrene show transmittance values close to 100 % in the visible light wavelength region, indicating good compatibility between phases.

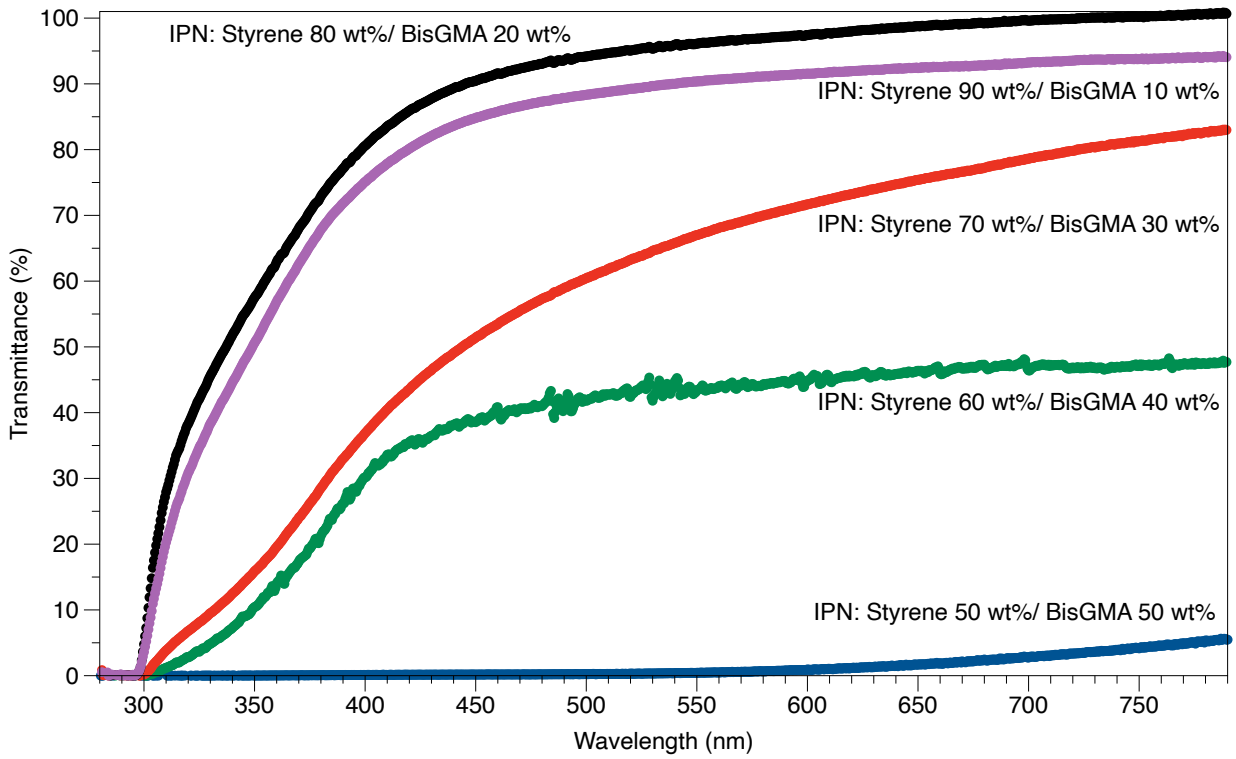

Figure 2.11. UV-Visible spectra of the IPNs with 25 wt% PU and 75 wt% acrylic copolymer with different copolymer composition.

2.3.5. Thermo-mechanical characterization

Thermo-mechanical properties of the synthesized IPNs were evaluated using DMA. Figure 2.12.a shows the storage modulus of the samples vs. temperature; samples with a higher percentage of styrene show higher initial moduli due to better compatibility between the two phases. Figure 2.12.b shows the *tan δ* results of the samples vs. temperature. The 50 wt% styrene IPN shows two peaks in *tan δ*, indicating the presence of two glass transition temperatures, and is an indication of phase separation between the polyurethane and acrylic copolymer constituents. The gap between the two peaks decreases with increasing styrene content due to the higher compatibility between the two phases. The 70 wt% styrene IPN (Figure 2.12.b) exhibits a flat peak in *tan δ*, due to improving compatibility but the remaining presence of phase separation. The IPN with 80 wt% of

the styrene shows only one peak in its *tan δ* demonstrating better compatibility between the two IPN constituents as observed with TEM and UV-Vis spectroscopy. The peak becomes sharper for the 90 wt% styrene IPN sample, further verifying enhanced phase compatibility. Broader peaks in samples with a lower percentage of styrene suggest that there are several relaxation mechanisms in the systems, which are more heterogeneous at the microscopic scale [25, 28, 40].

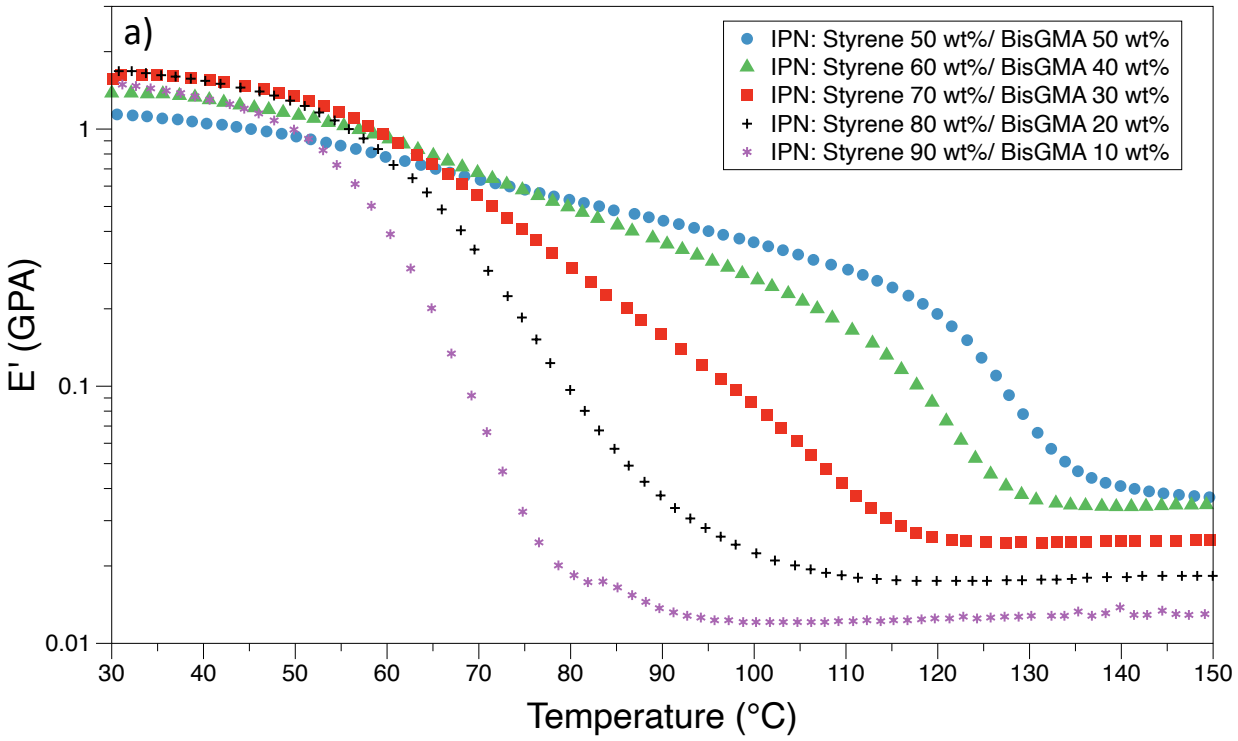
a)
IPN: Styrene 50 wt%/ BisGMA 50 wt%
IPN: Styrene 60 wt%/ BisGMA 40 wt%
IPN: Styrene 70 wt%/ BisGMA 30 wt%
IPN: Styrene 80 wt%/ BisGMA 20 wt%
IPN: Styrene 90 wt%/ BisGMA 10 wt%
E' (GPA)
1
0.1
0.01
30
40
50
60
70
80
90
100
110
120
130
140
150
Temperature (°C)

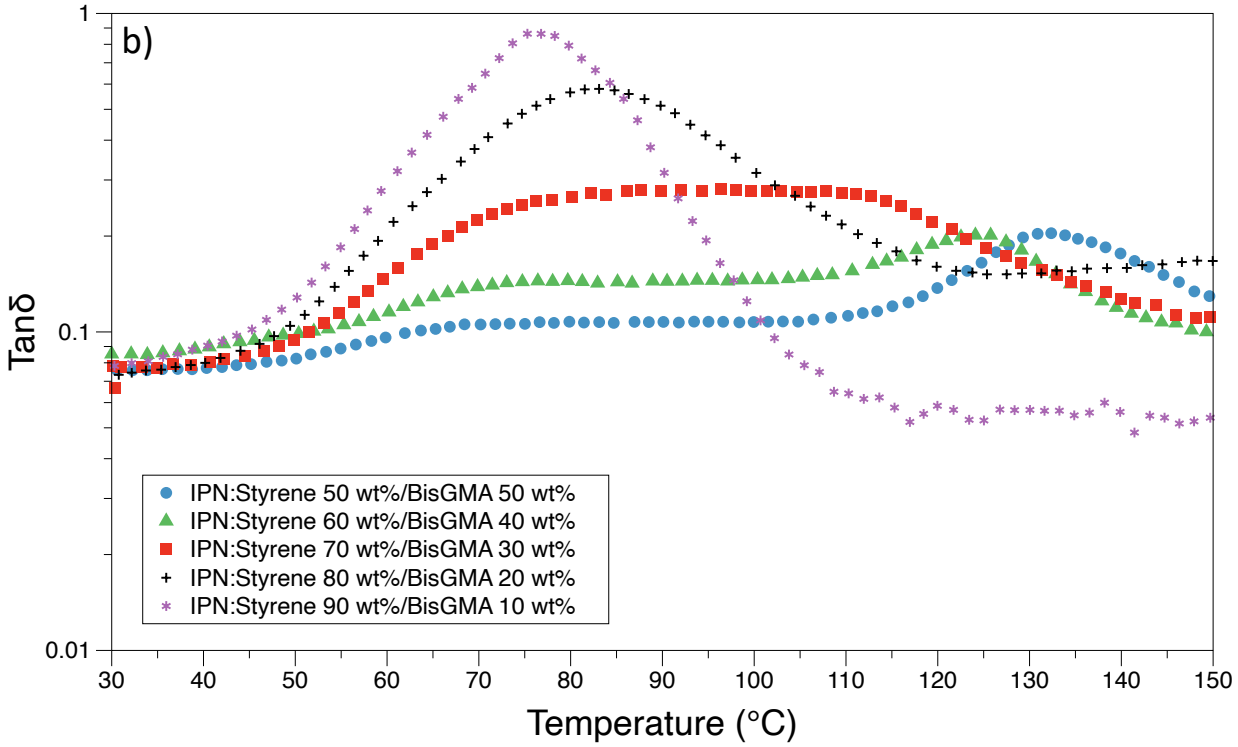
b)
IPN:Styrene 50 wt%/BisGMA 50 wt%
IPN:Styrene 60 wt%/BisGMA 40 wt%
IPN:Styrene 70 wt%/BisGMA 30 wt%
IPN:Styrene 80 wt%/BisGMA 20 wt%
IPN:Styrene 90 wt%/BisGMA 10 wt%
Tanδ
1
0.1
0.01
30
40
50
60
70
80
90
100
110
120
130
140
150
Temperature (°C)

Figure 2.12. Flexural test results a) storage modulus vs. temperature and b) *tan* δ vs. temperature for IPNs with 25 wt% PU and 75 wt% acrylic copolymer with varied acrylic copolymer precursors.

2.3.6. Fracture properties

Fracture toughness of the copolymer with 80 wt% styrene and 20 wt% BisGMA (COP80/20) and IPN with 75 wt% copolymer (80 wt% styrene) and 25 wt% PU (IPN80/20) were characterized, and a representative load vs. displacement plot is shown in Figure 2.13. Both samples show a linear elastic response up to the peak load, followed by brittle failure. IPN80/20 exhibited a higher load capacity at failure indicating enhanced fracture toughness and higher extension before brittle failure in comparison to the neat acrylic copolymer. Plane-strain fracture toughness, K_{Ic} of COP80/20 and IPN80/20 were 1.61 ±0.16 and 2.2 ±0.19 MPa.m$^{1/2}$, respectively. IPN80/20 shows approximately 40% improvement in fracture toughness compared to COP80/20 as the presence of polyurethane in the system improves the fracture properties by providing additional flexibility. Moreover, IPN80/20 shows more than 100% improvement in fracture toughness compared to virgin atactic polystyrene with 1.00 ± 0.20 fracture toughness and PMMA with 1.08 ± 0.18 MPa.m$^{1/2}$ fracture toughness [41, 42].

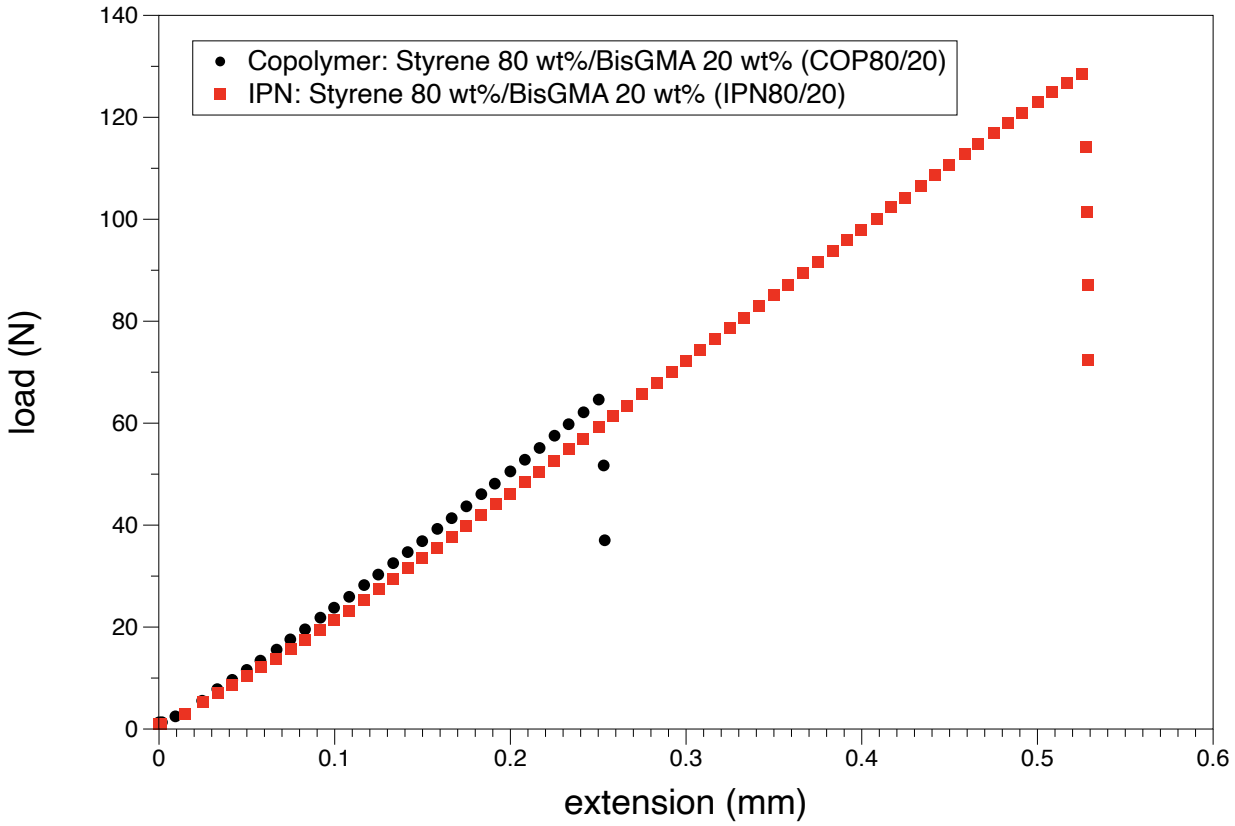

Figure 2.13. Representative load-displacement plots for acrylic copolymer and IPN with 25 wt% PU and 75 wt% acrylic copolymer.

SEM was used to investigate the fracture mechanism of the synthesized IPNs with varied acrylic network compositions. The SEM images of the fractured samples are shown in Figure 2.14. With increasing styrene content, an observable decrease in the roughness and surface area is observed, corresponding to less energy dissipation during fracture propagation. Although increasing the percentage of styrene increases the compatibility between two phases, it decreases the fracture toughness properties of the samples. Similar behavior has been observed in the literature where obtaining a rougher surface enhances the fracture toughness properties of the samples [20, 43].

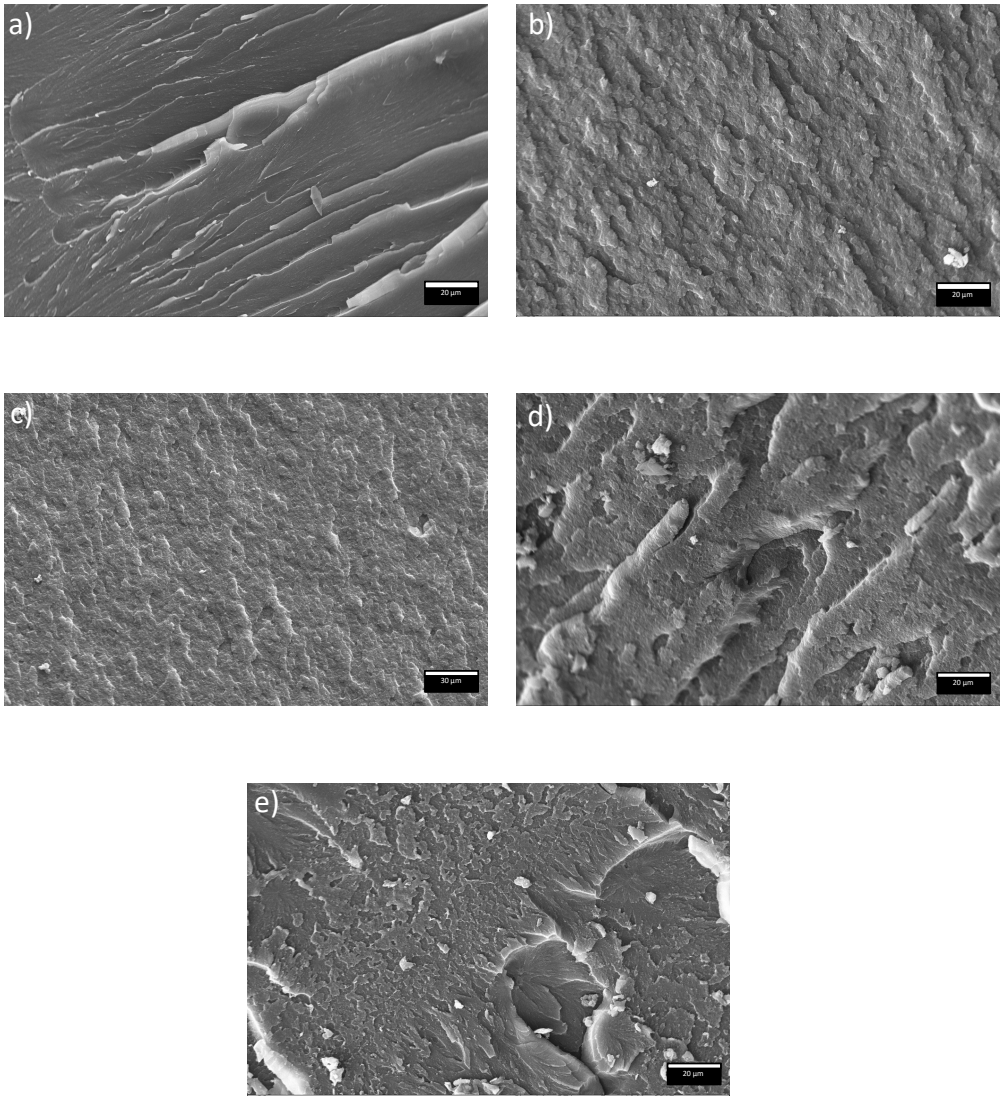

Figure 2.14. SEM images of a) copolymer: styrene 80 wt%/BisGMA 20 wt% and IPN samples with 25 wt% PU and 75 wt% acrylic copolymer with varied acrylic copolymer precursors: b) IPN: styrene 50 wt%/BisGMA 50 wt% c) IPN: styrene 60 wt%/BisGMA 40 wt% d) IPN: styrene 70 wt%/BisGMA 30 wt% e) IPN: styrene 80 wt%/BisGMA 20 wt%.

2.4. Conclusions

Acrylic-polyurethane based graft-IPNs were synthesized, and their reaction kinetics, thermo-mechanical, and optical properties were investigated. Chemical bonding between the two polymers was utilized to increase the interpenetration between two polymer networks. FTIR spectroscopy revealed complete isocyanate conversion and the formation of polyurethane linkages and chemical bonds between the two polymer networks. 1H NMR spectroscopy was also utilized to track the kinetics of polyurethane formation, and the results were found to be in good agreement with those from FTIR spectroscopy.

The interplay of IPN composition and related material properties was investigated as a function of IPN styrene content. The incorporation of the acrylic copolymer network provided higher rigidity and better thermomechanical properties to the material. In contrast, higher flexibility was imparted by the polyurethane phase, increasing the impact-resistant and the fracture toughness of the IPNs. DMA, TEM, and UV-Vis spectrophotometry results indicate that increasing the percentage of styrene into the system improves the interpenetration between two polymer networks and therefore enhances the compatibility between two polymer networks. SEM images suggest that increasing the styrene content decreases fracture toughness, as observed from the change in surface roughness upon fracture. Significant improvement was observed in fracture toughness of graft-IPN in comparison to an acrylic copolymer in graft-IPNs. Such graft-IPN with excellent transparency and fracture toughness better than PS and PMMA has considerable potential in high fracture toughness applications.

References

1. Parimal, J. P.; Gary, A. G.; Peter, G. D.; James, W. M. In *Transparent ceramics for armor and EM window applications*, Proc.SPIE, 2000.

2. Kobayashi, A.; Ohtani, N., Dynamic Fracture in Aerospace High Polymers. In *Resins for Aerospace*, American Chemical Society: 1980; Vol. 132, pp 367-377.

3. Martin, A. M. a. G., *Glass: A World History*. The University of Chicago Press: Chicago, USA,, 2002.

4. Rawson, H., *Properties and Applications of Glass*. Elsevier Scientific Publishing Co.: 1980.

5. Jajam, K. C.; Bird, S. A.; Auad, M. L.; Tippur, H. V., Tensile, fracture and impact behavior of transparent Interpenetrating Polymer Networks with polyurethane-poly(methyl methacrylate). *Polymer Testing* **2013,** *32* (5), 889-900.

6. Méndez, R. B. Sequential graft-Interpenetrating polymer networks based on polyurethane and acrylic/ester copolymers. Auburn University, Auburn, AL, 2015.

7. Sundaram, B. M.; Mendez, R. B.; Auad, M. L.; Tippur, H. V., Quasi-static and dynamic mechanical behavior of transparent graft-interpenetrating polymer networks (graft-IPNs). *Polymer Testing* **2018,** *70*, 348-362.

8. Robeson, L. M., *Polymer Blends A Comprehensive Review*. Carl Hanser Verlag GmbH & Co. KG: 2007.

9. Panapitiya, N. P.; Wijenayake, S. N.; Huang, Y.; Bushdiecker, D.; Nguyen, D.; Ratanawanate, C.; Kalaw, G. J.; Gilpin, C. J.; Musselman, I. H.; Balkus, K. J.; Ferraris, J. P., Stabilization of immiscible polymer blends using structure directing metal organic frameworks (MOFs). *Polymer* **2014,** *55* (8), 2028-2034.

10. Sperling, L. H.; Mishra, V., The current status of interpenetrating polymer networks. *Polymers for Advanced Technologies* **1996,** *7* (4), 197-208.

11. Sperling, L. H.; Klempner, D.; Utracki, L. A., *Interpenetrating polymer networks*. American Chemical Society: Washington, DC, 1994; p xvi, 638 p.

12. Dave, V. J.; Patel, H. S., Synthesis and characterization of interpenetrating polymer networks from transesterified castor oil based polyurethane and polystyrene. *Journal of Saudi Chemical Society* **2017,** *21* (1), 18-24.

13. Sheu, H. R.; El-Aasser, M. S.; Vanderhoff, J. W., Phase separation in polystyrene latex interpenetrating polymer networks. *Journal of Polymer Science Part A: Polymer Chemistry* **1990,** *28* (3), 629-651.

14. Pissis, P.; Georgoussis, G.; Bershtein, V. A.; Neagu, E.; Fainleib, A. M., Dielectric studies in homogeneous and heterogeneous polyurethane/polycyanurate interpenetrating polymer networks. *Journal of Non-Crystalline Solids* **2002,** *305* (1), 150-158.

15. Sperling, L. H., *Interpenetrating Polymer Networks and Related Materials*. Plenum Press,: New York, 1981; Vol. 12 (1).

16. Sperling, L. H., Interpenetrating polymer networks and related materials. **1977,** *12* (1), 141-180.

17. Sperling, L. H., Interpenetrating Polymer Networks: An Overview. In *Interpenetrating Polymer Networks*, American Chemical Society: 1994; Vol. 239, pp 3-38.

18. Mita, I.; Akiyama, S., Macromolecular Design of Polymeric Materials. In *PLASTICS ENGINEERING-NEW YORK*, Marcel Dekker, Inc.: 1997; pp 393-406.

19. Millar, J. R., 263. Interpenetrating polymer networks. Styrene–divinylbenzene copolymers with two and three interpenetrating networks, and their sulphonates. *Journal of the Chemical Society (Resumed)* **1960,** (0), 1311-1317.

20. Chen, C. H.; Chen, W. J.; Chen, M. H.; Li, Y. M., Simultaneous full-interpenetrating polymer networks of blocked polyurethane and vinyl ester Part I. Synthesis, swelling ratio, thermal properties and morphology. *Polymer* **2000,** *41* (22), 7961-7967.

21. Fan, L. H.; Hu, C. P.; Ying, S. K., Thermal analysis during the formation of polyurethane and vinyl ester resin interpenetrating polymer networks. *Polymer* **1996,** *37* (6), 975-981.

22. Sundararajan, S.; Samui, A. B.; Kulkarni, P. S., Interpenetrating phase change polymer networks based on crosslinked polyethylene glycol and poly(hydroxyethyl methacrylate). *Solar Energy Materials and Solar Cells* **2016,** *149*, 266-274.

23. Sibaja, B.; Matheus, C. P.; Mendez, R. B.; Vega-Baudrit, J. R.; Auad, M. L., Synthesis and Characterization of Interpenetrating Polymer Networks (IPNs) from Acrylated Soybean Oil and α-Resorcylic Acid: Part 1. Kinetics of Network Formation. *Journal of Renewable Materials* **2017,** *5* (3-4), 231-240.

24. Sibaja, B.; Matheus, C. P.; Mendez, R. B.; Farag, R.; Baudrit, J. R. V.; Auad, M. L., Synthesis and Characterization of Interpenetrating Polymer Networks (IPNs) from Acrylated Soybean Oil

α-Resorcylic Acid: Part 2. Thermo-Mechanical Properties and Linear Fracture Mechanics. *Journal of Renewable Materials* **2017,** *5* (3-4), 241-250.

25. Bird, S. A.; Clary, D.; Jajam, K. C.; Tippur, H. V.; Auad, M. L., Synthesis and characterization of high performance, transparent interpenetrating polymer networks with polyurethane and poly(methyl methacrylate). *Polymer Engineering & Science* **2013,** *53* (4), 716-723.

26. Jajam, K. C.; Tippur, H. V.; Bird, S. A.; Auad, M. L. In *Dynamic Fracture and Impact Energy Absorption Characteristics of PMMA-PU Transparent Interpenetrating Polymer Networks (IPNs)*, Dynamic Behavior of Materials, Volume 1, Cham, 2014//; Song, B.; Casem, D.; Kimberley, J., Eds. Springer International Publishing: Cham, 2014; pp 277-284.

27. Jajam, K. C.; Bird, S. A.; Auad, M. L.; Tippur, H. V. In *Development and Characterization of a PU-PMMA Transparent Interpenetrating Polymer Networks (t-IPNs)*, Dynamic Behavior of Materials, Volume 1, New York, NY, 2011//; Proulx, T., Ed. Springer New York: New York, NY, 2011; pp 117-121.

28. Ballestero, R.; Sundaram, B. M.; Tippur, H. V.; Auad, M. L., Sequential graft-interpenetrating polymer networks based on polyurethane and acrylic/ester copolymers. *Express Polymer Letters* **2016,** *10* (3), 204-215.

29. Hillerström, A.; Andersson, M.; Pedersen, J. S.; Altskär, A.; Langton, M.; van Stam, J.; Kronberg, B., Transparency and wettability of PVP/PDMS-IPN synthesized in different organic solvents. *Journal of Applied Polymer Science* **2009,** *114* (3), 1828-1839.

30. Qin, C.-L.; Cai, W.-M.; Cai, J.; Tang, D.-Y.; Zhang, J.-S.; Qin, M., Damping properties and morphology of polyurethane/vinyl ester resin interpenetrating polymer network. *Materials Chemistry and Physics* **2004,** *85* (2-3), 402-409.

31. Alizadeh, N.; Bird, S. A.; Mendez, R. B.; Jajam, K. C.; Alexander, A. C.; Tippur, H. V.; Auad, M. L., Chapter 11 - Synthesis and Characterization of High Performance Interpenetrating Polymer Networks With Polyurethane and Poly(methyl methacrylate). In *Unsaturated Polyester Resins*, Elsevier: 2019; pp 243-255.

32. Bird, S. A. Interpenetrating Polymer Networks with Polyurethane and Methacrylate-based Polymers. Auburn University, Auburn, AL, 2013.

33. Huang, J.; Zhang, L., Effects of NCO/OH molar ratio on structure and properties of graft-interpenetrating polymer networks from polyurethane and nitrolignin. *Polymer* **2002,** *43* (8), 2287-2294.

34. Kato, K., Osmium tetroxide fixation of rubber latices. *Journal of Polymer Science Part B: Polymer Letters* **1966,** *4* (1), 35-38.

35. ASTM D5045-14, Standard Test Methods for Plane-Strain Fracture Toughness and Strain Energy Release Rate of Plastic Materials, ASTM International, West Conshohocken, PA, 2014.

36. Pavia, D. L.; Lampman, G. M.; Kriz, G. S., *Introduction to spectroscopy, Third edition*. Thomson Learning: Washington, 2001.

37. Cateto, C. A.; Barreiro, M. F.; Rodrigues, A. E., Monitoring of lignin-based polyurethane synthesis by FTIR-ATR. *Industrial Crops and Products* **2008,** *27* (2), 168-174.

38. Anslyn, E. V.; Dougherty, D. A.; Sausalito, C. U. S., *Modern physical organic chemistry*. University Science Books www.uscibooks.com: CA, 2006.

39. Chakrapani, S. B.; Minkler, M. J.; Beckingham, B. S., Low-field 1H-NMR spectroscopy for compositional analysis of multicomponent polymer systems. *Analyst* **2019,** *144* (5), 1679-1686.

40. Auad, M. L.; Aranguren, M.; Borrajo, J., Epoxy-based divinyl ester resin/styrene copolymers: Composition dependence of the mechanical and thermal properties. *Journal of Applied Polymer Science* **1997,** *66* (6), 1059-1066.

41. Serrano, A.; Welsch, G.; Gibala, R., Fracture toughness and fatigue of polystyrene, polyphenylene oxide and their blends. *Polymer Engineering & Science* **1982,** *22* (15), 946-949.

42. Choi, S. R.; Salem, J. A., Fracture toughness of PMMA as measured with indentation cracks. *Journal of Materials Research* **1993,** *8* (12), 3210-3217.

43. Hsieh, K. H.; Han, J. L.; Yu, C. T.; Fu, S. C., Graft interpenetrating polymer networks of urethane-modified bismaleimide and epoxy (I): mechanical behavior and morphology. *Polymer* **2001,** *42* (6), 2491-2500.

Chapter 3
Mechanical performance of vinyl ester-polyurethane interpenetrating polymer network composites

3.1. Introduction

Polymers exhibit a range of characteristics, such as high impact and tensile strength, that are beneficial for a wide variety of applications [1-4]. Polymeric systems with novel properties can be obtained by combining different polymeric materials [5]. The new material is known as a multicomponent polymeric material, examples of which include blends, graft copolymers, block copolymers, and crosslinked copolymers [6]. The low compatibility of polymer networks, however, can be a significant challenge to the creation of these new multicomponent polymers as most polymer blends have low miscibility, making it very difficult to synthesize homogenous mixtures [7].

Interpenetrating polymer networks (IPNs), consisting of at least one polymer network in the presence of another polymer, are one class of polymer blend that restricts phase separation and thus increases the compatibility of the polymers in its mixture [4, 8, 9]. The polymer networks in the IPN can be connected via physical entanglement, and it is not always necessary for them to be chemically bonded to each other [10]. The physical bonds are enough to hold them together, just as in other polymer blends.

There are three main types of IPNs: semi-interpenetrating polymer networks, full-interpenetrating polymer networks, and graft-interpenetrating polymer networks. In semi-IPNs, one polymer is crosslinked while the other one is a linear, branched, or graft copolymer [6, 10]. In full-IPNs, both polymers are chemically crosslinked, although physical entanglements also contribute to the network formation [6, 10]. The polymers in graft-IPNs are both crosslinked, and they bond together

via chemical bonds. Therefore, in graft-IPNs, both physical entanglements and chemical crosslinking link the polymers together, thereby increasing the compatibility between the two phases. As a result, graft-IPNs are a combination of graft copolymers and IPNs [6, 10]. IPNs can be further broken up into simultaneous or sequential IPNs based on the synthesis mechanism employed. Pissis and co-workers studied the phase separation in semi- and full-IPNs consisting of polyurethane and polyisocyanurate. The results showed a homogenous product of both IPNs, although a heterogeneous mixture was observed at the nano and microscale [11]. Bird et al. investigated the degree of transparency and compatibility of polyurethane and polymethyl methacrylate (PMMA) in IPN form [12]. Their results indicated that using the sequential method for synthesizing the IPN reduced the degree of phase separation and therefore increased the transparency of the samples. The full-IPN synthesized by the group showed potential use for applications where high impact resistance is required due to the presence of the polyurethane [12]. Dave et al. synthesized an IPN using polyurethane and polystyrene [13]. No phase separation was observed in their samples, and better thermal stability was achieved by utilizing the polyurethane-based IPN compared to just the neat polystyrene. Ballestero and co-workers [14], as well as Sundaram et al. [15] studied the properties of the graft-IPNs containing polyurethane and PMMA. An improvement in phase separation was also observed due to the chemical bonds generated between the two polymer networks. They also concluded that high fracture toughness made this specific IPN a good candidate for applications where transparency, as well as high fracture toughness, are critical.

The main advantage of IPNs is the ability to design desirable materials for a specific application [16]. As IPNs are comprised of networks of polymers that are at least partially interlaced, the resultant properties of a synthesized IPN are dependent on their constituent polymers [16]. For example, an

IPN comprising a stiff polymer and a flexible polymer exhibit elastic properties that are intermediate between the two constituents. As a result, different amounts of each constituent can be used to influence the resultant IPN properties, allowing IPNs to be potential materials for a wide range of applications [17]. IPNs show promise for use in demanding fields, such as military and aerospace [4]. One proposed usage of IPNs is to create transparent materials that exhibit high strength and toughness that can be used for bullet-proof glass, canopies, face shields, protective structures, and transparent armored vehicles [14]. Pater and Hansen have patented a semi-IPN that exhibits a favorable balance between processability, toughness, and mechanical performance [18]. Their work implies that, in addition to customizing mechanical properties, the processing ability can be customized as well. For aerospace applications where challenging manufacturing environments exist, specific IPNs can be synthesized to overcome these hurdles and mitigate manufacturing errors. IPNs can also be used for less demanding applications such as noise and vibration damping [19], ion exchange [20], and adhesives [21]. Another potential application of IPNs is in the development of fiber reinforced composites with enhanced strength and toughness.

Composite materials comprise two or more constituents that have been physically combined to produce a new material whose properties are unique to, and often better than, those of its constituents [22, 23]. Polymer matrix composites (PMCs) have found widespread use due to their relatively easy manufacturing process, tailorable properties, and their relatively low cost when compared to metal and ceramic matrix composites [24, 25]. PMCs are utilized in aerospace and civil engineering, in recreational applications, and even in the biomedical industry [26-29]. Examples of PMC usage in the aerospace industry include Sierra Nevada's Dream Chaser space plane, which uses PMCs for primary and secondary structures, and SpaceX's Falcon Heavy's fairing, which is made entirely of PMCs [30].

Continuous fiber PMCs are ideal for applications where strength, weight, and thermomechanical stability are critical. Most notable are carbon fiber composites which exhibit a wide range of attractive properties such as high specific strength and specific stiffness, as well as good fatigue and creep resistance [24, 31, 32]. Much like an IPN, the resultant properties of composite materials can be customized based on the matrix and reinforcement materials chosen.

Traditionally, thermoset polymers such as epoxies, vinyl esters, and polyimides, with relatively high thermomechanical properties, have been used as the matrix material for carbon fiber composites [33-35]. The work presented here evaluates the potential of using IPNs as the matrix material for high-strength carbon fiber composites. Specifically, an IPN that is a mixture of a brittle commercial vinyl ester and a more ductile polyurethane (PU) was studied to ascertain the effect of the more ductile PU phase on the overall composite properties. While previous studies have explored the use of IPNs as the matrix material for short carbon- and glass-fiber composites [36, 37], the work presented here is the first demonstration and evaluation of an IPN laminate composite reinforced with woven carbon fibers. Methods of IPN synthesis and composite fabrication were investigated, and the mechanical and thermomechanical response of the resulting composites characterized.

3.2. Experimental

3.2.1. IPN synthesis

The IPN investigated in this study consisted of polyurethane (PU) as the continuous phase and an acrylic copolymer of epoxy vinyl ester and styrene dispersed in the PU phase. Two different components with hydroxyl groups were used to synthesize the PU phase. 2-ethyl-2-(hydroxymethyl)-1,3propanediol (Acros Organics, USA) was used as a TRIOL (MW = 134.18

g/mol) while poly (tetramethylene ether) glycol), PTMG, (MW ≈ 1400 g/mol, Aldrich, USA) was used as a diol. Hexamethylene diisocyanate, DCH, (TCI, Japan) served as the cyanate group that reacted with the hydroxyl groups. Dibutyltin dilaurate, DBTDL, and triphenylbismuth, TPB, (Pfaltz & Bauer, USA and Alfa Aesar, USA, respectively) were used as the catalysts for the polyaddition polymerization reaction of PU.

A commercially available vinyl ester resin containing 45 wt% styrene (Ashland Inc., USA) was used as the copolymer phase. The total percentage of styrene in the copolymer was further increased to 70 wt% by adding an additional amount of styrene (Alfa Aesar, USA) to the vinyl ester. The addition of styrene decreases phase separation between the vinyl ester and polyurethane, therefore enhancing the final properties of the composite [13]. 2,2'-azobis(2-methyl-propionitrile), AIBN, (Matrix Scientific, USA) served as the thermal initiator of the chain-growth polymerization at a temperature of 60°C.

To synthesize the IPN, the TRIOL and PTMG were first heated to 60°C. The molten TRIOL and PTMG with stoichiometric amounts were then mixed using a magnetic stirrer. Once the mixture was completely mixed, it was allowed to cool to room temperature to avoid any premature reaction. Isocyanate was then added to the mixture. The commercial vinyl ester and styrene were mixed in a separate beaker, to which 1 wt% AIBN was dissolved. Both solutions were then mixed. DBTDL and TPB were then added to the system as the catalyst for the PU phase. The final IPN contained 75 wt% of the acrylic copolymer and 25 wt% PU.

Two control matrix materials were also analyzed in this study. These controls were used to isolate the effect of the two-phase matrix system on fiber-matrix adhesion and mechanical performance. The first control matrix was an unaltered commercial vinyl ester (Vinyl ester). In contrast, the

second control (Vinyl ester - styrene) contained a copolymer matrix of the commercial vinyl ester mixed with styrene in a 70:30 ratio.

3.2.2. IPN matrix analysis

An AR-G2 TA Universal Rheometer with cone and plate geometry (60 mm diameter, 1º angle) was utilized to measure the rheological properties of the matrix materials at different shear rates. Steady-state flow tests were performed at 25ºC within 1- 50 s^{-1}shear rates.

Fourier transform infrared spectroscopy (FTIR) analysis was performed using a Nicolet 6700 FTIR Spectrometer from Thermo Scientific (USA). The attenuated total reflection (ATR) infrared mode was utilized for this purpose, and the FTIR analysis was conducted within a wave number range of 400-4000 cm^{-1}, with 64 scans and 2 cm^{-1} resolution.

A TA Instruments DSCQ2000 was used to perform differential scanning calorimetry (DSC) experiments. Four samples (5-10 mg of each) of the IPN matrix and its monomers, with different curing profiles, were evaluated; uncured monomers, monomers cured for 24 hours at 40ºC, monomers cured for 24 hours at 60ºC, and the IPN polymer post-cured for 24 hours at 80ºC. Each sample was first equilibrated at 25ºC for 5 minutes, then heated to 200ºC at a rate of 5°C/min in a nitrogen atmosphere. The enthalpy of curing and onset for curing were recorded for each sample. The percentage cure for each sample was determined using equation 3.1:

$$Percentage\ cure\ (\%) = \frac{\Delta H_{\mathrm{rxn}}{}^{0} - \Delta H_{\mathrm{rxn}}}{\Delta H_{\mathrm{rxn}}{}^{0}} \times 100 \qquad [3.1]$$

where $\Delta H_{\mathrm{rxn}}{}^{0}$ is the enthalpy of reaction for the IPN monomers without previous curing, and ΔH_{rxn} is the enthalpy of reaction for the IPN samples with different curing profiles.

Dynamic mechanical analysis (DMA) was used to measure the storage modulus (*E'*) and glass transition temperature (T_g) of the IPN matrices and composites. A TA Instruments RSA-G3 was used for this purpose. Rectangular specimens of dimensions 25 mm × 9.6 mm × 2.5 mm were subjected to 3-point bend testing (25 mm support span) and oscillated at 0.1% maximum strain as per ASTM 1640-13 [38]. The storage moduli of the matrix materials were determined as the *E'* value in the glassy region during a temperature ramp from 0°C to 200°C at 5°C/min at 1 Hz. The glass transition temperature was obtained from the temperature value at the peak of *tan δ*, and evaluated at 1 Hz, 10 Hz, and 50 Hz to evaluate the damping properties of each material. Damping is a measure of the rate at which each material can dissipate the energy. Therefore, a higher rate of dissipating energy in a material indicates better damping properties [39, 40]. The temperature range for which *tan δ* > 0.2 was used to evaluate the damping properties of the matrix and composite materials.

3.2.3. IPN composite fabrication and quality evaluation

After evaluating several composite manufacturing methods, a simple hand layup process was adopted to fabricate the IPN composites. Laminates were manufactured using eight plies of 5 oz. plain weave carbon fiber (U.S. Composites, Inc., USA) with dimensions of 127 mm × 127 mm. First, an aluminum baseplate was sprayed with a mold release agent. A base layer of peel ply was then placed on the mold release-coated baseplate to aid in laminate removal post-cure. The carbon fiber plies were then placed on the base plate with IPN matrix material applied liberally and uniformly between the plies to ensure complete wet out of the fabric.

The fully wet-out layup was then covered with a second layer of peel ply and vacuum bagged to prevent styrene evaporation during the curing process. No vacuum was applied during cure,

however. A steel plate was then set on top of the layup to compress and consolidate the plies, see Figure 3.1. The cure cycle utilized for the IPN composite (and controls) was 24 hours at 40°C, followed by 24 hours at 60°C, and then 24 hours at 80°C. After curing, the carbon fiber/IPN composite laminates were sectioned into rectangular specimens for mechanical characterization.

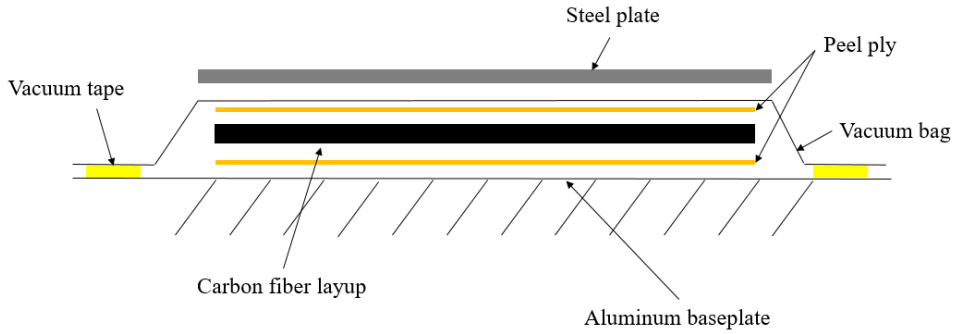

Figure 3.1. Simple hand layup method for fabricating vinyl ester - polyurethane IPN composite.

Specimens produced using this simple hand layup technique were fully compacted and had good adhesion between plies. Finished specimens also had minimum excess cured resin around the edges, indicative of the correct amount of resin being used. Final specimen thickness was consistent at 2.0 - 2.5 mm.

3.2.4. Mechanical testing

Flexural and tensile tests were performed on the IPN and control composites to examine the effect of the matrix on composite properties. Three-point-bend flexural test specimens were prepared with dimensions of 90 × 12.5 mm. Flexural tests were performed under displacement control using a screw-driven 5 kN Instron load frame (Model 5565) with a support span of 63 mm, as per ASTM D7264 [41]. Specimens were loaded at a constant displacement rate of 3 mm/min. Load and

displacement data were collected at 0.1 second intervals. Flexural strength (σ_f) and modulus (E_f) were calculated as per the ASTM standard.

Tensile test specimens were prepared with gage dimensions of 70 mm × 12 mm. Fiber-glass tabs were attached to each tensile specimen to minimize stress concentrations at the tensile grips. Tensile tests were performed under displacement control using a servo-hydraulic 100 kN Instron load frame (Model 1321), as per ASTM D3039 [42]. Specimens were loaded at a constant displacement rate of 2 mm/min. Load and displacement data were collected at 0.1 second intervals. Strain (ε) was measured via a 25.4 mm gauge length extensometer attached to the specimens using built-in clips. Ultimate tensile strength (σ_{ult}) was calculated from the maximum load attained by the specimens. Elastic modulus (E) was calculated from the linear portion of the stress-strain curve between 0.1% and 0.3% strain.

3.2.5. Surface morphology analysis

Scanning electron microscope (SEM) images of the composite specimens after testing were acquired using a Zeiss EVO50 variable pressure SEM with digital imaging and energy dispersive spectroscopy. Composite specimens were sputter-coated with gold using an EMS 550X auto sputter coater.

3.3. Results and discussion

3.3.1. Rheological properties of the matrix

The rheological properties of the vinyl ester, vinyl ester-styrene, and IPN matrix materials are summarized in Figure 3.2. Each material type exhibited a linear relationship between viscosity and shear rate. These results indicate the Newtonian behavior of the monomers before curing. The

vinyl ester matrix showed the highest viscosity (0.104 Pa.s) due to the lower percentage of styrene present in the system. The viscosity of the vinyl ester-styrene sample, however, was lower at 0.004 Pa.s due to the extra amount of styrene present in the system. Styrene is a small molecule that decreases the viscosity of monomers. The viscosity of the IPN matrix was 0.02 Pa.s, which is higher than vinyl ester-styrene. The addition of PTMG (MW ≈ 1400 g/mol) to the system is the most likely cause of the increase in viscosity. The viscosity of the IPN is lower than the vinyl ester monomers, however, indicating the significant impact of the additional styrene on decreasing the viscosity of the IPN precursors.

Lee et al. [43] also observed Newtonian behavior in polymer matrix composites consisting of pure polypropylene tested at low shear rates. However, the viscosity of the polymer matrix was determined to be on the order of 10^3-10^4 Pa.s, which is higher than the viscosity of the polymer matrix examined in our work. The lower viscosity of the polymer matrix makes the manufacturing process of the composite much easier and, therefore, more desirable. Xiao et al. [44] examined the viscosity of polyethylene matrix composites with different percentages of carbon nanotubes. Newtonian behavior was observed for pure low-density polyethylene tested at shear rates lower than 10 s^{-1}. The viscosity number was reported as 10^3 Pa.s. Their result also highlights the improved manufacturing capabilities offered by the IPN matrix utilized in this current work.

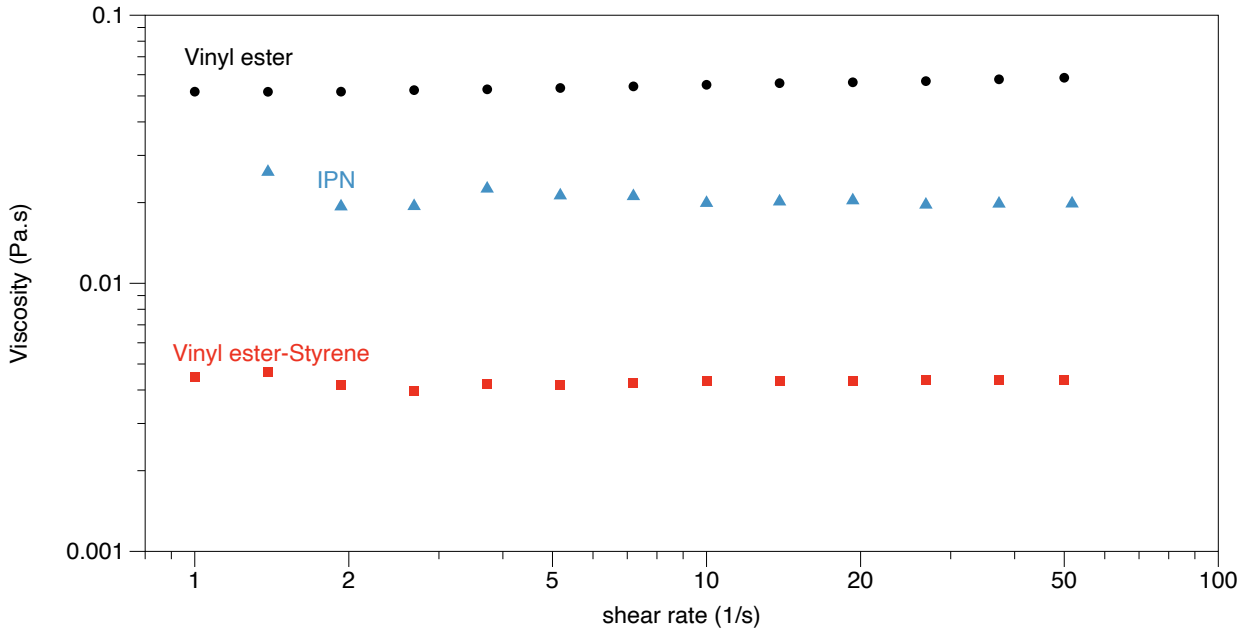

Figure 3.2. Viscosity behavior of IPN matrix material before curing as a function of the shear rate.

3.3.2. Analysis of matrix crosslinking via FTIR measurements

The FTIR technique was utilized to verify the successful synthesis of the vinyl ester, vinyl ester-styrene, and IPN matrix materials. In Figure 3.3, the FTIR spectra of vinyl ester, vinyl ester-styrene, and the IPN matrix before and after curing are illustrated. For the vinyl ester and vinyl ester-styrene matrix materials (Figure 3.3.a and Figure 3.3.b, respectively), the peaks circa 777 and 908 cm^{-1} can be attributed to out-of-plane (oop) bending of =C-H bonds. The intensity of these two peaks decreases after curing due to free radical polymerization between the double bonds. The peak around 1627 cm^{-1} belongs to the stretch of the C=C bond and disappears after curing, also due to the free radical polymerization that occurs. These results confirm the successful polymerization of the vinyl ester [45].

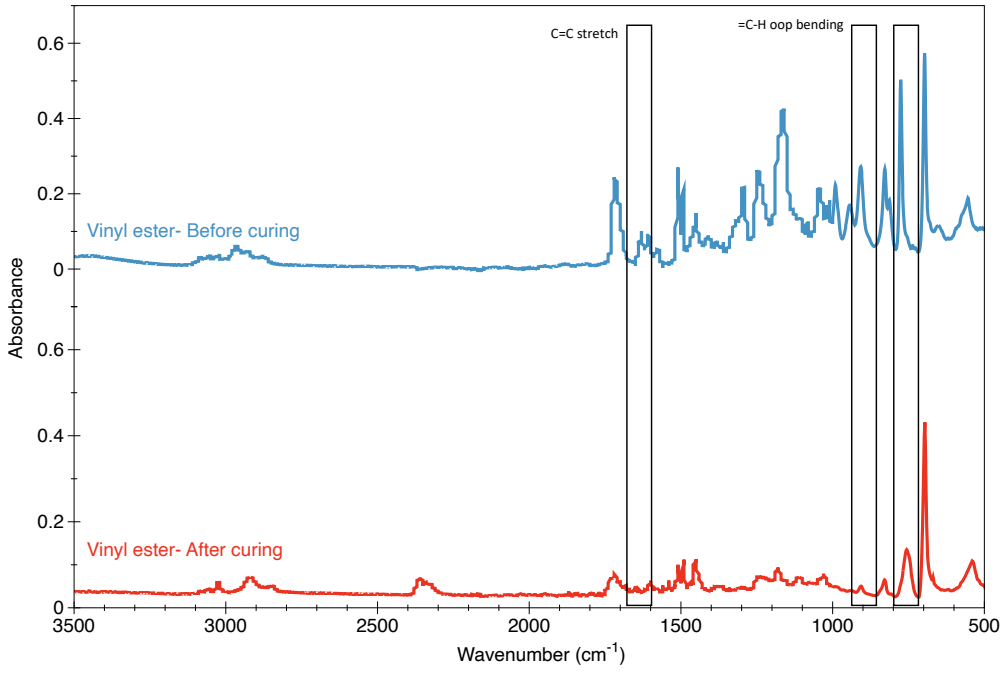
C=C stretch
=C-H oop bending
Vinyl ester- Before curing
Vinyl ester- After curing
Absorbance
Wavenumber (cm-1)

a)

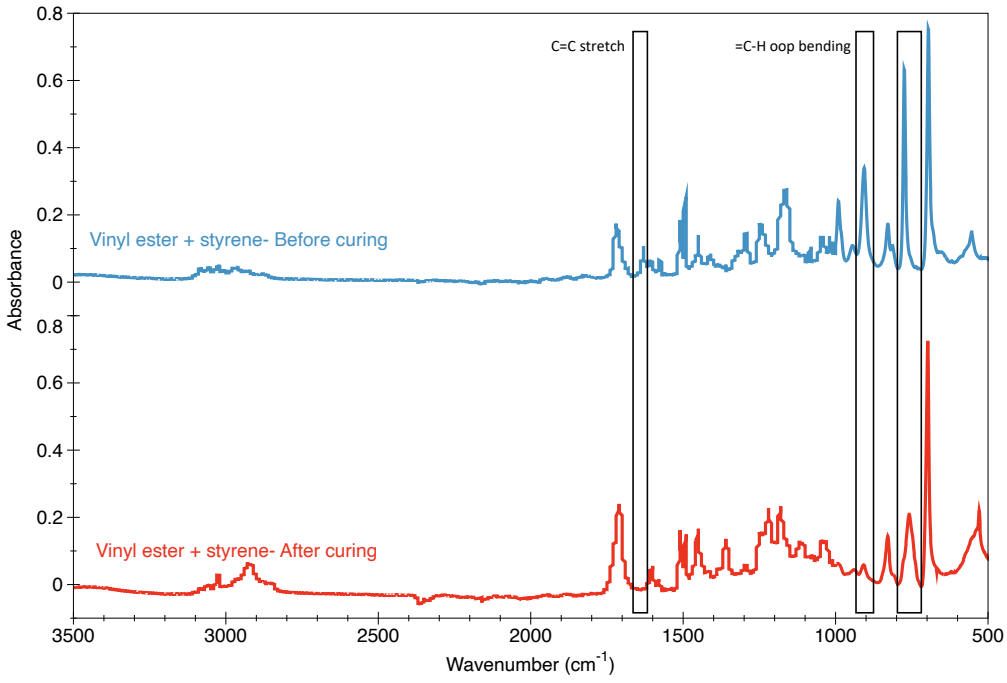
C=C stretch
=C-H oop bending
Vinyl ester + styrene- Before curing
Vinyl ester + styrene- After curing
Absorbance
Wavenumber (cm-1)

b)

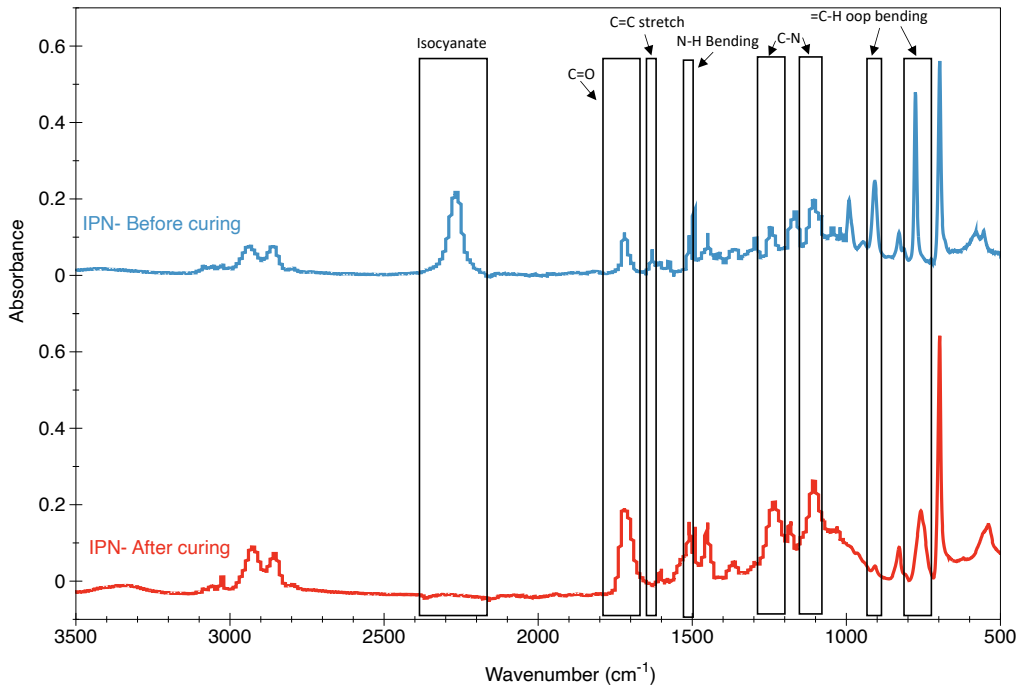

c)

Figure 3.3. FTIR spectra of IPN matrix materials before and after curing a) vinyl ester b) vinyl ester - styrene and c) vinyl ester - polyurethane IPN.

Figure 3.3.c shows the FTIR spectra of the IPN matrix before and after curing. Before curing, the peak between 3400 and 3500 cm^{-1} belongs to the hydroxyl groups of the PU precursors. This peak then shifts to a lower wavenumber after curing the hydroxyl groups and isocyanate group to form the amine groups. The peak at 2264 cm^{-1} belongs to the isocyanate peak, which also disappears after the polymerization process. The disappearance of this peak confirms the successful polymerization of PU in the system. The peak at 1721 cm^{-1} belongs to the carbonyl group and increases due to the formation of PU. The peak at 1627 cm^{-1} belongs to the C=C group, which also disappears due to the polymerization of the vinyl ester; a peak at 1618 cm^{-1} is also seen in a 20% PU-IPN prepared by Suresh and coworkers [46]. The peak at 1507 cm^{-1}, belonging to the bending of N-H, increases after curing due to the formation of PU. Peaks at 1224 cm^{-1} and 1107 cm^{-1} belong

to C-N, and these also increase after curing. Finally, peaks at 905 cm^{-1} and 777 cm^{-1} belong to the out-of-plane (oop) bending of =C-H, and decrease due to successful polymerization of the acrylic copolymer [45].

3.3.3. Analysis of matrix crosslinking via DSC analysis

The successful polymerization of each phase in the IPN system was examined via DSC experiments. A summary of the results are shown in Table 3.1. The enthalpy of the reaction decreases with increasing time and temperature due to curing of the two phases in the IPN, and the onset temperature also begin shifting to higher temperatures for the same reason. The percentage cure shows a similar trend to that observed via FTIR and confirms that the polymers achieve approximately 100% cure at the end of the curing process.

Table 3.1. DSC results for IPN matrix showing enthalpy of reaction and percentage cure.

Cure profile	ΔH_{rxn} **(J/g)**	T_{rxn} **(°C)**	**Percentage cure (%)**
None	284.7	58.9	0
24 hrs at 40ºC	50.3	64.3	82.3
24 hrs at 60ºC	17.2	76	94.0
24 hrs at 80ºC	1.5	100	99.5

ΔH_{rxn}: Enthalpy of reaction
T_{rxn}: Onset temperature

3.3.4. Dynamic mechanical analysis of IPN matrix and composites

The effects of matrix composition on the thermomechanical, as well as damping properties, were evaluated via DMA at 1, 10, and 50 Hz. A summary plot of *tan δ* as a function of temperature for the matrix materials and composites, at a frequency of 1 Hz, is shown in Figure 3.4. Here, the shifts in glass transition temperature based on matrix composition and the addition of the carbon fiber reinforcement are highlighted. Figure 3.5 illustrates the dependence of *tan δ* on temperature and frequency for vinyl ester - styrene and IPN, both matrix and composite materials. These plots indicate that as frequency increases, there is a corresponding increase in glass transition temperature and the temperature range for *tan δ* > 0.2. The rise in glass transition temperature is expected based on the Arrhenius dependence; $\omega = \omega_0 \, e^{\Delta H/RT}$ where R is the gas constant, ω_0 is a constant of the system, ω is the frequency, and ΔH is the activation energy for the polymer chain segments [40, 47]. Additionally, the increase in the temperature range for which *tan δ* > 0.2 can be explained by the overlap between glass transition and β relaxation, which both increase with increasing frequency [48]. In Table 3.2, the storage modulus (E'), glass transition temperature (T_g), and damping properties of the three matrix materials and their respective composites, evaluated at 1, 10, and 50 Hz, are summarized.

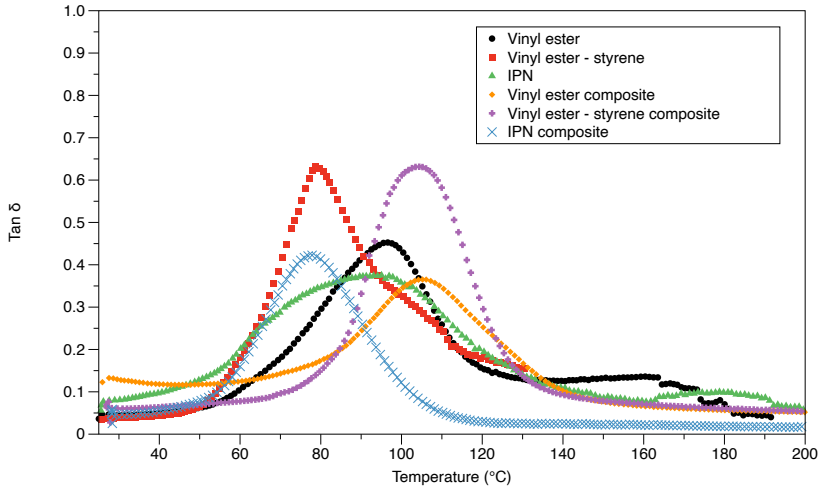

Figure 3.4. Representative plots of *tan δ* as a function of temperature for IPN matrices and composites, evaluated at a frequency of 1 Hz.

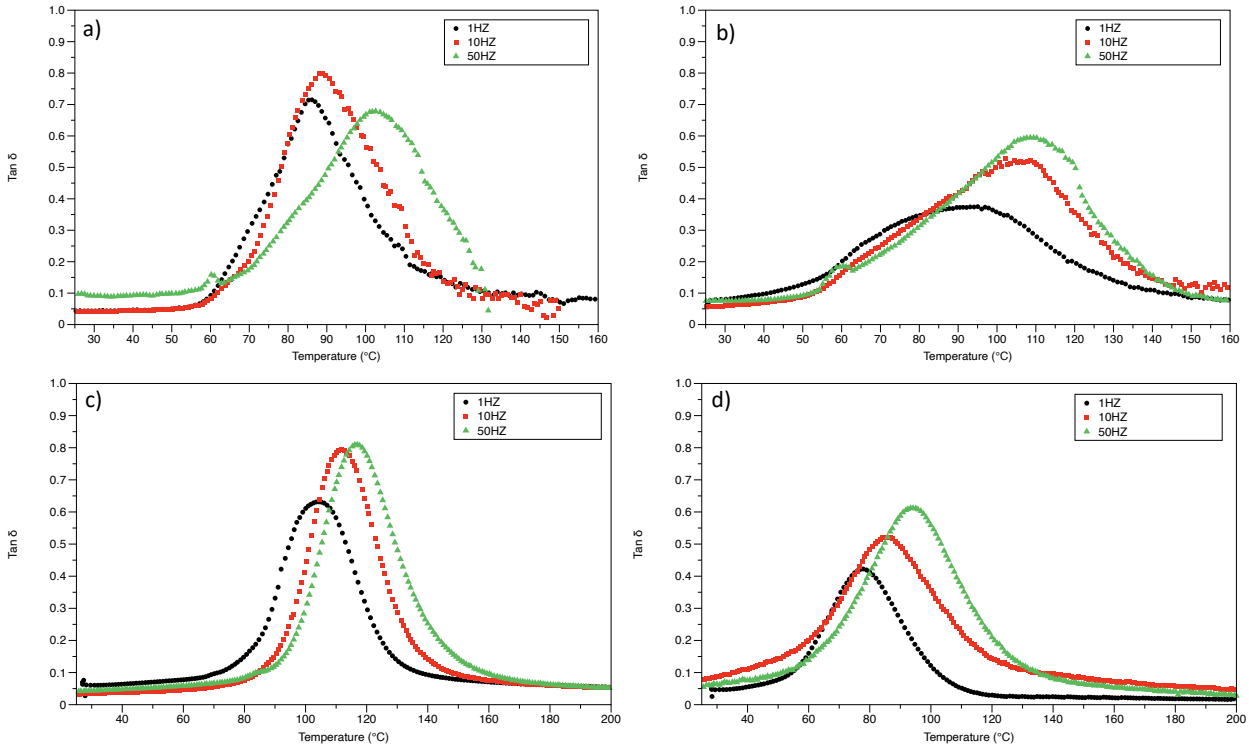

Figure 3.5. Comparison of *tan δ* as a function of temperature at different frequencies for IPN matrix and composite a) vinyl ester - styrene matrix b) vinyl ester - polyurethane IPN matrix c) vinyl ester - styrene composite and d) vinyl ester - polyurethane IPN composite.

As expected for the matrix materials, vinyl ester has the highest glass transition temperature and storage modulus among the three matrices at all frequencies investigated. Vinyl ester - styrene exhibits a lower glass transition temperature and storage modulus in comparison to vinyl ester. As discussed by Auad et al., higher free volume and mobility due to the presence of styrene is a possible reason for the lower glass transition temperature [49]. At 1 and 10 Hz, the storage modulus of the IPN matrix is lower than that of the vinyl ester- styrene due to the higher flexibility of PU. The glass transition of the IPN matrix measured at 1 Hz is essentially the same as that of vinyl ester- styrene but is the lowest of the three matrices when evaluated at the higher frequencies of 10 and 50 Hz. Significant improvements in both storage modulus and glass transition temperature, at all frequencies, were observed for all the composites reinforced with the high modulus, woven carbon fibers, as can be seen in Table 3.2.

Table 3.2. DMA characterization results of IPN matrix and composites evaluated at 1, 10 and 50 Hz.

Material	**1 Hz**			**10 Hz**			**50 Hz**		
	E'	***T_g***	**Range**	***E'***	***T_g***	**Range**	***E'***	***T_g***	**Range**
Matrix									
VE	2.8	93.9	36.7	2.9	102.9	47.4	3.1	108.3	57.1
VE-S	2.4	81.5	53.3	2.6	88.8	45.4	2.3	102.6	55.8
IPN	1.9	83.9	66.7	2.4	85.5	69.1	2.3	92.8	68.0
Carbon fiber composite									
VE	7.1	105.2	41.4	11.9	110.3	46.6	16.8	115.3	49.9
VE-S	14.1	103.5	40.6	16.7	110.9	41.7	10.0	116.1	47.3

IPN	9.3	79.2	37.9	12.0	85.9	40.7	21.6	92.8	42.2

VE: Vinyl ester
VE-S: Vinyl ester – styrene
IPN: Vinyl ester- polyurethane Interpenetrating Polymer Network
E': Storage modulus (GPa)
T_g: Glass transition temperature (°C)
Range: Temperature range over which $tan\ \delta > 0.2$ (°C)

The damping properties of each matrix material and its composite were assessed based on the temperature range over which $tan\ \delta > 0.2$. The results are summarized in Table 3.2. At all frequencies investigated, the temperature range for the matrix increases with the synthesis of the IPN from the brittle vinyl – ester copolymer and ductile PU. This increase shows the enhanced ability of the IPN matrix to dissipate energy due to the low storage modulus and flexibility of PU. The composites, however, exhibit a lower temperature range at which $tan\ \delta > 0.2$. There is also no significant difference observed in the damping properties among the composites, possibly due to the dominant stiffness of the carbon fibers.

3.3.5. IPN composite flexural properties

Flexural testing was performed on the IPN composites, as well as the controls. Representative plots of stress versus strain for the flexural tests of the IPN composites and controls are illustrated in Figure 3.6.a. Each composite exhibits linear elastic behavior followed by brittle fracture and subsequent failure characteristic of woven, continuous carbon fiber composites. Flexural properties are summarized in Figure 3.6.b. All three composite types exhibited similar flexural strengths, between 280 and 286 MPa, within error. The flexural modulus of the vinyl ester and IPN composites were also comparable. This behavior illustrates that the addition of polyurethane to the matrix system does not adversely affect flexural properties. The flexural strength and

modulus of these carbon fiber/IPN composites are higher than similarly prepared carbon fiber/epoxy control specimens, such as those produced by Kim et al [50]. The vinyl ester–styrene composite, however, exhibited lower flexural modulus compared to the other two composites. This result was not expected and may be due to the presence of internal material defects, such as voids or reduced fiber-matrix adhesion, within the composite specimens. Future work will seek to further enhance the flexural properties of the IPN composites by optimizing the matrix composition and composite fabrication process.

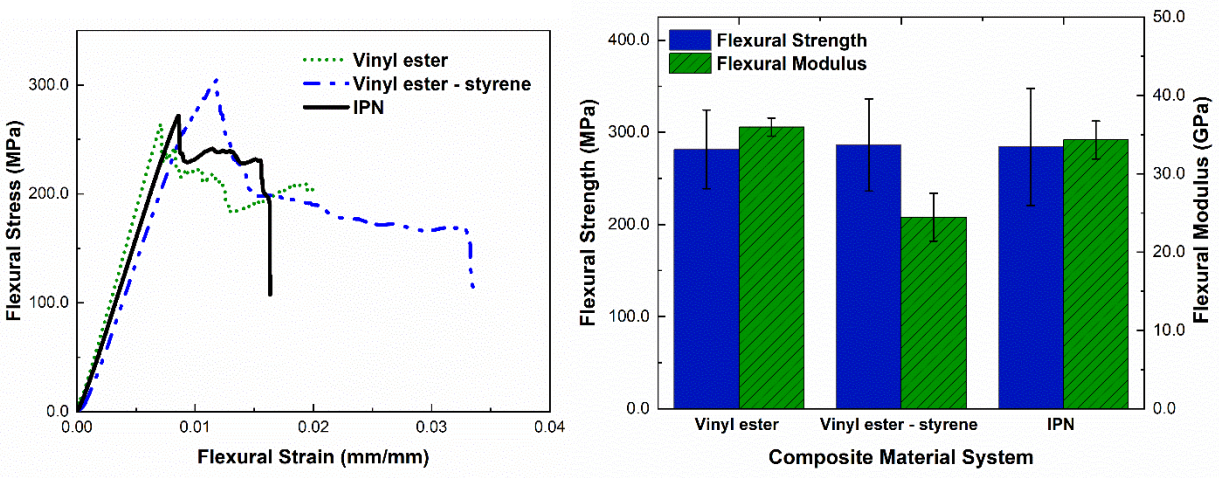

a) b)

Figure 3.6. Flexural response of IPN composites and controls a) representative plot of flexural stress versus flexural strain b) summary of flexural properties.

3.3.6. IPN composite tensile properties

Tensile testing was also performed on the three types of composites. Representative plots of tensile stress versus tensile strain are depicted in Figure 3.7.a. All composite materials show initial linear elastic behavior followed by brittle failure. Tensile properties are summarized in Figure 3.7.b. The

average failure stress for the vinyl ester and vinyl ester-styrene samples was comparable at 354 MPa and 334 MPa, respectively. This result illustrates that increasing the percentage of styrene in the copolymer does not adversely affect composite properties. Previous studies have shown, however, that the addition of the low viscous monomer like styrene is necessary for higher compatibility between the phases [4, 14]. The IPN composites failed at much lower stresses and with lower modulus values compared to the controls, 250 MPa and 36.7 GPa, respectively. These results illustrate a reduction in both tensile strength and modulus that occurs with the addition of the PU to the matrix and are in good agreement with those obtained via DMA testing, as well as the work of other researchers [36]. The decrease in strength with the addition of the PU (approximately 29%), however, is greater than the reduction in modulus (~ 16%), indicating a greater dependence on matrix properties for the tensile strength of the composite compared to its stiffness.

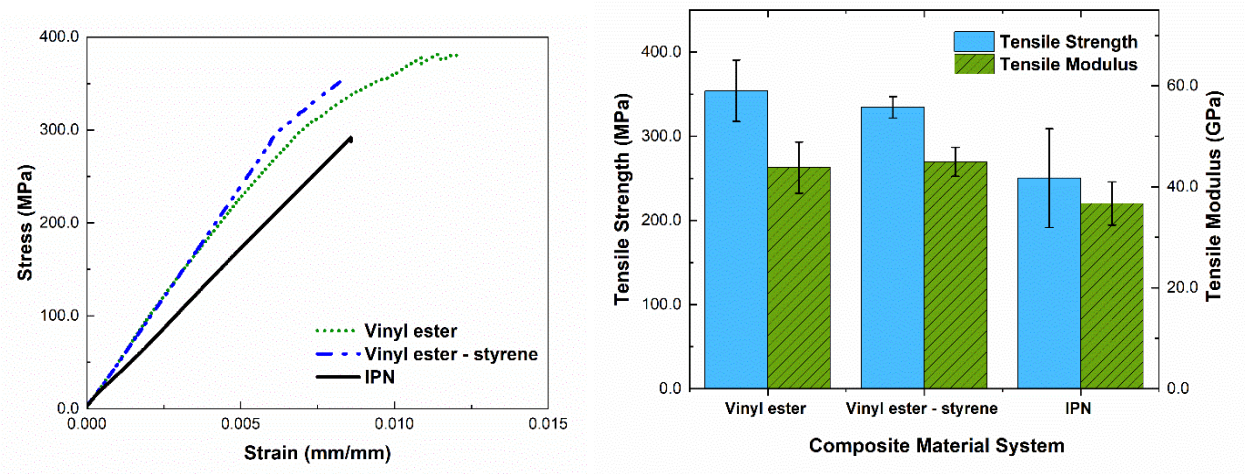

a) b)

Figure 3.7. Tensile response of IPN composites and controls a) representative stress versus strain plots b) summary of tensile properties.

3.3.7. SEM imaging

SEM images of fractured specimens were acquired for the vinyl ester and IPN composites, see Figure 3.8. In both composites, there is good wet out of the fibers by the matrix material, with virtually no signs of fiber-matrix debonding or fiber pull-out, indicating good interfacial adhesion and compatibility between the carbon fibers and the IPN matrix. Few voids are visible between the fibers, and these may be a source of reduced mechanical properties, specifically those dominated by the matrix.

Chen and co-workers examined the mechanical properties, as well as fracture surfaces of fiber-reinforced PMMA/polyurethane IPN composites and also observed good fiber wet out by the IPN matrix [51]. Work by Cardona et al. examining composites made from bioresins and jute fibers, however, demonstrated poor fiber-matrix adhesion with jute fibers and synthetic epoxy but enhanced adhesion with epoxidized bioresins [52].

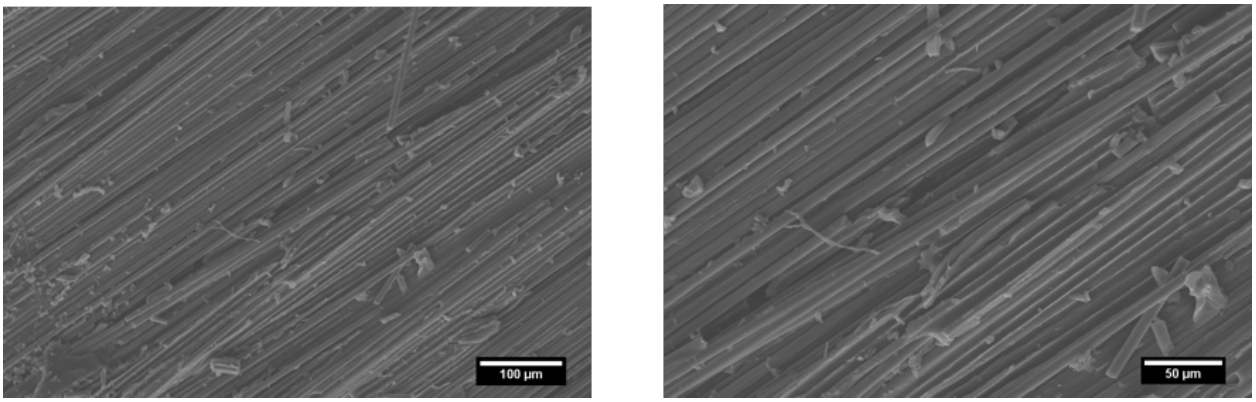

a)

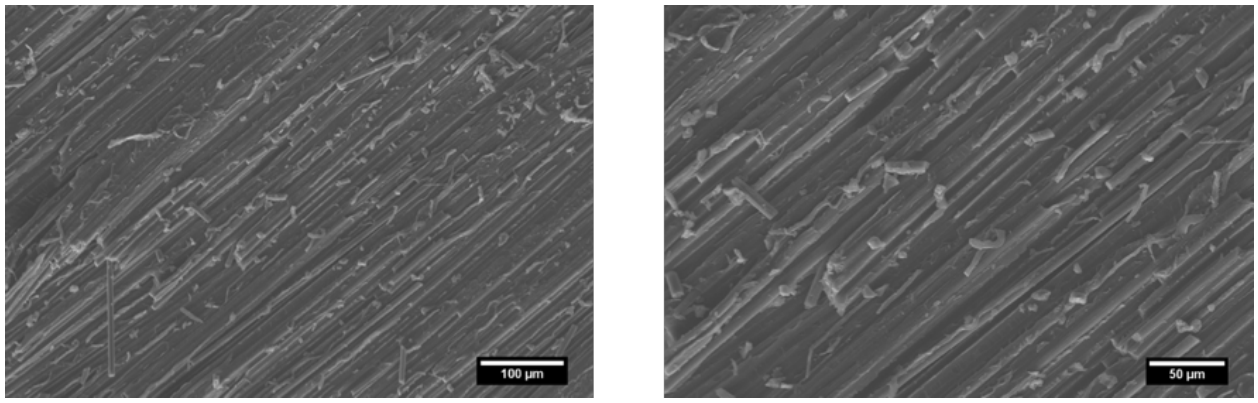

b)

Figure 3.8. Scanning electron microscope (SEM) images of IPN composites and controls a) vinyl ester composite b) IPN composite.

3.4. Conclusions

Woven carbon fiber reinforced composites with a vinyl ester - polyurethane-based IPN matrix were fabricated using a hand layup method. The full cure process of both polymers in the IPN was confirmed via FTIR spectroscopy and DSC analysis. Macroscopically, the finished composites were of good quality, and SEM imaging revealed good adhesion between the matrix and fibers. Compatibility between the copolymer and polyurethane was also illustrated via SEM imaging. DMA results revealed improved damping properties of the IPN matrix containing polyurethane compared to the other control matrices. Similar flexural strengths and moduli were observed for all composites revealing no degradation in flexural properties with the addition of the ductile polyurethane. The carbon fiber/IPN composites exhibited flexural strength and flexural modulus of 285 MPa and 34 GPa, respectively. The tensile response of the IPN composite, however, was affected by the addition of polyurethane, with the reduction in strength from 350 MPa for the vinyl ester composite to 250 MPa for the IPN composite (~29% decrease) and modulus reduction from

45 GPa to 38 GPa (16% decrease). These promising results demonstrate the potential for using acrylic-based IPNs in carbon fiber reinforced composites for demanding materials applications.

References

1. Sperling, L. H., *Introduction to physical polymer science*. 4th ed.; John Wiley & Sons: New Jersey, 2006.

2. McCrum, N. G.; Buckley, C. P.; Bucknall, C. B., *Principles of polymer engineering* 2nd ed.; Oxford University Press: 1988.

3. Odian, G., *Principles of polymerization*. John Wiley & Sons, Inc.: Hoboken, New Jersey, 2004.

4. Alizadeh, N.; Bird, S. A.; Mendez, R. B.; Jajam, K. C.; Alexander, A. C.; Tippur, H. V.; Auad, M. L., Chapter 11 – Synthesis and Characterization of High Performance Interpenetrating Polymer Networks With Polyurethane and Poly(methyl methacrylate). In *Unsaturated Polyester Resins*, Thomas, S.; Hosur, M.; Chirayil, C. J., Eds. Elsevier: 2019; pp 243-255.

5. Robeson, L. M., *Polymer Blends A Comprehensive Review*. Carl Hanser Verlag GmbH & Co. KG: 2007.

6. Cerclé, C.; Favis, B. D., Generalizing interfacial modification in polymer blends. *Polymer* **2012,** *53* (20), 4338-4343.

7. Panapitiya, N. P.; Wijenayake, S. N.; Huang, Y.; Bushdiecker, D.; Nguyen, D.; Ratanawanate, C.; Kalaw, G. J.; Gilpin, C. J.; Musselman, I. H.; Balkus, K. J.; Ferraris, J. P., Stabilization of immiscible polymer blends using structure directing metal organic frameworks (MOFs). *Polymer* **2014,** *55* (8), 2028-2034.

8. Albores-Velasco, M.; Gascon, R. I.; Rodriguez, O. A., Polymeric Compatibilizers. In *Concise Polymeric Materials Encyclopedia*, 1st ed.; Salamone, J., Ed. CRC Press LLC: 1998.

9. Porte, R. J. L., Polymer Coatings for Medical Devices: Structure/Properties, Development, Manufacture and Applications. CRC Press LLC.: 1997.

10. Garcia-Martinez, J. M.; Laguna, O.; Areso, S.; Collar, E. P., A dynamic-mechanical study of the role of succinil-fluoresceine grafted atactic polypropylene as interfacial modifier in polypropylene/tale composites. Effect of grafting degree. *Eur Polym J* **2002,** *38* (8), 1583-1589.

11. Pissis, P.; Georgoussis, G.; Bershtein, V. A.; Neagu, E.; Fainleib, A. M., Dielectric studies in homogeneous and heterogeneous polyurethane/polycyanurate interpenetrating polymer networks. *J Non-Cryst Solids* **2002,** *305* (1), 150-158.

12. Bird, S. A.; Clary, D.; Jajam, K. C.; Tippur, H. V.; Auad, M. L., Synthesis and characterization of high performance, transparent interpenetrating polymer networks with

polyurethane and poly(methyl methacrylate). *Polymer Engineering & Science* **2013,** *53* (4), 716-723.

13. Dave, V. J.; Patel, H. S., Synthesis and characterization of interpenetrating polymer networks from transesterified castor oil based polyurethane and polystyrene. *Journal of Saudi Chemical Society* **2017,** *21* (1), 18-24.

14. Ballestero, R.; Sundaram, B.; Tippur, H.; Auad, M., Sequential graft-interpenetrating polymer networks based on polyurethane and acrylic/ester copolymers. *Express Polym Lett* **2016,** *10*, 204-215.

15. Sundaram, B. M.; Mendez, R. B.; Auad, M. L.; Tippur, H. V., Quasi-static and dynamic mechanical behavior of transparent graft-interpenetrating polymer networks (graft-IPNs). *Polym Test* **2018,** *70*, 348-362.

16. Thapliyal, P. C., Interpenetrating Polymer Networks. *Composite Interfaces* **2010,** *17* (2-3), 85-89.

17. Alizadeh, N.; Barde, M.; Minkler, M.; Celestine, A.-D.; Agrawal, V.; Beckingham, B.; Auad, M. L., High-fracture-toughness acrylic–polyurethane-based graft-interpenetrating polymer networks for transparent applications. *Polymer International* **2020**.

18. Pater, R. H.; Yorktown, V.; Hansen, M. G.; Knoxville, T. Process for controlling morphology and improving thermal-mechanical performance of high performance interpenetrating and semi-interpenetrating polymer networks. 1997.

19. Sperling, L. H., *Interpenetrating Polymer Networks and Related Materials*. 1st ed.; Springer US: New York, 1981.

20. Hatch, M. J. Composite ion exchange resin bodies. 3,041,292, 1962.

21. Hilbelink, R. D.; Peters, G. H. Intercrossing resin/curing agent adhesive systems. 3,657,379, 1972.

22. Reinhart, T. J., Overview of Composite Materials. In *Handbook of Composites*, Peters, S. T., Ed. Springer US: Massachusetts, 1998.

23. Chawla, K. K., In *Composite Materials: Science and Engineering*, 4 ed.; Springer International Publishing: 2019; pp 3-5.

24. Chung, D. D. L., *Carbon Fiber Composites*. Butterworth-Heinemann: 1994.

25. Goren, A.; Atas, C., Manufacturing of polymer matrix composites using vacuum assisted resin infusion molding. *Archives of Materials Science and Engineering* **2008,** *34*, 117-120.

26. Xiong, W.; Cai, C. S.; Xiao, R. C., Chapter 8: The use of carbon fiber-reinforced polymer (CFRP) composites for cable-stayed bridges. In *Advanced Composites in Bridge Construction and Repair*, Kim, Y. J., Ed. Woodhead Publishing: 2014; pp 210-264.

27. Han, S.; Chung, D. D. L., Increasing the through-thickness thermal conductivity of carbon fiber polymer–matrix composite by curing pressure increase and filler incorporation. *Compos Sci Technol* **2011,** *71* (16), 1944-1952.

28. Ramakrishna, S.; Mayer, J.; Wintermantel, E.; Leong, K. W., Biomedical applications of polymer-composite materials: a review. *Compos Sci Technol* **2001,** *61* (9), 1189-1224.

29. Bai, X.; Li, N., The Application of Carbon Fiber Composite Material for Sports Equipment. *Advanced Materials Research* **2012,** *496*, 480-483.

30. Daily, C.; Barnard, D. J.; Jones, R. W.; McClelland, J. F.; Bowler, N., Dielectric and infrared inference of thermo-oxidative aging of a bismaleimide composite material. *Composites Part B: Engineering* **2016,** *101*, 167-175.

31. Pathak, A. K.; Borah, M.; Gupta, A.; Yokozeki, T.; Dhakate, S. R., Improved mechanical properties of carbon fiber/graphene oxide-epoxy hybrid composites. *Compos Sci Technol* **2016,** *135*, 28-38.

32. Choi, M. H.; Jeon, B. H.; Chung, I. J., The effect of coupling agent on electrical and mechanical properties of carbon fiber/phenolic resin composites. *Polymer* **2000,** *41* (9), 3243-3252.

33. Morgan, P., *Carbon Fibers and Their Composites*. CRC Press: 2005.

34. Malkapuram, R.; Kumar, V.; Yuvraj Singh, N., Recent Development in Natural Fiber Reinforced Polypropylene Composites. *J Reinf Plast Comp* **2008,** *28* (10), 1169-1189.

35. Stenzenberger, H. D., Recent developments of thermosetting polymers for advanced composites. *Composite Structures* **1993,** *24* (3), 219-231.

36. Suresh, G.; Jayakumari, L. S.; Dinesh, K. S., Finite Element Analysis of IPN Reinforced Woven Fabric Composite. *Matéria (Rio de Janeiro)* **2017,** *22*.

37. Wang, T.; Chen, S.; Wang, Q.; Pei, X., Damping analysis of polyurethane/epoxy graft interpenetrating polymer network composites filled with short carbon fiber and micro hollow glass bead. *Materials & Design* **2010,** *31* (8), 3810-3815.

38. ASTM E1640-13, Standard Test Method for Assignment of the Glass Transition Temperature By Dynamic Mechanical Analysis. ASTM International: West Conshohocken, PA, 2013.

39. Wu, G.; Gu, J.; Zhao, X., Preparation and dynamic mechanical properties of polyurethane-modified epoxy composites filled with functionalized fly ash particulates. *J Appl Polym Sci* **2007,** *105* (3), 1118-1126.

40. Wang, T. M.; Chen, S. B.; Wang, Q. H.; Pei, X. Q., Damping analysis of polyurethane/epoxy graft interpenetrating polymer network composites filled with short carbon fiber and micro hollow glass bead. *Materials & Design* **2010,** *31* (8), 3810-3815.

41. ASTM D7264 / D7264M-15, Standard Test Method for Flexural Properties of Polymer Matrix Composite Materials. ASTM International: West Conshohocken, PA, 2015.

42. ASTM D3039 / D3039M-17, Standard Test Method for Tensile Properties of Polymer Matrix Composite Materials. ASTM International: West Conshohocken, PA, 2017.

43. Lee, S. H.; Cho, E.; Jeon, S. H.; Youn, J. R., Rheological and electrical properties of polypropylene composites containing functionalized multi-walled carbon nanotubes and compatibilizers. *Carbon* **2007,** *45* (14), 2810-2822.

44. Xiao, K. Q.; Zhang, L. C.; Zarudi, I., Mechanical and rheological properties of carbon nanotube-reinforced polyethylene composites. *Compos Sci Technol* **2007,** *67* (2), 177-182.

45. Pavia, D. L.; Lampman, G. M.; Kriz, G. S., *Introduction to spectroscopy*. 3rd ed.; Thomson Learning: Washington, 2001.

46. Suresh, G.; Jayakumari, L. S., Evaluating the mechanical properties of E-Glass fiber/carbon fiber reinforced interpenetrating polymer networks. *Polímeros* **2015,** *25*, 49-57.

47. Meili, G., Dynamic mechanical thermal analysis of composite material and high polymer. Beijing: Chemical Industry Press: 2002.

48. Menard, K. P.; Menard, N. R., Dynamic Mechanical Analysis in the Analysis of Polymers and Rubbers. In *Encyclopedia of Polymer Science and Technology*, 2015; pp 1-33.

49. Auad, M. L.; Aranguren, M.; Borrajo, J., Epoxy-based divinyl ester resin/styrene copolymers: Composition dependence of the mechanical and thermal properties. *J Appl Polym Sci* **1997,** *66* (6), 1059-1066.

50. Kim, M. T.; Rhee, K. Y.; Lee, J. H.; Hui, D.; Lau, A. K. T., Property enhancement of a carbon fiber/epoxy composite by using carbon nanotubes. *Composites Part B: Engineering* **2011,** *42* (5), 1257-1261.

51. Chen, C.-H.; Ma, C.-C. M., Pultruded fibre-reinforced PMMA/PU IPN composites: processability and mechanical properties. *Composites Part A: Applied Science and Manufacturing* **1997,** *28* (1), 65-72.

52. Cardona, F.; Sultan, M. T.; Talib, A. R. A.; Ezzah, F.; Derahman, A., Interpenetrating polymer network (IPN) with epoxidized and acrylated bioresins and their composites with glass and jute fibres. *BioResources* **2016,** *11* (1), 2820-2838.

Chapter 4

Flexible acrylic-polyurethane based graft-interpenetrating polymer networks for high impact structural applications

4.1. Introduction

Transparent impact-resistant materials can be used in different applications such as electronic devices, windshields, protecting enclosures [1], canopies [2], and many general applications. Excellent transparency, impact resistance, ballistic resistance, and low density are essential features that each transparent protective material should have. Sands et al. indicated that, while transparent protective materials cover just 15% of the whole surface of body armors, they contribute to 30 % of the entire weight of body armor [3].

Traditionally, bulletproof glass (laminated glass) was used in high-performance transparent applications. Laminated glasses consist of a couple of glass layers with plastic layers between them [4]. Plastic layers with high toughness could withstand the harsh projectile and make the whole system impact resistance. However, laminated glasses lose their transparency after experiencing several strikes [5]. Transparent ceramics, which have better thermomechanical properties, are other options for the high-performance transparent application [6]. Nonetheless, the manufacturing process, price, and availability are the most important disadvantages of ceramics [5].

The recent transparent protective materials consist of three layers, a hard strike face, an intermediate layer, and a backing layer called a “spall” layer. The strike face is disturbing the energy, while the intermediate layer objection is absorbing the energy. Finally, the spall layer prevents outer and intermediate fractured layers from spraying or “spalling” into the passenger compartment or inside layer [7]. These layers stick to each other by an adhesive interlayer, usually manufactured from polyurethanes (PUs) [7]. Transparent protective materials are taking much

attention due to their unique properties [8]. Acrylates such as Plexiglas® and polycarbonates (PC) such as Lexan® are two main groups of amorphous polymers used for transparent impact resistant applications [5]. Amorphous polymers are mostly used in the intermediate and adhesive interlayer, where low density and transparency are critical [7]. However, PC, for instance, has low ultraviolet light (UV) resistance, chemical resistance, scratch resistance, and high price [9]. Vinyl ester resins (VER) such as bisphenol-A based dimethacrylate resins are widely used in military, high-performance applications and as a matrix in composites due to the excellent thermomechanical properties [10-12]. However, due to high viscosity, mostly lower viscosity co-monomers such as styrene, which has excellent transparency and low price, and methyl methacrylate (MMA) are mixed with the vinyl ester resins to increase processability [11, 13]. Poly(methyl methacrylate) (PMMA) is an amorphous polymer widely used in transparent applications due to the high similarity to glass [7]. Chemical resistance, wearing resistance, ease of processability, relatively high stiffness, and UV resistance are some of the desirable properties of PMMA in high-performance transparent applications [7].

Since VER resins are brittle, blending with rubbery materials such as PU is required to increase the toughness [14]. PU is an elastomeric material with high impact resistance better than PC. PU has tailorable properties that make it a great candidate in various applications, including protective applications [15, 16]. The choice of the molecular weight of monomers, catalysts, chemical configuration of isocyanate, and the synthesis method affect the final morphology of PU [17], therefore changing the structural properties [17-19].

Blending polymers is considered one method to enhance the desirable properties for specific applications [20, 21]. However, blending polymers has its challenges due to the low entropy of mixing

in big molecules [22, 23]. Different methods such as copolymerization, grafting, and interpenetrating polymer networks (IPNs) were introduced to solve the immiscibility of the polymers [24, 25].

IPNs include two polymers where both networks are physically entangled, and it is not possible to separate them without breaking their bonds [25]. IPNs are classified as semi-IPN, full-IPN, and graft-IPN based on their structure. Semi-IPN consists of a crosslinked polymer and a linear polymer trapped inside the crosslinked network. Full-IPN includes two crosslinked polymers with physical entanglements [26]. Finally, graft-IPN is similar to full IPN. However, selected chemical bonds between the two polymers are utilized to enhance the compatibility even further [24, 27].

IPNs can also be classified into simultaneous and sequential IPNs based on the polymerization method.

In sequential IPNs, the polymerization of the first polymer occurs first, while the monomers of the second polymer swell the system. Once the initial polymerization occurs, the polymerization of the second polymer begins. Simultaneous IPNs are different because the polymerization of two polymers coincides-with no interfering reaction [23, 28, 29].

Many different research groups, including authors, such as Millar et al. [27] and Frisch et al. [30], studied different aspects of IPNs [12, 23, 31-37]. Factors such as changing the composition of two polymers, curing profile [38-42], grafting two polymers [43], synthesis method [40], and choice of monomers and catalysts [39], were studied. It was mentioned that utilizing a sequential polymerization method with linear isocyanate rather than aromatic isocyanate, and using chemical bonds, synthesize the IPNs with the best compatibility, and therefore enhancing the transparency and fracture toughness [5, 11, 40, 43-47].

In this research, flexible graft-IPNs out of PU and styrene and MMA based acrylic copolymer were synthesized for the first time. Excellent transparency and impact properties were obtained in

all samples. Different properties of the IPNs, such as impact resistance, shear strength, thermomechanical, and tensile strength, were studied. Furthermore, the polymerization reaction between the two networks was analyzed using the FTIR method. The final results confirmed the potential of the synthesized novel flexible IPNs in high-performance applications such as interlayer adhesives in bulletproof transparent applications, windshields, and many other high-performance applications where high transparency, impact resistance, and elastomeric behavior are required.

4.2. Experimental

4.2.1. Materials

In this research, the polyurethane phase was synthesized by 2-ethyl-2-(hydroxymethyl)-1,3-propanediol (TRIOL, MW=134.18 g/mol) as a crosslinker purchased from Acros Organics, poly(tetramethylene ether) glycol (Tetrathane® 1400) (PTMG, MW=1400 g/mol) donated from Lycra. Hexamethylene diisocyanate (DCH) was purchased from TCI. Moreover, dibutyltin dilaurate (DBTDL) and triphenyl bismuth (TPB) as catalysts were purchased from Pfaltz & Bauer and Alfa Aesar, respectively. Both catalysts were dissolved in ethyl acetate, purchased from Alfa Aesar. Styrene, purchased from Alfa Aesar, Methyl methacrylate (MMA) purchased from Acros Organics, and bisphenol A bis(2-hydroxy-3-methacryloxypropyl) ether (BisGMA), purchased from Esstech, was used to synthesize acrylic copolymer phase. 2,2'-azobis(2-methyl-propionitrile) (AIBN, thermal initiator) was purchased from Matrix Scientific. 4Å molecular sieves, purchased from Alfa Aesar, were utilized to remove the moisture from DCH, styrene, MMA, TRIOL, and PTMG. Polycarbonate (PC) sheets (3.175 mm and 6.35 mm thickness) were purchased from the US sealing.

4.2.2. Methods

4.2.2.1. Synthesis of graft-IPNs

For the PU phase, TRIOL and PTMG with 0.19 eq. and 0.12 eq. respectively, were heated and mixed at 60°C. The mixture was cooled down first, and then 0.31 eq DCH was added.

For synthesis the acrylic copolymer phase, 20 wt% of BisGMA, was dissolved into 80 wt% Styrene or MMA. Then 1 wt% of the total mass of acrylic copolymer, AIBN, was dissolved into the mixture. Afterward, PU and acrylic copolymer monomers were mixed. Finally, 150 μL, 0.02 M ethyl acetate solution of DBTDL, and 75 μL, 0.001 M ethyl acetate solution of TPB per 50 grams of PU were added to the monomers to catalyze the poly-addition polymerization of the PU system. The mixture was then vacuumed under 95 kPa for 5 minutes, and it was cured at room temperature in closed glass molds, which was increased gradually to reach 40°C for 24 hours, followed by 24 hours at 60°C, and finally 24 hours at 80°C. The schematic of two poly-addition polymerizations happening to synthesize the PU phase and free radical polymerization of a mixture of styrene or MMA and BisGMA are shown in Figure 4.1.a and b. Figure 4.1.a shows the free radical polymerization of MMA and BisGMA to synthesize acrylic copolymer. Moreover, a simple schematic of the graft-IPN synthesis is shown in Figure 4.1.b. The free radical polymerization of Styrene and BisGMA to synthesize acrylic copolymer was shown elsewhere [34].

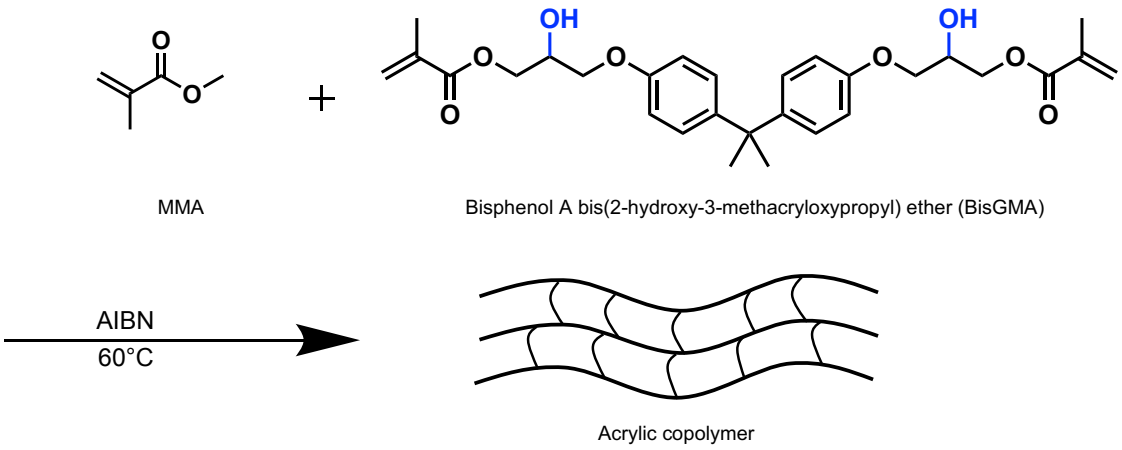

a)

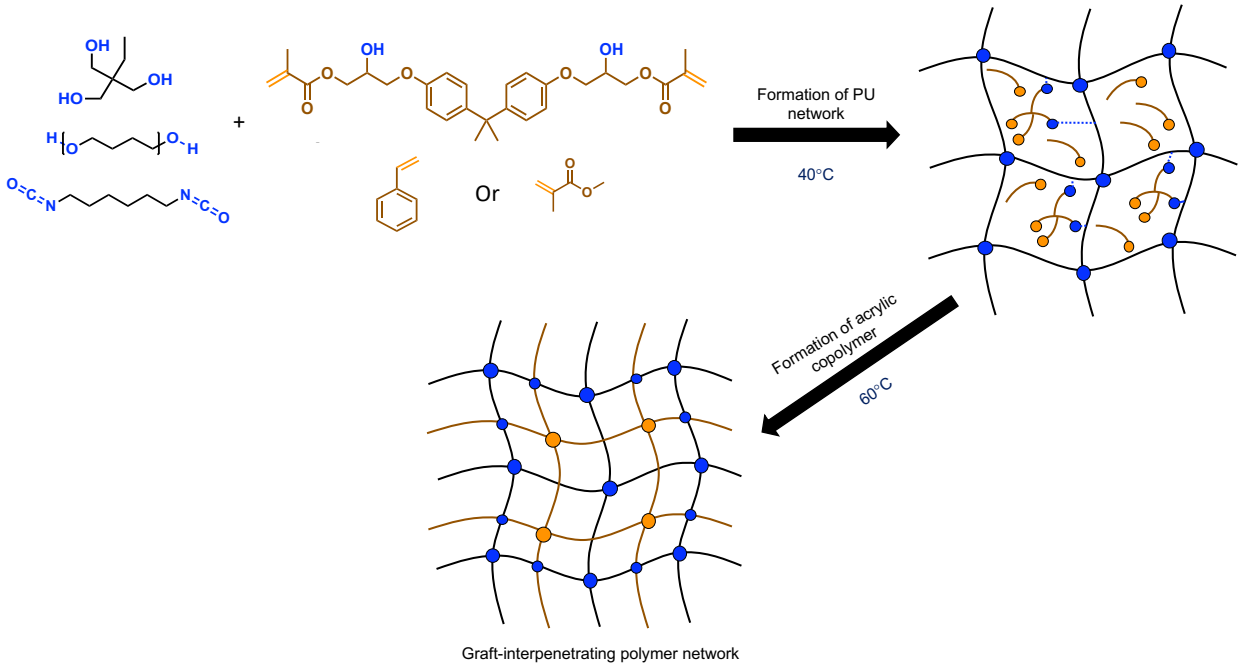

b)

Figure 4.1. a) Free radical polymerization of acrylic copolymer out of MMA and BisGMA b) schematic of the graft-IPN synthesis.

As shown in Figure 4.1.b, the poly-addition polymerization of the PU phase occurs at a lower temperature. The crosslinked polyurethane traps the monomers of the second polymer inside itself. Moreover, the hydroxyl groups of BisGMA start to react with the isocyanate group to account for the chemical bonds between the two networks. At 60°C, the thermal initiator of the acrylic copolymer decomposes, starting the free radical polymerization. Samples were post cured at 80°C to ensure that all of the active groups were reacted in systems. All samples prepared in this research were summarized in Table 4.1.

Table 4.1. Summary of samples made in this research.

Samples	PU (wt%)	Acrylic copolymer (wt%)
PU	100	0
IPN75-Styrene	75	25 (80 wt% Styrene and 20 wt% BisGMA as monomers)
IPN50-Styrene	50	50 (80 wt% Styrene and 20 wt% BisGMA as monomers)
IPN75-MMA	75	25 (80 wt% MMA and 20 wt% BisGMA as monomers)
IPN50-MMA	50	50 (80 wt% MMA and 20 wt% BisGMA as monomers)
COP-Styrene	0	100 (80 wt% Styrene and 20 wt% BisGMA as monomers)

4.2.2.2. Characterization

Modulated differential scanning calorimetry (DSC) experiment was performed on TA Instruments DSCQ2000. 5 to 10 mg of samples were used for each test. Samples were first equilibrated at -90 °C for 5 minutes, then heated to 200°C, cooled to -90°C, and finally heated to 200°C with 5°C/min heating rate in a nitrogen atmosphere.

Thermogravimetric analysis (TGA) was performed on TA Instruments TGAQ500. Between 10 – 20 mg of each sample was placed on a platinum pan and were heated from room temperature to 800°C with 10°C/min under a nitrogen atmosphere.

Fourier transform infrared spectroscopy (FTIR) analysis was performed using Nicolet 6700 FTIR spectrometer from Thermo Scientific (US) in attenuated total reflection (ATR) infrared mode. FTIR analysis uses 400-4000 cm^{-1} wavenumber with 64 scans and 4 cm^{-1} resolution.

Thermo-mechanical analysis experiments were performed using TA Instruments RSA 3 dynamic mechanical analyzer (DMA). The flexural test was performed on samples with 35 mm × 10 mm × 3 mm and measurements from -100 to 200°C at 5°C/min heating rate, with a sinusoidal strain amplitude of 0.5% and 1 Hz frequency, following ASTM E1640 [48]. At least 5 specimens for each sample were tested.

The tensile test was performed using a universal testing machine, Instron® 5565 with 1 kN static load cell according to ASTM D638 and Type V dog bone geometry with 63.5 mm overall length, 7.62 mm gage length, 3.18 mm width of narrow section, and ~ 3 mm thickness [49]. The test was performed under displacement control mode at 10 mm/min. At least 10 specimens were tested for each composition. Boss Laser LS 3655 was utilized to cut cured samples to the desired shape for tensile and DMA tests.

A Zeiss EVO 50 variable pressure scanning electron microscope (SEM) with digital imaging and energy dispersive spectroscopy was utilized to examine the cross-section of the tensile specimens after failure on their gauge. The samples were sputter-coated with an EMS 550X auto sputter coating device with carbon coating attachment.

PC sheets were cut to 152.4 mm × 152.4 mm squares in preparation for impact-resistant tests. Then IPN monomers were added between two sheets making a sandwich structure. Afterward, 1.2 kg

weight was put on the top of the sandwich to keep the PC sheets together and avoid introducing air bubbles between PC sheets. Finally, sandwich structures were cured similarly, as explained in the IPN synthesis section. The impact-resistant test was performed on the Instron® instrumented impact testing machine (Dynatup 8250), following ASTM D5420 [50] (GD geometry) and ASTM D3763 [51]. A mass of 22.58 kg falling from 82 centimeter height to hit the sample clamped to the platform having a hole of 76 mm by a dart with a hemispherical nose (tup) of 17.6 mm diameter was used for the impact-resistant test.

A Shimadzu UV-2450 spectrometer was used to verify the transparency of the samples (450-800 nm wavelength). For this purpose, similar samples prepared for impact resistance were cut into 25.4 mm × 25.4 mm with a saw. Moreover, Pure Pc sheets were used as background.

The IPNs strength as an adhesive in shear was performed by tension loading of single-lap-joint assemblies, ASTM D3165 [52]. The samples laminated assembly was prepared a similar procedure followed for preparing impact test samples with regard to putting the IPN monomers between the two layers of 152.4 mm × 152.4 mm squares and cure it. Then sandwich samples were cut into 25.4 mm × 152.4 mm specimens. Finally, prepared specimens were notched twice at the right angle to the long axis of the specimen at 12.7 mm from the middle of the opposite sides, providing an area of 25.4 mm × 25.4 mm joint. The notch depth is to cut the sheet and the adhesive material in the thickness direction. Figure 4.2.a, b, and c show different views of prepared shear samples, while Figure 4.2.d shows the sample loaded into the tensile testing machine, Instron® 5582, with a 100 kN static load cell. The test was performed under displacement control mode at 1 mm/min. At least 10 specimens were tested for each composition. Equation 4.1 was used to calculate the shear stress of the samples.

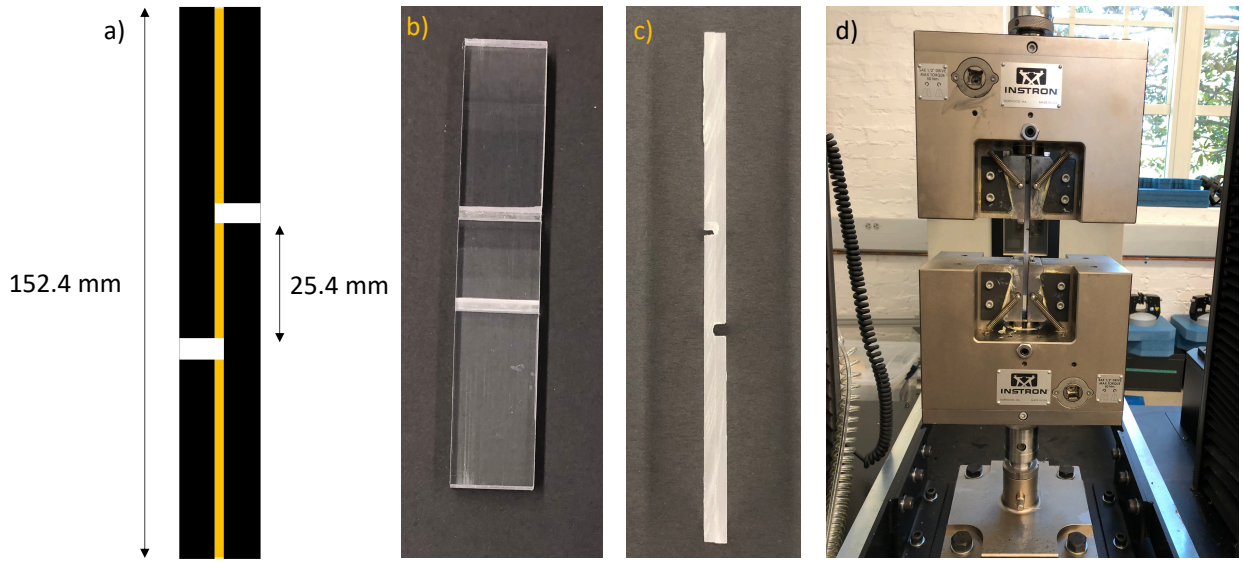

Figure 4.2. a) A simple schematic b) top view and c) cross-section view of samples prepared for lap shear test, d) loaded sample on the tensile instrument.

$$\tau = \frac{F}{A_0} \qquad [4.1]$$

Where τ is the shear stress, F is the maximum force, and A_0 is the initial cross-section.

4.3. Results and discussion

The heating cycle of DSC experiment indicated no crystallization with a minimum amount of post-curing in all samples, as shown in Figure 4.3.

TGA analysis was utilized to study the thermal stability of the IPN samples. As shown in Figure 4.4, the degradation for all samples starts at approximately 300°C and finishes at around 450°C. The degradation temperature obtained from TGA analysis was much higher than the application temperature of IPN samples. PU degrades at a higher rate than other IPN samples due to acrylic

copolymer presence, which increases the samples' thermal stability. However, All IPN samples follow the same trend regards to degradation.

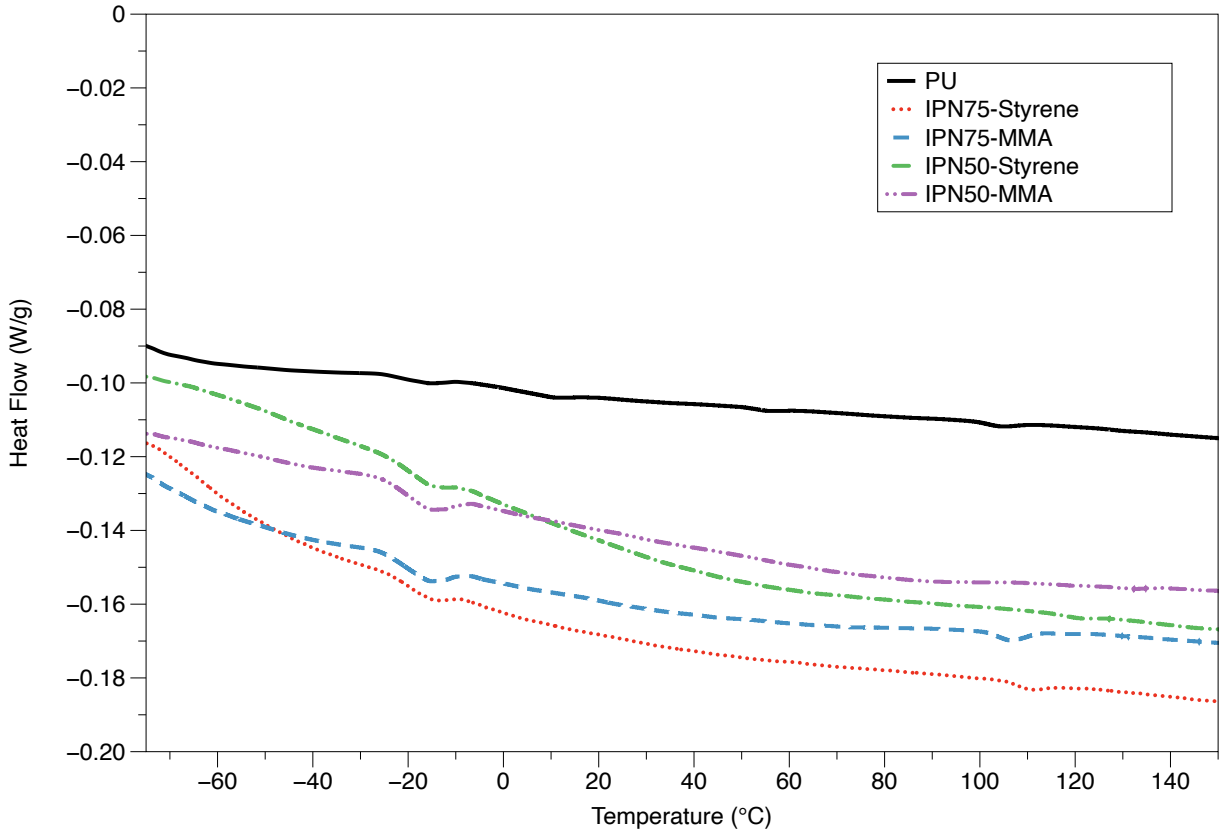

Figure 4.3. Heating cycle of differential scanning calorimetry (DSC) results of the IPN samples.

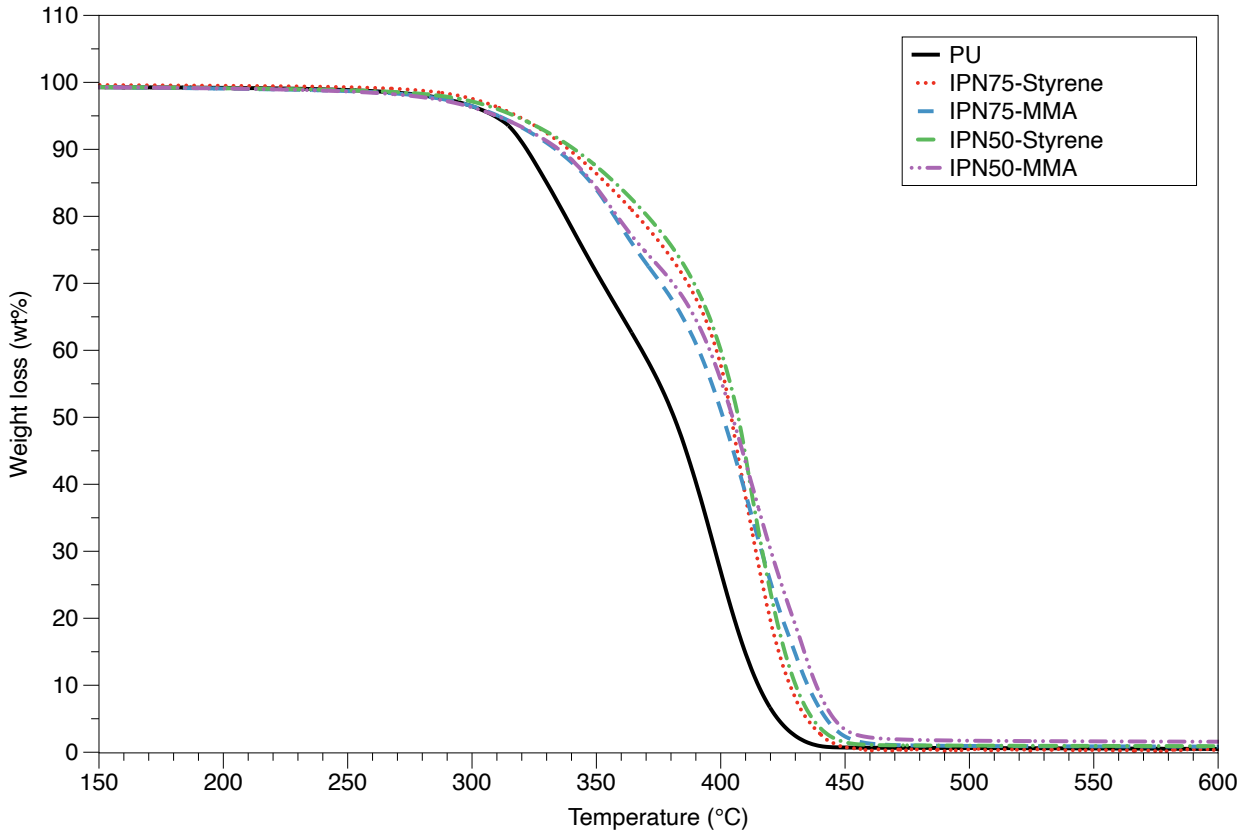

Figure 4.4. TGA analysis results of IPN samples.

The FTIR analysis was utilized to clarify the successful polymerization of each polymer in IPN systems. FTIR spectra of IPN75-Styrene at 0, 21, 41, 62 min and two days are shown in Figure 4.5. As it is displayed, the peak around 3454 cm^{-1} belongs to the O-H bond and shift to the lower wavenumber (around 3330 cm^{-1}), which belongs to the stretching of the N-H bond. It confirms the formation of the PU after polymerization. The disappearance of isocyanate (NCO) peak around 2257 cm^{-1} shows the total consumption of the isocyanate group, and it is another evidence for the formation of PU. The formation of amide C=O bond, bending of N-H bond, and C-N bond are other evidence to confirm the successful synthesis of PU. Peaks around 1627 cm^{-1} belong to the alkene C=C bond, which disappears after polymerization. The disappearance of the alkene peak

confirms the polymerization of the acrylic phase in the system. Moreover, peaks around 780 cm^{-1} and 910 $cm^{-1,}$ attributed to out-of-plane (oop) bending of =C-H bonds, disappear in IPN75-Styrene due to the free radical polymerization.

To analyze the isocyanate conversion of flexible IPN material during the polymerization, IPN75-Styrene was chosen. Isocyanate peak, which happens around 2270 cm^{-1}, was monitored during the polymerization while stretching C-H (within 2850-3000 cm^{-1}) was used as standard due to the constant concentration during the polymerization [53]. Equation 4.2 [54] was used to calculate the isocyanate conversion.

$$p = 1 - \frac{\frac{A_{NCO}}{A_{CH_2}}}{\left(\frac{A_{NCO}}{A_{CH_2}}\right)_0} \qquad [4.2]$$

Where p is isocyanate conversion, A_{NCO} is integrated absorbance for NCO peak, A_{CH_2} is integrated absorbance for stretching of C-H peak, and $\left(\frac{A_{NCO}}{A_{CH_2}}\right)_0$ is the relative absorbance extrapolated to time zero.

As shown in Figure 4.5, the isocyanate peak at approximately 2270 cm^{-1} starts to decrease during the polymerization due to the reaction between the isocyanate group and a hydroxyl group, which causes the formation of the PU structure. Moreover, the C-H stretch peak remains similar during the polymerization. The result for isocyanate conversion is shown in Figure 4.6.

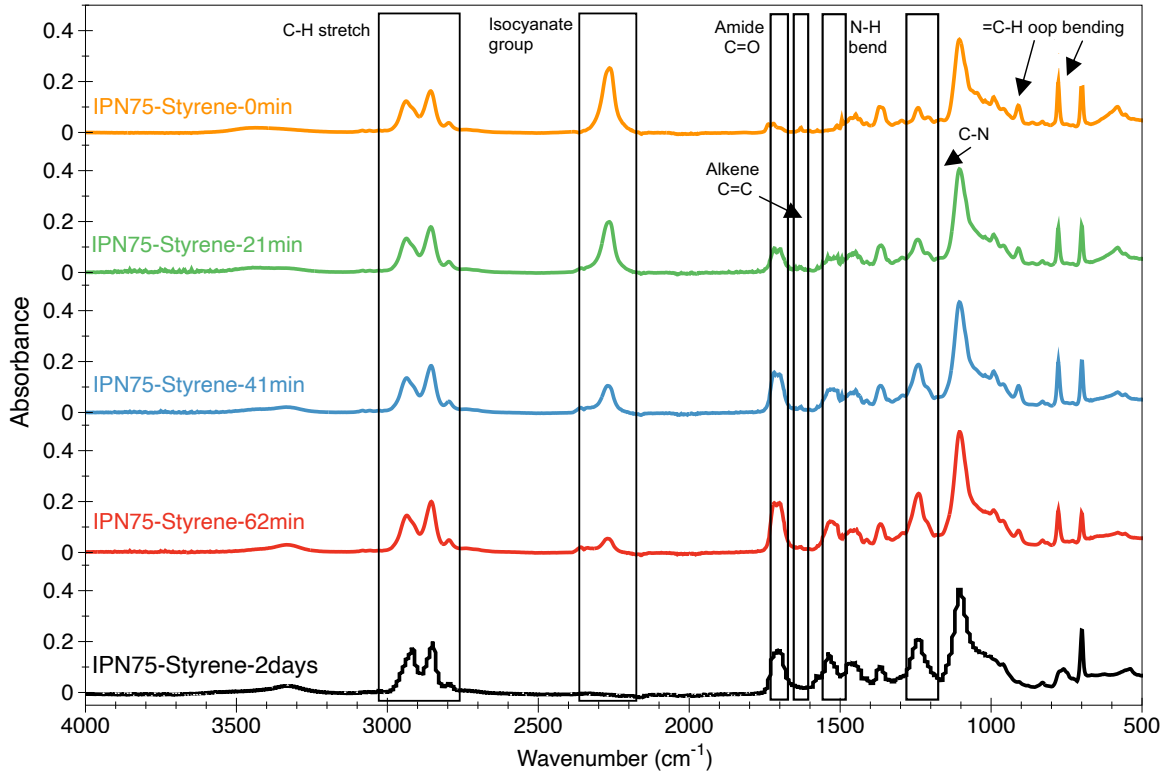

Figure 4.5. FTIR spectra of IPN75-Styrene at 5 different times.

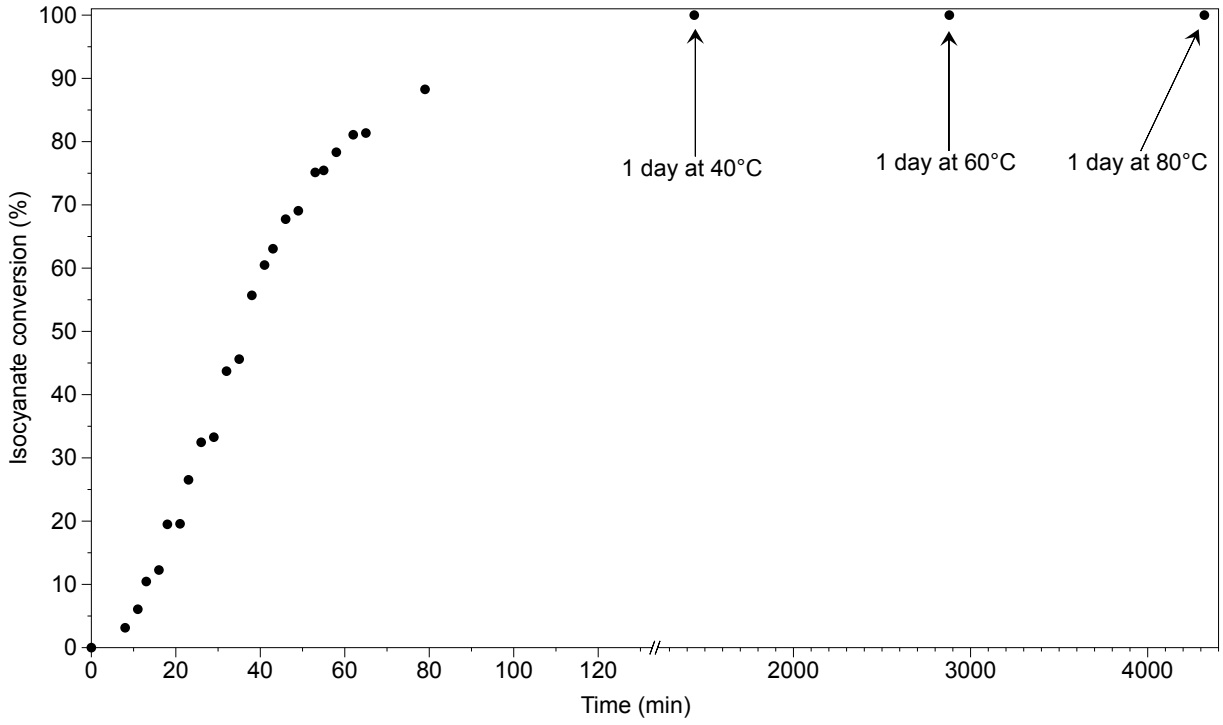

Figure 4.6. Isocyanate conversion of IPN75-Styrene.

As it is shown in Figure 4.6, IPN75-Styrene reaches to 50% of isocyanate conversion approximately after 40 minutes, and then conversion reaches to 90% after around 90 minutes. Finally, the conversion becomes 100% at the end of the polymerization process. IPN75-Styrene follows the same trend as rigid IPN with a composition of 75 wt% of copolymer and 25 wt% of PU explained elsewhere [34].

UV-Visible spectrophotometry was utilized to study the transparency of the samples. Figure 4.7 shows the sandwich structures (Figure 4.7.a), and results of transparency for different samples (Figure 4.7.b). As shown in Figure 4.7, All IPN samples show transparency higher than 80% in a visible light region. PU shows the lowest transparency in comparison to other samples. Slight tinting in PU structure decreases the transparency of the pure PU samples [7]. Adding more acrylic copolymer into the system increases the transparency of the samples. Furthermore, as it is shown, IPN75 samples show transmittance between 95-100%.

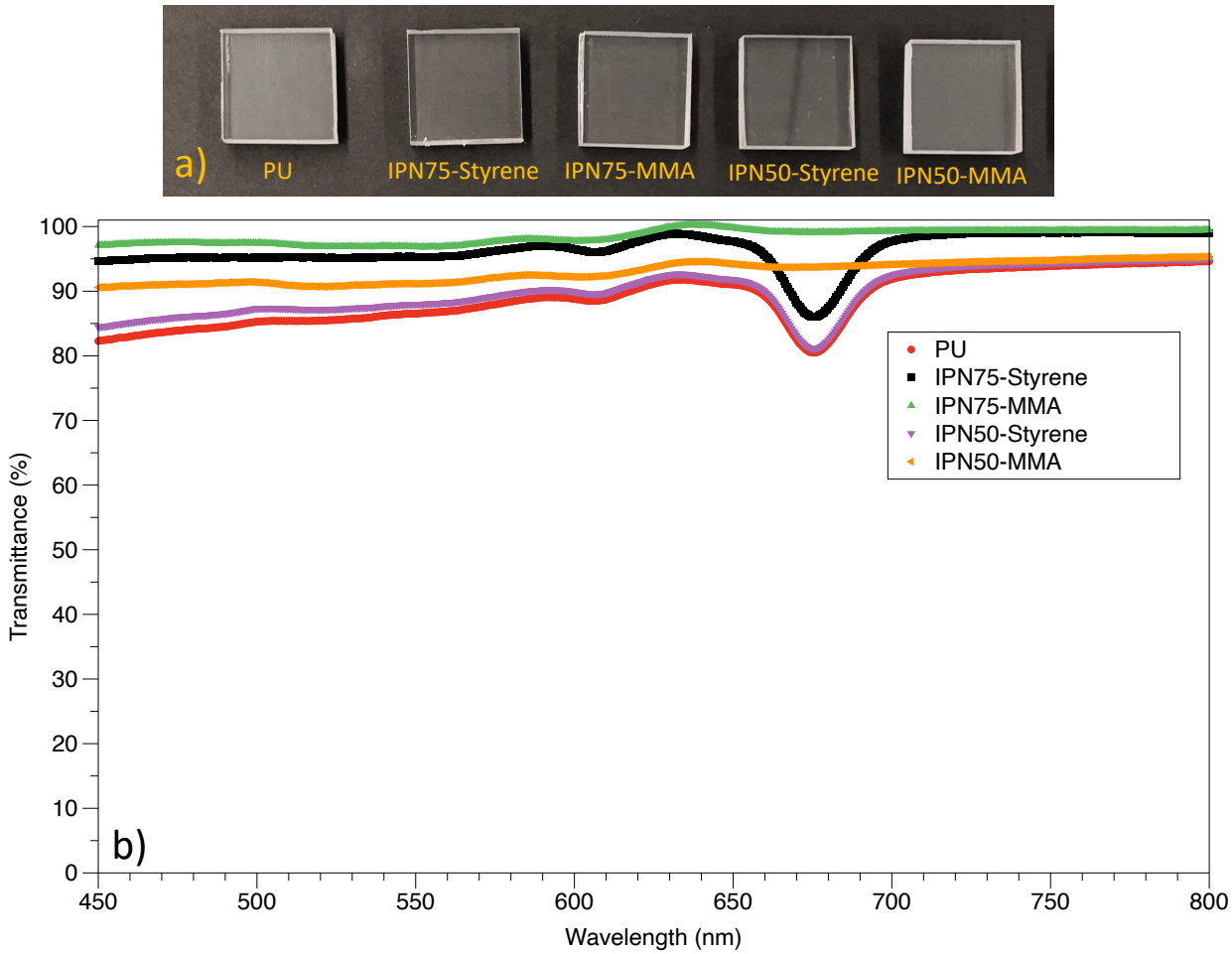

Figure 4.7. a) Sandwich structures prepared for transparency test b) UV-Visible spectra of the samples (The size of each sample is 25.4 mm × 25.4 mm).

Thermo-mechanical characterization of materials was performed by DMA. Figure 4.8 and Table 4.2 show the results for thermo-mechanical characterization. As it is shown, PU shows the lowest storage modulus (E') and glass transition temperature (T_g) due to the higher flexibility and mobility of the chains in PU structure. Glass transition of the samples and their storage modulus starts to increase by adding copolymer to PU and synthesizing IPN samples. The IPN50 sample shows the highest storage modulus and glass transition temperature due to the presence of 50 wt% copolymer, which restricts the mobility of chains. IPN samples with MMA show higher storage modulus and

T_g. Aminolysis reaction between the ester group of PMMA and amine groups of PU, which forms tertiary amine and, as a result, bring higher interpenetration between two polymer phases, is one of the reasons behind better thermomechanical properties in IPN-MMA samples [55].

Moreover, the nucleophilicity of double bonds in the MMA and BisGMA is relatively similar due to the ester group in their structure, while the nucleophilicity of BisGMA is lower than styrene. Since the ester group in BisGMA has a higher electronegativity than the benzene ring in styrene. Accordingly, styrene-based copolymer looks more like an alternating copolymer, and MMA based copolymer looks more like a random copolymer. This fact is another reason for the thermomechanical difference in two different systems [56-58]. Wide storage modulus and glass transition temperature show the potential of synthesized materials in various applications.

Figure 4.8.b shows the *tan δ* vs. temperature of the materials. As it is shown, all materials show a broad *tan δ* peak due to the several relaxation mechanisms occurring in the system [34, 40, 43, 59]. This fact shows the potential of these materials to be used in damping applications such as shock absorbers and isolators [60]. Moreover, the height of *tan δ* is another factor in predicting the damping ability of the materials [61]. As shown in Table 4.2, the height of *tan δ* starts to decrease by adding more copolymer into the IPN system. This result was expected due to the hindrance provided by acrylic copolymer against chain mobility and therefore reducing the damping ability of the materials.

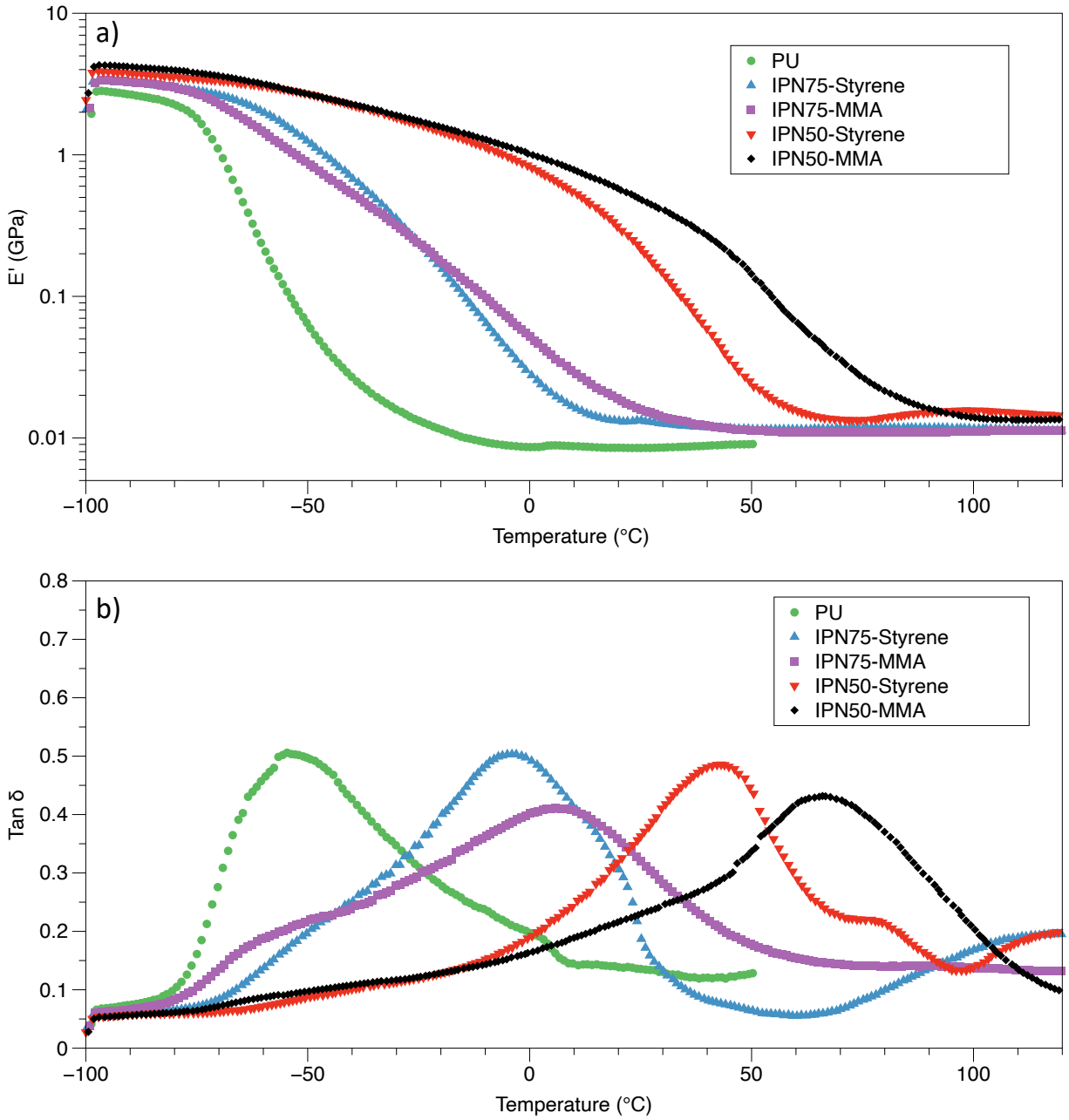

Figure 4.8. Thermo-mechanical analysis of materials a) *E'* vs. temperature and b) *tan δ* vs. temperature.

Table 4.2. Summary of thermo-mechanical results.

Sample	Storage modulus *E'* (GPa)	T_g (°C)	*Tan δ*
PU	2.80 ± 1.08	-52.44 ± 2.73	0.49 ± 0.01
IPN75-Styrene	3.16 ± 0.19	-2.80 ± 2.48	0.47 ± 0.05
IPN75-MMA	3.38 ± 0.20	10.74 ± 5.08	0.37 ± 0.04
IPN50-Styrene	3.50 ± 0.56	39.81 ± 2.78	0.43 ± 0.06
IPN50-MMA	3.92 ± 0.34	62.86 ± 3.04	0.44 ± 0.02

4.3.1. Tensile strength test

All tensile test IPN samples were failed in the gauge section, which shows the validity of the test. Figure 4.9 shows the tensile test graphs, while results are summarized in Table 4.3. As expected, PU shows the highest elongation and lowest tensile stress than other materials due to the higher mobility of the chains in the PU structure. It can be observed that the IPN75 samples show an increase in tensile strength and a decrease in elongation due to the 25 wt% of copolymers in IPN systems. Copolymer acts as reinforcements and therefore increases the tensile strength and, at the same time, decreases the flexibility of the samples. The modulus of the elasticity follows the same trend as it increases by adding more COP into the system. Finally, IPN50 samples show the lowest elongation with the highest tensile strength due to the reason mentioned above. PU shows completely elastomeric behavior in the tensile test, while the tensile behavior of IPN samples becomes more ductile by adding more copolymer as reinforcement. IPN-MMA samples exhibit higher modulus and tensile strength than IPN-Styrene samples due to the aminolysis reaction and different copolymer structures between IPN samples, which was discussed in the DMA section.

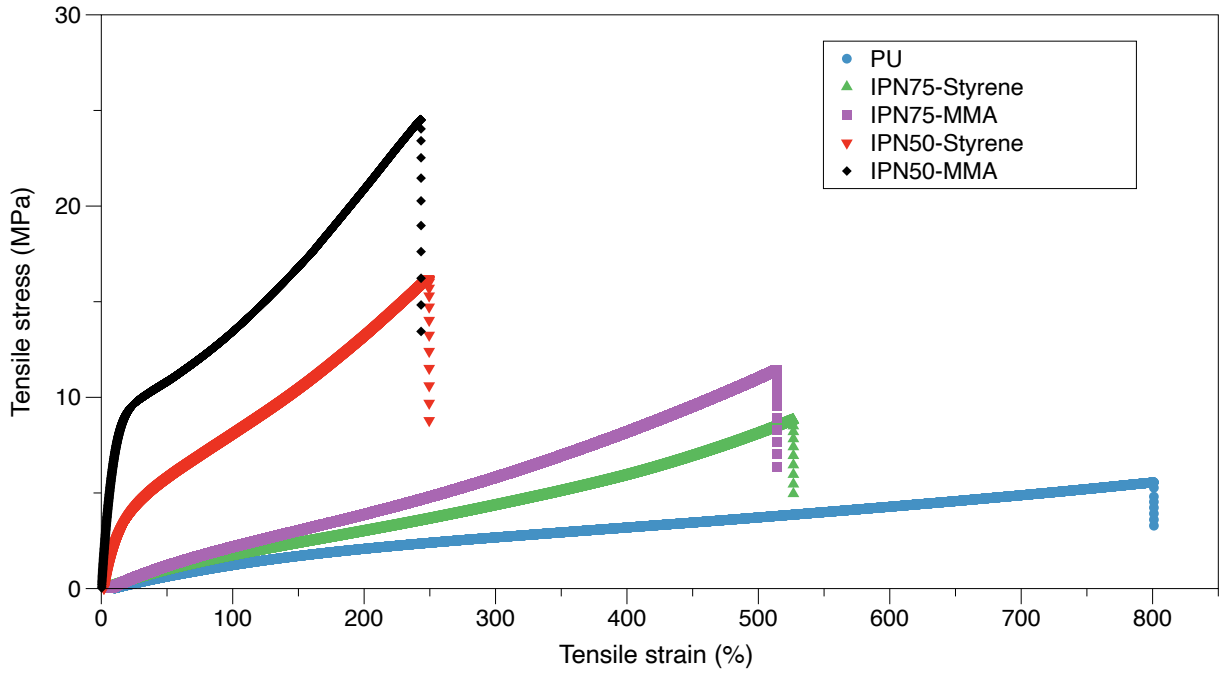

Figure 4.9. Tensile analysis of PU and IPN samples.

Table 4.3. Summary of tensile results for PU and IPN samples.

Sample	Modulus of elasticity (MPa)	Tensile stress at maximum load (MPa)	Tensile strain at maximum load (%)
PU	2.00	5.16 ± 2.49	738.39 ± 360.62
IPN75-Styrene	2.14 ± 0.36	6.12 ± 4.36	332.27 ± 206.43
IPN75-MMA	3.10 ± 0.32	9.01 ± 4.48	440.41 ± 162.72
IPN50-Styrene	19.36 ± 3.85	16.89 ± 3.23	269.64 ± 58.64
IPN50-MMA	86.08 ± 8.79	25.55 ± 3.50	256.23 ± 40.14

The cross-section of the fractured surface area after tensile test was studied using SEM. Mirror-like surfaces with no specific features were observed for all the analyzed samples, as shown in

Figure 4.10. The flat surface of all the IPN samples with no textured properties, similar to PU surface, is also evidence of good homogeneity with no phase separation between two phases [38].

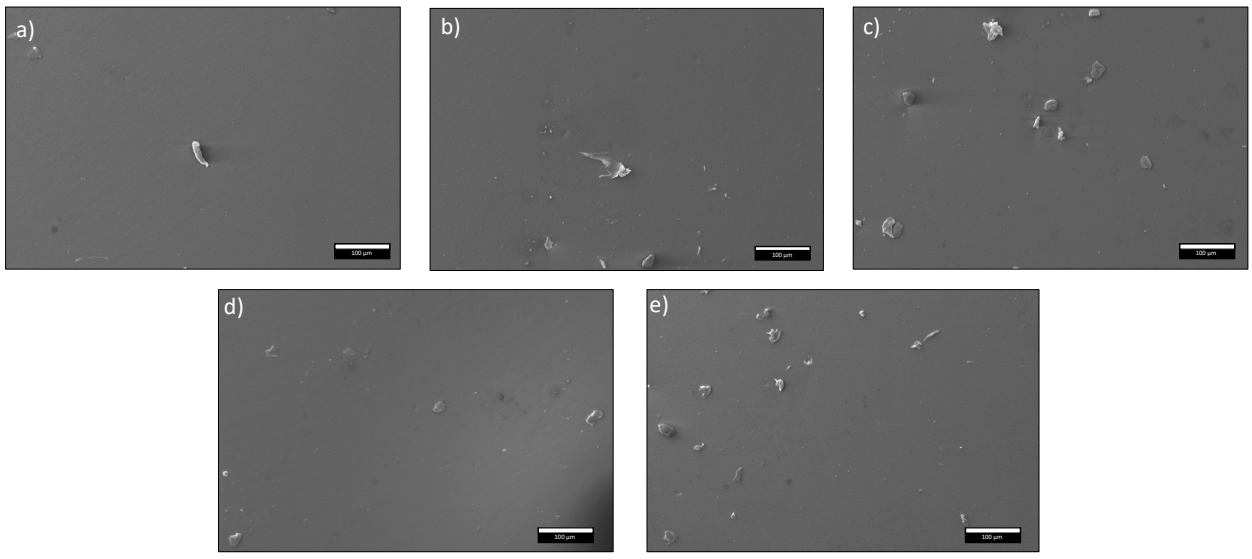

Figure 4.10. The cross-section SEM images of the fractured surface area of samples after tensile test a) PU b) IPN75-Styrene c) IPN75-MMA d) IPN50 Styrene e) IPN50-MMA.

4.3.2. Lap shear test

All samples were failed in shear through the adhesive. Table 4.4 shows a summary of the shear results for all the samples. In this experiment, COP-Styrene was used as the reference, which has the highest rigidity in comparison to other adhesive materials. As expected, PU shows the highest shear stress and displacement values due to the higher free volume and mobility of the chains in the PU structure. Shear stress value starts to decrease by synthesizing IPN samples out of PU. Reduction in the amount of PU in the system and the presence of acrylic copolymer into the system, which acts as a hindrance against free movement of polymer chains, are the reasons behind the decrease in shear stress. Surprisingly, IPN75-MMA shows smaller shear stress and displacement

in comparison to IPN-50 samples. However, as is shown in Table 4.4, the difference is not considerable for IPN samples. Finally, COP-Styrene shows the lowest displacement and shear stress due to the low free volume and less mobility of the chains in the acrylic copolymer structure.

Table 4.4. Summary of shear test results for PU, COP-Styrene, and IPN samples.

Sample	Shear Stress (MPa)	Tensile strain at maximum load (%)
PU	2.44 ± 0.32	4.10 ± 0.47
IPN75-Styrene	2.20 ± 0.33	2.78 ± 0.38
IPN75-MMA	1.94 ± 0.40	2.54 ± 0.50
IPN50-Styrene	2.13 ± 0.37	2.59 ± 0.51
IPN50-MMA	2.02 ± 0.39	2.46 ± 0.51
COP-Styrene	1.30 ± 0.43	1.57 ± 0.47

4.3.3. Impact resistant

The impact-resistant graphs for sandwich structures and a pure PC with similar thickness are shown in Figure 4.11 and summarized in Table 4.5. Initially, force fluctuation was observed in all samples, as shown within the dotted ellipse (Figure 4.11.a). The initial force fluctuation occurred due to the initial contact of the striker and the sample's surface. Elastic deformation, followed by elastic reflection, is the reason for the initial fluctuation. Next, the striker penetrates the sample and continues forming a neck shape on the other side. The slope of the load vs. time curves follows similar trends with approximately a similar slope for all samples. It shows that all samples show the same contact stiffness, determined by the slope of load vs. time curves [62]. It should be noted

that the slope of load vs. time curves for pure PC is lower; therefore, it has lower contact stiffness in comparison to IPN sandwich structures. After elastic deformation and yielding, samples show a steep drop in load, indicating that the samples experienced permanent plastic deformations.

Figure 4.11.b shows the energy absorbed vs. time for different sandwich samples in the impact test. All samples show the linear region of energy absorption showing the elastic deformation, followed by the plateau, which shows the permanent plastic deformation. From Figure 4.11 and Table 4.5, it could be observed that the PU sandwich sample shows the highest energy absorption, deflection, and time before failure due to the higher mobility and free volume of the chains in the PU structure. All of these factors start to decrease by synthesizing IPN out of PU. As shown, PC sheets with IPN products between them show a little higher energy absorption compared to the PC sheets alone. IPN-Styrene sandwich samples show higher energy absorption due to the higher stiffness in IPN-MMA samples coming from aminolysis reaction between the ester group of PMMA and amine groups of PU, and different copolymer structure of IPN samples [55]. COP-Styrene sample shows much lower values of force and energy absorption compared to the pure PC and IPN sandwich structures. This fact shows the applications of these novel graft-IPN systems where high toughness is required. It also shows the capability of these materials to be used as an adhesive with high impact resistance properties. It should be noted that energy absorption is indicative of the toughness of the material, which could be defined as an optimum number for strength and ductility in different materials [38, 63].

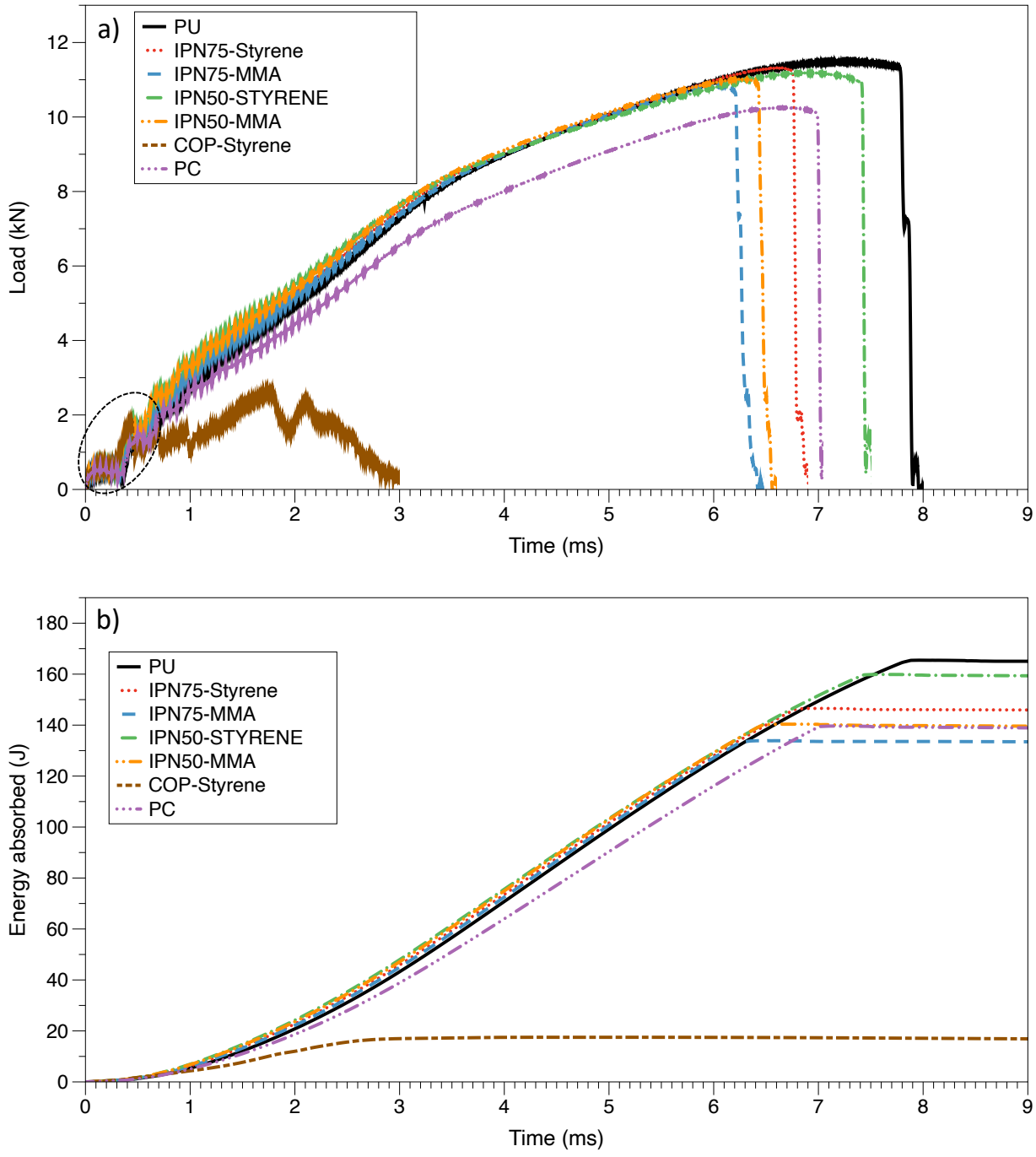

Figure 4.11. Impact resistance results a) load vs. time b) energy absorbed vs. time.

Table 4.5. Summary of impact resistance results.

Sample	Time to max load (ms)	Deflection at max load (mm)	Maximum load (kN)	Energy to max load (J)
PU	7.02 ± 0.26	22.47 ± 0.48	11.37 ± 0.44	149.95 ± 6.81
IPN75-Styrene	6.61 ± 0.33	21.55 ± 0.58	11.17 ± 0.33	141.56 ± 8.33
IPN75-MMA	6.15 ± 0.35	20.67 ± 0.77	10.77 ± 0.22	129.64 ± 8.08
IPN50-Styrene	6.62 ± 0.29	21.45 ± 0.53	11.11 ± 0.45	143.31 ± 7.73
IPN50-MMA	6.18 ± 0.45	20.57 ± 1.00	11 ± 0.28	132.98 ± 10.80
COP-Styrene	1.15 ± 0.44	4.56 ± 1.73	1.69 ± 0.50	4.96 ± 2.92
PC	6.58 ± 0.28	22.12 ± 0.64	10.44 ± 0.37	131.10 ± 7.35

Figure 4.12 shows the photograph of the samples before the test (first row), the top surface after the test (second row), and the bottom surface after the test (third row). As it is shown, all the samples except COP-Styrene show excellent resistance against the strike due to the high toughness coming from PC sheets and IPN samples in between them. The striker made a hole in all of the samples; however, no crack propagation was observed in any of the specimens. This fact shows the massive potential of these graft-IPN materials in high toughness applications. COP-Styrene sandwich, however, shows the catastrophic failure. Circular opening with cracks propagating all over samples is evidence of spallation failure mode in this sample.

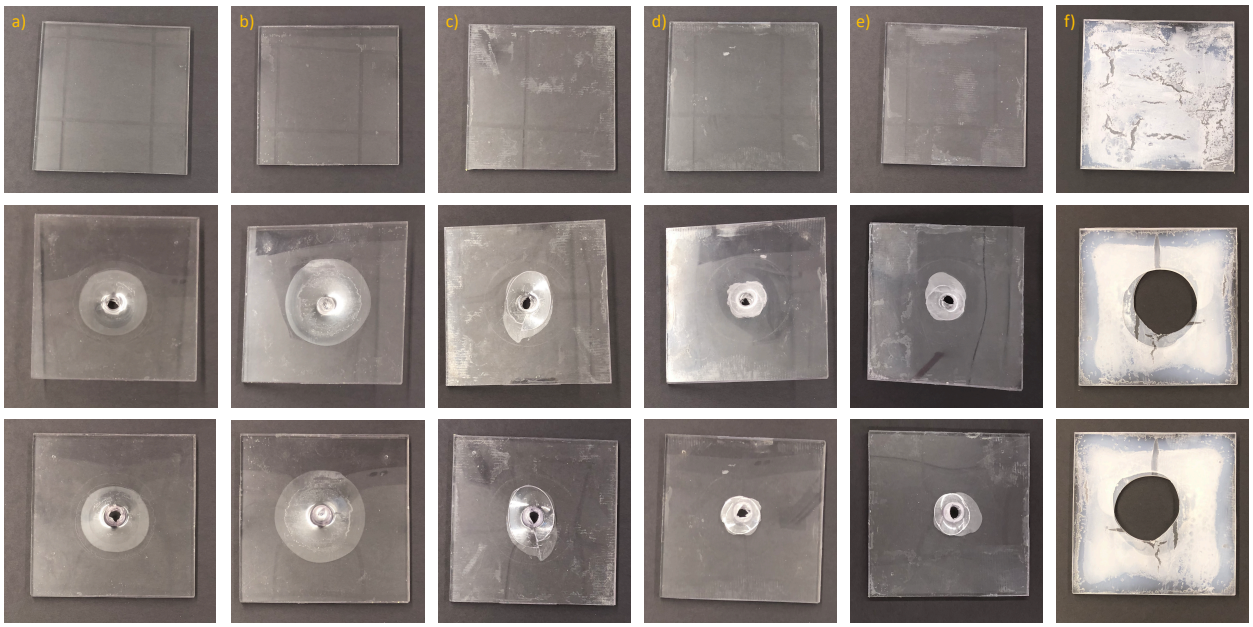

Figure 4.12. Photographs of sandwich samples before and after test a) PU b) IPN75-Styrene c) IPN75-MMA d) IPN50-Styrene e) IPN50-MMA f) COP-Styrene (The size of each sample is 152.4 mm × 152.4 mm).

4.4. Conclusions

Flexible graft-IPNs were successfully synthesized out of PU and acrylic copolymer. The effect of changing the composition of the two polymers on different strength properties was studied. Two different graft-IPN with two different monomers (Styrene and MMA) in the acrylic copolymer structure were synthesized in this research. Two polymers in the IPN system were grafted to minimize the phase separation and maximize the properties of the graft-IPNs. FTIR analysis confirms the successful synthesis of two phases in graft-IPN. DMA, Tensile, and shear analysis show a wide range of properties, from elastomeric properties to more ductile properties. IPN samples with a higher percentage of PU show more elastomeric behavior, while adding more

acrylic copolymer into the system changes the behavior to more ductile. Impact analysis shows high toughness impact resistance for IPN sandwich structures. Moreover, shear analysis shows the potential of synthesized IPN to be used as an adhesive. Finally, excellent transparency was observed in all IPN samples. These results indicate the considerable potential of the novel synthesized IPNs in transparent, high-impact applications.

References

1. Holden, H., To Be a U.S. Secret Service Agent. 2006: Zenith Press.

2. Jarrett, D.N., Cockpit Engineering. 2005: Ashgate Publishing Limited.

3. Hazell, P. J.; Edwards, M. R.; Longstaff, H.; Erskine, J., Penetration of a glass-faced transparent elastomeric resin by a lead–antimony-cored bullet. *International Journal of Impact Engineering* **2009,** *36* (1), 147-153.

4. Varasdi, J.A., *Myth Information. 1989, New York: Ballantine Books.*

5. Bird, S. A. Interpenetrating Polymer Networks with Polyurethane and Methacrylate-based Polymers. Auburn University, Auburn, AL, 2013.

6. Basu, B.; Balani, K., *Advanced Structural Ceramics.Hoboken: John Wiley & Sons, Inc.* Hoboken: John Wiley & Sons, Inc.: 2011.

7. Grujicic, M.; Bell, W. C.; Pandurangan, B., Design and material selection guidelines and strategies for transparent armor systems. *Materials & Design* **2012,** *34*, 808-819.

8. Girard, J. E., *Criminalistics: forensic science, crime, and terrorism.* 2 ed.; Jones &Bartlett Learning. 3.: 2011.

9. Krauthammer, T.; Marchand, K. A.; Mlakar, P. F.; Conrath, E. J., *Structural Design for Physical Security*. American Society of Civil Engineers.: 1999.

10. Scott, T. F.; Cook, W. D.; Forsythe, J. S., Kinetics and network structure of thermally cured vinyl ester resins. *European Polymer Journal* **2002,** *38* (4), 705-716.

11. Méndez, R. B. Sequential graft-Interpenetrating polymer networks based on polyurethane and acrylic/ester copolymers. Auburn University, Auburn, AL, 2015.

12. Alizadeh, N.; Thorne, D. P.; Auad, M. L.; Celestine, A.-D. N., Mechanical performance of vinyl ester—polyurethane interpenetrating polymer network composites. *Journal of Applied Polymer Science* **2021,** *138* (19), 50411.

13. Pham, S.; Burchill, P. J., Toughening of vinyl ester resins with modified polybutadienes. *Polymer* **1995,** *36* (17), 3279-3285.

14. Liang, G. Z.; Zuo, R. L.; Lu, T. L.; Wang, J. L., Modification of vinyl ester resin by a new thermoset liquid crystalline diacrylate. *Journal of Materials Science* **2005,** *40* (8), 2089-2091.

15. Petrovic, Z. S., *Handbook of Polymer Synthesis, Characterization, Processing*. A John Wiley & Sons, Inc.: 2013.

16. Patel, P. J.; Gilde, G. A.; Dehmer, P. G.; McCauley, J. W., Transparent armour. *The AMPTIAC Newsletter 4 (3)* 2000.

17. Chattopadhyay, D. K.; Raju, K. V. S. N., Structural engineering of polyurethane coatings for high performance applications. *Progress in Polymer Science* **2007,** *32* (3), 352-418.

18. Frisch, K. C.; Rumao, L. P., Catalysis in Isocyanate Reactions. *Journal of Macromolecular Science, Part C* **1970,** *5* (1), 103-149.

19. Luo, S.-G.; Tan, H.-M.; Zhang, J.-G.; Wu, Y.-J.; Pei, F.-K.; Meng, X.-H., Catalytic mechanisms of triphenyl bismuth, dibutyltin dilaurate, and their combination in polyurethane-forming reaction. *Journal of Applied Polymer Science* **1997,** *65* (6), 1217-1225.

20. Robeson, L. M., *Polymer Blends A Comprehensive Review*. Carl Hanser Verlag GmbH & Co. KG: 2007.

21. Raee, E.; Avid, A.; Kaffashi, B., Effect of compatibilizer concentration on dynamic rheological behavior and morphology of thermoplastic starch/polypropylene blends. *Journal of Applied Polymer Science* **2020,** *137* (22), 48742.

22. Panapitiya, N. P.; Wijenayake, S. N.; Huang, Y.; Bushdiecker, D.; Nguyen, D.; Ratanawanate, C.; Kalaw, G. J.; Gilpin, C. J.; Musselman, I. H.; Balkus, K. J.; Ferraris, J. P., Stabilization of immiscible polymer blends using structure directing metal organic frameworks (MOFs). *Polymer* **2014,** *55* (8), 2028-2034.

23. Sperling, L. H.; Mishra, V., The current status of interpenetrating polymer networks. *Polymers for Advanced Technologies* **1996,** *7* (4), 197-208.

24. Sperling, L. H.; Klempner, D.; Utracki, L. A., *Interpenetrating polymer networks*. American Chemical Society: Washington, DC, 1994; p xvi, 638 p.

25. BOUDENNE, A.; IBOS, L.; CANDAU, Y., *Handbook of Multiphase Polymer Systems*. A John Wiley & Sons, Ltd., Publication: 2011.

26. Pissis, P.; Georgoussis, G.; Bershtein, V. A.; Neagu, E.; Fainleib, A. M., Dielectric studies in homogeneous and heterogeneous polyurethane/polycyanurate interpenetrating polymer networks. *Journal of Non-Crystalline Solids* **2002,** *305* (1), 150-158.

27. Sperling, L. H., *Interpenetrating Polymer Networks and Related Materials*. Plenum Press,: New York, 1981; Vol. 12 (1).

28. Sperling, L. H., Interpenetrating Polymer Networks: An Overview. In *Interpenetrating Polymer Networks*, American Chemical Society: 1994; Vol. 239, pp 3-38.

29. Mita, I.; Akiyama, S., Macromolecular Design of Polymeric Materials. In *PLASTICS ENGINEERING-NEW YORK*, Marcel Dekker, Inc.: 1997; pp 393-406.

30. Frisch, H. L.; Klempner, D.; Frisch, K. C., A topologically interpenetrating elastomeric network. *Journal of Polymer Science Part B: Polymer Letters* **1969,** *7* (11), 775-779.

31. Chen, C. H.; Chen, W. J.; Chen, M. H.; Li, Y. M., Simultaneous full-interpenetrating polymer networks of blocked polyurethane and vinyl ester Part I. Synthesis, swelling ratio, thermal properties and morphology. *Polymer* **2000,** *41* (22), 7961-7967.

32. Fan, L. H.; Hu, C. P.; Ying, S. K., Thermal analysis during the formation of polyurethane and vinyl ester resin interpenetrating polymer networks. *Polymer* **1996,** *37* (6), 975-981.

33. Dave, V. J.; Patel, H. S., Synthesis and characterization of interpenetrating polymer networks from transesterified castor oil based polyurethane and polystyrene. *Journal of Saudi Chemical Society* **2017,** *21* (1), 18-24.

34. Alizadeh, N.; Barde, M.; Minkler, M.; Celestine, A.-D.; Agrawal, V.; Beckingham, B.; Auad, M. L., High-fracture-toughness acrylic–polyurethane-based graft-interpenetrating polymer networks for transparent applications. *Polymer International* **2020**.

35. Sundararajan, S.; Samui, A. B.; Kulkarni, P. S., Interpenetrating phase change polymer networks based on crosslinked polyethylene glycol and poly(hydroxyethyl methacrylate). *Solar Energy Materials and Solar Cells* **2016,** *149*, 266-274.

36. Sibaja, B.; Matheus, C. P.; Mendez, R. B.; Vega-Baudrit, J. R.; Auad, M. L., Synthesis and Characterization of Interpenetrating Polymer Networks (IPNs) from Acrylated Soybean Oil and α-Resorcylic Acid: Part 1. Kinetics of Network Formation. *Journal of Renewable Materials* **2017,** *5* (3-4), 231-240.

37. Sibaja, B.; Matheus, C. P.; Mendez, R. B.; Farag, R.; Baudrit, J. R. V.; Auad, M. L., Synthesis and Characterization of Interpenetrating Polymer Networks (IPNs) from Acrylated Soybean Oil α-Resorcylic Acid: Part 2. Thermo-Mechanical Properties and Linear Fracture Mechanics. *Journal of Renewable Materials* **2017,** *5* (3-4), 241-250.

38. Jajam, K. C.; Bird, S. A.; Auad, M. L.; Tippur, H. V., Tensile, fracture and impact behavior of transparent Interpenetrating Polymer Networks with polyurethane-poly(methyl methacrylate). *Polym. Test* **2013,** *32* (5), 889-900.

39. Sundaram, B. M.; Mendez, R. B.; Auad, M. L.; Tippur, H. V., Quasi-static and dynamic mechanical behavior of transparent graft-interpenetrating polymer networks (graft-IPNs). *Polymer Testing* **2018,** *70*, 348-362.

40. Bird, S. A.; Clary, D.; Jajam, K. C.; Tippur, H. V.; Auad, M. L., Synthesis and characterization of high performance, transparent interpenetrating polymer networks with polyurethane and poly(methyl methacrylate). *Polymer Engineering & Science* **2013,** *53* (4), 716-723.

41. Jajam, K. C.; Tippur, H. V.; Bird, S. A.; Auad, M. L. In *Dynamic Fracture and Impact Energy Absorption Characteristics of PMMA-PU Transparent Interpenetrating Polymer Networks (IPNs)*, Dynamic Behavior of Materials, Volume 1, Cham, 2014//; Song, B.; Casem, D.; Kimberley, J., Eds. Springer International Publishing: Cham, 2014; pp 277-284.

42. Jajam, K. C.; Bird, S. A.; Auad, M. L.; Tippur, H. V. In *Development and Characterization of a PU-PMMA Transparent Interpenetrating Polymer Networks (t-IPNs)*, Dynamic Behavior of Materials, Volume 1, New York, NY, 2011//; Proulx, T., Ed. Springer New York: New York, NY, 2011; pp 117-121.

43. Ballestero, R.; Sundaram, B. M.; Tippur, H. V.; Auad, M. L., Sequential graft-interpenetrating polymer networks based on polyurethane and acrylic/ester copolymers. *Express Polymer Letters* **2016,** *10* (3), 204-215.

44. Hillerström, A.; Andersson, M.; Pedersen, J. S.; Altskär, A.; Langton, M.; van Stam, J.; Kronberg, B., Transparency and wettability of PVP/PDMS-IPN synthesized in different organic solvents. *Journal of Applied Polymer Science* **2009,** *114* (3), 1828-1839.

45. Qin, C.-L.; Cai, W.-M.; Cai, J.; Tang, D.-Y.; Zhang, J.-S.; Qin, M., Damping properties and morphology of polyurethane/vinyl ester resin interpenetrating polymer network. *Materials Chemistry and Physics* **2004,** *85* (2-3), 402-409.

46. Alizadeh, N.; Bird, S. A.; Mendez, R. B.; Jajam, K. C.; Alexander, A. C.; Tippur, H. V.; Auad, M. L., Chapter 11 – Synthesis and Characterization of High Performance Interpenetrating Polymer Networks With Polyurethane and Poly(methyl methacrylate). In *Unsaturated Polyester Resins*, Elsevier: 2019; pp 243-255.

47. Huang, J.; Zhang, L., Effects of NCO/OH molar ratio on structure and properties of graft-interpenetrating polymer networks from polyurethane and nitrolignin. *Polymer* **2002,** *43* (8), 2287-2294.

48. ASTM E1640-18, Standard Test Method for Assignment of the Glass Transition Temperature By Dynamic Mechanical Analysis, ASTM International, West Conshohocken, PA, 2018.

49. ASTM D638-14, Standard Test Method for Tensile Properties of Plastics, ASTM International, West Conshohocken, PA, 2014.

50. ASTM D5420-16, Standard Test Method for Impact Resistance of Flat, Rigid Plastic Specimen by Means of a Striker Impacted by a Falling Weight (Gardner Impact), ASTM International, West Conshohocken, PA, 2016.

51. ASTM D3763-18, Standard Test Method for High Speed Puncture Properties of Plastics Using Load and Displacement Sensors, ASTM International, West Conshohocken, PA, 2018.

52. ASTM D3165-07(2014), Standard Test Method for Strength Properties of Adhesives in Shear by Tension Loading of Single-Lap-Joint Laminated Assemblies, ASTM International, West Conshohocken, PA, 2014.

53. Pavia, D. L.; Lampman, G. M.; Kriz, G. S., *Introduction to spectroscopy, Third edition*. Thomson Learning: Washington, 2001.

54. Cateto, C. A.; Barreiro, M. F.; Rodrigues, A. E., Monitoring of lignin-based polyurethane synthesis by FTIR-ATR. *Industrial Crops and Products* **2008,** *27* (2), 168-174.

55. Jin, Y.; Wong, K. H.; Granville, A. M., Developing localized surface plasmon resonance biosensor chips and fiber optics via direct surface modification of PMMA optical waveguides. *Colloids and Surfaces A: Physicochemical and Engineering Aspects* **2016,** *492*, 100-109.

56. Fried, J. R., *Polymer Science and Technology*. Prentice Hall Press: New Jersey 07458, 1996; Vol. 118.

57. Anslyn, E. V.; Dougherty, D. A., *Modern physical organic chemistry*. University Science: Sausalito, Calif., 2006; p xxviii, 1095 p.

58. Sulca, N. M.; Lungu, A.; Zaharia, C.; Stan, R.; Iovu, H., Determination of the Monomer Reactivity Ratios in Copolymerization of Two Distinct Dimethacrylates for Dental Use. *MATERIALE PLASTICE* **2010,** *47* (2), 254.

59. Auad, M. L.; Aranguren, M.; Borrajo, J., Epoxy-based divinyl ester resin/styrene copolymers: Composition dependence of the mechanical and thermal properties. *Journal of Applied Polymer Science* **1997,** *66* (6), 1059-1066.

60. Askarbekov, R.; Herak, D.; Mizera, C. In *Mechanical Behavior of Rubber Samples Under Relaxation*, Proceedings of the International Scientific Conference, 2016.

61. Wang, T. M.; Chen, S. B.; Wang, Q. H.; Pei, X. Q., Damping analysis of polyurethane/epoxy graft interpenetrating polymer network composites filled with short carbon fiber and micro hollow glass bead. *Materials & Design* **2010,** *31* (8), 3810-3815.

62. Hosur, M. V.; Chowdhury, F.; Jeelani, S., Low-Velocity Impact Response and Ultrasonic NDE of Woven Carbon/ Epoxy—Nanoclay Nanocomposites. *Journal of Composite Materials* **2007,** *41* (18), 2195-2212.

63. Ritchie, R. O., The conflicts between strength and toughness. *Nature Materials* **2011,** *10* (11), 817-822.

Chapter 5
Mechanical characterization and modeling stress relaxation behavior of acrylic-polyurethane-based graft-interpenetrating polymer networks

5.1. Introduction

The study of time-dependent, viscoelastic behavior of polymers is essential for many applications such as manufacturing processes where fast and large strains occur [1], shape memory, and self-repairing materials [2, 3], and bioengineering [4]. Traditionally, stress relaxation experiments are used to monitor the time-dependent changes in modulus in polymers. Stress relaxation behavior is observed when materials under a fixed strain relax over time [5, 6]. As the stress slowly decreases, the modulus (E) changes from E_0 to E_∞ [7]. The speed of this process is denoted as the stress relaxation time constant, τ. In polymeric materials, this decrease in stress occurs because the macromolecular conformation is not in the same state. Therefore, the movement of the chain segments occurs to relax internal stresses [8]. Considering the viscoelastic behavior of crosslink points in polymers with dynamic chemical bonds are time-dependent, the stress relaxation study of these materials is important [9-12].

Blending polymers is one of the many methods employed to enhance polymer properties [13]. Mixing polymers, however, introduces challenges due to polymers' inherent low entropy of mixing compared with the enthalpy [14, 15]. Polymerization techniques that utilize graft and block copolymers, and interpenetrating polymer networks (IPNs) are proposed to overcome the low miscibility of polymers and therefore enhance their final properties [16, 17]. IPNs consists of two polymers entangled with each other, where it is not possible to separate them without breaking the chemical bonds [17]. Entanglements bring forced compatibility between the two polymers and cause uniform structure within the IPNs [18]. IPNs are not soluble in solvents; however, solvents can swell

the IPN network [19]. Synthesis methods, degree of crosslinking, and degree of polymerization are some factors that can affect the final morphology of the IPNs [20].

The final properties of IPNs are influenced significantly by their morphology [21] and, as such, IPNs can be classified based on their final structures. Full-IPNs are one kind of IPNs where both polymers are crosslinked, while in semi-IPNs, only one of the polymers is crosslinked, and the other polymer has a linear structure [22]. Graft-IPNs are similar to full-IPNs, except that in graft-IPNs the chemical bonds between the two polymers are utilized to further enhance the compatibility of the two polymers [23, 24]. IPNs are also classified based on their synthesis methods. In sequential IPNs, the polymerization of Polymer A proceeds first while swelling the monomers of Polymer B. In simultaneous IPNs, however, polymerization of the two polymers begins at the same time, and no interfering reaction occurs [15, 16, 25].

Various studies, such as those by Millar et al. and Aylsworth and Edison, have examined the different aspects of IPNs [15, 26-29] and their synthesis [30, 31]. Factors such as the composition of the constituent polymers in the IPNs, the curing processes involved [31-35], the molecular weight of the polymer precursors [32], synthesis methods [33], and utilization of the chemical bonds between the two polymers [36, 37] play an essential role in the overall performance of the network. Different approaches to enhance polymers' compatibility have also been investigated [21, 33, 36, 38-42]. Graft-IPNs, which are synthesized via a sequential polymerization method, exhibit the best thermomechanical properties due to improved compatibility between the two polymers. It has also been observed that mixing a flexible polymer with a stiff one in the IPN structure enhances fracture toughness [36]. As a result, IPNs have found use in a wide range of applications, including biomedicine [43], dental applications [44], damping applications [45], coatings [24], adhesives [24], and many others [24, 45-51].

Bisphenol-A based dimethacrylate resins are highly viscous materials; therefore, vinyl ester resins (VER) are usually synthesized with low viscosity materials such as styrene and methyl methacrylate (MMA) [38, 52]. Their rapid curing properties, which arise from unsaturated polyesters, as well as excellent thermal and mechanical properties, low cost, and low weight, make vinyl ester resins great candidates in high-performance applications [38, 53]. Their brittle nature can be enhanced by adding flexible materials such as polyurethane (PU). The tailorable properties of PU, along with its high impact resistance properties, which is better than that of polycarbonate and acrylic copolymers, make PU an excellent candidate for improving fracture toughness properties of vinyl ester resins. IPNs consisting of PU and VER possess not only excellent thermal and mechanical properties but also exceptional toughening properties [54, 55]. These IPNs have the potential to be used as actuators for noise and vibration damping [49], and in shape memory and self-healing applications [1-4]. Understanding and modeling their stress relaxation behavior is therefore essential. In this paper, the stress relaxation behavior of acrylic-PU based graft-IPNs under tension and flexure was studied via experiments and finite element method (FEM) analysis. While FEM analysis has been widely used to study the viscoelastic and viscoplastic response of polymers [56], numerical modeling of IPNs is still in its infancy. The FEM model utilized in this work is based on a Generalized Maxwell model integrating Prony series data obtained from the stress relaxation experiments. A variational dissipation energy-based model was implemented in FEniCS [57, 58], a widely used open-source FEM software. This provides a basis for modeling time-dependent mechanical behavior such as stress relaxation and creep of IPNs. Additionally, this model can be coupled with micromechanics-based models to explicitly incorporate microstructural information such as chain unfolding and cross-linking. Flexural and tensile stress relaxation tests were simulated for IPN samples, and the decay in modulus was compared to experimental observations.

With only four terms in the Prony series, the FEM model showed a good, but not perfect, the match between experimental data and simulation predictions. The results can be improved by increasing the number of terms in the Prony series, as well as performing relaxation experiments under shear.

This paper is organized as follows: Section 2 outlines the experimental methods, including materials used, synthesis steps, and characterization of IPNs. Section 3 describes the numerical component of this work, including the Prony series model and results, and the variational dissipation energy-based formulation implemented in FEniCS along with results. Finally, the conclusions of this work are described in Section 4.

5.2. Experimental

5.2.1. Materials

The polyurethane (PU) precursors consisted of 2-ethyl-2-(hydroxymethyl)-1,3propanediol (TRIOL) with 134.18 g/mol purchased from Acros Organics, and poly(tetramethylene ether) glycol (PTMG) with approximately 1400 number average molecular weight purchased from Aldrich (USA) as the diol. Hexamethylene diisocyanate (DCH) purchased from TCI (USA) was also used in the synthesis. Dibutyltin dilaurate (DBTDL) and triphenyl bismuth (TPB) purchased from Pfaltz & Bauer (USA) and Alfa Aesar (USA), respectively, were used as the two catalysts for the step-growth polymerization of PU. Ethyl acetate, purchased from Alfa Aesar (USA), was used as a solvent to dissolve the catalysts. Molecular sieves, 4Å, 3-5 mm beads purchased from Alfa Aesar (USA), were utilized to remove the moisture from the DCH, styrene, TRIOL, and

PTMG. Molecular sieves were used to reduce the formation of bubbles in the IPNs caused by the reaction of water with isocyanate and subsequent production of carbon dioxide [59, 60].

Styrene purchased from Alfa Aesar (USA), and bisphenol A bis(2-hydroxy-3-methacryloxypropyl) ether (BisGMA) purchased from Esstech (USA) were utilized as the two monomers for the acrylic copolymer phase. 2,2'-azo bis(2-methyl-propionitrile) (AIBN) purchased from Matrix Scientific was used as the initiator.

5.2.2. Methods

5.2.2.1. Synthesis of graft-IPNs

Sequential polymerization was chosen to synthesize the graft-IPNs to enable better interpenetration between the two polymers [33]. In this method, the polymerization of one of the polymers begins first, while monomers of the second polymer are swelling in the first polymer network. This step is then followed by the polymerization of the second polymer to form the graft-IPN. For the PU phase, PU precursors were heated at 60°C, and molten TRIOL and PTMG were mixed in with the help of a mixer. As noted by Ballestero et al. [38], PTMG 1400 g/mol has ideal molecular weight necessary to provide the optimum PU network size and avoid phase separation in the system. After the mixture was allowed to cool, DCH was added into the mixture as an isocyanate group to react with the hydroxyl groups of the PU precursors and form PU via polyaddition polymerization. DCH was chosen due to the higher transparency provided, as reported by Bird et al. [21, 33]. A stoichiometric amount of PU precursors was used in this work.

For the acrylic copolymer phase, BisGMA was dissolved into styrene. Two hydroxyl groups in the BisGMA structure form the chemical bonds between two polymers and therefore increase the compatibility between the two phases. Subsequently, 1 wt% of total copolymer weight AIBN was

added into the mixture as a thermal initiator to initiate the free radical polymerization. AIBN breaks and forms free radicals at 60°C to start the polymerization of the acrylic copolymer. Next, the monomers of both polymers were mixed, and then the solution of the two catalysts was added to the mixture.

The graft-IPN was cured in a closed aluminum mold. The curing process began at a temperature of 40°C for 24 hours, where polymerization of PU begins. Next, the temperature was increased to 60°C and held for 24 hours. Free radical polymerizations of acrylic copolymer occur at this stage. Finally, to cure any residual monomers, the temperature was increased to 80°C and held for 24 hours. Copolymer (COP) samples with different percentages of styrene/BisGMA and IPN samples with varying proportions of PU/acrylic copolymer and styrene/BisGMA were synthesized for this study. Samples with low concentrations of PU were denoted as glassy IPNs (IPN_G) with glass transition higher than room temperature, while those with high concentrations of PU were denoted as rubbery IPNs (IPN_R) with glass transition lower than room temperature, as shown in Table 5.2. All the COP samples and IPN_G samples were rigid/glassy, while IPN_R and PU samples were flexible/rubbery. A summary of the different material samples examined is shown in Table 5.1.

Table 5.1. Composition of copolymer and graft-interpenetrating polymer network materials.

Materials	**PU (wt%)**	**Acrylic copolymer (wt%)**	**Styrene (wt%)**	**BisGMA (wt%)**
COP70/30	0	100	70	30
COP80/20	0	100	80	20
COP90/10	0	100	90	10
IPN_G70/30	25	75	70	30
IPN_G80/20	25	75	80	20

IPN_G90/10	25	75	90	10
IPN_R80/20	75	25	80	20
PU	100	0	0	0

COP: Copolymer
IPN_G: Glassy IPNs
IPN_R: Rubbery IPNs

5.2.2.2. Characterization of graft-IPNs

A TA Instruments RSA 3 dynamic mechanical analyzer (DMA) was used to study the stress relaxation behavior of the materials. Flexural tests were performed on the rigid/glassy samples (~ 10 mm width, ~ 2.5 mm thickness) using 3-point bend geometry with a 25 mm support span. For the rubbery materials, tensile tests were performed (with a 10 mm grip gap) on samples measuring ~ 10 mm width and ~ 2.5 mm thickness. All flexural tests and tensile tests were performed at 25°C with a fixed strain of 0.1% to determine the storage modulus (E') as a function of time in accordance with the ASTM E328 standard [61]. Dynamic temperature ramp tests (DTRT) were also performed on specimens measuring approximately 35 mm × 10 mm × 3 mm to determine the glass transition temperature (T_g) of each material. Tests were conducted using 3-point bend geometry with a 25 mm support span, 5°C/min heating rate, with a sinusoidal strain amplitude of 0.1% and 1 Hz frequency in accordance with ASTM E1640 [62]. The peak of $tan\ \delta$ was used to determine the glass transition temperature of each material. Both the initial storage modulus $E_0 = E'(t = 0)$, obtained from stress relaxation experiment, and glass transition T_g for each material type, obtained from DTRT, are summarized in Table 5.2. The storage modulus and $tan\ \delta$ plots for different samples are shown in Figure 5.1.

Table 5.2. Experimental results: storage modulus at the beginning of stress relaxation experiments (E_0) and glass transition temperature (T_g) of samples.

Materials	E_0 **(Mpa)**	T_g **(°C)**
COP70/30	1870.70	105.38
COP80/20	1250.00	100.95
COP90/10	810.53	107.27
IPN$_G$70/30	857.35	82.14
IPN$_G$80/20	1407.97	81.28
IPN$_G$90/10	1811.90	75.34
IPN$_R$80/20	10.14	-4.03
PU	3.48	-53.73

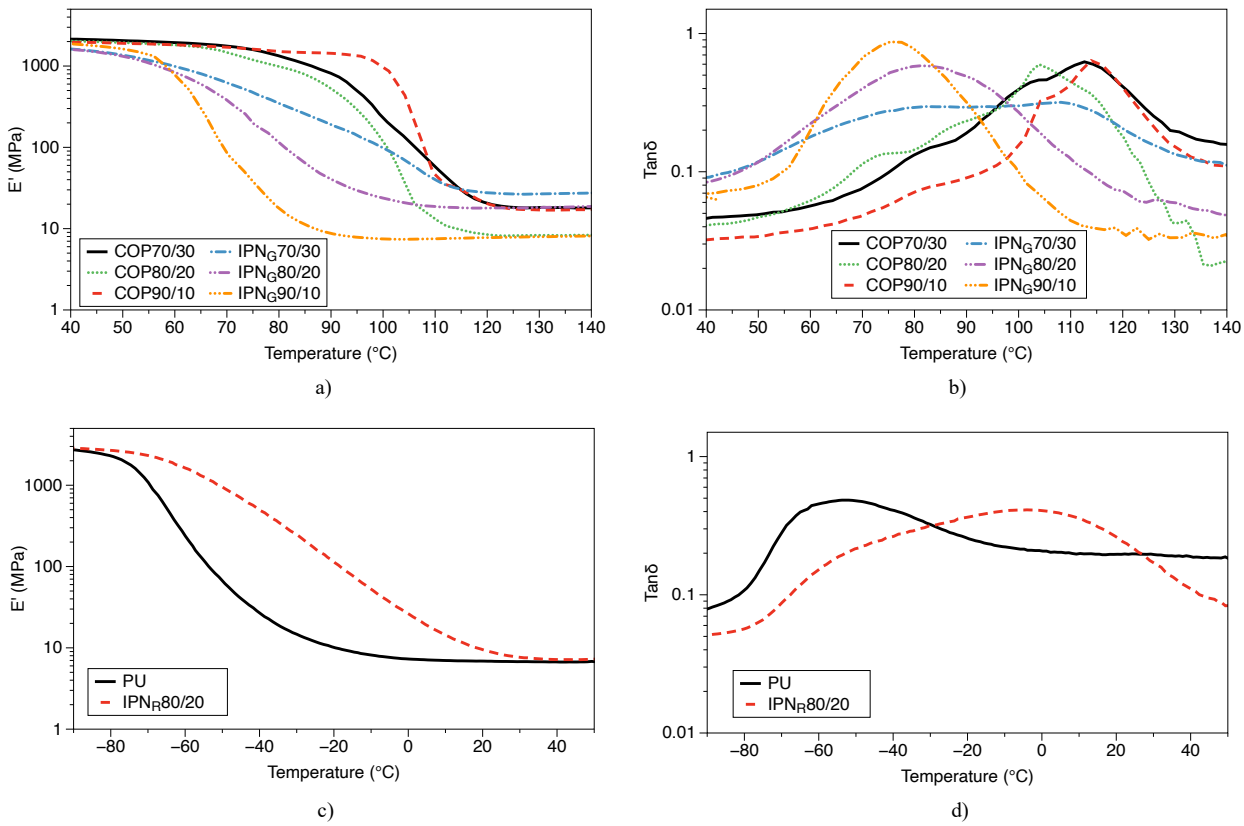

Figure 5.1. DTRT results for a) E' vs. temperature of glassy samples b) $tan\ \delta$ vs. temperature of glassy samples c) E' vs. temperature of rubbery samples d) $tan\ \delta$ vs. temperature of rubbery samples.

As shown in Figure 5.1, The $tan\ \delta$ for pure COP and PU samples show only one sharp peak. However, $IPN_G70/30$ and $IPN_R80/20$ show a broader $tan\ \delta$ peak, which indicates the heterogeneous microscopic structures in IPN systems, and it is due to the several relaxation mechanisms happening in IPNs. The $tan\ \delta$ peak becomes sharper for $IPN_G80/20$ and $IPN_G90/10$, indicating higher homogeneity and better compatibility between the two phases [33, 63, 64]. The peak for $IPN_G90/10$ becomes similar to the pure COP samples due to the excellent compatibility of two phases in $IPN_G90/10$. The presence of a higher percentage of styrene as small molecules enhances

the mobility of the acrylic copolymer and therefore provides better interpenetration between two phases in IPN_G90/10.

The stress relaxation behavior of glassy and rubbery samples is shown in Figure 5.2.a and Figure 5.2.b, respectively. The values on the vertical axis are normalized with respect to the modulus measured at $t = 0$ to better illustrate the stress relaxation behavior. As shown in Figure 5.2 and Table 5.2, most of the stress relaxation in all samples occurs at the beginning of the test. COP70/30 exhibits the highest modulus at the beginning of stress relaxation experiments (E_0) due to the lowest mobility and high rigidity of polymer chains in COP70/30. The initial modulus then decreases as the concentration of styrene increases. Styrene provides greater free volume and mobility and therefore reduces the modulus. Glassy IPN samples with a higher percentage of styrene, however, show higher initial modulus due to the better interpenetration between two phases in the IPN system, which brings less mobility and high rigidity, as mentioned before.

IPN_G70/30 shows a lower initial modulus compared to COP70/30 due to the presence of PU and heterogeneity in IPN_G70/30. In fact, IPN_G70/30 has the lowest initial modulus in all glassy IPN samples. However, IPN_G80/20 and IPN_G90/10 both show higher initial modulus than their COP counterpart samples due to the higher concentration of BisGMA in the PU phase, which enhances the mechanical properties of the IPNs and better compatibility between the two phases. A higher styrene content in COP80/20 and COP90/10 compared to COP70/30 is another reason behind this observation. As expected, PU exhibits the lowest initial modulus due to its high flexibility. IPN_R80/20 displays the lowest initial modulus after PU due to 75 wt% flexible PU, which acts as the continuous phase.

As depicted in Figure 5.2.a, IPN_G70/30 offers the lowest resistance to relaxation in glassy samples due to the heterogonous structure and low compatibility of IPN_G70/30, which affects the stress

relaxation behavior of the mentioned sample. Low interpenetration and low compatibility between two phases let two polymers relax with less resistance against the relaxation. Qualitatively, specimens with higher E_∞/E_0 or $E'(t=\infty)/E'(t=0)$ ratio are said to exhibit higher resistance to relaxation. As shown, $IPN_G80/20$ reveals better resistance than $IPN_G70/30$ against relaxation due to the better interpenetration between two phases in $IPN_G80/20$. In addition, $IPN_G90/10$ offers a much higher resistance to relaxation than $IPN_G80/20$. In fact, $IPN_G90/10$ shows resistance to relaxation similar to COP samples due to the excellent interpenetration between two polymers. Each network supports one another and therefore provides high resistance against relaxation. As expected, COP samples with the high rigidity and storage modulus reveal the highest resistance against relaxation due to the highly crosslinked network, which opposes the chains to move and relax.

The flexible/rubbery specimens (Figure 5.2.b) exhibit excellent resistance during the stress relaxation experiments. This behavior indicates their capacity to damp vibrations, finding application in shock absorbers and isolators [65]. Surprisingly, between the two flexible/rubbery specimens, PU shows better resistance to relaxation than $IPN_R80/20$. Low interpenetration between two polymers in $IPN_R80/20$, which prevents two polymers to support each other and therefore $IPN_R80/20$ relax with less resistance against relaxation is the reason behind this phenomena.

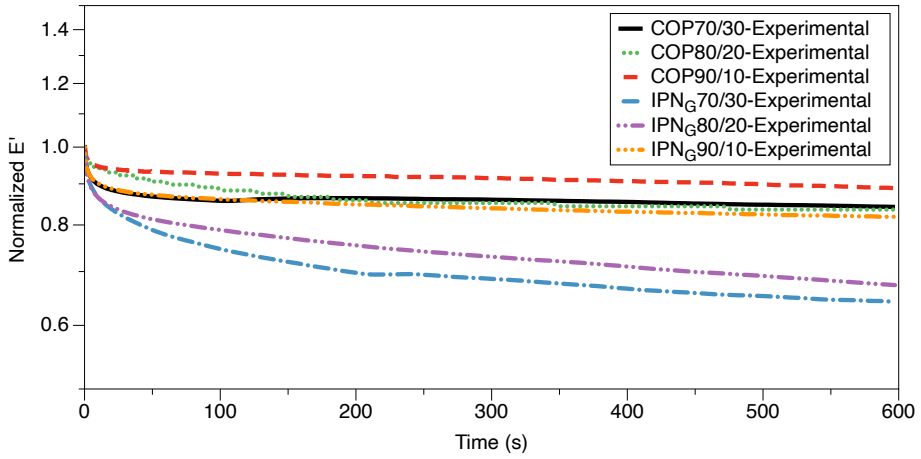

a)

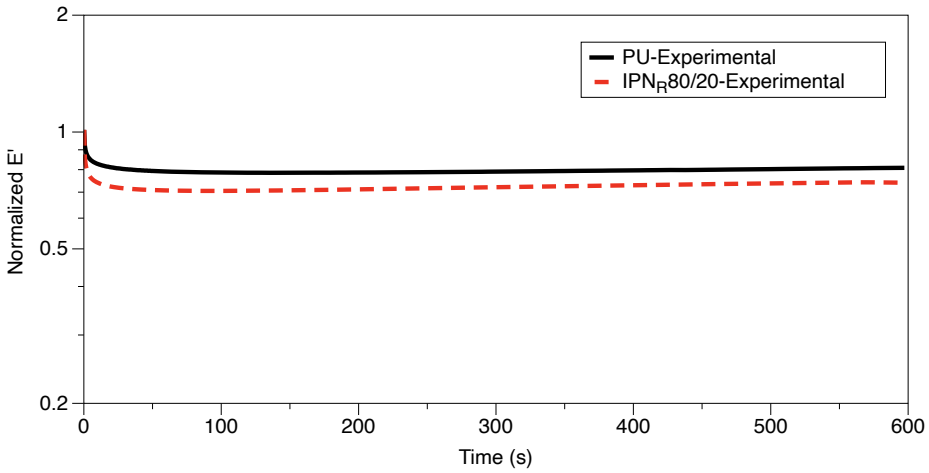

b)

Figure 5.2. Experimentally measured modulus (normalized with the modulus at $t = 0$) as a function of time illustrating the stress relaxation behavior of a) glassy samples b) rubbery samples.

5.3. Numerical modeling

5.3.1. Prony-series based model

The stress relaxation behavior of the IPN system was modeled using a Generalized Maxwell model in a three-dimensional setting. A schematic of the system used in this work is shown in Figure 5.3. The model shown in Figure 5.3 consists of a spring with modulus κ connected to a series of springs and dashpots systems. Springs start to deform immediately by applying force and reach equilibrium. Then the dashpot begins to move. When the force is removed, the spring returns to its original shape. However, the dashpot stays in this final shape. This model predicts the viscoelastic behavior of the polymers [65].The system consists of one spring with modulus μ_∞ connected to n parallel elements of springs μ_i and dashpots η_i, $(i = 1,2, \dots, n)$. The relaxation time τ_i for the i^{th} spring-dashpot branch is given by

$$\tau_i = \frac{\eta_i}{\mu_i} \qquad [5.1]$$

The total strain tensor ε is decomposed into a volumetric strain ε_{vol} and a deviatoric strain ε_{dev} as

$$\varepsilon = \varepsilon_{dev} + \varepsilon_{vol} \qquad [5.2]$$

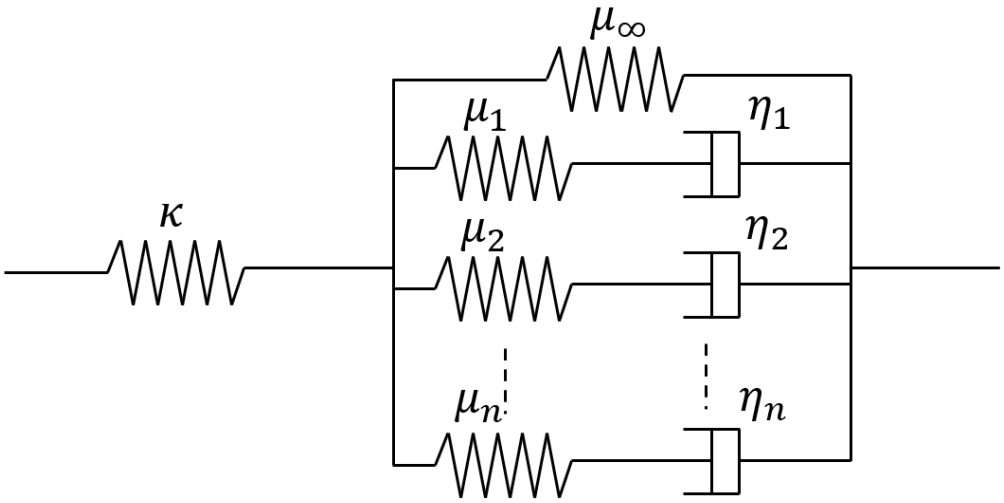

Figure 5.3. Schematic of the material model based on Generalized Maxwell model.

Where

$$\varepsilon_{vol} = \frac{1}{3} tr(\varepsilon)\, I, \quad \varepsilon_{dev} = \varepsilon - \varepsilon_{vol} \tag{5.3}$$

Next, a viscous strain $\varepsilon_i^v, (i = 1,2, \dots, n)$ is introduced corresponding to every spring-dashpot branch. The viscous strain is an internal variable that accounts for strain in the dashpot element. The total stress is now given as

$$\sigma = \sigma_{vol} + \sigma_{dev} \tag{5.4}$$

where

$$\sigma_{vol} = 3\kappa\, \varepsilon_{vol}, \qquad \sigma_{dev} = \mu_\infty\, \varepsilon_{dev} + \sum_{i=1}^{n} \mu_i\, (\varepsilon_{dev} - \varepsilon_i^v) \qquad [5.5]$$

Finally, the evolution of the viscous strain ε_i^v can be obtained from the internal force balance in the i^{th} spring-dashpot element as

$$\eta_i\, \dot{\varepsilon_i^v} = \mu_i(\varepsilon_{dev} - \varepsilon_i^v) \;\; \Rightarrow \;\; \dot{\varepsilon_i^v} = \frac{\mu_i}{\eta_i}(\varepsilon_{dev} - \varepsilon_i^v) = \frac{1}{\tau_i}(\varepsilon_{dev} - \varepsilon_i^v) \qquad [5.6]$$

The parameters in this Prony series model were determined from the stress relaxation experiments.

5.3.2. Results and discussion

5.3.2.1. Prony series parameters

Prony series constants for young modulus were obtained using stress relaxation experiments. The stress relaxation experiments were performed using three-point bend tests for rigid/glassy samples and tensile tests for flexible/rubbery samples. Results were fit to the equation below for four terms in the Prony series.

$$E = E_\infty + \sum_{i=1}^{4} E_i\, e^{-\frac{t}{\tau_i}} \qquad [5.7]$$

Constants E_∞, E_i $(i = 1, \dots, 4)$ and τ_i $(i = 1, \dots, 4)$ were obtained using the Curve Fitting toolbox in MATLAB with constraints $E_\infty > 0$, $E_i > 0$ and $\tau_i > 0$. The fitting search criterion was adjusted to obtain fitted values with R^2 value of above 0.99. The fitted values are listed in Table 5.3.

Table 5.3. Fitted parameters obtained from MATLAB curve fitting toolbox.

	Modulus (MPa)					**Relaxation Time (s)**			
	$\boldsymbol{E_1}$	$\boldsymbol{E_2}$	$\boldsymbol{E_3}$	$\boldsymbol{E_4}$	$\boldsymbol{E_\infty}$	$\boldsymbol{\tau_1}$	$\boldsymbol{\tau_2}$	$\boldsymbol{\tau_3}$	$\boldsymbol{\tau_4}$
COP70/30	142.0	111.6	1.074	905.5	718.7	1.313	15.44	718.5	12330
COP80/20	35.38	29.41	114.7	637.1	459.9	1.061	6.824	98.03	12980
COP90/10	33.26	22.8	19.21	757.7	8218	0.2283	2.113	14.45	12870
IPN$_G$70/30	52.74	49.18	112.5	159.3	482.7	0.98	5.976	55.36	684.9
IPN$_G$80/20	121.2	65.06	365.7	86.4	779.2	1.14	47.38	783.4	8.493
IPN$_G$90/10	135.0	76.12	67.61	151.7	1434	0.589	4.166	22.53	532.6
IPN$_R$80/20	2.39	0.7198	0.379	0.0366	8.243	0.882	7.149	28.14	1267
PU	0.4187	0.2028	0.189	0.722	2.243	0.832	5.022	28.14	10400

5.3.2.2. FEM modeling

The spring-dashpot model was implemented in FEniCS [57, 58, 66], an open-source finite-element framework, being actively developed and maintained by the scientific community. The equations presented were reformulated as a variational problem for ease of implementation within FEniCS. An incremental potential $\mathcal{E}$ was defined as,

$$\mathcal{E} = \int_{\Omega} w(\varepsilon, \varepsilon_i^v)\, d\Omega + \Delta t \int_{\Omega} \phi(\dot{\varepsilon}_i^v)\, d\Omega - W_{ext}(u) \quad [5.8]$$

where u is the displacement, W_{ext} is the work done by external forces, w is the internal strain energy density, and ϕ is the dissipation potential. The strain energy density and dissipation potential were given by

$$w(\varepsilon, \varepsilon_i^v) = \frac{1}{2} 3\kappa\, \varepsilon_{vol} : \varepsilon_{vol} + \frac{1}{2}\mu_\infty \varepsilon_{dev} : \varepsilon_{dev} + \sum_{i=1}^{n} \frac{1}{2}\mu_i (\varepsilon_{dev} - \varepsilon_i^v) : (\varepsilon_{dev} - \varepsilon_i^v),$$

$$\phi(\dot{\varepsilon}_i^v) = \sum_{i=1}^{N} \frac{1}{2}\eta_i \dot{\varepsilon}_i^v : \dot{\varepsilon}_i^v \quad [5.9]$$

A backward Euler approximation was introduced for time-discretization as

$$\dot{\varepsilon}_i^v \approx \frac{\varepsilon_i^{v,n+1} - \varepsilon_i^{v,n}}{\Delta t} \quad [5.10]$$

where $\boldsymbol{\varepsilon}_i^{v,n+1}$ denotes the viscoelastic strain in the i^{th} dashpot at time t_{n+1}, and Δt is the time-step. The problem was rewritten as a minimization problem of incremental potentials as,

$$\min_{\boldsymbol{\varepsilon}^{n+1},\boldsymbol{\varepsilon}_i^{v,n+1}} \mathcal{E}_{n+1} = \int_\Omega w\left(\boldsymbol{\varepsilon}^{n+1}, \boldsymbol{\varepsilon}_i^{v,n+1}\right) d\Omega + \Delta t \int_\Omega \phi\left(\frac{\boldsymbol{\varepsilon}_i^{v,n+1} - \boldsymbol{\varepsilon}_i^{v,n}}{\Delta t}\right) d\Omega \qquad [5.11]$$

which depends on the values at the previous time step. Finally, the strain was defined in terms of displacement as,

$$\varepsilon = \frac{1}{2}(grad\ u + (grad\ u)^T) \qquad [5.12]$$

A cuboidal sample, $L = 25$ mm, $W = 10$ mm, and $H = 2$ mm, was chosen with $50 \times 20 \times 4$ tetragonal mesh elements. Cubic polynomial shape functions were used for this analysis. A three-point bend test was simulated (Figure 5.4.a) with boundary conditions

$$u_z = \begin{cases} 0 & at \quad x = 0, z = 0 \\ 0 & at \quad x = L, z = 0 \\ D & at \quad x = L/2, z = H \end{cases} \qquad [5.13]$$

where $D = -0.05$ mm and u_z is the z component of u. The tensile test was simulated (Figure 5.4.b) with boundary conditions as

$$u_x = \begin{cases} 0 & at \quad x = 0 \\ D & at \quad x = L \end{cases} \qquad [5.14]$$

where $D = -0.05$ mm and u_x is the x component of u. The displacement was held constant, and the material was allowed to relax. Figure 5.5.a shows the actual meshed geometry and the color plot of u_z in the domain under a three-point bend test. The total vertical force necessary to maintain

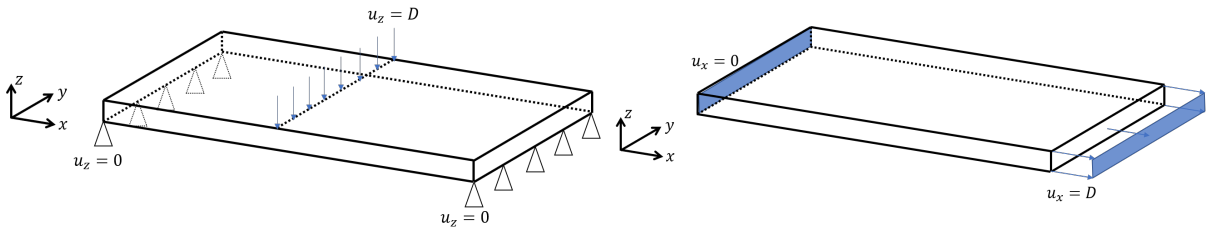

a) b)

Figure 5.4. a) Schematic of the stress relaxation model with constrained u_z boundary conditions b) schematic of the tensile test with u_x boundary conditions.

The applied displacement was calculated by integrating the shear stress σ_{13} as,

$$F = 2\int_0^W \int_0^H \sigma_{13}\left(x = \frac{L}{4}, y, z\right) dz\, dy \qquad [5.15]$$

Next, flexural stresses, strains, and modulus were calculated using standard three-point test formulation as

$$\sigma_f = \frac{3FL}{2WH^2}\ ,\ \varepsilon_f = \frac{6DH}{L^2}\ , E_f = \frac{\sigma_f}{\varepsilon_f} \qquad [5.16]$$

Figure 5.5.b shows u_x profile in the sample for the tensile test boundary conditions. The total horizontal force in the mid-plane or gauge section was calculated as

$$F = \int_0^W \int_0^H \sigma_{11}\left(x = \frac{L}{2}, y, z\right) dz\, dy \qquad [5.17]$$

The effective young's modulus was then calculated as

$$\sigma_t = \frac{F}{WH}, \varepsilon_t = \frac{D}{L}, E_t = \frac{\sigma_t}{\varepsilon_t} \qquad [5.18]$$

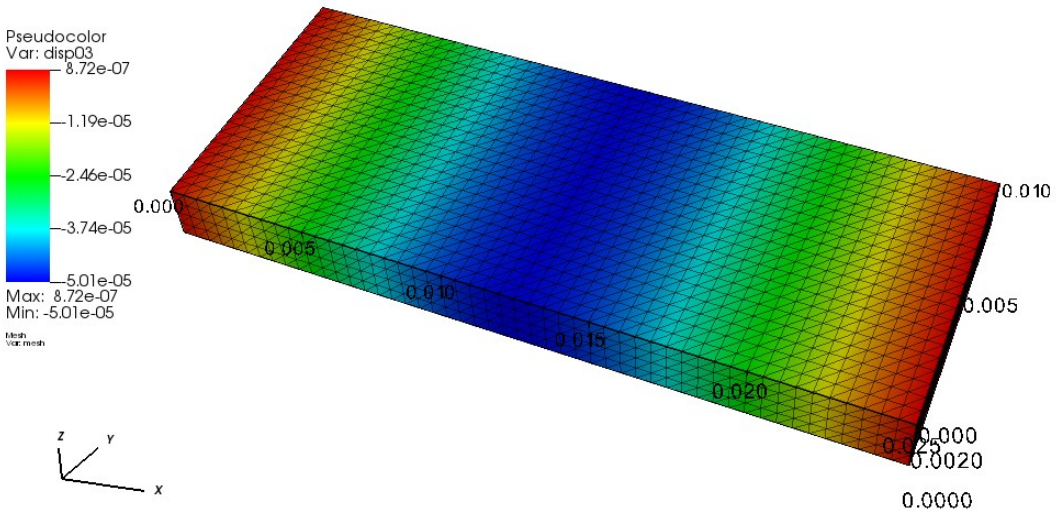

a)

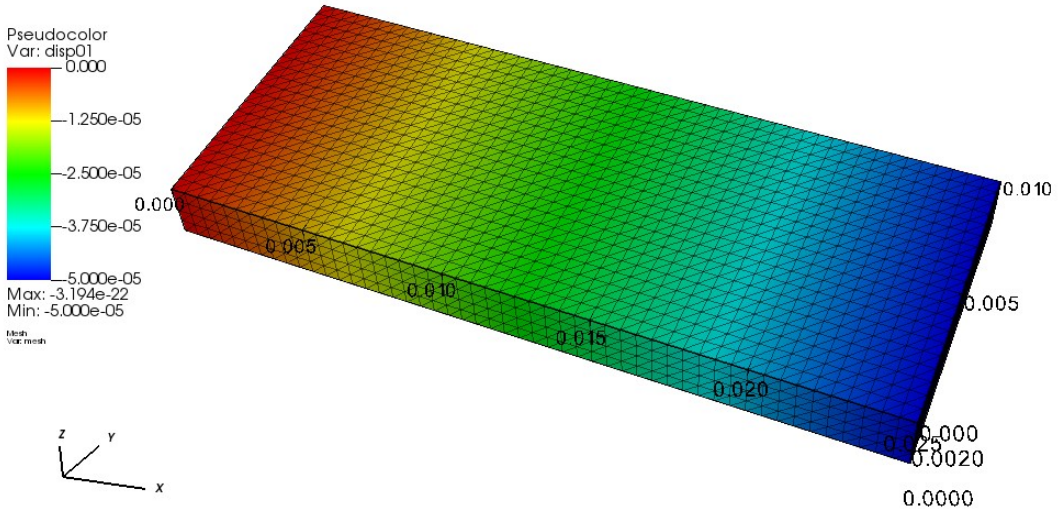

b)

Figure 5.5. a) Color plot of u_z generated by the model along with the meshed geometry under the flexure test b) color plot of u_x generated by the model along with the meshed geometry under tensile test. The minimum value (blue) is −0.05 mm, and the maximum value (red) is 0.0.

The values for κ, μ_∞, and μ_i were obtained using Prony series constants in Table 5.3 with a scaling factor of 0.6 for flexure samples (COP70/30, COP80/20, COP90/10, IPN_G70/30, IPN_G80/20, IPN_G90/10), 0.85 for tensile samples (IPN_R80/20, PU), and a Poisson's ratio of 0.3 for all materials.

Figure 5.6 shows the plot of flexural and tensile modulus obtained from simulations for all the samples in log scale. Experimental data is overlaid for comparison. A good correlation is observed between experiments and simulations. The model performs well for COP and IPN_G samples and successfully predicts their relaxation behavior with reasonable accuracy. On the other hand, it cannot accurately capture rubbery samples such as IPN_R80/20 and PU. This is because the model uses dashpots for the deviatoric components of the strain tensor, which dominates during the

relaxation of rigid samples. To accurately capture softer materials, the model in Figure 5.3 must be updated to incorporate dashpots in both volumetric and deviatoric components. The calibration of the model would require relaxation experiments in different configurations, including tension and shear. It should also be noted that the model only takes data from the stress relaxation experiments. Additionally, the model uses only four terms for the Prony series model, which governs the relaxation in shear modulus. Further improvements can be made using experiments focused on measuring shear stress relaxation. Model predictions can also be improved by increasing the number of terms in the Prony series model. These steps will be reserved for future work.

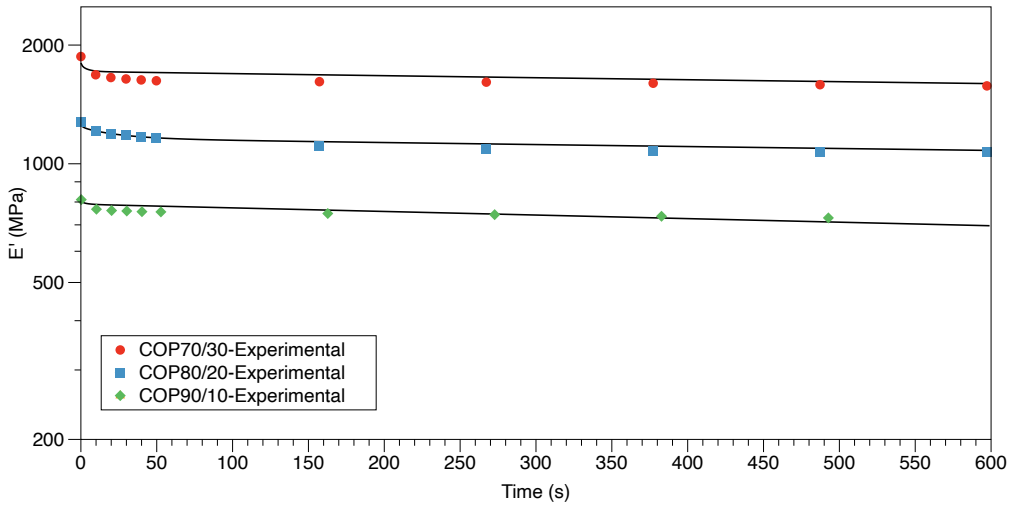

a)

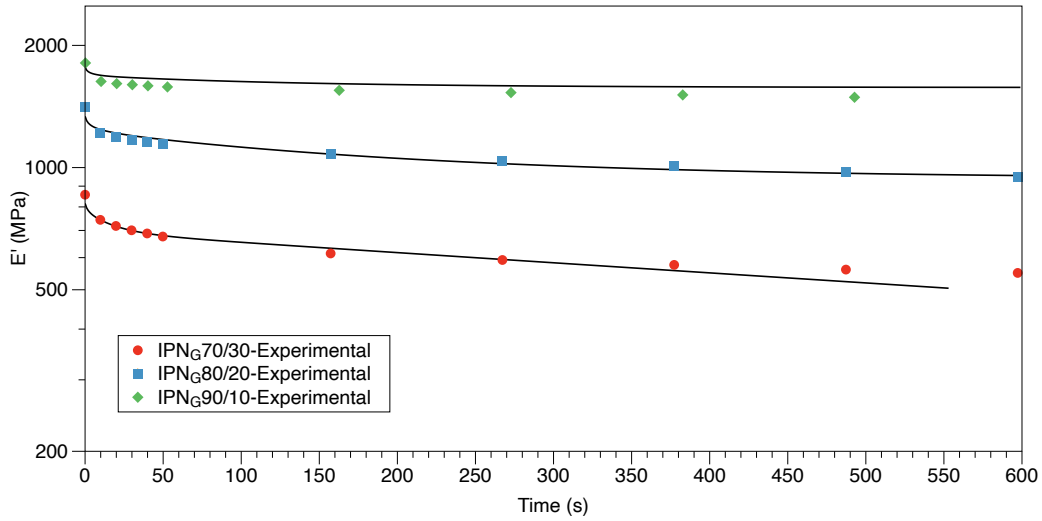

b)

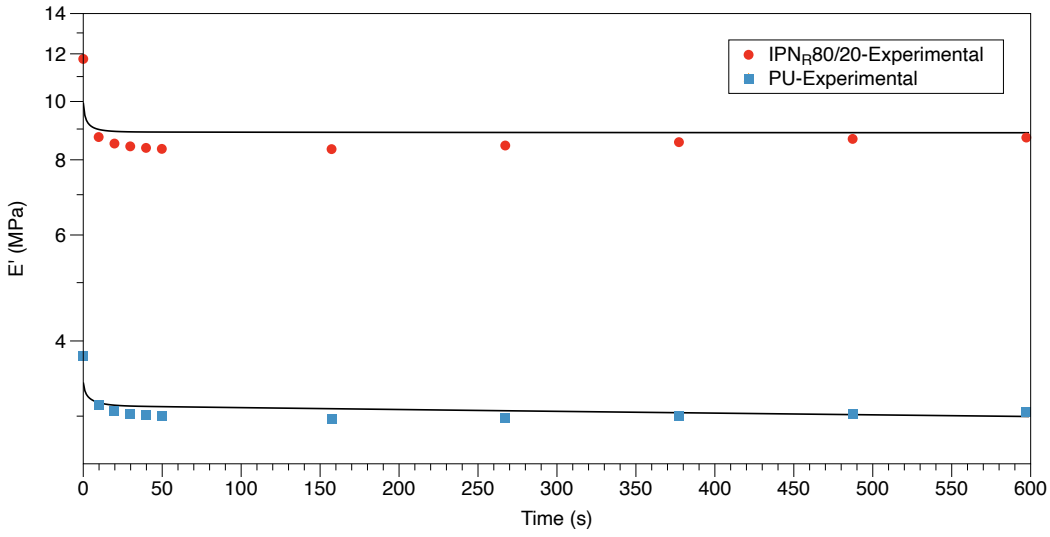

c)

Figure 5.6. Plot of modulus vs. time for a) COP b) IPN_G (glassy IPN) c) IPN_R (rubbery IPN) and PU samples as a function of time. Model results are represented by a solid line. The model captures the experimental data with reasonable accuracy.

5.4. Conclusions

In this paper, the stress relaxation behavior of the graft-IPN samples was characterized by tensile and flexural geometry. The miscibility of two phases in IPN systems was also examined using DTRT. It was observed that the IPN structure's homogeneity starts to enhance by adding more styrene to the system. Most of the stress relaxation behavior for samples was observed at the beginning of the stress relaxation test, and then the curve becomes flattened. The results suggested that a higher percentage of styrene in acrylic copolymer samples decreases the relaxation modulus. However, Glassy IPNs indicated that the relaxation modulus increases by adding more styrene to the system due to the better interpenetration between the two polymers. The lowest relaxation modulus was observed in PU and IPN_R80/20 due to the high flexibility of the samples. IPN_G90/10 shows the resistance against relaxation comparable to COP samples due to the excellent interpenetration between two phases. As expected, COP samples show the highest resistance against relaxation coming from the low mobile chain in the acrylic copolymer system. Moreover, PU reveals higher resistance against relaxation compared to IPN_R80/20 due to the low interpenetration in rubbery IPNs that makes it difficult for two phases to support each other and avoid high relaxation.

Flexible/rubbery samples show excellent relaxation resistance, which indicates their potential to be used in shock damping applications. A three-dimensional Prony series based finite element model was developed for IPNs. The FEM model was based on the Generalized Maxwell model and used the volumetric-deviatoric decomposition of the strain tensor. Prony series constants were extracted from stress relaxation experiments, and three-point bend and tension tests were simulated using FEniCS. A good match was observed between simulation predictions and experimental observations. The model is limited in its current state has the following limitations.

First, the model uses dashpots in the shear/deviatoric component of modulus/strain. As such the model predictions deviate from experimental data for softer materials. Second, the model uses four term Prony series model which can be extended to more standard six or eight term series. Third, the model only takes information from stress relaxation experiment. Improvements can be made by a) introducing relaxation in the volumetric component of the strain, b) including more terms in the Prony series and a number of spring-dashpot branches in Figure 5.3, and c) calibrating the model with more experimental data. It should be emphasized that the model performs with good accuracy despite these limitations.

References

1. Chen, J.; Gu, C.; Lin, H.; Chen, S.-C., Soft mold-based hot embossing process for precision imprinting of optical components on non-planar surfaces. *Optics express* **2015,** *23* (16), 20977-20985.

2. Schiavi, A.; Prato, A., Evidences of non-linear short-term stress relaxation in polymers. *Polymer Testing* **2017,** *59*, 220-229.

3. Huang, W. M.; Ding, Z.; Wang, C. C.; Wei, J.; Zhao, Y.; Purnawali, H., Shape memory materials. *Materials Today* **2010,** *13* (7), 54-61.

4. Nayar, V. T.; Weiland, J. D.; Nelson, C. S.; Hodge, A. M., Elastic and viscoelastic characterization of agar. *Journal of the Mechanical Behavior of Biomedical Materials* **2012,** *7*, 60-68.

5. Ginta, L.; Rimvydas, M., Behaviour of Long-Lasting Stress Relaxation of Various Types of Yarns. *Autex Research Journal* **2017,** *17* (4), 379-385.

6. Baszczyński, K., Effect of repeated loading on textile rope and webbing characteristics in personal equipment protecting against falls from a height. *Fibres & Textiles in Eastern Europe* **2015**.

7. Schiavi, A.; Prato, A. In *Non-Linear Stress Relaxation of Polymers: Experimental Evidences and Stretched-Exponential Model*, 23nd International Congress of Sound and Vibration, 2016.

8. Obaid, N.; Kortschot, M. T.; Sain, M., Understanding the Stress Relaxation Behavior of Polymers Reinforced with Short Elastic Fibers. *Materials (Basel)* **2017,** *10* (5).

9. Hayashi, M.; Yano, R., Fair Investigation of Cross-Link Density Effects on the Bond-Exchange Properties for Trans-Esterification-Based Vitrimers with Identical Concentrations of Reactive Groups. *Macromolecules* **2020,** *53* (1), 182-189.

10. Liu, B.; Tang, Z.; Wang, Z.; Zhang, L.; Guo, B., Integrating transient and sacrificial bonds into biobased elastomers toward mechanical property enhancement and macroscopically responsive property. *Polymer* **2019,** *184*, 121914.

11. Wang, C.; Deitrick, K.; Seo, J.; Cheng, Z.; Zacharia, N. S.; Weiss, R. A.; Vogt, B. D., Manipulating the Mechanical Response of Hydrophobically Cross-Linked Hydrogels with Ionic Associations. *Macromolecules* **2019,** *52* (16), 6055-6067.

12. Brutman, J. P.; Fortman, D. J.; De Hoe, G. X.; Dichtel, W. R.; Hillmyer, M. A., Mechanistic Study of Stress Relaxation in Urethane-Containing Polymer Networks. *The Journal of Physical Chemistry B* **2019,** *123* (6), 1432-1441.

13. Robeson, L. M., *Polymer Blends A Comprehensive Review*. Carl Hanser Verlag GmbH & Co. KG: 2007.

14. Panapitiya, N. P.; Wijenayake, S. N.; Huang, Y.; Bushdiecker, D.; Nguyen, D.; Ratanawanate, C.; Kalaw, G. J.; Gilpin, C. J.; Musselman, I. H.; Balkus, K. J.; Ferraris, J. P., Stabilization of immiscible polymer blends using structure directing metal organic frameworks (MOFs). *Polymer* **2014,** *55* (8), 2028-2034.

15. Sperling, L. H.; Mishra, V., The current status of interpenetrating polymer networks. *Polymers for Advanced Technologies* **1996,** *7* (4), 197-208.

16. Sperling, L. H., Interpenetrating Polymer Networks: An Overview. In *Interpenetrating Polymer Networks*, American Chemical Society: 1994; Vol. 239, pp 3-38.

17. BOUDENNE, A.; IBOS, L.; CANDAU, Y., *Handbook of Multiphase Polymer Systems*. A John Wiley & Sons, Ltd., Publication: 2011.

18. Li, B.; Bi, X.; Zhang, D.; Whang, F., Forced Compatibility and Mutual Entanglements in Poly (Vinyl Acetate)/Poly (Methyl Acrylate) IPNs. *Technomic Publishing Company, Advances in Interpenetrating Polymer Networks.* **1989,** *1*, 203-220.

19. Sperling, L. H., Interpenetrating polymer networks and related materials. **1977,** *12* (1), 141-180.

20. Sheu, H. R.; El-Aasser, M. S.; Vanderhoff, J. W., Phase separation in polystyrene latex interpenetrating polymer networks. *Journal of Polymer Science Part A: Polymer Chemistry* **1990,** *28* (3), 629-651.

21. Bird, S. A. Interpenetrating Polymer Networks with Polyurethane and Methacrylate-based Polymers. Auburn University, Auburn, AL, 2013.

22. Pissis, P.; Georgoussis, G.; Bershtein, V. A.; Neagu, E.; Fainleib, A. M., Dielectric studies in homogeneous and heterogeneous polyurethane/polycyanurate interpenetrating polymer networks. *Journal of Non-Crystalline Solids* **2002,** *305* (1), 150-158.

23. Sperling, L. H.; Klempner, D.; Utracki, L. A., *Interpenetrating polymer networks*. American Chemical Society: Washington, DC, 1994; p xvi, 638 p.

24. Sperling, L. H., *Interpenetrating Polymer Networks and Related Materials*. Plenum Press,: New York, 1981; Vol. 12 (1).

25. Mita, I.; Akiyama, S., Macromolecular Design of Polymeric Materials. In *PLASTICS ENGINEERING-NEW YORK*, Marcel Dekker, Inc.: 1997; pp 393-406.

26. Chen, C. H.; Chen, W. J.; Chen, M. H.; Li, Y. M., Simultaneous full-interpenetrating polymer networks of blocked polyurethane and vinyl ester Part I. Synthesis, swelling ratio, thermal properties and morphology. *Polymer* **2000,** *41* (22), 7961-7967.

27. Fan, L. H.; Hu, C. P.; Ying, S. K., Thermal analysis during the formation of polyurethane and vinyl ester resin interpenetrating polymer networks. *Polymer* **1996,** *37* (6), 975-981.

28. Dave, V. J.; Patel, H. S., Synthesis and characterization of interpenetrating polymer networks from transesterified castor oil based polyurethane and polystyrene. *Journal of Saudi Chemical Society* **2017,** *21* (1), 18-24.

29. Sundararajan, S.; Samui, A. B.; Kulkarni, P. S., Interpenetrating phase change polymer networks based on crosslinked polyethylene glycol and poly(hydroxyethyl methacrylate). *Solar Energy Materials and Solar Cells* **2016,** *149*, 266-274.

30. Sibaja, B.; Matheus, C. P.; Mendez, R. B.; Farag, R.; Baudrit, J. R. V.; Auad, M. L., Synthesis and Characterization of Interpenetrating Polymer Networks (IPNs) from Acrylated Soybean Oil α-Resorcylic Acid: Part 2. Thermo-Mechanical Properties and Linear Fracture Mechanics. *Journal of Renewable Materials* **2017,** *5* (3-4), 241-250.

31. Jajam, K. C.; Bird, S. A.; Auad, M. L.; Tippur, H. V., Tensile, fracture and impact behavior of transparent Interpenetrating Polymer Networks with polyurethane-poly(methyl methacrylate). *Polymer Testing* **2013,** *32* (5), 889-900.

32. Sundaram, B. M.; Mendez, R. B.; Auad, M. L.; Tippur, H. V., Quasi-static and dynamic mechanical behavior of transparent graft-interpenetrating polymer networks (graft-IPNs). *Polymer Testing* **2018,** *70*, 348-362.

33. Bird, S. A.; Clary, D.; Jajam, K. C.; Tippur, H. V.; Auad, M. L., Synthesis and characterization of high performance, transparent interpenetrating polymer networks with polyurethane and poly(methyl methacrylate). *Polymer Engineering & Science* **2013,** *53* (4), 716-723.

34. Jajam, K. C.; Tippur, H. V.; Bird, S. A.; Auad, M. L. In *Dynamic Fracture and Impact Energy Absorption Characteristics of PMMA-PU Transparent Interpenetrating Polymer Networks (IPNs)*, Dynamic Behavior of Materials, Volume 1, Cham, 2014//; Song, B.; Casem, D.; Kimberley, J., Eds. Springer International Publishing: Cham, 2014; pp 277-284.

35. Jajam, K. C.; Bird, S. A.; Auad, M. L.; Tippur, H. V. In *Development and Characterization of a PU-PMMA Transparent Interpenetrating Polymer Networks (t-IPNs)*, Dynamic Behavior of Materials, Volume 1, New York, NY, 2011//; Proulx, T., Ed. Springer New York: New York, NY, 2011; pp 117-121.

36. Ballestero, R.; Sundaram, B. M.; Tippur, H. V.; Auad, M. L., Sequential graft-interpenetrating polymer networks based on polyurethane and acrylic/ester copolymers. *Express Polymer Letters* **2016,** *10* (3), 204-215.

37. Alizadeh, N.; Barde, M.; Minkler, M.; Celestine, A.-D.; Agrawal, V.; Beckingham, B.; Auad, M. L., High-fracture-toughness acrylic–polyurethane-based graft-interpenetrating polymer networks for transparent applications. *Polymer International* **2020**.

38. Méndez, R. B. Sequential graft-Interpenetrating polymer networks based on polyurethane and acrylic/ester copolymers. Auburn University, Auburn, AL, 2015.

39. Hillerström, A.; Andersson, M.; Pedersen, J. S.; Altskär, A.; Langton, M.; van Stam, J.; Kronberg, B., Transparency and wettability of PVP/PDMS-IPN synthesized in different organic solvents. *Journal of Applied Polymer Science* **2009,** *114* (3), 1828-1839.

40. Qin, C.-L.; Cai, W.-M.; Cai, J.; Tang, D.-Y.; Zhang, J.-S.; Qin, M., Damping properties and morphology of polyurethane/vinyl ester resin interpenetrating polymer network. *Materials Chemistry and Physics* **2004,** *85* (2-3), 402-409.

41. Alizadeh, N.; Bird, S. A.; Mendez, R. B.; Jajam, K. C.; Alexander, A. C.; Tippur, H. V.; Auad, M. L., Chapter 11 - Synthesis and Characterization of High Performance Interpenetrating Polymer Networks With Polyurethane and Poly(methyl methacrylate). In *Unsaturated Polyester Resins*, Elsevier: 2019; pp 243-255.

42. Huang, J.; Zhang, L., Effects of NCO/OH molar ratio on structure and properties of graft-interpenetrating polymer networks from polyurethane and nitrolignin. *Polymer* **2002,** *43* (8), 2287-2294.

43. Qadri, M. F.; Malviya, R.; Sharma, P. K., Biomedical Applications of Interpenetrating Polymer Network System. *Open Pharmaceutical Sciences Journal* **2015,** *2* (1), 21-30.

44. Vallittu, P. K., Interpenetrating Polymer Networks (IPNs) in Dental Polymers and Composites. *Journal of Adhesion Science and Technology* **2009,** *23* (7-8), 961-972.

45. Sperling, L.; Thomas, D. Vibration or sound damping coating for vibratory structures. 3,833,404, Sept. 3, 1974.

46. Peterson, A. M.; Kotthapalli, H.; Rahmathullah, M. A. M.; Palmese, G. R., Investigation of interpenetrating polymer networks for self-healing applications. *Composites Science and Technology* **2012,** *72* (2), 330-336.

47. Jeevananda, T.; Siddaramaiah, Synthesis and characterization of polyaniline filled PU/PMMA interpenetrating polymer networks. *European Polymer Journal* **2003,** *39* (3), 569-578.

48. Zhang, Y.; Xiu, J.; Tang, B.; Lu, R.; Zhang, S., Novel semi-interpenetrating network structural phase change composites with high phase change enthalpy. *AIChE Journal* **2018,** *64* (2), 688-696.

49. Ha, S. M.; Yuan, W.; Pei, Q.; Pelrine, R.; Stanford, S., Interpenetrating Polymer Networks for High-Performance Electroelastomer Artificial Muscles. *Advanced Materials* **2006,** *18* (7), 887-891.

50. Bruno, V. Impact-resistant plastic compositions comprising a styrene polymer and a cross-linked acrylic acid ester polymer, and process for preparing same. 3,055,859, Sept. 25, 1962.

51. Solak, T. A.; Duke, J. T. Polymerizates of olefinic nitriles and diene-nitrile rubbers. 3,426,102, Feb. 4, 1969.

52. Pham, S.; Burchill, P. J., Toughening of vinyl ester resins with modified polybutadienes. *Polymer* **1995,** *36* (17), 3279-3285.

53. Scott, T. F.; Cook, W. D.; Forsythe, J. S., Kinetics and network structure of thermally cured vinyl ester resins. *European Polymer Journal* **2002,** *38* (4), 705-716.

54. Petrovic, Z. S., *Handbook of Polymer Synthesis, Characterization, Processing*. A John Wiley & Sons, Inc.: 2013.

55. Patel, P. J.; Gilde, G. A.; Dehmer, P. G.; McCauley, J. W., Transparent armour. *The AMPTIAC Newsletter 4 (3)* 2000.

56. Nassehi, V., *Practical aspects of finite element modelling of polymer processing*. Wiley: 2002.

57. Alnæs, M.; Blechta, J.; Hake, J.; Johansson, A.; Kehlet, B.; Logg, A.; Richardson, C.; Ring, J.; Rognes, M. E.; Wells, G. N., The FEniCS project version 1.5. *Archive of Numerical Software* **2015,** *3* (100).

58. Logg, A.; Wells, G. N., DOLFIN: Automated finite element computing. *ACM Trans. Math. Softw.* **2010,** *37* (2), Article 20.

59. Chattopadhyay, D. K.; Raju, K. V. S. N., Structural engineering of polyurethane coatings for high performance applications. *Progress in Polymer Science* **2007,** *32* (3), 352-418.

60. Shkapenko, G.; Gmitter, G. T.; Gruber, E. E., Mechanism of the Water-lsocyanate Reaction. *Industrial & Engineering Chemistry* **1960,** *52* (7), 605-608.

61. ASTM E328-13, Standard Test Methods for Stress Relaxation Tests for Materials and Structures, ASTM International, West Conshohocken, PA, 2013.

62. ASTM E1640-18, Standard Test Method for Assignment of the Glass Transition Temperature By Dynamic Mechanical Analysis, ASTM International, West Conshohocken, PA, 2018.

63. Jones, B. H.; Alam, T. M.; Lee, S.; Celina, M. C.; Allers, J. P.; Park, S.; Chen, L.; Martinez, E. J.; Unangst, J. L., Curing behavior, chain dynamics, and microstructure of high Tg thiol-acrylate networks with systematically varied network heterogeneity. *Polymer* **2020,** *205*, 122783.

64. Araujo, S.; Batteux, F.; Li, W.; Butterfield, L.; Delpouve, N.; Esposito, A.; Tan, L.; Saiter, J.-M.; Negahban, M., A structural interpretation of the two components governing the kinetic fragility from the example of interpenetrated polymer networks. *Journal of Polymer Science Part B: Polymer Physics* **2018,** *56* (20), 1393-1403.

65. Askarbekov, R.; Herak, D.; Mizera, C. In *Mechanical Behavior of Rubber Samples Under Relaxation*, Proceedings of the International Scientific Conference, 2016.

66. Kirby, R. C.; Logg, A., A compiler for variational forms. *ACM Trans. Math. Softw.* **2006,** *32* (3), 417–444.

Chapter 6
Acrylic-polyurethane based graft semi-interpenetrating polymer networks for thermal energy storage

6.1. Introduction

Phase change materials (PCMs) undergo a phase transition in a narrow temperature range, making them a good candidate for thermal applications. The critical factor for PCMs is their high latent heat, making them capable of thermal energy storage (TES) [1, 2]. PCMs have a wide variety of applications, including thermal storage and thermal protection. For thermal storage applications, high heat conductivity is required, while for thermal protection, low heat conductivity is desirable. Thermal storage in solar energy, different cooling and heating applications such as ice bank and underground cooling systems, medical applications such as smart packaging for transferring food and medicine, temperature maintenance for building, food, and electrical instruments, different military and civil applications such as collectors for microwave antenna in ships and helicopters, and controlled greenhouse are just a few examples for use of PCMs [1, 3-13].

PCMs are classified into three different kinds based on their transition phase: solid-solid PCMs, solid-liquid PCMs, and liquid–gas PCMs. Solid-solid PCMs are materials where the crystalline structure changes to another crystalline structure or amorphous phase. Solid-solid PCMs consist of inorganic, organic, and polymer-based PCMs [14-17].

Fatty acids [18], paraffin waxes [19], fatty hydrocarbon [20], fatty alcohols [21], and poly(ethylene glycol) (PEG) are traditional materials widely used as PCMs. However, all these materials suffer from material leakage, which makes them undesirable for phase change applications [22, 23]. Therefore, new kinds of methods such as utilizing capsules and copolymerization of polymers were introduced to minimize the leakage in PCM applications [24].

The essential benefits of polymer-based PCMs compared to traditional PCMs are the absence of leakage, no requirement to seal, no generation of gas or liquid, low-cost and straightforward fabrication process, long cycling stability, and minimum volume change [12, 13, 25, 26].

There are two different types of polymeric solid-solid PCMs. One type consists of a mixture of two polymers where one of the polymers acts as the supports with a higher melting point, while the other changes phase from solid to liquid. Therefore, as long as the supporting polymer does not reach its melting point, the whole system can maintain its structure. This type is called shape stabilized PCMs [27]. The most significant disadvantage of these materials is the phase segregation after a couple of cycles [12]. The second type of polymeric solid-solid PCMs is synthesized by grafting or copolymerizing two polymers with each other. Overall, low thermal stability, high transition temperature, low transition enthalpy were reported as the most important disadvantages of polymeric solid-solid PCMs. Therefore, semi-interpenetrating polymer networks (IPNs) are used as polymeric solid-solid PCMs with excellent stability [28] and high latent heat of fusion for the system. Semi-IPNs are benefiting from all of the advantages of polymeric solid-solid PCMs as well [28].

Semi-IPN is one kind of polymer blend where one of the polymers is crosslinked. In contrast, the other polymer is linear, making the polymer chains move freely and align in the crystalline structure [29, 30]. Two polymers in the IPN structure are entangled, and it is impossible to separate them without breaking their bonds. Li et al. mentioned that although IPNs show phase separation, these materials exhibit a uniform morphology from forced compatibility due to the structure's physical entanglement [31]. Graft semi-IPN is one kind of IPN system where chemical bonds between two polymers are utilized to increase the compatibility of two polymers and increase the shape stability [29, 30, 32, 33]. IPNs can be classified as simultaneous and sequential IPNs based on the

polymerization method. In the sequential process, the first polymer is synthesized while being swollen by monomers of the second polymer. Then polymerization of the second polymer starts to happen. In simultaneous IPN, polymerization of two polymers occurs together, and there is no interfering reaction between two polymer phases [29, 33, 34].

Extensive work has been published related to different aspects of IPNs [23, 29, 35-37]. Various elements affecting the final morphology and properties of IPNs such as the ratio of two polymers, choice of precursors and their ratio [38, 39], diol molecular weight, polymerization process [40], utilizing chemical bonds between two polymers [41, 42], and curing profile [38, 40, 43-45] were investigated. It was concluded that synthesizing graft-IPNs with linear isocyanate enhances the compatibility of two IPNs and therefore improves the final properties [46-52].

PEG is considered one of the best polymeric materials for PCM applications due to its high latent heat ~ 200 J/g, good corrosion resistance, and wide melting temperature [53]. However, it needs to be sealed in packages to avoid leakage in the system, limiting the opportunities and increasing the final cost of PEG-based PCMs [54]. Different research groups tried to solve the leakage problem of PEG by synthesizing polyurethane (PU) and copolymer out of PEG [11, 13]. For instance, Su et al. [55] synthesized PEG-based PU. Calorimetry results suggested high latent heat for synthesized PU with no shape change at high temperatures. Sari et al. [12] synthesized polystyrene-graft-PEG6000 copolymers for use as PCMs. The results indicated good thermal stability with high latent heat for copolymer samples. It was also suggested that enthalpy increases by an increase in the amount of PEG in the system.

Different research groups utilized PEG in the IPN structure to reach shape stability with high latent heat. Zhang et al. fabricated semi-IPN out of PEG and a gel for phase change applications. Excellent latent heat and shape stability were observed in the synthesized samples [28].

Sundararajan et al. fabricated PEG based graft semi-IPN with the simultaneous method. The authors observed enthalpies in the order of 145 J/g. [23] Jiang et al. synthesized graft semi-IPN out of PEG and cellulose diacetate as a support phase. Semi-IPN samples with 90 wt% PEG10000 showed the highest enthalpy of fusion in research [56]. Liu et al. was another research group that synthesized semi-IPN out of PEG/poly(polyethylene glycol diacrylate). The highest heat enthalpy, which was achieved in research, was 117 J/g. All semi-IPN samples showed excellent shape stability as well [57].

In this research, graft semi-IPN out of PEG8000 based PU, and bisphenol A bis(2-hydroxy-3-methacryloxypropyl) ether (BisGMA) and methyl methacrylate (MMA) based acrylic copolymer was synthesized for the first time. PU acted as the phase transition materials, while acrylic copolymer acted as a skeleton to keep the whole structure together at high temperature. The polymerization of two phases was studied utilizing Fourier transform infrared spectroscopy (FTIR) analysis. Moreover, the crystallization properties of semi-IPN samples were analyzed using x-ray diffraction (XRD) and polarized optical microscopy (POM). Cycling stability, as one of the essential features of the PCMs, was also examined. Overall, IPN synthesized in this research shows tremendous potential in PCM applications such as solar cells, biomedical and biological containers, heat management for buildings and electronics, the cooling system in the collector of a microwave antenna in ships, and helicopters, among others.

6.2. Experimental

6.2.1. Materials

Poly(ethylene glycol) (PEG, MW = approximately 8000 g/mol) was purchased from Acros Organics. Hexamethylene diisocyanate (DCH) was received from Tokyo Chemical Industry Co.,

Ltd. (TCI). Dibutyltin dilaurate (DBTDL) was purchased from Pfaltz & Bauer. MMA and BisGMA were purchased from Acros Organics and Esstech, respectively. Moreover, 2,2'-azobis(2-methyl-propionitrile) (AIBN) was purchased from Matrix Scientific. 4Å molecular sieves, purchased from Alfa Aesar, were used to remove the moisture from MMA and DCH.

6.2.2. Methods

6.2.2.1. Synthesis of graft-semi-IPNs

PEG8000 was dried before the experiment using an oven. Then, it was melted by transferring into an oil bath at 70 °C.

In a separate container, 20 wt% of BisGMA was dissolved into 80 wt% of MMA. Then 1 wt % of AIBN based on the total mass of the copolymer was dissolved into the mixture. Afterward, DCH and 4 drops of DBTDL were added to the mixture and mixed for 3 minutes. Finally, the mixture was added to the molten PEG8000 placed in the oil bath at 70°C. Afterward, the mixture was transferred to closed glass molds and cured at 80°C for 6 hours. A simultaneous polymerization method was followed to synthesize the graft-IPN system as two polymers do not follow interfering reactions. Figure 6.1 shows the chemical reactions of graft semi-IPN samples.

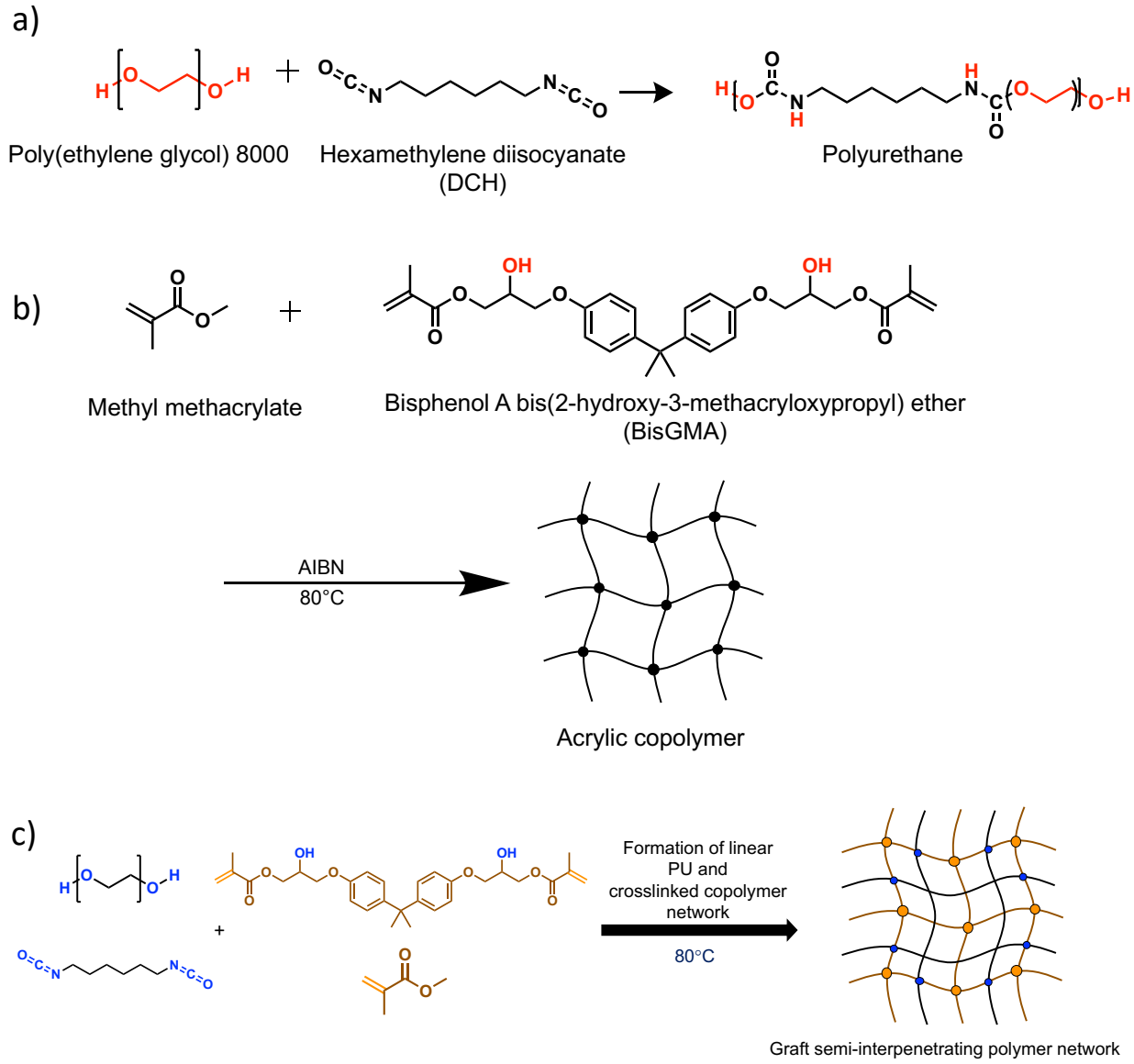

Figure 6.1. a) Poly-addition polymerization to synthesize linear PU b) free radical polymerization of acrylic copolymer c) simple schematic of semi graft-IPN synthesis.

As shown in Figure 6.1, PEG and DCH follow the poly-addition polymerization to synthesize linear PU. Extra isocyanate also reacts with hydroxyl groups of BisGMA to make bonds between two polymers. PU is a polymer phase with high latent heat to fulfill requirements in phase change applications. Monomers in the acrylic copolymer, however, follow free radical polymerization to

make a crosslinked acrylic copolymer. The acrylic copolymer acts as a support to maintain the original form of IPN at a temperature higher than PEG's melting point. The final product is graft semi-IPN with chemical bonds between two polymer phases. Five different IPN samples with varied PU and acrylic copolymer compositions were synthesized, where numbers in front of IPN exhibit the wt% of PU in the IPN system. For instance, IPN90 has 90 wt% of PU.

6.2.2.2. Characterization

A Nicolet 6700 FTIR spectrometer from Thermo Scientific (USA) in attenuated total reflection (ATR) infrared mode was utilized to study the FTIR spectra of the synthesized samples. FTIR analysis was performed within the 400-4000 cm^{-1} wavenumber range with 64 scans and a 4 cm^{-1} resolution.

A differential scanning calorimetry (DSC) experiment was performed on a TA Instruments DSCQ2000. Approximately 5-10 mg of the sample was tested each time. The sample was first equilibrated at 0°C for 5 minutes, and then the temperature was increased to 150°C to remove any thermal history in the samples, followed by decreasing the temperature to 0°C, and finally brought back to 150°C all with a 5°C/min heating rate, in a nitrogen atmosphere. The second heat was utilized to determine the thermal properties of the IPN samples. Three replicas were tested for each sample to confirm the validity of the results. Equation 6.1 [58] was used to calculate the percentage of crystallinity:

$$X_c(\%) = \frac{\Delta H_m}{\Delta H^0{}_m} \times 100 \qquad [6.1]$$

Where χ_c is the crystallinity percentage, ΔH_m is the enthalpy of fusion of the IPN sample, and $\Delta H^0{}_m$ = 196.8 J/g [58] is the enthalpy of fusion for totally crystalline PEG.

XRD analysis was performed on a Proto manufacturing powder diffraction system having a CuKα source with a 1.54 nm wavelength, 40 kV, and 30 mA. Approximately 500 mg of sample in the powder form was tested in the range of 2θ within 15 – 40° with around 15 minutes scan time. The scherrer formula [59] (equation 6.2) was utilized to calculate the mean size of crystallites in IPN samples:

$$L = \frac{K\lambda}{\beta \cos\theta} \qquad [6.2]$$

Where λ is the wavelength of the X-ray source in nanometers (0.15406 nm), K is the Scherrer constant, which is related to the crystallite shape (generally taken as 0.9), β is the diffraction peak width at half maximum height in radians, θ is the peak positions in radians, and L is the average crystallite size.

An Olympus BH-2 polarized optical microscope with a FMA050 digital camera was utilized to study the samples' crystalline morphology. IPN samples were cured between two micro slides to reach the thin, consistent thickness for all the samples.

A Zeiss EVO 50 variable pressure scanning electron microscope with digital imaging and energy dispersive spectroscopy was used to study the surface morphology of the fractured samples. Samples were immersed in liquid nitrogen and then were broken to make a brittle failure in samples and avoid fracturing of the samples below their glass transition, which could alter the surface morphology, and fractured surfaces were utilized for scanning electron microscopy (SEM)

imaging. The samples were sputter-coated with an EMS 550X auto sputter coating device with carbon coating attachment before SEM imaging.

Samples were cut to circles with a 12 mm diameter using a Boss Laser LS 3655 and kept in a hot plate at 80°C for 30 minutes to test the shape stability of the IPN samples.

Thermogravimetric analysis (TGA) was performed under a nitrogen atmosphere using a platinum pan on TA Instruments TGAQ500. 10-20 mg of samples was heated from room temperature to 800°C with 10°C/min.

The thermal cycling stability of the IPN samples was studied by placing the samples into glass vials and then transfer to an oven at 90°C for 20 minutes, followed by 20 minutes in a refrigerator at 10°C to make sure that solid-liquid-solid transition is occurring in the system. The phase transition cycle was done 25 times. Then, DSC, TGA, FTIR, XRD, and wetting experiments were performed on thermal cycled samples.

The contact angle of 1.5 µl of ultrapure water (UPW) with the IPNs' surface was monitored for 20 seconds using a DataPhysics OCA 50 instrument. The reported results are the average contact angles of UPW with at least 4 different IPN sample areas. A Thermo Scientific Barnstead Nanopure (18.2 MΩ.cm) was employed to deionize and purify the water. The measurement was analyzed using SCA 20 software.

6.3. Results and discussion

6.3.1. Chemical structure analysis

FTIR analysis was utilized to confirm the successful polymerization of two phases in graft semi-IPN. Values on the Y-axis were normalized based on the peak at 2880 cm^{-1}. Figure 6.2 shows the FTIR spectra for all of the samples after polymerization. As shown, a peak at approximately 3320

cm^{-1} indicates the stretching of the N-H bond due to PU formation in the IPN structure. No peak was observed at around 2270 cm^{-1}, which corresponds to the isocyanate bond and confirms the isocyanate consumption to synthesize PU [60]. The peak at about 1720 cm^{-1} is attributed to Amide C=O, the peak at 1240 cm^{-1} belongs to the C-N bond, and the peak at about 1538 cm^{-1} corresponds to the N-H bend. These signals are evidence of the successful polymerization of PU. Moreover, there is no peak at approximately 1630 cm^{-1}, which belongs to the alkene C=C bond, indicating successful free radical polymerization to synthesize the acrylic copolymer.

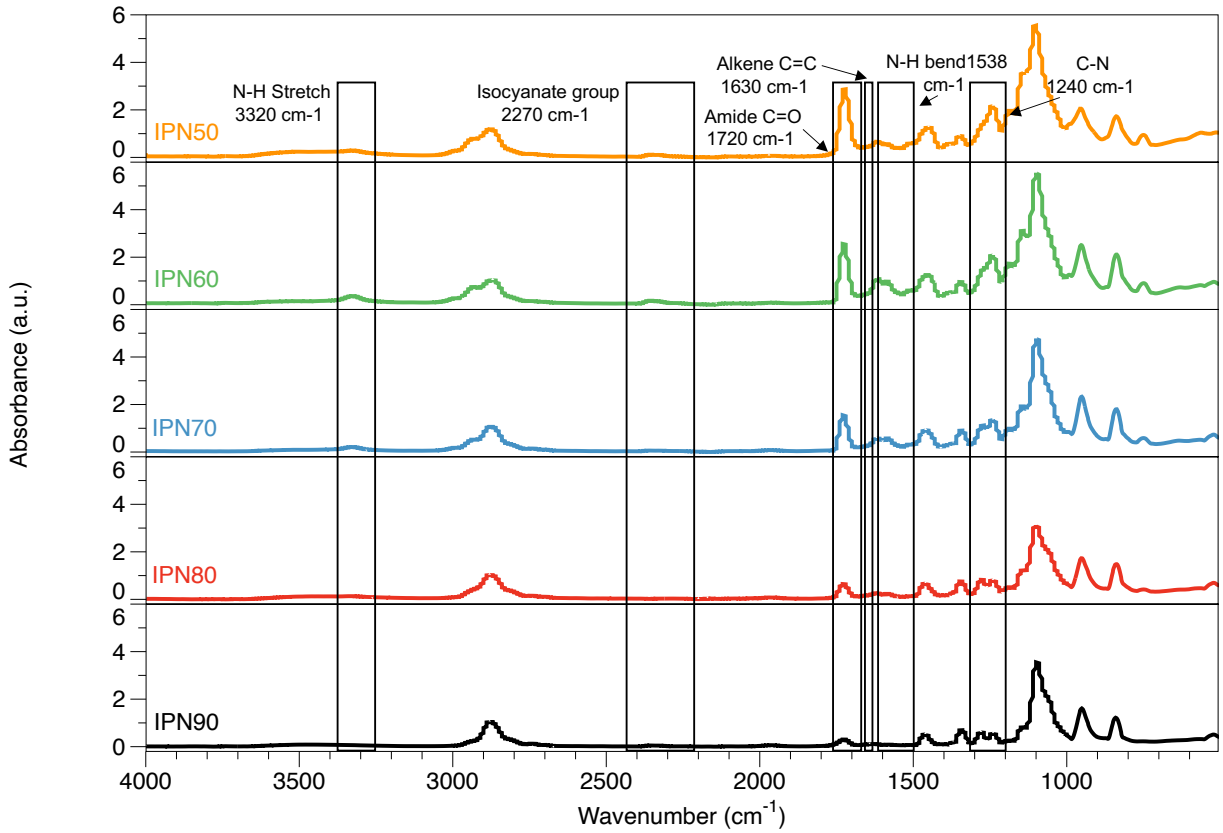

Figure 6.2. FTIR spectra of IPN samples with different composition.

6.3.2. Thermal analysis

Thermal properties are critical for phase change materials. DSC was used in this research to study the thermal properties of the IPNs. Table 6.1 exhibits a summary of thermal results for pure PEG and IPN samples. As shown, pristine PEG8000 shows the highest enthalpy of fusion. This result is expected due to the perfection of the crystalline structure in pure PEG. However, synthesizing IPNs out of PU and the acrylic copolymer hinders the free movements of PEG chains and therefore decreases the crystalline structure in the system. The enthalpy of fusion declines, and as shown, IPN50 shows the smallest number in comparison to other IPN samples due to the high percentage of the acrylic copolymer in the system. Crystallization results show the same trends due to the reason mentioned above. IPN90 shows the highest latent heat of fusion with 177.5 J/g, which is still lower than that of pure PEG. However, this number is higher than the reported latent heat of fusion for IPNs and copolymers used in phase change applications [12, 28, 56]. For instance, Zhou et al. [13] synthesized the PEG4000/MDI/PVA copolymer with a 72.8 J/g enthalpy of fusion and a 61.1°C transition temperature. Chen et al. [61] synthesized PEG/PU phase change materials with the enthalpies of fusion within 103–124 J/g. Sundararajan et al. [23] synthesized PEG8000 based graft semi-IPN. 145 J/g was the highest enthalpy of fusion observed in the paper. Li et al. [11] fabricated the PEG10000/MDI/PE tertiary copolymer with the highest enthalpy of fusion at 152.97 J/g. Liu et al. [57] also manufactured PEG-based semi-IPN, and the highest enthalpy of fusion obtained in the research was 117 J/g. Su et al. [55] fabricated PEG10000-based PU with a 138.7 J/g enthalpy of fusion. Finally, Cao et al. [25] synthesized PEG6000 based hyperbranched PU with a 138.3 J/g enthalpy of fusion. Transition temperatures increase with the PU wt% because PEG chains have more free volume and mobility to align and make a perfect crystalline structure.

Table 6.1. Summary of DSC results for IPN samples.

Sample	Enthalpy of fusion (ΔH_m) (J/g)	Melting temperature (T_m) (°C)	Enthalpy of crystallization (ΔH_c) (J/g)	Crystallization temperature (T_c) (°C)
PEG8000	196.0	61.8	198.2	43.6
IPN90	177.5	59.9	174.3	43.9
IPN80	140.3	59.8	141.4	44.2
IPN70	108.7	59.9	105.1	43.3
IPN60	78.1	58.9	74.0	38.6
IPN50	47.7	54.4	41.3	33.7

6.3.3. Crystallization behavior analysis

XRD was utilized to study the crystallization properties of the samples. Figure 6.3 shows the diffraction peaks of the samples. As shown, pristine PEG8000 shows the peaks at 19° and 23°, which are characteristic peaks for PEG8000. All IPN samples show a peak at the same diffraction angles, which shows that the crystallization properties of PEG8000 do not change after the synthesis of the IPN samples. However, the height of the peak starts to decrease in IPN90, and it continues to decline by reducing the amount of PEG in systems. IPN50 shows the lowest height in diffraction peak due to the reduction of PEG in the reactive system and the presence of the acrylic copolymer, which destroys the perfection of the crystallization in PEG. Moreover, although the chemical interaction between the -OH group of PEG and BisGMA with the isocyanate group in

DCH brings shape stability into the system, it decreases the perfection of the crystallization even more [23].

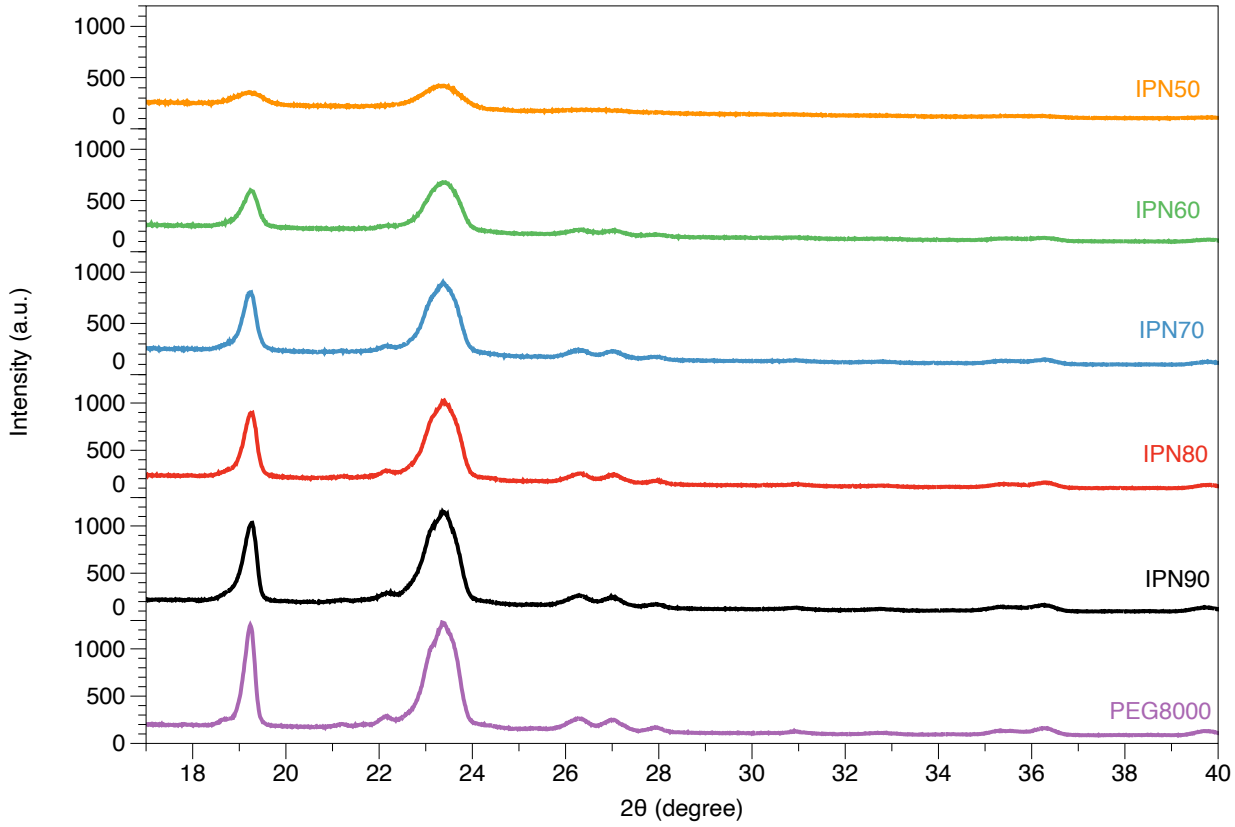

Figure 6.3. XRD curves of PEG8000 and IPN samples.

The Scherrer equation (Equation 6.2) was utilized to calculate the mean size of crystallites in IPN samples. Moreover, the percentage of crystallinity for each sample was calculated using Equation 6.1. Table 6.2 shows a summary of the results.

Table 6.2. Mean size of crystallites and percentage of crystallinity for IPN samples.

Sample	Mean crystallite size (nm)	Crystallinity percentage (%)
PEG8000	19.9	99.6
IPN90	16.8	90.2
IPN80	16.8	71.3
IPN70	16.5	55.2
IPN60	14.6	39.7
IPN50	9.4	24.2

As shown, the crystallite size and percentage of crystallinity confirm the results from XRD analysis. Pure PEG8000 shows the most significant crystallite size and crystallinity percentage. The crystallite size and crystallinity percentage start to decrease by adding the acrylic copolymer to form the IPN network, as expected.

The crystalline morphology of the samples was studied using POM. Figure 6.4 shows the photograph of the pristine PEG8000 (Figure 6.4.a), IPN samples at room temperature (Figure 6.4.b, c, and d), and IPN samples at 80°C (Figure 6.4.e, and f). As shown, pristine PEG and IPN samples exhibit similar spherulitic crystalline structures. This fact indicates that the crystalline structure of PEG8000 in IPN samples does not change.

Furthermore, the crystallite size becomes smaller by adding more acrylic copolymer to the system due to a decrease in the amount of the PEG8000 and the presence of acrylic copolymer, which acts as a hindrance in IPN samples, therefore destroying the perfection of the PEG crystallization. The crystalline structure of the IPN samples at 80°C faded away due to the crystalline structure's

disappearance at higher temperatures. In other words, the crystalline structure of PEG8000 in the IPN structure was transformed into an amorphous structure. This fact is due to the free movements of PEG8000 chains at 80°C, which therefore do not align to make the crystalline structure. POM images confirm the results from XRD analysis.

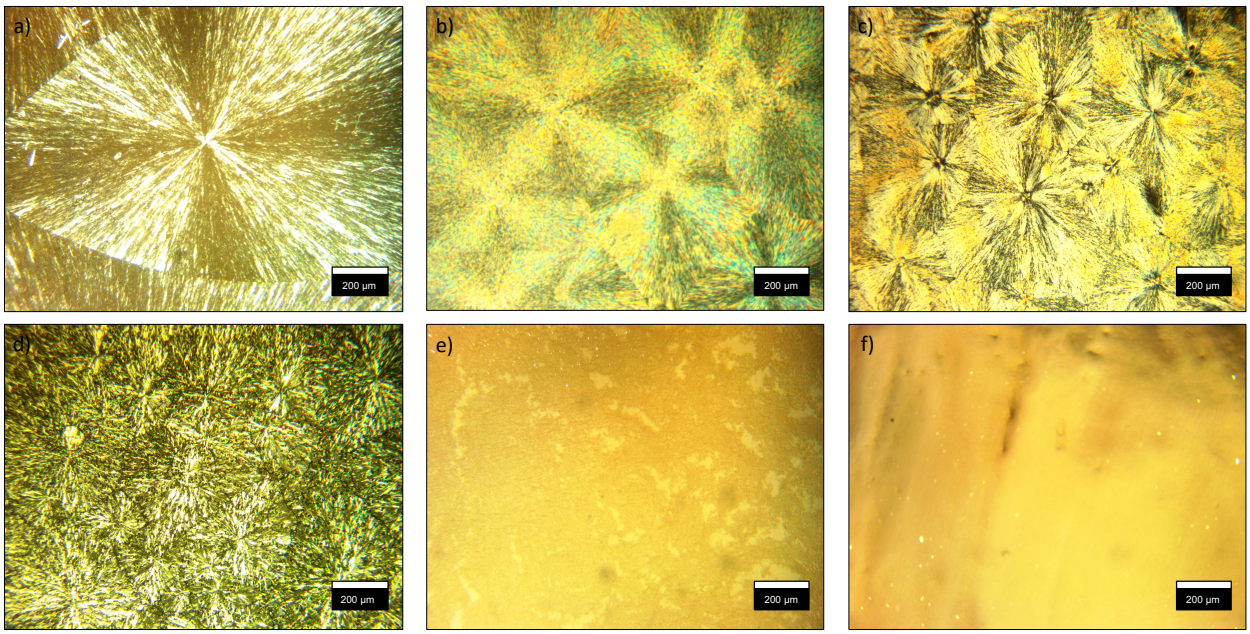

Figure 6.4. POM photographs of a) PEG8000 at room temperature b) IPN90 at room temperature c) IPN80 at room temperature d) IPN50 at room temperature e) IPN90 at 80°C, and f) IPN80 at 80°C.

Figure 6.5 shows The SEM images of fractured IPN samples. As shown, IPN50 (Figure 6.5.c) shows the flat surface with ductile behavior on fractured samples. However, the surface starts to show brittle failure with cracks all over the surfaces by adding more PU to the system due to higher crystallization (Figure 6.5.a, and b). Higher crystallization and alignment of chains in IPN90 and IPN80 increase the brittle behavior of the IPN samples. However, the presence of more amorphous

regions with many chains entangled in each other is the reason for ductile behavior in the fractured surface of IPN50. SEM images support DSC, XRD, and POM results, indicating higher crystallization by increasing wt% of PU into the IPN system.

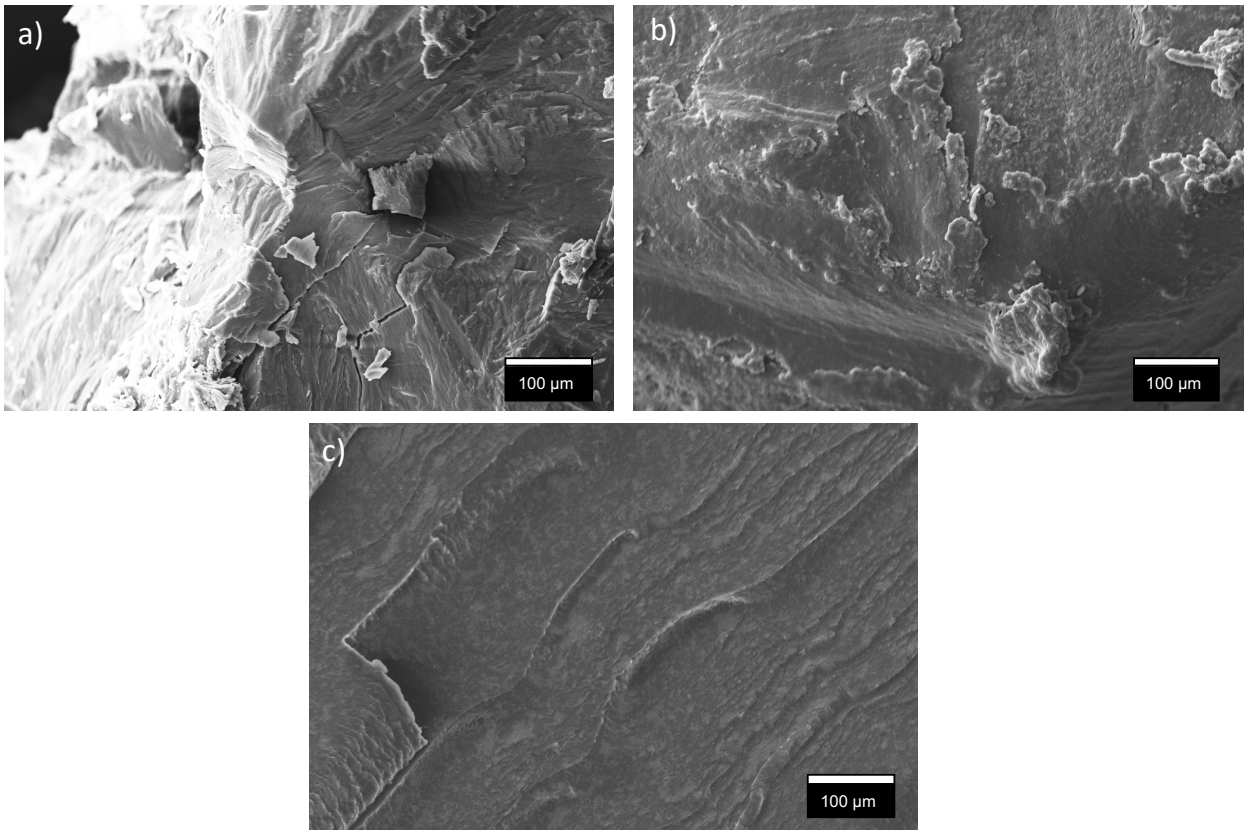

Figure 6.5. SEM images of a) IPN90 b) IPN80 c) IPN50.

6.3.4. Shape stability analysis

IPN samples were put on the 80°C hot plate for 30 minutes to examine the shape stability. Figure 6.6 shows the digital photographs of the pristine PEG8000, IPN90, IPN80, and IPN50 before (first row) and after (second row) of the shape stability experiment. PEG8000 loses its shape immediately after reaching 80°C and starts to flow because of passing its melting point. In contrast,

IPN samples maintain their shape even after 30 minutes at 80°C. The presence of the crosslinked acrylic copolymer phase in graft semi-IPN and chemical bonds between the hydroxyl group of PEG and BisGMA with the isocyanate group in DCH, which act as a boundary and trapped long chains of PEG8000, are the reasons behind the excellent shape stability of the IPN samples even at a temperature higher than that of the melting point of PEG8000. It should be added that the transparency of the IPN50 sample is higher than other IPN samples. The transparency starts to decrease by adding more PU into the system due to the crystallization increase, as mentioned before.

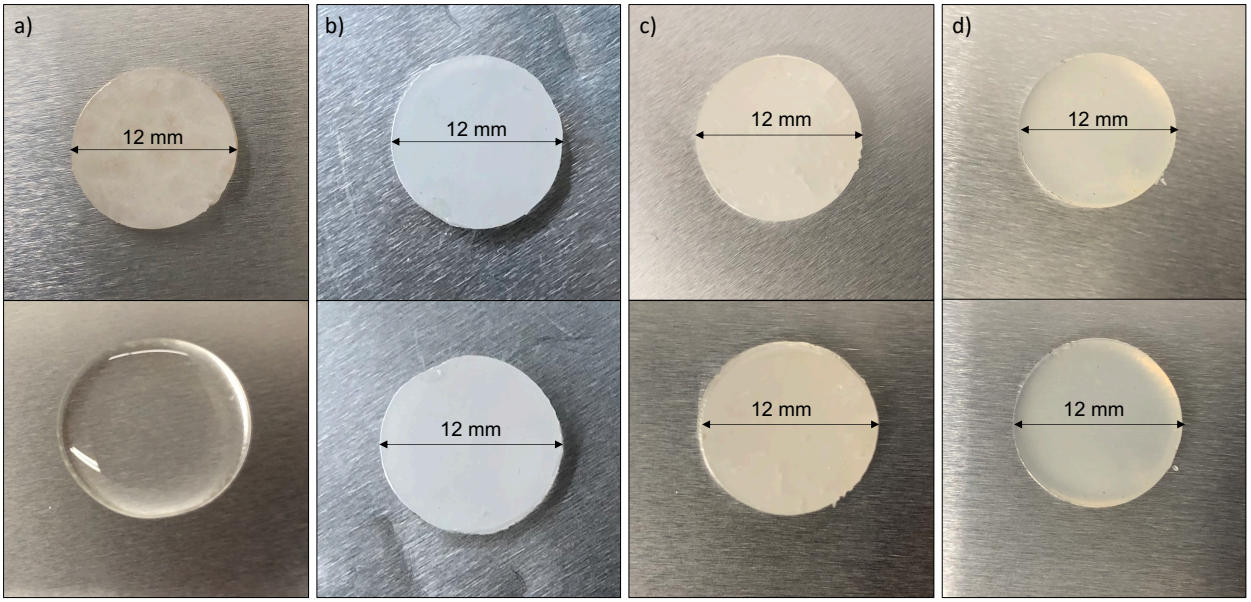

Figure 6.6. Digital photograph of a) pristine PEG8000 b) IPN90 c) IPN80 d) IPN50 before and after the shape stability experiment.

6.3.5. Thermal and cycling stability

Cycling stability is a critical property in PCMs. TGA results before and after cycling experiments for IPN90 and IPN80 are shown in Figure 6.7. As shown, the degradation process for samples starts at around 300°C and ends at about 460°C. The degradation temperature of IPN samples is much higher than the application temperature for phase change applications. These data are in good agreement with literature works on phase change applications of materials [11, 12, 23, 28, 57]. Moreover, TGA results approximately overlap before and after cycling experiments.

Table 6.3 summarizes DSC results for IPN90 and IPN80 before and after the cycling stability experiment. Table 6.3 indicates that phase transition temperatures and enthalpies are very close before and after 25 times of melt-freeze-melt cycles.

FTIR results for IPN90 and IPN80 before and after the thermal cycling exhibit good overlap, as shown in Figure 6.8. This implies that the chemical structure for IPN samples did not change after the thermal cycling experiment.

Furthermore, Figure 6.9 shows the XRD analysis results for IPN90 and IPN80 before and after the thermal cycling experiment. The good overlap is observed with a small drop in peak intensities in both samples. The mean crystallite size for IPN90 and IPN80 after thermal cycling are 15.6 nm and 15.8 nm, respectively, which are close to their crystallite sizes before thermal cycling (16.8 nm for both). These findings confirm the TGA, DSC, and FTIR results and indicate excellent thermal cycling stability of the IPN samples.

The contact angle and hydrophilicity of the IPN sample surfaces after thermal cycling were checked. IPN90 and IPN80 showed 29.1 ± 4.0° and 22.2 ± 1.9° contact angles with UPW, respectively. The low contact angle in both IPN samples indicates high hydrophilicity of the samples due to urethane groups in PU and esters in the acrylic copolymer.

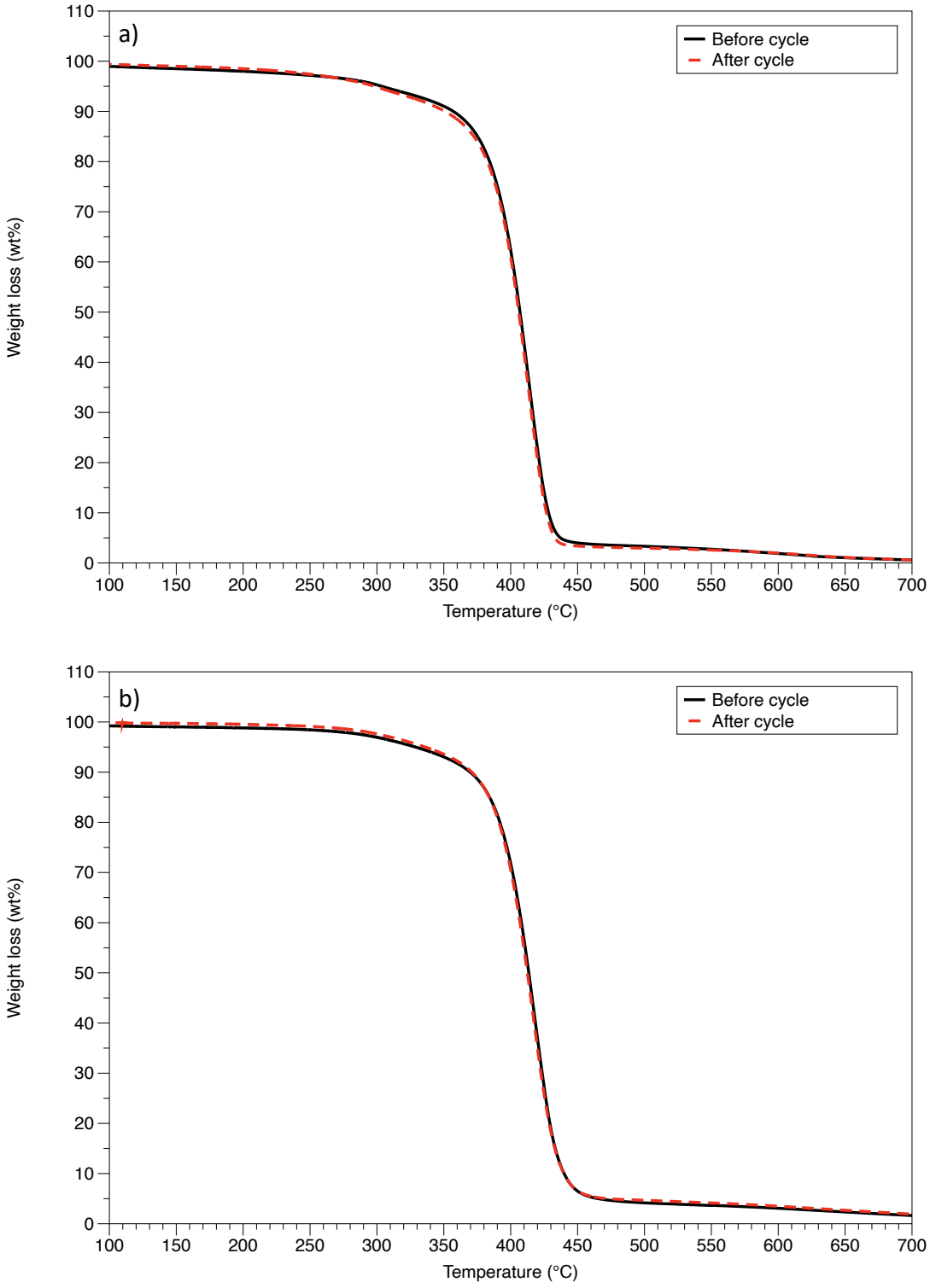

Figure 6.7. TGA results before and after the thermal cycling test a) IPN90, and b) IPN80.

Table 6.3. Summary of DSC results for IPN samples before and after the cycling test.

Sample		Enthalpy of fusion (ΔH_m) (J/g)	Melting temperature (T_m) (°C)	Enthalpy of crystallization ΔH_c (J/g)	Crystallization temperature T_c (°C)
IPN90	**Before cycle**	177.5	59.9	174.3	43.9
	After cycle	177.7	60.2	176.6	43.9
IPN80	**Before cycle**	140.3	59.8	141.4	44.2
	After cycle	140	60.3	142.9	44.8

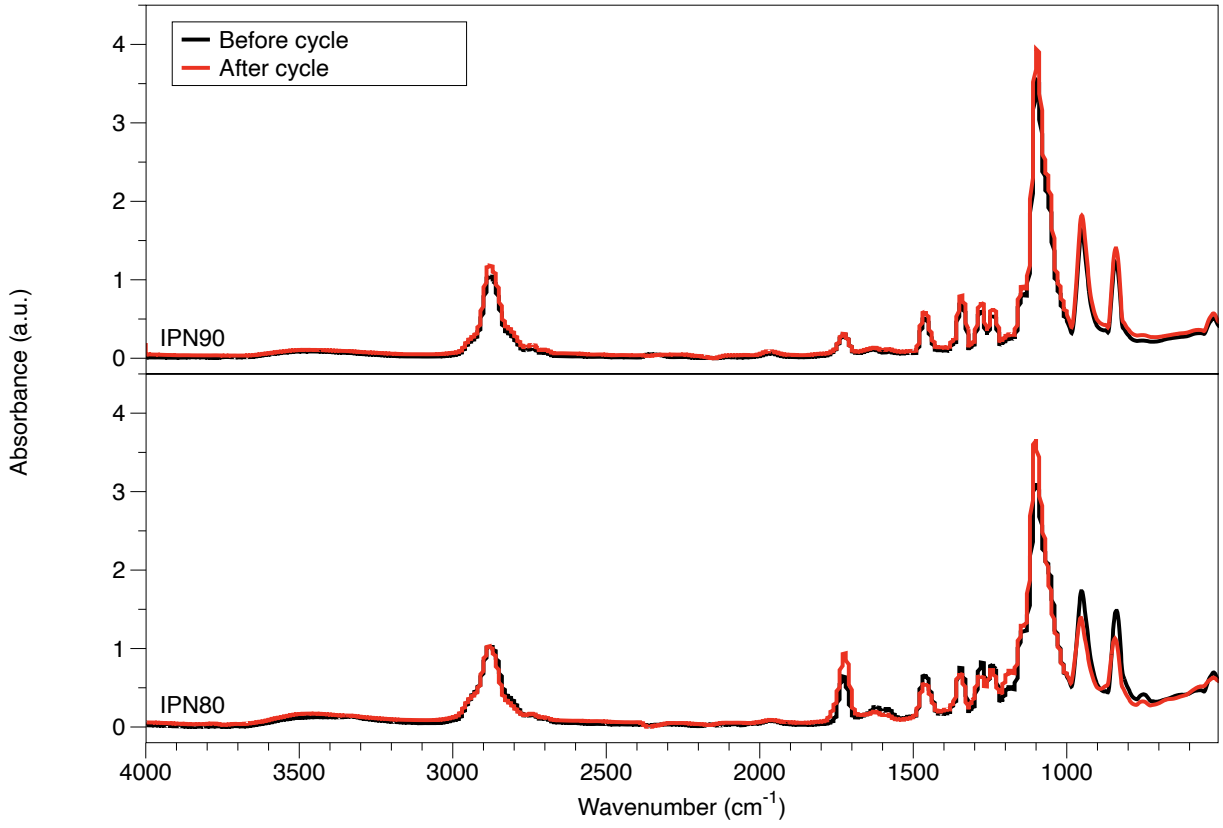

Figure 6.8. FTIR results of IPN90 and IPN80 before and after the thermal cycling test.

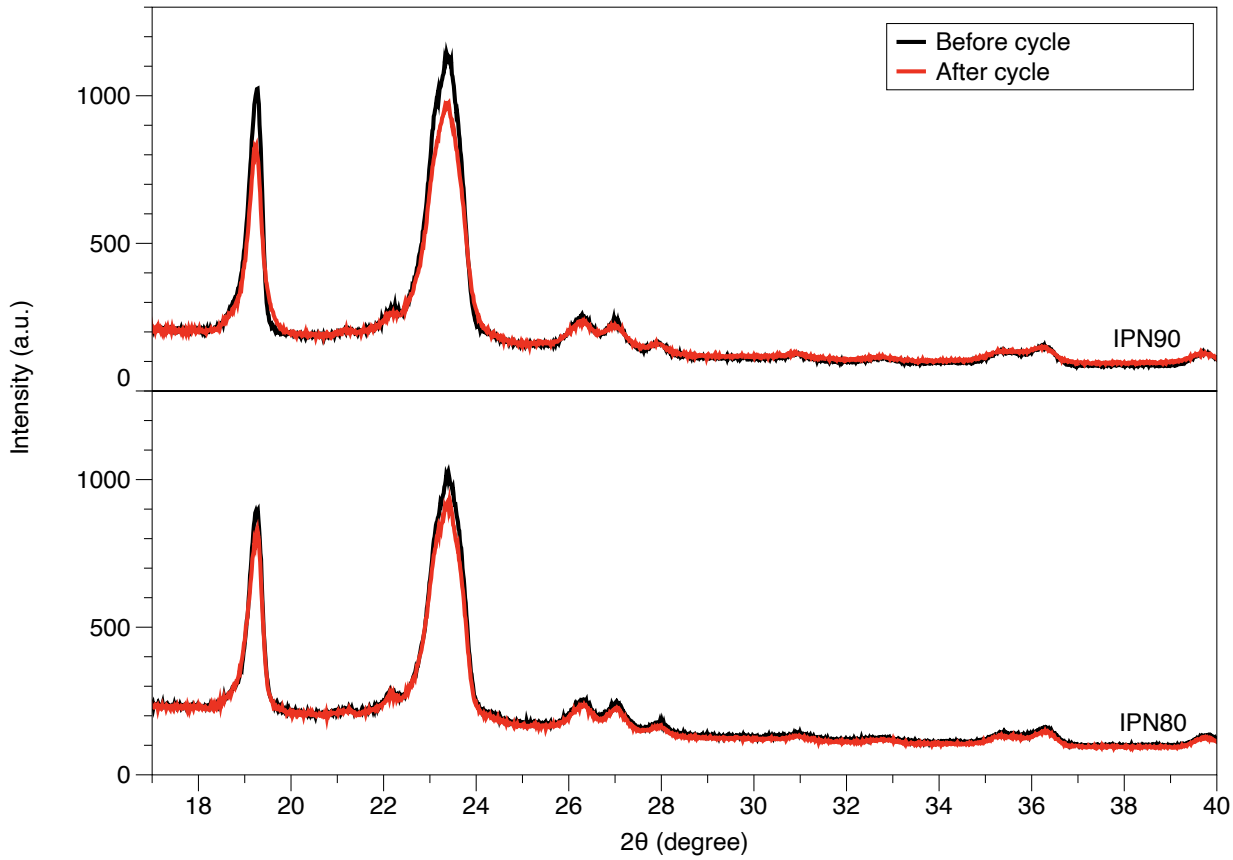

Figure 6.9. XRD curves of IPN90 and IPN80 before and after the thermal cycling test.

6.4. Conclusions

Graft semi-IPNs with the high latent heat of fusion were synthesized in this research. Chemical bonds between two polymers were used to enhance the compatibility between two phases and improve the shape stability of the IPNs. PEG-based PU is the polymer phase with high latent heat, while acrylic copolymer acts as a skeleton to keep the whole structure together even at a temperature higher than the melting point of PEG8000. FTIR spectra of IPN samples confirm the successful polymerization of both phases. DSC results show excellent enthalpies higher than other literature with a proper phase transition temperature. TGA indicates excellent thermal stability for

IPN samples, which is required for phase change applications. XRD analysis and POM images show that the crystalline properties of PEG8000 do not change after the synthesis of IPNs. However, the latent heat and phase transition temperature becomes smaller by adding more acrylic copolymer to the system due to a decrease in crystal size and perfection. IPNs exhibit excellent shape stability at 80°C in comparison to pure PEG8000, which starts to flow immediately after reaching 80°C. Finally, excellent cycling stability with overlap between DSC, TGA, FTIR, and XRD results before and after cycling experiments was observed. Overall, synthesized IPN shows promising results required in a wide variety of thermal energy storage applications.

References

1. Zalba, B.; Marín, J. M.; Cabeza, L. F.; Mehling, H., Review on thermal energy storage with phase change: materials, heat transfer analysis and applications. *Applied Thermal Engineering* **2003,** *23* (3), 251-283.

2. Khan, Z.; Khan, Z.; Ghafoor, A., A review of performance enhancement of PCM based latent heat storage system within the context of materials, thermal stability and compatibility. *Energy Conversion and Management* **2016,** *115*, 132-158.

3. Abhat, A.; Aboul-Enein, S.; Malatidis, N. A. In *Heat-of-Fusion Storage Systems for Solar Heating Applications*, Thermal Storage of Solar Energy, Dordrecht, 1981//; den Ouden, C., Ed. Springer Netherlands: Dordrecht, 1981; pp 157-171.

4. Ismail, K. A. R.; Henríquez, J. R., Thermally effective windows with moving phase change material curtains. *Applied Thermal Engineering* **2001,** *21* (18), 1909-1923.

5. Vakilaltojjar, S. M.; Saman, W., Analysis and modelling of a phase change storage system for air conditioning applications. *Applied Thermal Engineering* **2001,** *21* (3), 249-263.

6. Bédécarrats, J. P.; Strub, F.; Falcon, B.; Dumas, J. P., Phase-change thermal energy storage using spherical capsules: performance of a test plant. *International Journal of Refrigeration* **1996,** *19* (3), 187-196.

7. Espeau, P.; Mondieig, D.; Haget, Y.; Cuevas-Diarte, M. A., 'Active' Package for Thermal Protection of Food Products. *Packaging Technology and Science* **1997,** *10* (5), 253-260.

8. Salyer, I. O.; Sircar, A. K. In *Phase Change Katerials For Heating And Cooling Of Residential Buildings And Other Applications*, Proceedings of the 25th Intersociety Energy Conversion Engineering Conference, 12-17 Aug. 1990; 1990; pp 236-241.

9. Pal, D.; Joshi, Y., Application of phase change materials for passive thermal control of plastic quad flat packages: a computational study. *Numerical Heat Transfer, Part A: Applications* **1996,** *30* (1), 19-34.

10. Mulligan, J. C.; Colvin, D. P.; Bryant, Y. G., Microencapsulated phase-change material suspensions for heat transfer in spacecraft thermal systems. *Journal of Spacecraft and Rockets* **1996,** *33* (2), 278-284.

11. Li, W.-D.; Ding, E.-Y., Preparation and characterization of cross-linking PEG/MDI/PE copolymer as solid–solid phase change heat storage material. *Solar Energy Materials and Solar Cells* **2007,** *91* (9), 764-768.

12. Sarı, A.; Alkan, C.; Biçer, A., Synthesis and thermal properties of polystyrene-graft-PEG copolymers as new kinds of solid–solid phase change materials for thermal energy storage. *Materials Chemistry and Physics* **2012,** *133* (1), 87-94.

13. Zhou, X.-M., Preparation and characterization of PEG/MDI/PVA copolymer as solid–solid phase change heat storage material. *Journal of Applied Polymer Science* **2009,** *113* (3), 2041-2045.

14. Al-Ahmed, A.; Sarı, A.; Mazumder, M. A. J.; Hekimoğlu, G.; Al-Sulaiman, F. A.; Inamuddin, Thermal energy storage and thermal conductivity properties of Octadecanol-MWCNT composite PCMs as promising organic heat storage materials. *Scientific Reports* **2020,** *10* (1), 9168.

15. Al-Ahmed, A.; Sarı, A.; Mazumder, M. A. J.; Salhi, B.; Hekimoğlu, G.; Al-Sulaiman, F. A.; Inamuddin, Thermal energy storage and thermal conductivity properties of fatty acid/fatty acid-grafted-CNTs and fatty acid/CNTs as novel composite phase change materials. *Scientific Reports* **2020,** *10* (1), 15388.

16. Nazir, H.; Batool, M.; Bolivar Osorio, F. J.; Isaza-Ruiz, M.; Xu, X.; Vignarooban, K.; Phelan, P.; Inamuddin; Kannan, A. M., Recent developments in phase change materials for energy storage applications: A review. *International Journal of Heat and Mass Transfer* **2019,** *129*, 491-523.

17. Comtois, E.; Favis, B. D.; Dubois, C., Phase transitions and mechanical properties of nitrocellulose plasticized by glycidyl azide polymer and nitroglycerine. *Polymer Engineering & Science* **2020,** *60* (9), 2301-2313.

18. Sarı, A.; Alkan, C.; Altıntaş, A., Preparation, characterization and latent heat thermal energy storage properties of micro-nanoencapsulated fatty acids by polystyrene shell. *Applied Thermal Engineering* **2014,** *73* (1), 1160-1168.

19. Xiao, X.; Zhang, P.; Li, M., Preparation and thermal characterization of paraffin/metal foam composite phase change material. *Applied Energy* **2013,** *112* (C), 1357-1366.

20. Schiffres, S. N.; Harish, S.; Maruyama, S.; Shiomi, J.; Malen, J. A., Tunable Electrical and Thermal Transport in Ice-Templated Multilayer Graphene Nanocomposites through Freezing Rate Control. *ACS Nano* **2013,** *7* (12), 11183-11189.

21. Gunasekara, S. N.; Pan, R.; Chiu, J. N.; Martin, V., Polyols as phase change materials for surplus thermal energy storage. *Applied Energy* **2016,** *162* (C), 1439-1452.

22. Farid, M. M.; Khudhair, A. M.; Razack, S. A. K.; Al-Hallaj, S., A review on phase change energy storage: materials and applications. *Energy Conversion and Management* **2004,** *45* (9), 1597-1615.

23. Sundararajan, S.; Samui, A. B.; Kulkarni, P. S., Interpenetrating phase change polymer networks based on crosslinked polyethylene glycol and poly(hydroxyethyl methacrylate). *Solar Energy Materials and Solar Cells* **2016,** *149*, 266-274.

24. Sari, A.; Alkan, C.; Doguscu, D. K.; Bicer, A., Micro/nano-encapsulated n-heptadecane with polystyrene shell for latent heat thermal energy storage. *Solar Energy Materials and Solar Cells* **2014,** *126*, 42-50.

25. Cao, Q.; Liu, P., Hyperbranched polyurethane as novel solid–solid phase change material for thermal energy storage. *European Polymer Journal* **2006,** *42* (11), 2931-2939.

26. Hong, Y.; Xin-shi, G., Preparation of polyethylene–paraffin compound as a form-stable solid-liquid phase change material. *Solar Energy Materials and Solar Cells* **2000,** *64* (1), 37-44.

27. Sarı, A., Form-stable paraffin/high density polyethylene composites as solid–liquid phase change material for thermal energy storage: preparation and thermal properties. *Energy Conversion and Management* **2004,** *45* (13), 2033-2042.

28. Zhang, Y.; Xiu, J.; Tang, B.; Lu, R.; Zhang, S., Novel semi-interpenetrating network structural phase change composites with high phase change enthalpy. *AIChE Journal* **2018,** *64* (2), 688-696.

29. Sperling, L. H.; Mishra, V., The current status of interpenetrating polymer networks. *Polymers for Advanced Technologies* **1996,** *7* (4), 197-208.

30. Sperling, L. H., *Interpenetrating Polymer Networks and Related Materials*. Plenum Press,: New York, 1981; Vol. 12 (1).

31. Li, B.; Bi, X.; Zhang, D.; Whang, F., Forced Compatibility and Mutual Entanglements in Poly (Vinyl Acetate)/Poly (Methyl Acrylate) IPNs. *Technomic Publishing Company, Advances in Interpenetrating Polymer Networks.* **1989,** *1*, 203-220.

32. BOUDENNE, A.; IBOS, L.; CANDAU, Y., *Handbook of Multiphase Polymer Systems*. A John Wiley & Sons, Ltd., Publication: 2011.

33. Sperling, L. H., Interpenetrating Polymer Networks: An Overview. In *Interpenetrating Polymer Networks*, American Chemical Society: 1994; Vol. 239, pp 3-38.

34. Mita, I.; Akiyama, S., Macromolecular Design of Polymeric Materials. In *PLASTICS ENGINEERING-NEW YORK*, Marcel Dekker, Inc.: 1997; pp 393-406.

35. Chen, C. H.; Chen, W. J.; Chen, M. H.; Li, Y. M., Simultaneous full-interpenetrating polymer networks of blocked polyurethane and vinyl ester Part I. Synthesis, swelling ratio, thermal properties and morphology. *Polymer* **2000,** *41* (22), 7961-7967.

36. Fan, L. H.; Hu, C. P.; Ying, S. K., Thermal analysis during the formation of polyurethane and vinyl ester resin interpenetrating polymer networks. *Polymer* **1996,** *37* (6), 975-981.

37. Dave, V. J.; Patel, H. S., Synthesis and characterization of interpenetrating polymer networks from transesterified castor oil based polyurethane and polystyrene. *Journal of Saudi Chemical Society* **2017,** *21* (1), 18-24.

38. Sundaram, B. M.; Mendez, R. B.; Auad, M. L.; Tippur, H. V., Quasi-static and dynamic mechanical behavior of transparent graft-interpenetrating polymer networks (graft-IPNs). *Polymer Testing* **2018,** *70*, 348-362.

39. Alizadeh, N.; Thorne, D. P.; Auad, M. L.; Celestine, A.-D. N., Mechanical performance of vinyl ester—polyurethane interpenetrating polymer network composites. *Journal of Applied Polymer Science* **2021,** *138* (19), 50411.

40. Bird, S. A.; Clary, D.; Jajam, K. C.; Tippur, H. V.; Auad, M. L., Synthesis and characterization of high performance, transparent interpenetrating polymer networks with polyurethane and poly(methyl methacrylate). *Polymer Engineering & Science* **2013,** *53* (4), 716-723.

41. Ballestero, R.; Sundaram, B. M.; Tippur, H. V.; Auad, M. L., Sequential graft-interpenetrating polymer networks based on polyurethane and acrylic/ester copolymers. *Express Polymer Letters* **2016,** *10* (3), 204-215.

42. Alizadeh, N.; Barde, M.; Minkler, M.; Celestine, A.-D.; Agrawal, V.; Beckingham, B.; Auad, M. L., High-fracture-toughness acrylic–polyurethane-based graft-interpenetrating polymer networks for transparent applications. *Polymer International* **2020**.

43. Jajam, K. C.; Bird, S. A.; Auad, M. L.; Tippur, H. V., Tensile, fracture and impact behavior of transparent Interpenetrating Polymer Networks with polyurethane-poly(methyl methacrylate). *Polym. Test* **2013,** *32* (5), 889-900.

44. Jajam, K. C.; Tippur, H. V.; Bird, S. A.; Auad, M. L. In *Dynamic Fracture and Impact Energy Absorption Characteristics of PMMA-PU Transparent Interpenetrating Polymer Networks (IPNs)*, Dynamic Behavior of Materials, Volume 1, Cham, 2014//; Song, B.; Casem, D.; Kimberley, J., Eds. Springer International Publishing: Cham, 2014; pp 277-284.

45. Jajam, K. C.; Bird, S. A.; Auad, M. L.; Tippur, H. V. In *Development and Characterization of a PU-PMMA Transparent Interpenetrating Polymer Networks (t-IPNs)*, Dynamic Behavior of

Materials, Volume 1, New York, NY, 2011//; Proulx, T., Ed. Springer New York: New York, NY, 2011; pp 117-121.

46. Méndez, R. B. Sequential graft-Interpenetrating polymer networks based on polyurethane and acrylic/ester copolymers. Auburn University, Auburn, AL, 2015.

47. Hillerström, A.; Andersson, M.; Pedersen, J. S.; Altskär, A.; Langton, M.; van Stam, J.; Kronberg, B., Transparency and wettability of PVP/PDMS-IPN synthesized in different organic solvents. *Journal of Applied Polymer Science* **2009,** *114* (3), 1828-1839.

48. Alizadeh, N.; Bird, S. A.; Mendez, R. B.; Jajam, K. C.; Alexander, A. C.; Tippur, H. V.; Auad, M. L., Chapter 11 - Synthesis and Characterization of High Performance Interpenetrating Polymer Networks With Polyurethane and Poly(methyl methacrylate). In *Unsaturated Polyester Resins*, Thomas, S.; Hosur, M.; Chirayil, C. J., Eds. Elsevier: 2019; pp 243-255.

49. Qin, C.-L.; Cai, W.-M.; Cai, J.; Tang, D.-Y.; Zhang, J.-S.; Qin, M., Damping properties and morphology of polyurethane/vinyl ester resin interpenetrating polymer network. *Materials Chemistry and Physics* **2004,** *85* (2-3), 402-409.

50. Bird, S. A. Interpenetrating Polymer Networks with Polyurethane and Methacrylate-based Polymers. Auburn University, Auburn, AL, 2013.

51. Alizadeh, N.; Celestine, A.-D. N.; Auad, M. L.; Agrawal, V., Mechanical characterization and modeling stress relaxation behavior of acrylic–polyurethane-based graft-interpenetrating polymer networks. *Polymer Engineering & Science* **2021**.

52. Huang, J.; Zhang, L., Effects of NCO/OH molar ratio on structure and properties of graft-interpenetrating polymer networks from polyurethane and nitrolignin. *Polymer* **2002,** *43* (8), 2287-2294.

53. Zalipsky, S.; Harris, J. M., Introduction to Chemistry and Biological Applications of Poly(ethylene glycol). In *Poly(ethylene glycol)*, American Chemical Society: 1997; Vol. 680, pp 1-13.

54. Natta, G.; Corradini, P.; Bassi, I. W., Crystal structure of isotactic polystyrene. *Il Nuovo Cimento (1955-1965)* **1960,** *15* (1), 68-82.

55. Su, J.-C.; Liu, P.-S., A novel solid–solid phase change heat storage material with polyurethane block copolymer structure. *Energy Conversion and Management* **2006,** *47* (18), 3185-3191.

56. Jiang, Y.; Ding, E.; Li, G., Study on transition characteristics of PEG/CDA solid–solid phase change materials. *Polymer* **2002,** *43* (1), 117-122.

57. Liu, Z.; Zhang, Y.; Hu, K.; Xiao, Y.; Wang, J.; Zhou, C.; Lei, J., Preparation and properties of polyethylene glycol based semi-interpenetrating polymer network as novel form-stable phase change materials for thermal energy storage. *Energy and Buildings* **2016,** *127*, 327-336.

58. Pielichowski, K.; Flejtuch, K., Differential scanning calorimetry studies on poly(ethylene glycol) with different molecular weights for thermal energy storage materials. *Polymers for Advanced Technologies* **2002,** *13* (10-12), 690-696.

59. Scherrer, P., Nachrichten von der Gesellschaft der Wissenschaften zu Göttingen. *Mathematisch-Physikalische Klasse* **1918,** *2*, 98-100.

60. Pavia, D. L.; Lampman, G. M.; Kriz, G. S., *Introduction to spectroscopy, Third edition*. Thomson Learning: Washington, 2001.

61. Chen, C.; Chen, J.; Jia, Y.; Topham, P. D.; Wang, L., Binary shape-stabilized phase change materials based on poly(ethylene glycol)/polyurethane composite with dual-phase transition. *Journal of Materials Science* **2018,** *53* (24), 16539-16556.

General Conclusions

Interpenetrating polymer networks were synthesized to prepare high-performance polymers. Although IPNs bring physical entanglement as forced compatibility between the two networks, chemical bonds between two polymers were used to enhance compatibility. PU was used as a rubbery phase which brings high toughness and high flexibility properties to the system, while the acrylic copolymer was utilized to bring high mechanical properties such as modulus and strength to the IPN system.

In chapter 2, aliphatic isocyanate with 1400 g/mol PTMG as diol was used to avoid phase separation between two polymers. Moreover, a Stoichiometric amount of diol and triol was utilized to prevent phase separation between two polymers. Following the sequential polymerization also helped in this improvement. FTIR and NMR spectroscopies confirm the successful polymerization of both phases in the IPN system. Thermomechanical and TEM analysis show that phase separation starts to decrease by increasing the ratio of styrene, and IPN samples with 80 and 90 wt% of styrene show minimum phase separation in the system. The UV-Vis spectroscopy results indicate that IPNs with 80 and 90 wt% styrene have transparency close to 100%, which confirms the observation in thermomechanical and TEM analysis. Besides, a thermomechanical study exhibits the glass transition of IPNs is higher than 80°C, which is a considerable improvement compared to pure PU due to acrylic copolymer in the system. Finally, SEM was used to study the samples' surface morphology. SEM results show that even though adding more styrene to the network increases transparency, it decreases the surface's roughness, decreasing the fracture toughness of the samples. Thus IPN with 80 wt% styrene with excellent transparency and the rigged texture was utilized to determine the fracture toughness of IPN. Approximately 40% improvement in fracture toughness is observed in the IPN than acrylic copolymer with 80 wt%

styrene. Moreover, fracture toughness is improved around 120% compared to PMMA and PS. Such graft-IPNs have considerable potential in transparent, high-performance applications such as canopies and enclosures.

In chapter 3, the graft-IPN synthesized out of commercial vinyl ester, was employed to manufacture polymer matrix composite. The hand layup process was applied to synthesize the carbon fiber reinforced composite. The IPN monomers show low viscosity, which helps to make the manufacturing process easier. DSC and FTIR analyses confirm the successful polymerization of the IPNs. The dynamic mechanical analysis reveals the enhancement in the IPN samples' damping properties due to flexible PU. Mechanical characterization of composite samples exhibits modulus and strength comparable to numbers reported in the literature. Finally, SEM results show good adhesion between fibers and matrix with no debonding and fiber pull out. The simple manufacturing method and excellent mechanical properties show the vast potential of synthesized composites in high-performance applications.

In chapter 4, rubbery graft-IPNs were synthesized by increasing the ratio of PU in IPN systems. FTIR results confirm the successful polymerization of both phases. DMA and tensile analysis show a wide range of Tg and E' for samples with different ratios of PU and different monomers (MMA and styrene) in acrylic copolymer structures. This fact shows the wide variety of applications for synthesized graft-IPN. The tensile shear test results reveal comparable shear strength for IPN samples as an adhesive with literature. Finally, the sandwich structure of pure PC with IPN samples in between them exhibits excellent transparency and impact resistance, which indicates the considerable potential of novel IPN in transparent high impact structural applications.

In chapter 5, the IPN and copolymer samples' stress relaxation behavior with different percentages of PU and different acrylic copolymer precursors' ratios were studied and modeled using the FEM.

Acrylic Copolymers show the highest relaxation modulus and resistance against relaxation due to acrylic copolymers' highest stiffness. However, the relaxation modulus for COP samples drops by adding more styrene into the system. As expected, rubbery specimens show the lowest relaxation modulus among all samples. Moreover, rubbery samples exhibit high resistance against relaxation, making them the right candidate for damping applications. It should be added that $IPN_G90/10$ shows relaxation modulus and resistance against relaxation comparable to COP samples due to the higher percentage of styrene, making better interpenetration between two polymers. A Generalized Maxwell model with four-term Prony series was utilized to model the samples' stress relaxation behavior. Overall, a good overlap between experimental and simulation data for stress relaxation behavior of all samples is observed. This fact shows the potential of a developed model to predict the stress relaxation behavior of IPNs, which has not been vastly studied before.

In the final chapter, graft-semi-IPN was synthesized to be used in thermal energy storage applications. Linear PEG-based PU with long chains was used as the first phase due to its high capability of phase change applications. The stiff Acrylic copolymer was used as a skeleton to keep the structure of IPN together in high temperatures. Chemical bonds between two polymers were also employed to enhance the shape stability of the samples even more. FTIR analysis confirms the successful polymerization of both phases. DSC and TGA exhibit excellent thermal properties in the semi-IPN samples. It is observed that thermal properties are enhanced by adding more PU to IPN. The presence of acrylic copolymer acts as a hindrance in the IPN system and limits the thermal properties in IPN samples. XRD, POM, and SEM analysis confirm the results from DSC and show that the PEG's crystal properties does not change by utilizing it in the IPN system. Finally, excellent shape and cycling stability were obtained in all samples, which shows

the massive potential of novel IPNs in high-performance thermal energy storage applications such as antennas for ships and helicopters.

Overall, we conclude that the synthesized IPNs show vast potential in high fracture toughness and impact structural applications, polymer matrix composite, and thermal energy storage applications. The unique properties of each phase (PU and acrylic copolymer) in the IPN structure enhance each polymer's weakness and provide desirable properties for the high-performance applications mentioned above. The model generated in this research is one of the first in the field and can predict the stress relaxation behavior of synthesized IPNs.

In order to synthesize the novel IPNs with complex structure, low cost, and less waste of energy and materials, It is beneficial to utilize additive manufacturing technology to print and synthesize the IPNs. The thermal initiator should change to the photoinitiator such as irgacure 184 and diphenyl(2,4,6-trimethylbenzoyl)phosphine oxide which can be cured by UV light in 365 nm and 405 nm, respectively. Utilizing a different photoinitiator with the capability to cure in different wavelengths expands the application of IPNs in this research to be used with different additive manufacturing technologies. Such technologies include direct ink writing and stereolithography. Synthesized IPNs with additive manufacturing could be used in a wide range of applications where high resolution is required such as aerospace. Moreover, different kinds of fillers such as layered silicates could be utilized to improve the mechanical properties, flame and chemical resistance, and etc. Finally, The generated model in this research could be modified to be used for heterogeneous systems.